

UNIVERSIDAD DE MÁLAGA  
DEPARTAMENTO DE FÍSICA APLICADA II

PROGRAMA DE DOCTORADO INTERUNIVERSITARIO:  
DINÁMICA DE LOS FLUJOS BIOGEOQUÍMICOS Y SUS APLICACIONES

Tesis Doctoral

# Unraveling the physics of connectivity and dispersal in Mediterranean coastal marine populations: the case of the Alboran and Adriatic seas

Irene Nadal Arizo

Directores: Jesús García Lafuente y Simone Sammartino

Málaga, 2024





UNIVERSIDAD  
DE MÁLAGA

Universidad de Málaga

Departamento de Física Aplicada II

Programa de Doctorado Interuniversitario:  
**Dinámica de los Flujos Biogeoquímicos y sus Aplicaciones**

TESIS DOCTORAL

por compendio de publicaciones

**Unraveling the physics of connectivity and  
dispersal in Mediterranean coastal marine  
populations: the case of the Alboran and  
Adriatic seas**

**Irene Nadal Arizo**

**Málaga, 2024**

Los directores:

**Jesús García Lafuente**

Catedrático del Dpto. de Física  
Aplicada II de la Universidad de  
Málaga

**Simone Sammartino**

Profesor Titular del Dpto. de Física  
Aplicada II de la Universidad de  
Málaga





Memoria presentada por Irene Nadal Arizo para optar al grado de Doctora por la Universidad de Málaga con Mención Internacional en el Programa de Doctorado en Dinámica de los Flujos Biogeoquímicos y sus Aplicaciones.



## DECLARACIÓN DE AUTORÍA Y ORIGINALIDAD DE LA TESIS PRESENTADA PARA OBTENER EL TÍTULO DE DOCTOR

D./Dña. IRENE NADAL ARIZO

Estudiante del programa de doctorado DINÁMICA DE LOS FLUJOS BIOGEOQUÍMICOS Y SUS APLICACIONES de la Universidad de Málaga, autor/a de la tesis, presentada para la obtención del título de doctor por la Universidad de Málaga, titulada: UNRAVELING THE PHYSICS OF CONNECTIVITY AND DISPERSAL IN MEDITERRANEAN COASTAL MARINE POPULATIONS: THE CASE OF THE ALBORAN AND ADRIATIC SEAS





Realizada bajo la tutorización de JESÚS GARCÍA LAFUENTE y dirección de JESÚS GARCÍA LAFUENTE y SIMONE SAMMARTINO

DECLARO QUE:

La tesis presentada es una obra original que no infringe los derechos de propiedad intelectual ni los derechos de propiedad industrial u otros, conforme al ordenamiento jurídico vigente (Real Decreto Legislativo 1/1996, de 12 de abril, por el que se aprueba el texto refundido de la Ley de Propiedad Intelectual, regularizando, aclarando y armonizando las disposiciones legales vigentes sobre la materia), modificado por la Ley 2/2019, de 1 de marzo.

Igualmente asumo, ante a la Universidad de Málaga y ante cualquier otra instancia, la responsabilidad que pudiera derivarse en caso de plagio de contenidos en la tesis presentada, conforme al ordenamiento jurídico vigente.

En Málaga, a 12 de junio de 2024

 Fdo.: Irene Nadal Arizo Doctorando/a	 Fdo.: Jesús García Lafuente Tutor/a
 Fdo. Jesús García Lafuente	 Fdo. Simone Sammartino Director/es de tesis





D. **Jesús García Lafuente**, Catedrático del Departamento de Física Aplicada II de la Universidad de Málaga, y D. **Simone Sammartino**, Profesor Titular del Departamento de Física Aplicada II de la Universidad de Málaga,

HACEN CONSTAR:

Que el trabajo recogido en la presente memoria, titulada “Unraveling the physics of connectivity and dispersal in Mediterranean coastal marine populations: the case of the Alboran and Adriatic seas”, presentada por Irene Nadal Arizo, ha sido realizada bajo nuestra dirección y tiene, a nuestro juicio, contenido científico suficiente, de lo que informamos favorablemente en orden a su presentación y defensa para optar grado de Doctora Internacional por la Universidad de Málaga.

Para ello, firmamos la presente en Málaga a 12 de junio de 2024:



Jesús García Lafuente

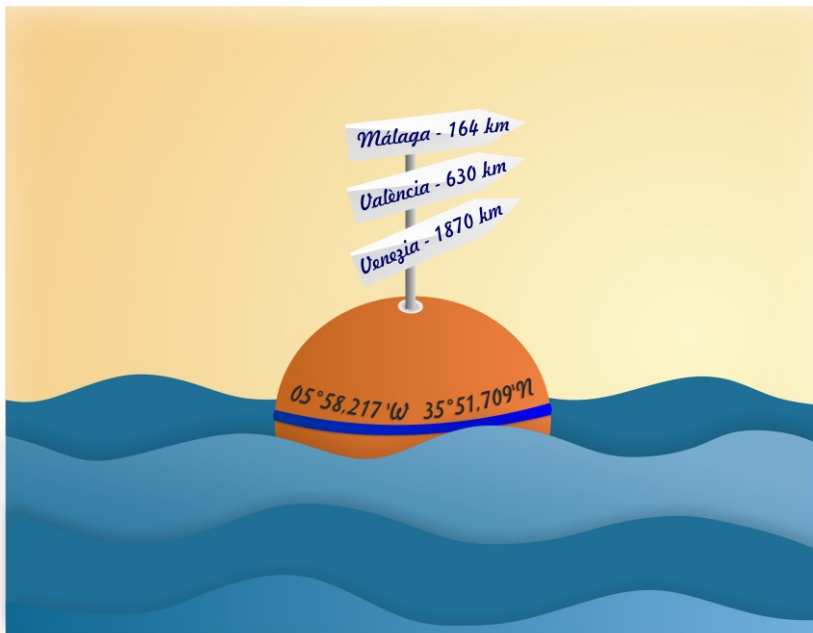


Simone Sammartino



*“El mar  
me alimenta,  
el mar  
me sustenta.  
A mí,  
a mi familia...  
El mar me contenta,  
el mar  
me atormenta...  
El mar  
es mi vida,  
el mar  
es mi hogar...”*

Ricardo Villar Martínez, *El poeta de los mares*





## Agradecimientos

Cuando acaba un doctorado, en cierto modo, se cierra un ciclo para dejar paso a otra etapa de la vida. Ahora, mirando atrás, reconozco lo importante que ha sido este periodo y todas aquellas personas que han formado parte de él. Sin ellas, no sería quien soy hoy, así que quiero dar las gracias a todos los que, de una forma u otra, me han guiado, acompañado y apoyado, ya sea en el ámbito profesional o personal, en este viaje tan especial.

El primer agradecimiento es, sin duda, para mis dos directores de tesis, el Dr. Jesús García Lafuente y el Dr. Simone Sammartino, a quienes admiro profundamente y por los que me he sentido una estudiante muy afortunada. Jesús, eres un referente en la oceanografía física para muchas personas, y también para mí. Gracias por haberme dado la oportunidad de formarme en el grupo, pero, sobre todo, gracias por todo lo que me has enseñado sobre el océano, por los valiosos consejos que sin duda recordaré y aplicaré en mi futuro profesional, y por tu paciencia y capacidad para hacerme una crítica constructiva y darme un empujón cuando lo necesitaba, científica y personalmente. Simone, mi primer contacto contigo fue que, sin apenas conocerme, dedicaste todo el tiempo que hizo falta para enseñarme paciente y entusiastamente el procesado de datos geofísicos con Matlab. Más tarde descubriría que sería una herramienta y un aprendizaje imprescindibles en mi trabajo, pero también que ese mismo entusiasmo y dedicación los seguiría recibiendo durante el resto de mi periodo académico. Aprender contigo ha sido una suerte de la que no muchos gozan. Me has enseñado a hacer ciencia, a plantearme preguntas, a ser resolutiva, a hacerlo siempre lo mejor posible y, en definitiva, a ser mejor oceanógrafa. Eres un gran científico y profesor, pero sobre todo eres una gran persona.

Un enorme agradecimiento es para el resto de los miembros del Grupo de Oceanografía Física de la Universidad de Málaga (GOFIMA), José Carlos, Javi, Jorge, Cristina, Francis y Pablo, por los valiosos consejos que me habéis dado y por todos por los buenos momentos que hacen que ahora ya no seáis sólo “compañeros”, sino amigos. En especial, gracias a Jorge y Cristina, que en distintas partes de esta etapa me han escuchado, apoyado, y aconsejado, y



a Pablo, por ser un amigo y compañero de estudios en esta fase. Nos hemos ayudado y escuchado mutuamente, y sólo me queda darte ánimos para completar tu tesis.

I would also like to thank the Institute of Marine Science of Venice (ISMAR), which hosted me during three wonderful months of my PhD. A big "Grazie" is undoubtedly to my supervisors at this center, Dr. Michol Ghezzo and Dr. Francesco Falcieri, for their constant kind appreciation, availability and enthusiasm, for their scientific advice and knowledge, and for all the fruitful and insightful discussions and suggestions we had during my stay. Thanks also to the colleagues who gave me precious scientific and personal advices during and after my stay, Dr. Marta Picciulin, Dr. Christian Ferrarin and Dr. Katrin Schroeder, and to all the friends I left there (or scattered all over the world): Sofi, Lorenzo, Matt, Laura, Daphnie, Francesco, Malek, Taha, Marina, Luca, Silvio, Giovanni, and all the people I have unintentionally forgotten. Especially to Lorenzo, for being a great support during all my time in Venice, and to Sofi, for visiting me in Malaga and being such a great friend. But in general, thank you all for making my stay there so pleasant and enjoyable. Grazie amici!!

Durante estos años he tenido la oportunidad de participar en once maravillosas campañas en el Estrecho de Gibraltar, en las que he tenido la suerte de disfrutar y aprender de grandes oceanógrafos y, aún mejores personas. Agradezco en especial al equipo STOCA: Ricardo, Susana, Carmela, Izaskun, Ana, Tere, Juan, y Silvia; y al equipo TRANSBORAN: Raúl, Alberto y JM Quintanilla. Muchas gracias a tod@s por los bonitos momentos compartidos a bordo.

Mi experiencia no habría sido ni de lejos la misma sin las personas que me han acompañado en mi vida malagueña y que han hecho que ésta fuera bonita, divertida y definitivamente más fácil cuando las cosas no han sido sencillas. Gracias Andy, fuiste un apoyo incondicional durante gran parte del doctorado. Nunca olvidaré esos paseos en medio de la tarde por teleco que pasábamos riendo, explorando y hablando de la vida, con las que desconectábamos y volvíamos al trabajo con más energía. Gracias a mis

compañeras de piso que al final se convirtieron en mis amigas. A Tere, mi amiga gaditana, con la que tan buenos momentos he pasado. La vida no ha sido nada fácil para ti estos últimos años, pero no has perdido la sonrisa y el optimismo, y no sabes lo mucho que he aprendido de ti. A María, la amiga con quien más he reído, llorado y disfrutado en Málaga. Qué bonito ha sido compartir esta etapa contigo. Y a Alba, quien siempre me recibe con una sonrisa, me escucha y apoya, sin importar cuanto tiempo llevemos sin vernos.

La distancia, inevitablemente, dificulta mantener el contacto con muchas personas, pero existen amistades que, sin importar cuánto tiempo pase, hacen que cada reencuentro se sienta como si nos hubiéramos visto ayer. En concreto, quiero agradecer a algunos de mis amig@s oceanógraf@s, quienes han seguido de cerca mi trayectoria académica y han estado presentes en momentos muy especiales de esta etapa. Gracias, Carmen, por ser un apoyo incondicional desde que nos conocemos y por sacar siempre un momento para mí cuando voy a Valencia. Eres de esas amistades de verdad, en las que puedes confiar sin pensar, sin importar cuánto tiempo pase y sin que te pidan nada a cambio. Gracias por estar ahí “siempre, siempre, siempre...”. Gracias, Ana, por acordarte de avisarme cada vez que estás de campaña y paras en el Puerto de Málaga, y por dedicarme tan bonitas palabras de ánimo cuando más falta me hacen. Eres un sol. Gracias a Uxue y Samu, por hacer que viviera la experiencia de congreso más divertida y especial que he tenido hasta la fecha. Pero, sobre todo, gracias a dos compañeros con quienes hace más de diez años comencé a estudiar Ciencias del Mar y que, con el tiempo, se convirtieron en los amigos más importantes de mi vida: Alejandro y Judith.

Gracias, Ale. Eres ese amigo que un día llega para quedarse, con quien sé que puedo contar para todo y que, sin importar hasta dónde nos lleven los caminos, siempre estará ahí. Hemos compartido un montón de buenos ratos juntos, dentro y fuera del agua, y nos hemos apoyado y entendido como nadie. Ahora que ya estamos aquí, por fin, sólo me queda mandarte un abrazo enorme y todo el ánimo para esta última parte. Decir que estoy orgullosa de ti es poco. Te aprecio muchísimo.

Y, en especial, gracias, Judith, por ser mi mejor amiga, confidente y compañera en este viaje. Por ver y sacar siempre lo mejor de mí. Por conocerme tan bien que, con sólo una mirada, nos entendemos. Por estar siempre ahí, sin importar la distancia y hacer que, aunque vivamos a casi 1000 km, te sienta cerca. No hay palabras suficientes para agradecerte todo el apoyo y la ayuda que me has dado durante toda esta etapa, especialmente en estos últimos meses. Sin ti, no habría llegado hasta aquí. Llevas el sol dentro, y me siento muy afortunada de tenerte en mi vida. Sé que siempre será así. Te quiero, y me siento querida por ti.

Sin duda, gracias infinitas también a ti, Adri, por animarme siempre a cumplir mis sueños, por aportar tu lado racional cuando mi mente es un caos de emociones, por todo el apoyo que me has brindado en estos últimos meses, en los que la tesis ha protagonizado nuestras vidas. Pero, sobre todo, gracias por respetar y aceptar mi pasión, eligiendo subir a este barco en el que compartimos una nostalgia y un profundo cariño que nos une de una forma muy especial. Quizá no sepamos hacia dónde nos llevará este rumbo, pero lo que sí sé con certeza es que navegando contigo he encontrado la calma, y de ti he aprendido que el viaje importa más que el destino. Sense tu, no hauria pogut fer-ho. Gràcies per tant. Et vuic un món.

Mi último y más sincero agradecimiento es para mis padres, quienes han sufrido más de cerca los inconvenientes de que mi pasión estuviera a más de 600 km de casa. Sé que mis elecciones no siempre han sido las más convencionales, pero nunca me habéis puesto impedimento alguno y sin vosotros, no habría llegado hasta aquí. Así que gracias, de corazón, por vuestro amor, por el apoyo incondicional en cada paso que he dado, tanto personal como académico, y vuestra confianza para afrontar cada reto de la vida. Os quiero, y no podría estar más agradecida por teneros a mi lado.

# Table of contents

List of publications .....	19
List of abbreviations.....	23
List of figures.....	25
List of tables .....	35
Scheme of the research: one-page thesis .....	37
1 General Introduction.....	39
1.1 State of the art.....	39
1.1.1 Motions in the marine environment: an overview .....	39
1.1.2 The idea and relevance of connectivity and dispersal.....	42
1.1.3 Some notions on the methods to estimate connectivity .....	46
1.1.4 Methodological challenges .....	48
1.2 Motivation, objectives, and structure of the PhD thesis .....	50
1.3 General hydrodynamics of the study regions.....	53
1.3.1 The Alboran Sea .....	54
1.3.2 The Adriatic Sea .....	58
2 Methodology .....	61
2.1 Numerical model .....	61
2.1.1 Governing equations.....	61
2.1.2 General considerations on the setup of ocean models .....	62
2.1.3 MITgcm.....	66
2.1.4 SHYFEM.....	70
2.2 Lagrangian particle tracking .....	72
2.2.1 Applications .....	74
2.3 Connectivity computation .....	76
3 Hydrodynamic connectivity and dispersal patterns of a transboundary species ( <i>Pagellus bogaraveo</i> ) in the Strait of Gibraltar and adjacent basins.....	79

3.1	Abstract.....	79
3.2	Introduction .....	80
3.2.1	Life cycle of blackspot seabream .....	83
3.2.2	Relevant hydrodynamic features of the area .....	83
3.3	Numerical data and methods .....	85
3.3.1	The hydrodynamic model .....	85
3.3.2	Releasing boxes and landing areas selection .....	87
3.3.3	Lagrangian particle tracking and experimental setup.....	89
3.3.4	Pool of experiments and connectivity computation .....	90
3.4	Results and discussion.....	93
3.4.1	MPoP and ToMC averages .....	93
3.4.2	Release area dependency .....	96
3.4.3	Tide dependence: A case study in the northern shore .....	101
3.4.4	Depth dependence .....	103
3.4.5	A sensitivity analysis on PLD .....	106
3.4.6	Release time dependency (replicas) .....	108
3.4.7	Implications for the species assessment and management.....	108
3.5	Summary and future works.....	109
3.6	Supplementary material.....	115
4	Spatio-temporal connectivity and dispersal seasonal patterns in the Adriatic Sea using a retention clock approach .....	117
4.1	Abstract.....	117
4.2	Introduction .....	118
4.3	Study area.....	120
4.3.1	Relevant hydrologic features.....	121
4.3.2	Ichthyo-biodiversity in the AS .....	122
4.4	Experimental procedure.....	125
4.4.1	Hydrodynamic model.....	125



4.4.2	Particle tracking module.....	127
4.4.3	Construction and analysis of connectivity .....	131
4.5	Results and discussion .....	134
4.5.1	Connectivity matrix.....	134
4.5.2	Time-dependent connectivity .....	138
4.5.3	Auto-connectivity .....	138
4.5.4	Effects of PLD on connectivity .....	146
4.5.5	Implications for the species inhabiting the AS .....	148
4.6	Conclusions.....	149
4.7	Supplementary material.....	151
5	Could secondary flows have made possible the cross-strait transport and explosive invasion of <i>Rugulopteryx okamurae</i> algae in the Strait of Gibraltar? .....	155
5.1	Abstract .....	155
5.2	Introduction .....	156
5.3	Possible mechanisms for cross-strait connection.....	160
5.4	Summary of current meter observations and other data sets .....	164
5.5	Assessment of the possible cross-strait transport.....	167
5.5.1	Observation-based cross-strait mean secondary circulation ...	167
5.6	Time variability of the cross-strait secondary circulation .....	169
5.6.1	Meteorologically-induced fluctuations.....	170
5.6.2	The fortnightly tidal cycle .....	171
5.7	Other requirements for a successful connection.....	172
5.7.1	Reaching the right depth for crossing and returning to illuminated layers.....	173
5.7.2	Keeping the right conditions for spreading .....	175
5.8	Summary and final remarks .....	176
5.9	Annex 5A: Summary of current meter observations .....	178

5.9.1	Eastern section.....	178
5.9.2	Camarinal sill section .....	179
6	Modeling spread of an alien alga under different temporal scenarios in the Strait of Gibraltar and adjacent basins .....	181
6.1	Abstract.....	181
6.2	Introduction .....	182
6.3	Relevant hydrodynamic features of the study area .....	185
6.4	Hydrodynamic model .....	187
6.4.1	Model description and initialization.....	187
6.4.2	Model validation.....	189
6.5	Lagrangian setup.....	191
6.6	Results and discussion.....	193
6.6.1	March 2021 as a case of study .....	198
6.6.2	Sinking velocity dependence.....	200
6.6.3	Implications of the results for invasion management .....	202
6.7	Final remarks .....	203
6.8	Supplementary material.....	205
7	Integrated discussion and conclusion.....	207
7.1	Thesis synthesis: patterns of connectivity.....	207
7.1.1	Alboran Sea.....	207
7.1.2	Adriatic Sea.....	211
7.2	Applicability of results and obstacles on current connectivity applications .....	212
7.3	Modelling limitations and future paths.....	215
7.4	Concluding remarks .....	218
	Resumen en español.....	223
	Bibliography .....	233
	Annex: Publications.....	283

## List of publications

### Publications arising from this thesis

The present thesis is presented in the form of a "thesis by compendium of publications". To this aim, a total of four scientific papers are collected, which have been published (1-, 2-, 3-) or are being prepared for submission for publication (4-) in scientific journals, all of which belong to the first quartile in the Journal Citation Report (JCR). The listed works deal with the hydrodynamics that regulate the connectivity and dispersal patterns of different populations of interest in the regions of the Strait of Gibraltar and the Alboran Sea (1-, 3-, 4-) on the one hand, and the Adriatic Sea (2-) on the other.

- 1- **Nadal, I.**, Sammartino, S., García-Lafuente, J., Sánchez Garrido, J. C., Gil-Herrera, J., Hidalgo, M., & Hernández, P. (2022). Hydrodynamic connectivity and dispersal patterns of a transboundary species (*Pagellus bogaraveo*) in the Strait of Gibraltar and adjacent basins. *Fisheries Oceanography*, 31(4), 384-401. <https://doi.org/10.1111/fog.12583>.
- 2- **Nadal, I.**, Picciulin, M., Falcieri, F. M., García-Lafuente, J., Sammartino, S., & Ghezzi, M. (2024) Spatio-temporal connectivity and dispersal seasonal patterns in the Adriatic Sea using a retention clock approach. *Frontiers in Marine Science*, 11:1360077. <https://doi.org/10.3389/fmars.2024.1360077>.
- 3- García-Lafuente, J., **Nadal, I.**, Sammartino, S., Korbee, N., Figueroa, F.L. (2023) Could secondary flows have made possible the cross-strait transport and explosive invasion of *Rugulopteryx okamurae* algae in the Strait of Gibraltar?. *PLOS ONE*, 18(5): e0285470. <https://doi.org/10.1371/journal.pone.0285470>.
- 4- **Nadal, I.**, Sammartino, S., Sánchez Garrido, J. C., García-Lafuente, J., Korbee, N., Figueroa, F.L. Modeling spread of an alien alga under different temporal scenarios in the Strait of Gibraltar and adjacent basins. In preparation for submission to the journal *Marine Pollution Bulletin* in the following months of the year 2024.

## Other scientific publications during the doctoral period

During the period of my doctoral thesis, I contributed to two additional scientific works that are not included in this dissertation. These contributions are hereby listed as scientific merits:

- 5- García-Lafuente, J., Sammartino, S., Huertas, I. E., Flecha, S., Sánchez-Leal, R. F., Naranjo, C., **Nadal, I.**, & Bellanco, M. J. (2021). Hotter and Weaker Mediterranean Outflow as a Response to Basin-Wide Alterations. *Frontiers in Marine Science*, 8. <https://doi.org/10.3389/fmars.2021.613444> .
- 6- Sánchez-Garrido, J. C., & **Nadal, I.** (2022). The Alboran Sea circulation and its biological response: A review. *Frontiers in Marine Science*, 9. <https://doi.org/10.3389/fmars.2022.933390>.

Eleven contributions to national congresses are listed below as additional merits:

- 7- **Nadal, I.**, Sánchez Garrido, J. C., Sammartino, S., García-Lafuente, J., Korbee, N. & López-Figueroa, F. (2024, July 10-12). Dispersal modeling of the invasive algae *Rugulopteryx okamuræ* in the Strait of Gibraltar and adjacent basins [Oral presentation]. Physical Oceanography Encounter 2024 (EOF) - IX International Symposium on Marine Science (ISMS2024). Catholic University of Valencia. Valencia, Spain.
- 8- **Nadal, I.**, Picciulin, M., Falcieri, F. M., García-Lafuente, J., Sammartino, S., & Ghezzi, M. (2024, July 10-12). Spatio-temporal patterns of connectivity and dispersal in the Adriatic Sea [Poster]. Physical Oceanography Encounter 2024 (EOF) - IX International Symposium on Marine Science (ISMS2024). Catholic University of Valencia. Valencia, Spain.
- 9- **Nadal, I.**, Ghezzi, M., Falcieri, F.M., Sammartino, S., & García-Lafuente, J. (6-9 septiembre 2023). Patrones de dispersión y conectividad en el Mar Adriático [Poster]. I Congreso Iberoamericano Jóvenes Investigadores del Mar. University of Almería. Almería, Spain.
- 10- **Nadal, I.**, García-Lafuente, J., Sammartino, S., Sánchez-Garrido J. C., Korbee, N. & López-Figueroa, F. (6-8 julio 2022). On the interaction

- between the macroalgae *Rugulopteryx okamurae* and the hydrology of the Alboran Sea [Poster]. VII Expanding Ocean Frontiers conference (EOF) – VIII International Symposium on Marine Science (ISMS2022). University of Las Palmas de Gran Canaria. Las Palmas de Gran Canaria, Spain.
- 11- **Nadal, I.**, Sammartino, S., García-Lafuente, J., Sánchez Garrido, J. C., Gil-Herrera, J., Hidalgo, M., & Hernández, P. (6-8 julio 2022). Hydrodynamic connectivity and dispersal patterns in the Strait of Gibraltar: Implications for a transboundary species [Oral presentation]. VII Expanding Ocean Frontiers conference (EOF) – VIII International Symposium on Marine Science (ISMS2022). University of Las Palmas de Gran Canaria. Las Palmas de Gran Canaria, Spain.
  - 12- **Nadal, I.**, Muñoz López, P., Sammartino, S., García-Lafuente, J., & Cabello, J. (6-9 septiembre 2021). Estructura y variabilidad de las propiedades termohalinas y corriente en el Estuario del Guadalquivir [Oral presentation]. III Congress of Young Researchers (JISDELMAR). University of Granada. Motril, Spain.
  - 13- **Nadal, I.**, García-Lafuente, J., Sammartino, S., Muñoz López, P., & Cabello, J. (6-9 septiembre 2021). Interacciones entre la propagación de la onda de marea y el efecto de la fricción en el Estuario del Guadalquivir [Poster]. III Congress of Young Researchers (JISDELMAR). University of Granada. Motril, Spain.
  - 14- **Nadal, I.**, García-Lafuente, J., Sammartino, S., Muñoz López, P., & Cabello, J. (5-7 julio 2021). Interacciones entre la propagación de la onda de marea y el efecto de la fricción en el Estuario del Guadalquivir [*Online* oral presentation]. VI Expanding Ocean Frontiers conference (EOF). Polytechnic University of Catalonia. Barcelona (Virtual conference), Spain.
  - 15- **Nadal, I.**, García-Lafuente, J., Sammartino, S., Cabello, J. & Muñoz López, P., (16-18 junio 2021). Tidal propagation and frequency responses in the Guadalquivir Estuary [*Online* oral presentation]. 9th International Workshop On Marine Technology (MARTECH). University of Vigo (Virtual conference). Vigo, Spain.



- 16- **Nadal, I.**, Sammartino, S., Sánchez Garrido, J. C., & García-Lafuente, J. (1-4 octubre 2019). Connectivity patterns of the blackspot seabream (*Pagellus bogaraveo*) in the Alboran Sea [Poster]. II Congress of Young Researchers (JISDELMAR). University of Málaga. Málaga, Spain.
- 17- **Nadal, I.**, Sammartino, S., Sánchez Garrido, J. C., & García-Lafuente, J. (1-4 octubre 2019). Tidal dynamics effect on the connectivity patterns of the blackspot seabream (*Pagellus bogaraveo*) in the Alboran Sea [Oral presentation]. II Congress of Young Researchers (JISDELMAR). University of Málaga. Málaga, Spain.

## List of abbreviations

Abbreviation		Chapter(s)
<b>AdDW</b>	Adriatic Deep Water	1, 4
<b>ADCP</b>	Acoustic Doppler Current Profiler	5, 6
<b>AJ</b>	Atlantic Jet	1, 3, 6
<b>AOF/AO</b>	Almería-Oran front	1, 3
<b>AS</b>	Alboran Sea	3
<b>AS</b>	Adriatic Sea	4
<b>CCG</b>	Central Cyclonic Gyre	1, 3, 6
<b>CS</b>	Camarinal Sill	5, 6
<b>EAC</b>	Eastern Adriatic Current	1, 4, 7
<b>EAG</b>	Eastern Alboran Gyre	1, 3, 6, 7
<b>ELS</b>	Early-Life-Stages	3
<b>GSA</b>	Geographical Sub-Area	3, 4
<b>ISW</b>	Ionian Surface Water	1
<b>LIW</b>	Levantine Intermediate Water	1, 2, 3
<b>MITgcm</b>	Massachusetts Institute of Technology General Circulation Model	2, 3, 6
<b>MPoP</b>	Maximum Percentage of Particles	3
<b>NACW</b>	North Atlantic Central Water	1, 6
<b>NAdDW</b>	North Adriatic Dense Water	1, 4
<b>PLD</b>	Pelagic Larval Duration	1, 2, 3, 4
<b>RCM</b>	Retention Clock Matrix	4
<b>SAW</b>	Surface Atlantic Water	1
<b>SHYFEM</b>	Shallow water HYdrodynamic Finite Element Model	2, 4
<b>SoG</b>	Strait of Gibraltar	1, 3, 5, 6, 7
<b>Sv</b>	Sverdrup (1 Sv = 10 <sup>6</sup> m·s <sup>-1</sup> )	1, 3, 6

<b>ToMC</b>	Time of Maximum Connectivity	3
<b>WAC</b>	Western Adriatic Current	1, 4, 7
<b>WAG</b>	Western Alboran Gyre	1, 3, 6, 7
<b>WMDW</b>	Western Mediterranean Deep Water	1, 6

## List of figures

Chapter 1		page
<b>Figure 1.1</b>	Spatio-temporal scale at which different oceanographic phenomena occur. Adapted from Dickey, 2001.	40
<b>Figure 1.2</b>	Hypothetical linkage between spawning of eggs and adult ontogenetic migrations in sheltered (a) and exposed (b) regions. Sketch adapted from Brown et al. (2016).	45
<b>Figure 1.3</b>	Map showing the Mediterranean Sea, the Strait of Sicily dividing the Mediterranean into western and eastern basins, and the two regions of interest, the Alboran and Adriatic Seas, connected to the Mediterranean by the Straits of Gibraltar and Otranto, respectively. Some relevant sites mentioned in the text are also indicated.	54
<b>Figure 1.4</b>	Map of the Gulf of Cádiz and Alboran Sea, showing the Strait of Gibraltar, and patching its general circulation: on the Atlantic Side, the Coastal Counter Current (CCC) and the Cape San Vicente gyre (SVE), and on the Mediterranean Side, the Atlantic Jet (AJ), the Western and Eastern Alboran Gyres (WAG and EAG, respectively), the Central Cyclonic Gyre (CCG) and the Almería-Oran front (AOF). The Canary, Azores, and Portuguese currents alluded to in the text flow southward, eastward, and northerly, respectively, in the North part of the Atlantic not shown. For illustration purposes, an imaginary branch representing the course of these currents is shown in red. The most relevant water masses are also displayed, following sketches from Kinder & Bryden (1990)	57
<b>Figure 1.5</b>	Map of the Adriatic Sea sketching its general circulation: the Western and Eastern Adriatic Currents (WAC and EAC, respectively) and the North, Central and South Cyclonic Gyres. The most relevant water masses are displayed, following sketches from Russo & Artegiani (1996). Some of the relevant locations are also displayed.	59

Chapter 2		page
<b>Figure 2.1</b>	Schematic diagram of some of the typical stages required for a hydrodynamic model setup.	63
<b>Figure 2.2</b>	Numerical grid and bathymetry of MITgcm application in the Strait of Gibraltar and adjacent basins.	68
<b>Figure 2.3</b>	Numerical grid and bathymetry of SHYFEM application in the Adriatic Sea.	71
Chapter 3		page
<b>Figure 3.1</b>	Map of the Alboran Sea showing the Strait of Gibraltar (SoG) and sketching its general surface circulation: the Atlantic Jet (AJ) and the western and eastern Alboran Gyres (WAG and EAG, respectively). CCG stands for Central Cyclonic Gyre, a weaker structure that normally develops whenever the WAG and EAG are fully developed (adapted from Sánchez-Garrido et al., 2013). Smaller cyclonic eddies, represented by dashed lines, are often found rightwards and leftwards of the AJ main path. Some relevant locations are displayed and the GSAs (1-4), defined by the GFCM (2021) are patched.	85
<b>Figure 3.2</b>	Surface current direction and kinetic energy per unit of mass ( $m^2 \cdot s^{-2}$ ) in the AS (lower panels) and in the SoG region (upper panels) during neap (left side) and spring tide (right side). The main surface structures sketched in Figure 3.1 have been tagged in the lower right panel using the same acronyms.	87
<b>Figure 3.3</b>	Map of the study area showing the releasing boxes of Tarifa, Tangier and Tangier-Med (brown polygons in the inset) and the landing areas of Cadiz, Estepona, Malaga, Roquetas, Carboneras, Oran, Melilla, Al Hoceima, Tetuan, and Arcila (green polygons). Adapted from CopeMed II, 2019.	88
<b>Figure 3.4</b>	Sea level in Tarifa (blue line) during the period used for ELS release. Releasing times are shown by symbols whose meaning is indicated in the legend. It makes use of the following code to specify tidal conditions: first letter refers to tidal phase according to: H, high water; L, low water; F, maximum flood (westward) tidal	90

current; E, maximum ebb (eastward) tidal current. Second letter specifies the fortnightly cycle according to: S, spring; N, neap tides. The gray vertical lines divide the series into four pieces that correspond to each replica.

- Figure 3.5** Time series of the percentage of ELS released in Tarifa box at the surface that were found in Estepona landing area as a function of time, in a high-spring (HS) tide scenario. Red dot indicates the maximum value of 94.85% on day 7. 92
- Figure 3.6** (a) Diagrams of MPoP (%) in each landing area, averaged over the four replicas of the ELS released at Tarifa box (red rectangle) for the 40 combinations of spatial (5 depths, Y-axis) and temporal (8 tidal conditions, X-axis; see acronym code in Figure 3.4) conditions. (b) Same as panel (a) for ToMC (days). Notice the changing Z-axis scale in the different diagrams of both panels. 97
- Figure 3.7** Same as Figure 3.6 for Tangier-Med releasing box, indicated by the red polygon. 99
- Figure 3.8** Time series of percentage of particles released at the surface in Tarifa releasing box collected in Estepona (left panel) and Malaga (right panel) for all tidal combinations discussed in text (see legend). The inset shows trajectories for the whole combination of phases in spring (blue lines) and neap (red lines) tides during the first 6 days after the release. 102
- Figure 3.9** Time series of percentage of particles released in Tangier-Med releasing box under HN conditions and collected in Estepona landing area for the five depths considered (1, 12, 25, 52, and 81 m). Inset map shows trajectories for surface and 81 m depth spawning levels after 30 days of simulation using the same color code as in the main panel. 104
- Figure 3.10** ELS trajectories after 3.5 days of simulation for particles released in Tarifa box at 52 m (left panel) and 150 m (right panel) in case of FS (blue lines) and FN (orange lines) initial conditions. 105

Chapter 4		page
<b>Figure 4.1</b>	Map of the AS showing bathymetry from EMODnet, and sketching its general surface circulation: the Western and Eastern Adriatic Currents (WAC and EAC, respectively) and the North, Central and South Cyclonic Gyres. Orange dashed lines show the virtual boundaries of the three sub-basins, Northern, Middle and Southern Adriatic (NA, MA, SA, respectively), while semitransparent gray bands show the limits of the two Geographical Subareas (GSA17 in the north and GSA18 in the south; see Section 4.3.2). Maps were created using ArcGIS® 10.8 software from ESRI.	121
<b>Figure 4.2</b>	(a) Numerical grid and bathymetry of SHYFEM-Tiresias (i.e., the SHYFEM application in the AS; Ferrarin et al., 2019). (b) Modeled surface velocity (color scale) and direction (arrows), in cm·s <sup>-1</sup> , in winter (January-March). (c) Same as panel (b) for summer (July-September).	127
<b>Figure 4.3</b>	Map of the study area with the subareas of source and destination of particles and bathymetric features. A summarizing table that illustrates the code numbers, associated names and surface areas in km <sup>2</sup> of each box is included.	129
<b>Figure 4.4</b>	(a) An example of a connectivity matrix estimated in ten artificial subareas with fictitious ratios of connectivity varying from 0 (blank cells, null connectivity) to 1 (brownest colored cells, maximum connectivity). Rows correspond to the release zones of virtual larvae, whilst columns correspond to the destination areas of the released larvae. Diagonal stands for self-recruitment, which is the number of virtual larvae retained within the area from which they were released. (b) RCM applied to the same example, with an inset that zooms an example of a box connection with itself. In the inset, time progresses clockwise from 0 to a time scale T (e.g. 60 days) as concentration of particles decreases from 1 to 0, with a given temporal resolution of $\Delta t$ (e.g. 12 slices of 5 days each).	132

<b>Figure 4.5</b>	Average connectivity matrices representing the mean exchange of particles between sub-zones in winter (A) and summer (B). The color scale represents the particle concentration at the selected time scale. A small map of the study area showing the sub-areas is displayed in the summer scenario to facilitate interpretation.	136
<b>Figure 4.6</b>	Clocks of auto-connectivity extracted from the diagonal of RCMs estimated at winter (A) and summer (B) and displayed spatially in the centered positions of the 40 defined subareas.	139
<b>Figure 4.7</b>	RCM representing the time-dependent exchange of particles between sub-zones in winter, with the diagonal cells highlighted in blue color. A small map of the study area showing the 40 sub-areas and their corresponding codes is displayed to facilitate the interpretation of results.	141
<b>Figure 4.8</b>	Same as Figure 4.7 for the summer experimental configuration.	144
<b>Figure 4.9</b>	Pie charts showing the proportions of connectivity at each area at the distinct temporal bands of PLD (see legend for interpretation) for the winter (A) and summer (B) experimental configurations.	147
<b>Chapter 5</b>		page
<b>Figure 5.1</b>	Map of the Strait of Gibraltar showing bathymetric features and locations and geographic sites mentioned in the text. Dots labelled N, C, and S in the eastern part and CsN and CsS in Camarinal section are the stations where current meter data used in this study come from. Red dot in the inset indicates Palma de Mallorca in the Balearic Islands. Sources: Esri, GEBCO, NOAA, National Geographic, DeLorme, Geonames.org, and other contributors. Maps were created using ArcGIS® software by Esri. ArcGIS® and ArcMap™ are the intellectual property of Esri and are used herein under license. Copyright Esri. All rights reserved. For more information about Esri® software, please visit <a href="http://www.esri.com">www.esri.com</a> .	157
<b>Figure 5.2</b>	A) Tuna fishing net (Almadraba) pulled from the sea in Tarifa nearly covered with <i>Rugulopteryx okamurae</i> . B)	159



Massive *Rugulopteryx okamurae* beaching nearby Tarifa. C) Frame taken from a video recorded by a Remotely Operated Vehicle during a rescue operation of a mooring line off Cape Espartel (see Figure 5.1) showing thalli of *Rugulopteryx okamurae* drifted by the Mediterranean outflow. Sea floor (identified by the grey spots in the background) is at 360m depth. D) Frame taken from a video recorded by a camera attached to a trawling net showing several fragments of *Rugulopteryx okamurae*. The fishing vessel was working to the northeast, but near of, the eastern limit of the SoG and the videocamera was at 120m depth. E) Fragments of *Rugulopteryx okamurae* attached to scientific equipment deployed at 350m depth off Espartel which were collected when the instruments were brought to the surface for maintenance.

**Figure 5.3** Black lines: Stick diagram of the velocity (scale on the right) recorded at 50m depth in site “C”, station C2 (Figure 5.1, Table 5.1 in Annex 5A). Vectors are oriented with reference to the East, indicated in the upper-right corner. Red line is the sea level difference between south (Ceuta, see Figure 5.1) and north (Algeciras) shores. Positive values indicate northward sea surface downslope (higher sea level in the south) as predicted by the geostrophic adjustment of an eastward surface current. (Adapted from García Lafuente, Delgado, et al., 2002). 161

**Figure 5.4** A) Schematic of a two-layer exchange through a channel of half-circular geometry, adapted from Johnson & Ohlsen (1994). Encircled white cross (dot) indicates flow into (out of) the page, thus resembling the exchange through the SoG as observed from the Atlantic looking to the Mediterranean, with the north (south) shore in the left (right). Northward downslope of the free surface and southward downslope of the interface (solid red line) are disclosed. Thick arrows indicate the solid boundary and interfacial boundary Ekman layers, whereas thin arrows illustrate the return flow in the interior (secondary circulation). B) Sketch of the interior ageostrophic circulation (thin arrows) driven by the convergence and divergence of the 162

Ekman transport (horizontal thicker arrows) in the Ekman boundary layer (EBL, dashed red line) beneath a spatially-variable jet, represented by the (size) of the white encircled dots. Since outside of the EBL the flow is geostrophic (water moves along isobars) the secondary circulation represented by the thin arrows crosses the isobars and is therefore ageostrophic or out of geostrophic balance.

- Figure 5.5** Time-average cross-strait (blue and red line) and along-strait (black line) velocity as a function of depth in the stations of the eastern section. Panel A corresponds to site N, panels B and C are for site C in two different periods, and panel D is for site S (see Figure 5.1 and Annex 5A for details). Horizontal black line is the depth of null time-average along-strait velocity, that is, the interface that separates inflow and outflow (notice the greater depth towards the south, in agreement with the sketch of Figure 5.4A). Shaded rectangle indicates  $\pm$ std (standard deviation) of the subinertial fluctuations of this interface estimated in station CsS2 (see text for details). In all panels, solid lines are interpolated profiles from observations, whose depths are indicated by yellow circles. The depth range of positive (northwards) cross-strait velocity is marked in red. The  $\pm 1$  std interval of this velocity is indicated by light-blue thin lines. 165
- Figure 5.6** Same as Figure 5.5 for Camarinal sill section. Panel A is for site CsN and panels B and C are for site CsS in two different periods (see Figure 5.1 for locations). The profiles are directly computed from ADCP observations (no interpolation required) and circles indicating instrument depths do not apply. 166
- Figure 5.7** A) Pressure oscillations (converted to meters of water column) recorded by the pressure sensor of the ADCP after removing the mean pressure. The spring-neap tidal cycle is easily recognizable and has been made clearer by the smoothed low-water envelope represented by the thick red line. B) Contours (every 5 cm·s<sup>-1</sup>) of the subinertial cross-strait velocity. Reddish colors indicate positive (northwards) velocity whereas bluish tones are for negative, the white line being the contour of cross-strait null velocity. Solid red line indicates the depth of along-strait null velocity (interface) 167

flanked by two dashed red lines at  $\pm 1$  std of the mean interface depth. All time series correspond to station CsS2 in Camarinal sill.

**Figure 5.8** Left panels: contours of lagged correlation as a function of depth between the modulus of along-strait velocity with A) the atmospheric pressure in Palma de Mallorca (see red dot in Figure 5.1), taken as representative of the Western Mediterranean basin, B) the local zonal component of wind, C) the meridional component of wind and D) the strength of the spring-neap tidal cycle as determined by the envelope displayed in Figure 5.7A. Contour lines are every 0.05 units of correlation with the zero contour shown in green. Horizontal red line indicates the depth of zero-crossing of the along-strait velocity (see Figure 5.6C). Right panels: same as left panels but for the cross-strait velocity. Red lines indicate the depths of cross-strait zero velocity. In all cases, positive lags correspond to “forcing” (i.e., atmospheric pressure, wind, strength of the tide) leading the “response” (i.e., the velocity components).

**Figure 5.9** A) Vertical velocity recorded at stations CsN and CsS1 at depths of 104m and 120m, respectively, close to the time-averaged interface depth. Dates on the top axis correspond to September 2013. Velocities were recorded every two minutes and have been smoothed by a 5min cut-off period filter. B) Vertical profile of the time-averaged vertical velocity at station CsN (blue line). Shaded area stretches over  $\pm 1$ std and the horizontal grey line indicates the (mean) interface depth. C) Same as B) but for station CsS1.

Chapter 6 page

**Figure 6.1** Figure 6.1. (a) Map of the study area showing bathymetric features and outlining its prevailing surface circulation: the Atlantic Jet (AJ), the Western and Eastern Alboran Gyres (WAG, EAG, respectively), and the Central Cyclonic Gyre (CCG). (b) Map of the northeastern Atlantic Ocean and the Mediterranean Sea, highlighting the location of the Alboran Sea (white square) and the SoG (purple square), and spotting records of *Rugulopteryx okamurae* through a sequential

number code, where 1 is the first reported detection in the SoG in 2016 and 14 is, to our knowledge, the last reported record to date. (c) Zoomed-in-view of map (b) in the SoG, with a label that indicates the position of the main sill of the Camarinal (CS). (d) Timeline plot of the 14 records of *Rugulopteryx okamurae* spotted in maps (b,c) from the existing scientific literature.

- Figure 6.2** Computational grid and bottom topography of the two nested domains, where the regional model (a), of larger extent and less horizontal resolution, embeds the local model (a, b), of less spatial extent and higher horizontal resolution. In the insets, a zoomed-in view of the outer (blue lines) and inner (grey lines) grids in Tarifa (maroon box) and Ceuta (yellow box) are displayed. 188
- Figure 6.3** Observed (black line) and modeled (blue line) time series of zonal (U) and meridional (V) velocity obtained in the Camarinal Sill (CS) at the representative depths of the Atlantic inflow (50 m), the interface between inflow and outflow (150 m), and the Mediterranean outflow (250 m). Mean values of each time series are shown at the top of each panel in the corresponding color code. 190
- Figure 6.4** (a) Initial positions of particle release in the SoG, with crosses marking the locations where *Rugulopteryx okamurae* has been detected (Figure 6.1). (b) Zonal (blue) and meridional (orange) wind components extracted from the ECMWF ERA5 reanalysis model at Tarifa in a fraction of the month of March 2021. (c) Simulated sea level extracted at the node closest to the Tarifa tide gauge in the same fraction of the month of March 192
- Figure 6.5** Accumulation ratios ( $A_n/A_T$ ) at the end of the tracking period (30 days) averaged over all the 108 simulations described in section 6.5. The classification “null” corresponds to zero accumulation values; “low” corresponds to accumulation values below P20; “medium-low”, between P20 and P40; “medium”, between P40 and P60; “medium-high”, between P60 and P80; and “high”, above P80. 194

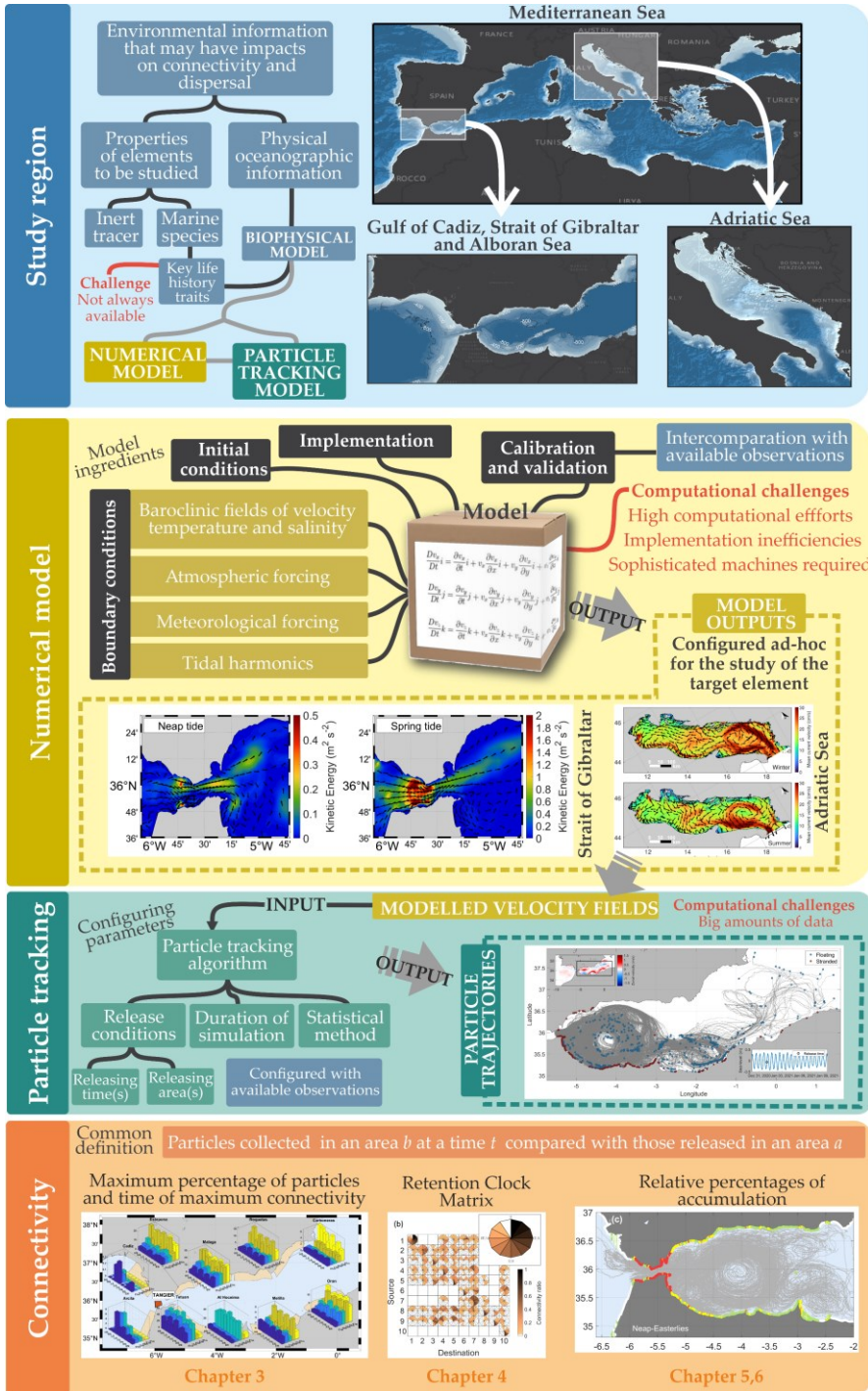
<b>Figure 6.7</b>	Accumulation ratios in the SoG and the Alboran Sea coastlines at the middle of the tracking period (15 days) for the four scenarios illustrated in Figure 6.4: a) an easterly wind during spring tide on March 14, 2021 [#24 in Figure 6.4c], b) a westerly wind during spring tide on March 11, 2021 [#23 in Figure 6.4c], c) an easterly wind during neap tide on March 5, 2021 [#21 in Figure 6.4c], d) a westerly wind during neap tide on March 8, 2021 [#22 in Figure 6.4c]. Particle trajectories are displayed for each scenario. Some relevant locations are displayed in map (a).	199
<b>Figure 6.8</b>	(a) Depth time-series of a particle released at surface with a sedimentation velocity of 1 (dark blue), 2 (blue) and 3 (light blue) cm·s <sup>-1</sup> , superimposed on the vertical velocities encountered by the 2 cm·s <sup>-1</sup> particle during the first 15 days after the release. (b) Particle trajectory from the 2 cm·s <sup>-1</sup> sedimentation velocity simulation. The trajectories followed by the 1 cm·s <sup>-1</sup> and 3 cm·s <sup>-1</sup> particles diverge only slightly from the 2 cm·s <sup>-1</sup> trajectories, and are not shown for clarity.	201
<b>Chapter 7</b>		page
<b>Figure 7.1</b>	Sketch of the main connectivity patterns of particles released from the northern (solid line) and southern (dashed line) Strait under conditions of spring (orange) and neap (blue) tide, based on the information described in Chapter 3.	208
<b>Figure 7.2</b>	Sketch of the main connectivity patterns of particles released throughout the Adriatic Sea during summer (orange) and winter (blue), based on the information described in Chapter 4.	211

## List of tables

Chapter 3		page
<b>Table 3.1</b>	Summary of the different spatial and temporal conditions configured in each numerical experiment.	90
<b>Table 3.2</b>	Maximum percentage of particles (MPoP column) and time of maximum connectivity (ToMC column) of ELS with their corresponding standard deviations for all landing areas and releasing boxes, averaged for all scenarios of initial conditions.	93
<b>Table 3.3</b>	Differences of MPoP computed using PLD windows of 60 and 30 days ( $\Delta_{30}$ column) and 60 and 15 days ( $\Delta_{15}$ column) for the three releasing boxes and the Alboran Sea landing areas.	107
Chapter 4		page
<b>Table 4.1</b>	Table 4.1. Literature review of biological traits for some emblematic species relevant for modeling in relation to the AS oceanographic conditions.	130
Chapter 5		page
<b>Table 5.1</b>	Information on the acquisition of current meter data at the eastern section of the SoG used in this study. The two deployments at site "C" have a 16-month gap and, although close to each other, were not at the very same geographical position. For these reasons, they have been considered as two separated stations ("C1" and "C2").	178
<b>Table 5.2</b>	Information on the acquisition of the current meter data at Camarinal sill section of the SoG used in this study. The two deployments at site "CsS" were several years apart and have been considered as separated stations ("CsS1" and "CsS2", the former simultaneous with "CsN").	179



# Scheme of the research: one-page thesis







# 1 General Introduction

## 1.1 State of the art

### 1.1.1 Motions in the marine environment: an overview

The marine environment is a vast, complex and dynamic system encompassing a broad range of fluid motions interacting at several spatio-temporal scales (Pineda et al., 2007). At the seaside, the occurrence of wind-driven surface waves with periods ranging from seconds to minutes and wave heights from centimeters to several meters is a common observation (Ocampo-Torres, 2001). Tides are an ever-present phenomena throughout the ocean, although generally more pronounced in proximity to large bathymetric features such as the entrance to a gulf, bay, channel, or estuary (Sirvienta et al., 2023). Longshore currents are another visible phenomenon within the surf zone (Boon, 2004). Even propagating internal waves, often generated through the interaction of the tidal flows with the bottom topography, may be detected by the naked eye in specific spots (Sánchez-Garrido & Vlasenko, 2009).

The set of oceanic fluid motions readily observable to the human eye represents a subset of the full spectrum of ocean motions known (Figure 1.1), ranging from molecular processes to decadal oscillations and climate variability on scales from seconds to centuries and from centimeters to thousands of kilometers. These motions are responsible for transporting seawater properties along with plankton, larvae, and debris, over long distances (van Sebille et al., 2020). It is a start to have an idea of how diverse processes and variables occurring in the ocean might influence the distribution of such matter at different spatio-temporal scales.

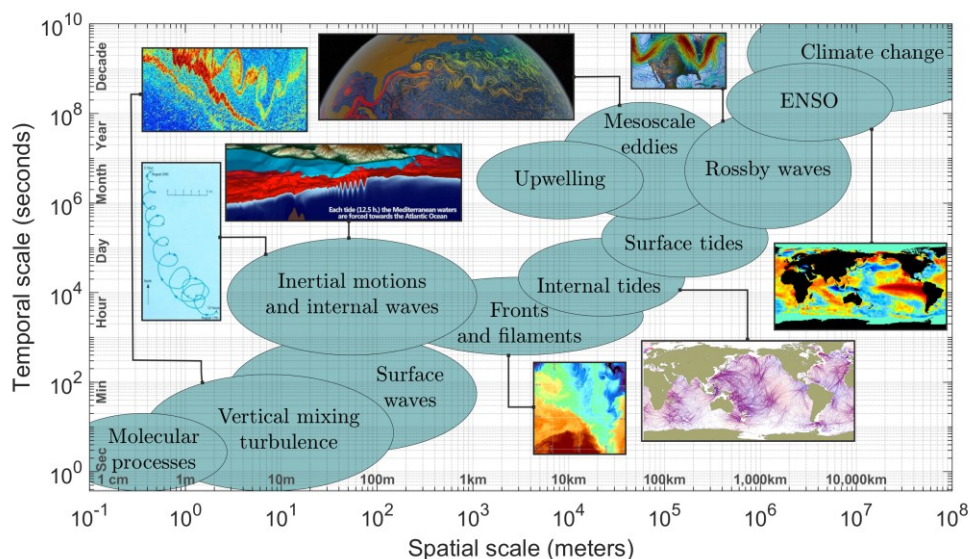


Figure 1.1. Spatio-temporal scale at which different oceanographic phenomena occur. Adapted from Dickey, 2001.

Small-scale turbulence is an ubiquitous eddy motion state of geophysical fluids responsible for mixing that influences sediment resuspension, mediates nutrient uptake, and affects the community structure of planktonic organisms in a multitude of ways (Margalef López, 1997), including alterations in grazing activity, motility, and growth (Megrey, 2001; Zhao et al., 2020). At similar spatio-temporal scales, surface waves generated in the upper layer of the ocean, have an effect on both mean currents through the action of the flux of momentum (Xue et al., 2023), and on the net transport of organisms and solutes in the nearshore environment, thereby influencing the dynamics of certain marine populations (Monismith & Fong, 2004).

In most coastal areas worldwide, oscillatory flow driven by tidal currents represents a dominant form of motion advecting shallow-water organisms. A relevant mechanism for this transfer is the interaction between topography and stratified tidal flow, which generates freely propagating internal waves that regulate the magnitude of vertical transport of certain organisms within the water column (Sentchev & Korotenko, 2003). Inertial oscillations, often resulting from extreme wind events such as storms, operate similarly to tidal processes and have been reported to pump nutrients from below the mixed

layer into the euphotic zone, where they can be utilized by phytoplankton, thus altering the grazing activity (Esposito et al., 2023). Persistent winds also influence upwelling and downwelling, which affect nutrient availability, particularly during certain seasons, and are crucial to the coast-wide and regional ecology (Trautman & Walter, 2021).

At the opposite extreme of the spectrum, planetary processes such as those linked to interannual (North Atlantic Oscillation, NAO; El Niño Southern Circulation, ENSO), and decadal (Pacific Decadal Oscillation, PDO) climatic modes also have environmental impacts through alterations in ocean-atmosphere interactions and nutrient and light availability (Daud et al., 2019; Graham et al., 2023; Pineda & López, 2002). For instance, anomalously high temperatures and diminished wind-driven upwelling in the Northeastern Pacific during El Niño events, occurring every two to seven years, have been shown to reduce larval abundance and settlement, potentially resulting in wide-scale ecological disruption (Pineda et al., 2018; Pineda & López, 2002).

The complex environment in which marine organisms reside offers a multitude of pathways and scales that ultimately determine the extent of connection or separation of individuals within and among local populations (Cowen & Sponaugle, 2009). An understanding of the spatial and temporal variability in the exchanges of such individuals is of paramount importance in numerous theoretical and practical applications (Brown et al., 2016). When applied to marine organisms, biological traits and the life history of the species concerned, particularly during the earliest stages of life, are of equal importance (Demmer et al., 2022). These biophysical interactions ultimately determine and regulate population dynamics. The focus of the subsequent Section is on these issues.

### 1.1.2 The idea and relevance of connectivity and dispersal

Most marine species are distributed in geographically discrete locations across their spatial range (Antell et al., 2020), resulting from the interactions between the biological and ecological characteristics of the species and the spatially diverse marine habitats (Costello & Chaudhary, 2017). The relationships between these habitat units are maintained through the transport of individuals at various life stages, from eggs and larvae to juveniles and adults (Lipcius et al., 2019). Over the years, researchers have employed a variety of key terms to describe these dynamics of populations in the marine environment (Pineda et al., 2007), the most widely used being "dispersal" and "connectivity" (Cowen & Sponaugle, 2009).

In a general sense, dispersal can be defined as the outcome of all processes responsible for the transport (advection) and spread (diffusion) of a cloud of passive particles representing small fluid parcels, small amounts of tracers, or passively drifting individuals (Mayorga-Adame et al., 2022). When applied specifically to the context of marine organisms, dispersal represents the tendency of individuals to move, settle, and ultimately reproduce away from their native habitats and parents, a behavior that influences numerous evolutionary and ecological processes (Monroy et al., 2017). This usage is common in the terrestrial literature, where dispersal is typically described as a probability density function of dispersing individuals versus distance from a source (Pineda et al., 2007). The patterns of linkage or isolation of dispersants are summarized under the concept of connectivity. Connectivity refers to the extent to which passive particle exchange occurs between distinct locations (P. D. Taylor et al., 1993). It may therefore be applied not only to analyze interactions between individuals within a population (Ormerod et al., 2011), but also to estimate heat (Tamsitt et al., 2018) and momentum fluxes (Edson et al., 2013), and exchanges of other suspended particulate matter, including sediments (Najafi et al., 2021) and pollutants (Fifani et al., 2021).

Because of its broad definition and growing relevance, the term "connectivity" has been introduced and applied in a multitude of fields. As such, several interpretations exist, with the main differences between them

being the scale of applicability of the study (Kadoya, 2009). In ecological terms, population connectivity is of common usage (Cowen et al., 2007; Cowen & Sponaugle, 2009; Fogarty & Botsford, 2007; Pineda et al., 2007). It refers to the degree to which spatially separated populations are linked by dispersal of individuals that are part of a metapopulation, defined as an ensemble of populations of the same species distributed across habitable areas (Cowen et al., 2007). Demographic connectivity is used to describe the number of dispersers that are exchanged between populations (Kendrick et al., 2017). Genetic connectivity concerns the efficient transfer of gene flow between distant populations (Legrand et al., 2022). Sediment connectivity refers to the degree to which a system controls the transfer of sediment between different landforms or landscape units (Bracken et al., 2015). Such definitions represent only a sample of the multitude of potential usages, with arguably the most relevant being those that link the influence of connectivity processes on ecological function and ecosystem services, a definition that is often referred to as functional connectivity (Hidalgo et al., 2017).

Depending on the magnitude of the environmental phenomena involved and other biological parameters, such as the size of the dispersing agents, diverse spatial differences can be identified in the exchange of individuals. These differences range from very low levels of connectivity between populations, where population structure and size are maintained only through self-recruitment (i.e., closed populations), to high levels of connectivity that occur through large dispersal of larvae between metapopulations (i.e., open populations) (Cowen et al., 2000). It is therefore essential to have detailed knowledge of not only the magnitude, but also the spatio-temporal scales over which connectivity operates, in order to understand the structure of marine populations and their interrelationships (Siegel et al., 2008).

Spatio-temporal scales of connectivity are mediated by the successful exchange of individuals (Gaines et al., 2007). This is particularly relevant for early life stages, when spores, eggs, and developing larvae can be treated, at least to some extent, as passive plankton (Simpson et al., 2013). Examples

include most pelagic species, some of which spend their entire lives as plankton (holoplankton) or only their larval stages as plankton (meroplankton and ichthyoplankton) (Ibáñez-Tejero et al., 2019), but also many benthic species, which typically are characterized by a relatively stationary phase (sessile or sedentary juveniles and adults) preceded by a planktonic stage (propagules and larvae) during which dispersal occurs (Legrand et al., 2019). As such, dispersal distances, hence connectivity, is determined by the time that individuals spend in planktonic life stages (D'Aloia et al., 2015), commonly defined as spore or propagule duration, or pelagic larval duration (PLD, hereafter). The duration of this stage varies greatly from species to species, ranging from hours (e.g. giant kelp, with a spore duration of ~30 hours, Reed et al., 2006), to days (e.g. black-faced blenny fish; with a PLD of ~16 days, Schunter et al., 2019), and up to months (e.g. black rockfish, with a PLD of ~6 months, Miller & Shanks, 2004; or rock lobster, with a PLD up to ~18 months, Bradford et al., 2015).

The temporal and spatial scales over which connectivity varies during the pelagic stage rely on the spawning phase (Le Corre et al., 2012), the timing and location of which is in turn determined by multiple external factors, including system hydrodynamics and larval behavior (Shanks, 2009). Certain hydrodynamic conditions may increase larval dispersal distances (e.g., wind-driven surface currents and tides), while others may act to decrease them (e.g., eddies, turbulence). Therefore, it is reasonable to expect variability in connectivity patterns not only among species, but also among regions and time periods of a given study (Le Corre et al., 2012). In this regard, marine populations residing in environmentally sheltered regions may be less susceptible to strong directional advection, implying relatively limited dispersal, which in turn could lead to higher local retention and juvenile survival, and increased population connectivity within the region (Figure 1.2a). In contrast, in exposed environments, where the confluence of tides, wind-driven currents, and small-scale turbulence is present, dispersal may lead to lower individual retention, resulting in lower juvenile survival and reduced population connectivity (Figure 1.2b). By the time individuals reach maturity, they are too large to be influenced by the beneficial or detrimental

effects of these environmental parameters and are expected to migrate to their adult habitat by ontogenetic migration.

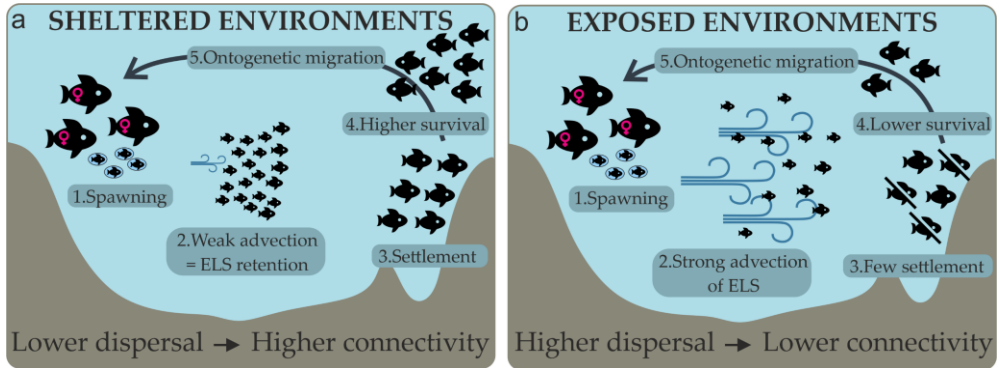


Figure 1.2. Hypothetical linkage between spawning of eggs and adult ontogenetic migrations in sheltered (a) and exposed (b) regions. Sketch adapted from Brown et al. (2016).

Dispersal and connectivity between different sites or populations is of particular relevance in the context of the design of marine protected areas (MPAs), with several studies having already demonstrated the effectiveness of such areas for the long-term conservation of the ecosystem and surrounding fisheries (Batista et al., 2011; Dominique, 2011; Gaines et al., 2010; Marcos et al., 2021). Particularly, defining the MPA optimal size and structure has been shown to directly influence their effectiveness (Muntoni, 2015). This is directly related to the objectives of the definition of an MPA. When designed for ecosystem conservation, MPAs should be large enough to retain a substantial portion of early life stages production (Marcos et al., 2021). If the objective is to optimize fisheries, the dimension of the MPA should be sufficient to increase the density and size of fish populations, and allow a proportion of individuals to spillover beyond their boundaries into surrounding fished areas (Guidetti & Claudet, 2010). If the MPA is designed as a network, individual MPAs should be self-sustaining or adequately connected to other MPAs via larval dispersal (Planes et al., 2009).

Connectivity knowledge can be employed not only to oversee specific marine areas of conservation concern, but also to identify, monitor and



regulate marine invasive alien species, i.e., organisms introduced outside their natural range (Assis et al., 2015; Hansen et al., 2024; Schilling et al., 2023). Additionally, understanding the dynamics of species with pelagic planktonic larval phases capable of long-range dispersal via ocean currents may enable the identification of sites suitable for early warning systems (Crivellaro et al., 2022). In many respects, knowledge of dispersal patterns and resulting connectivity estimates is of paramount importance to the management of a given marine ecosystem.

### 1.1.3 Some notions on the methods to estimate connectivity

As awareness of connectivity as a key component for understanding and managing certain marine populations has emerged, considerable effort has been invested in developing and applying a variety of methods to obtain information on population dynamics (Gaines et al., 2007; Hidalgo et al., 2017). Even so, knowledge of connectivity of specific marine species and specific geographic regions remains scarce (Podda & Porporato, 2023). This is certainly true in the case of the Mediterranean Sea, despite being an ideal location for such studies due to its well-studied oceanographic patterns (Bethoux et al., 1999; Calò et al., 2013; Daskalaki et al., 2022). Yet, the importance of the Mediterranean environment as a biodiversity hotspot (Beca-Carretero et al., 2024) and the cumulative human threats that marine populations continuously face (Micheli et al., 2013), make the connectivity research an urgent endeavor.

In their comprehensive literature review on methods for estimating population connectivity, particularly in the Mediterranean context, Calò et al. (2013) identified genetic techniques, otolith analysis, and modeling tools as the most advanced and commonly used approaches for estimating marine connectivity in the nearshore environment. Estimating population connectivity through genetics requires measuring gene flow (Pascual & Macpherson, 2016), which is often inferred indirectly by analyzing the movement of alleles or genes between populations (Palumbi, 2003), but can also be assessed directly through parentage analyses (Planes et al., 2009), which calculate the probability that a given individual originated from a

particular source population or set of parents (Hedgecock et al., 2007). Both approaches rely on molecular markers, such as microsatellites, allozymes, and mitochondrial DNA (Hauser & Ward, 1998; Féral, 2002; Meer et al., 2015), which are powerful tools for identifying genetic differentiation between populations (Ferrari et al., 2023), detecting barriers to gene flow for specific species (Schunter et al., 2011), and estimating the origins and number of migrants of a given population, among others (Deudero et al., 2017). Otolith analysis through morphometrics and microchemistry techniques also provides valuable information on aging, growth, and, by back-calculation, the date of spawning, hatching, and settlement of propagules for certain fish populations (Campana, 1999; Morat et al., 2014).

Yet, knowledge of population connectivity usually requires an understanding of the origins and trajectories of dispersing individuals within local or sub-populations (Cowen et al., 2007; Pineda et al., 2007). Visual tracking is the only direct method available to accomplish this but, mainly for practical reasons, has been less applied to dispersing larvae (Nolasco et al., 2018). Alternatively, advances in computational abilities have led to non-direct estimation progress based on circulation models coupled with Lagrangian particle-based algorithms (van Sebille et al., 2018). Lagrangian connectivity studies involve the analysis of sets of virtual particles representing fluid parcels, tracers, or passively drifting individuals, to identify their pathways, associated timescales and transports between distinct oceanic regions (Rühs, 2018). Classic applications involve forward simulations, where particles virtually released from potential source regions are tracked through simulated currents to their final settlement sites (Torrado et al., 2021). Other techniques include backtracking the particles from the settlement areas by running the particle tracking simulations in reverse (Y. Wang et al., 2019), which yields insights into the origin of specific species and enables the delineation and monitoring of the path's history of established populations (Kwon et al., 2019). The primary objective of both techniques is to estimate dispersal kernels, i.e. the probability distributions of spatial spread (Nathan & Muller-Landau, 2000), which can inform decisions

regarding the management of certain populations and geographic regions (D'Aloia et al., 2015).

By now, the study of connectivity with Lagrangian algorithms has been of great benefit for interdisciplinary applications. For instance, it has revealed the impacts of marine currents on certain populations, providing valuable information for ecosystem management (Hariri et al., 2024). It has been utilized to understand the migratory pathways of several marine populations, such as plankton blooms (Ser-Giacomi et al., 2023), bluefin tuna eggs and larvae (P. Mariani et al., 2010), rays and skates (Marandel et al., 2018), marine birds (Schneider, 1991), juvenile turtles (Lalire & Gaspar, 2019), and juvenile sharks (Bonnin et al., 2021), among other specimens (Rodríguez-Díaz & Gómez-Gesteira, 2017). It has been used to assess the accumulation of plastic debris in the Mediterranean (Soto-Navarro et al., 2020) and on the world's shorelines (Lebreton et al., 2019). It has been implemented even to provide rapid and accurate forecasts to minimize damage during maritime emergencies, including the search and rescue of a person lost at sea (Ličer et al., 2020), and the evaluation and management of oil spills, such as the Prestige accident in NW Spain in 2002 (Sotillo et al., 2008), and the Deepwater Horizon oil spill in the Gulf of Mexico in 2010 (Mariano et al., 2011).

The cited examples represent only a selection from a growing array of novel tools, methods, and multidisciplinary approaches that are being applied to provide efficient solutions for marine ecosystem assessment and management (van Sebille et al., 2018). At the same time, several of the cited studies also raise concerns about the methodological challenges facing marine connectivity research. The following Section focuses on these issues.

#### 1.1.4 Methodological challenges

Despite the considerable progress that has been achieved in the development of techniques for studying connectivity in the marine environment, the efforts are still limited by numerous processes related to physical oceanography, ecology (Cowen & Sponaugle, 2009), ocean modeling, marine spatial planning, and even administration and jurisdiction

(Popova et al., 2019). The multitude of available tools is itself a challenge, as it can be laborious to navigate and find the optimal technique for estimating connectivity (Novi et al., 2021). The selection of a methodology introduces further complexities into the development of complex and often expensive research tasks, which usually require sophisticated instrumentation and technology (Hidalgo et al., 2017).

Challenges in understanding population connectivity arise from the difficulty of obtaining direct observations of target individuals and tracking their movements, especially during early developmental stages (Sale & Kritzer, 2003), given their small size and still poorly understood interactions with the physical realm (Darnaude et al., 2022). Its knowledge is further constrained by the frequent inaccessibility to the marine environment (Hidalgo et al., 2017), although the literature suggests that even when accessed, certain population aspects, such as the phenotype-environment mismatch or the specific-species reproductive strategy, are not directly measurable (Pineda et al., 2007). Once accessible, large sample sizes are demanded to achieve high accuracy in inferring population structure using experimental approaches, both genetic and otolith based, which are often constrained by the limited number of individuals available and the associated costs (Deudero et al., 2017; Fumagalli, 2013; Schemmel et al., 2022). However, several genetic studies indicate that even with the most sensitive molecular markers and the largest sample sizes, there may still be small discrepancies in the level of gene flow between populations (Hauser & Ward, 1998; Fumagalli, 2013), and molecular markers, that are highly sensitive to such changes, may not be sufficient to identify populations with minimal degrees of isolation (Hauser & Ward, 1998; Kasapidis & Magoulas, 2008)

Ultimately, this leads to uncertainties in the knowledge of small-scale, biologically dominated processes and information, such as larval taxonomy, community diversity, biomass, and abundance, which are essential for predicting effective dispersal patterns (Ferraro & Failler, 2022). The consequences of these limitations are twofold, as ecological information, especially on the spatio-temporal distribution of spawners (e.g. where, when

and how many), is crucial for initializing biophysical coupled models of passive larval modeling and for interpreting their results (Hidalgo et al., 2017). Therefore, most biophysical models are hypothesis-driven and assume poorly known biological parameters, leading to uncertainty in population connectivity estimates (Calò et al., 2018).

The difficulty of quantifying connectivity is particularly acute in the nearshore environment, which is challenging to measure by both experimental and numerical approaches (Siegel et al., 2003). The transition from small spatio-temporal scales within the coastal environment to larger scales offshore requires a balance between fine-scale sampling strategies nearshore and more extensive offshore (Greenberg et al., 2007). Variation across scales of specific processes is also a challenge for modeling efforts, as simultaneous resolution of mesoscale (and even smaller) scales is currently problematic (Werner et al., 2007), despite recent advances in model nesting techniques (e.g., Mogé et al., 2019). Notwithstanding these constraints and the inevitable simplification of the biotic component, numerical models are still optimal tools that provide reliable results to delineate the main patterns of connectivity, with some studies having already demonstrated their high explanatory capacity in reproducing the observed inter-annual recruitment variability (Hidalgo, Rossi, et al., 2019). In particular, the low cost associated with exploring different environmental scenarios provides a valuable tool for assessing population connectivity and its variability across different spatiotemporal scales (B. Jones, 2014).

## 1.2 Motivation, objectives, and structure of the PhD thesis

From the preceding analysis, it becomes evident that a comprehensive understanding of the dynamics of marine ecosystems, the management of fishery resources to optimize fisheries, the regulation of marine invasive species, as well as the design of marine protected areas, necessitate an in-depth knowledge of dispersal and connectivity. These processes are significantly influenced by oceanographic features, the magnitude of which is usually enhanced in nearshore environments, which normally are highly

complex dynamic regions dominated by small-scale turbulence processes, advection and diffusion acting at different spatio-temporal scales.

Certain regions of the Mediterranean, widely recognized as one of the world's most important environmental biodiversity hotspots, provide specific examples of such complexity. Among these, the Alboran Sea and the Adriatic Sea are of particular note. Advances in connectivity and dispersal in these regions, along with guidance on how to integrate this information into management actions, require urgent attention. However, the difficulties encountered in quantifying nearshore connectivity, whether by observational or numerical methods, have led to a lack of understanding of the linkages between the hydrodynamics of those Mediterranean regions and the biological characteristics of the species present there.

Aiming to contribute to a better understanding of these dynamics-of-populations, the objective of this PhD is to provide a picture of the potential patterns of connectivity and dispersal of important population groups at different regional scales in the Mediterranean Sea. It focuses on the two aforementioned relevant regions: (1) the Strait of Gibraltar and the adjacent Alboran Sea, a transition basin between the Mediterranean Sea and the Atlantic Ocean strongly influenced by the Atlantic water flow, and (2): the Adriatic Sea, a semi-enclosed water body characterized by a peculiar topography and a large number of freshwater sources. Lagrangian transport algorithms coupled with results from high-resolution hydrodynamic models implemented in these regions, are the numerical tools applied to the study of application cases of species of interest.

The dissertation is organized as follows:

- (I) The present chapter (**Chapter 1**) is divided into two main sections. The first (1.1. State of the art) has thus far presented an overview of the fluid motions responsible for the transport of tracers in the marine environment (1.1), a discussion of the main concepts of population dynamics (1.1.2), and a description of the commonly used methodologies and encountered challenges in the applications of such studies (1.1.3 and 1.1.4). Subsequent section

(1.3. General hydrodynamics of the study regions) describes the hydrodynamic processes occurring within the study areas, whose knowledge is essential for conducting population-dynamics studies.

- (II) **Chapter 1** outlines the methodology employed for the study of connectivity in subsequent chapters. It is divided into three main sections. The first part (2.1. Numerical model) provides an overview of the necessary background material about the numerical models used in this thesis. The second part (2.2. Lagrangian particle tracking) examines the basis of Lagrangian particle trajectory calculations. The third part (2.3. Connectivity computation) briefly describes the methodologies employed for the quantification of connectivity.
  
- (III) In **Chapter 3**, a high-resolution circulation model implemented in the regions of the Strait of Gibraltar, Gulf of Cadiz and Alboran Sea, is coupled to a Lagrangian tracking algorithm to gain insight into the sustainability of an appreciated and overexploited resource of the Spanish and Moroccan fisheries, the blackspot seabream (*Pagellus bogaraveo*). Several scenarios consisting of different spatial (depths and sites) and temporal (tidal phase and strength) initial conditions simulating spawning are analyzed to identify the most likely pathways of dispersal.
  
- (IV) In **Chapter 4**, a high-resolution model is coupled to a Lagrangian tracking software to examine the hydrodynamics that regulate connectivity of particles in the Adriatic Sea. Lagrangian particles, representing eggs and larvae with typical biological characteristics of generic marine organisms inhabiting the region, are released throughout the basin at different times during a test year to identify the most likely pathways of individual dispersal.

- (V) In **Chapter 5**, the plausible causes of the spreading of the marine invasive alien algae *Rugulopteryx okamurae* in the Strait of Gibraltar is evaluated by revisiting historical current-meter profiles collected in the Strait of Gibraltar. Cross-strait connections are analyzed, and favorable opportunity windows and unfavorable scenarios are provided.
  
- (VI) In **Chapter 6**, the trajectories of the invasive algae *Rugulopteryx okamurae* as vectors of biological pollution are examined, by means of a high-resolution model coupled to a Lagrangian algorithm in the Strait of Gibraltar and adjacent basins. Various scenarios consisting of different temporal initial conditions (tidal phase and strength, and winds) are analyzed to identify the most unfavorable scenarios of particle accumulation in the shorelines.
  
- (VII) **Chapter 7** offers an integrated discussion of the findings presented in previous chapters, presents the directions for future works, and provides a comprehensive overview of the thesis.

### 1.3 General hydrodynamics of the study regions

Hydrodynamic models applied to studies of connectivity should reach sufficient resolution in coastal areas and resolve at least the mesoscale satisfactorily (Fox-Kemper & Menemenlis, 2008). These processes are essential for connectivity and, therefore, knowledge of the hydrodynamics, circulation patterns, and variability of the interest regions is fundamental to construct numerical models and interpret their outcomes in the interest regions (García-Lafuente, Sanchez-Garrido, et al., 2021).



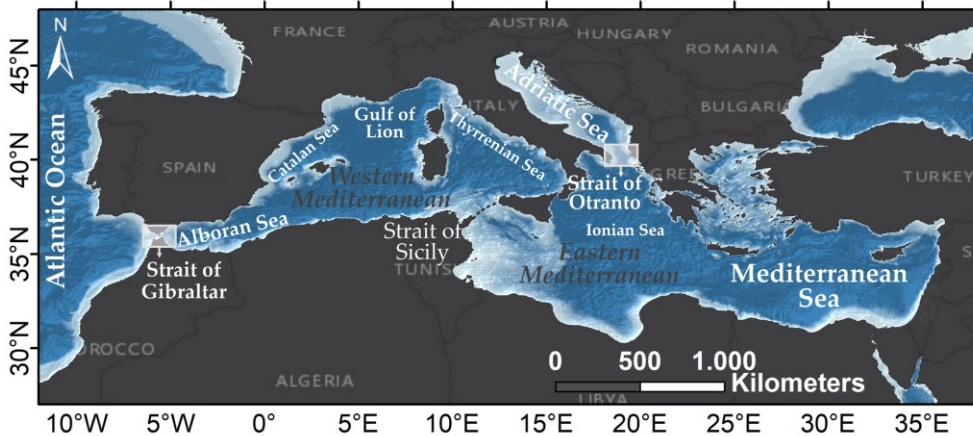


Figure 1.3. Map showing the Mediterranean Sea, the Strait of Sicily dividing the Mediterranean into western and eastern basins, and the two regions of interest, the Alboran and Adriatic Seas, connected to the Mediterranean by the Straits of Gibraltar and Otranto, respectively. Some relevant sites mentioned in the text are also indicated.

This dissertation deals with the dynamics of dispersal and connectivity occurring within two relevant sub-basins of the Mediterranean Sea (Figure 1.3), namely, the Alboran Sea and the Adriatic Sea. A summary of the oceanographic characteristics of both regions follows.

### 1.3.1 The Alboran Sea

The Alboran Sea is the westernmost basin of the Mediterranean Sea, bounded on the west by the Strait of Gibraltar (SoG, hereafter), and on the east by the north-south line connecting the locations of Almeria and Oran (Sánchez-Garrido & Nadal, 2022). It is the first to receive Atlantic waters flowing through the SoG, of clear interest to the Alboran Sea, for which a preliminary description of its dynamics follows. The SoG is the narrow ( $\sim 14$  km at its narrowest section) and shallow ( $\sim 300$  m at its shallowest section in Camarinal Sill) gateway that separates the Mediterranean Sea from the Atlantic Ocean (Farmer et al., 1988; García Lafuente, Alvarez Fanjul, et al., 2002). The horizontal density gradients drive a two-way exchange with a surface inflow of Atlantic waters and a counterflow of Mediterranean waters beneath (García-Lafuente et al., 2017), which is ultimately forced by the

freshwater deficit of the Mediterranean Sea (Bethoux et al., 1999). On average, the volume transport through the Strait is slightly less than 1 Sv in both directions (1 Sv =  $10^6$  m<sup>3</sup>/s, Sammartino et al., 2015).

Two water masses contribute to the inflow: the North Atlantic Central Water (NACW), which are mode waters originated at mid-high latitudes of the North Atlantic by isopycnal convection (Soto Navarro, 2012), and the Surface Atlantic Water (SAW), which results from shallow NACW that is modified by atmosphere-ocean interactions (Criado-Aldeanueva et al., 2012). The main water masses of the outflow are the Levantine Intermediate Water (LIW) and the Western Mediterranean Deep Water (WMDW). The LIW is formed in the Eastern Mediterranean (see Figure 1.3) by evaporation and is characterized by a salinity maximum of 38.5 when it reaches the Strait of Gibraltar (Millot, 2013). The WMDW is formed by diapycnal convection in the Gulf of Lion, in the northwestern part of the Western Mediterranean basin (see Figure 1.3) associated to strong winter heat loss and is among the coldest Mediterranean Waters ( $\theta=12.9$  °C) (García-Lafuente et al., 2021). Other less common water masses present in the Mediterranean outflow are the Winter Intermediate Water (WIW), formed in the continental shelf of the Catalan Sea (Juza et al., 2013), and the Tyrrhenian Dense Water (TDW), formed mostly by the mixing between WMDW and LIW in the Tyrrhenian Sea (Iacono et al., 2021).

The exchange flow through the SoG is strongly influenced by tides (García-Lafuente et al., 2000), especially in the vicinity of the Camarinal Sill, where the flow direction in either layer, Atlantic and Mediterranean, is periodically reversed. During the ebb tide (high-to-low water), water flows to the east in both layers, while during the flood (low-to-high water), it flows to the west. The eastern exit of the strait, although still subject to tidal modulation, does not undergo a change in direction, maintaining an eastward current (the outflow undergoes a change in direction with the tide). The contrary happens in the western exit, where it is the outflow that tends to keep direction whereas the inflow changes periodically with the tide. The sub-inertial modulation, related to the meteorological forcing (Candela et al., 1989; García Lafuente, Alvarez Fanjul, et al., 2002), also modifies the

baroclinic exchange by significant fractions of their average values at few-days' timescale, although it is much less than tidal fluctuations of flows.

The circulation in the uppermost 100-150 m of the Alboran Sea is therefore mainly driven by the Atlantic water, which enters the Alboran Sea from the Strait in the form of a frontal baroclinic jet, the so-called Atlantic Jet (AJ) (Viúdez, 1997), with flow velocities of up to  $1 \text{ m}\cdot\text{s}^{-1}$ . In its way eastward, the AJ surrounds two mesoscale anticyclonic and oligotrophic gyres usually present in the basin, the Western and the Eastern Alboran Gyres (WAG and EAG, respectively, see Figure 1.4) (Sánchez-Garrido et al., 2013), the EAG being less common, especially in winter (Renault et al., 2012). Between the WAG and the EAG lies a third mesoscale cyclonic gyre of smaller size (CCG).

Regarding the deeper circulation, the LIW flows towards the Strait close to the Spanish shelf, whereas the WMDW does it along the African coast in the south, possibly conveyed by the bottom topography (García-Lafuente et al., 2017). The accumulation of LIW flow along the north shelf shallows the pycnocline towards the north Alboran Sea and therefore favors nutrient pumping to the photic layer by eventual wind-driven upwelling events. Primary productivity on the north coast is thus enhanced with regards to the African coast. Another source of surface fertilization is the AJ itself, which is locally enriched in its entrance due to strong tidal mixing (Sánchez-Garrido et al., 2015). Local fertilization along the AJ has been also reportedly associated to its ageostrophic frontal dynamics (Oguz et al., 2014). Sub-mesoscale cyclonic eddies released from the Strait and advected by the AJ along its periphery represent another potential source of nutrient supply into the Alboran Sea (Sánchez-Garrido et al., 2015).

The Gulf of Cadiz, situated on the Atlantic side of the Strait of Gibraltar, is the source of the waters of the AJ. Consequently, it is also of evident interest to the Alboran Sea, for which a brief description is provided below.

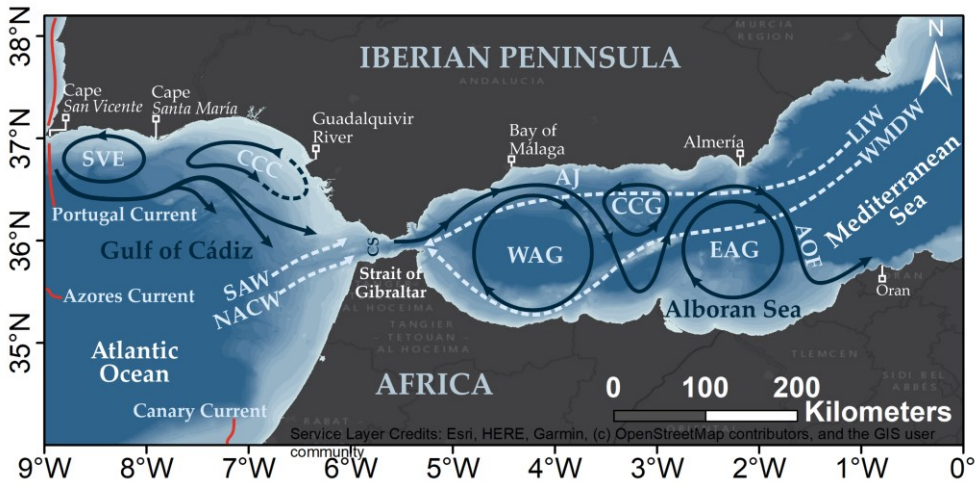


Figure 1.4. Map of the Gulf of Cádiz and Alboran Sea, showing the Strait of Gibraltar, and patching its general circulation: on the Atlantic Side, the Coastal Counter Current (CCC) and the Cape San Vicente gyre (SVE), and on the Mediterranean Side, the Atlantic Jet (AJ), the Western and Eastern Alboran Gyres (WAG and EAG, respectively), the Central Cyclonic Gyre (CCG) and the Almería-Oran front (AOF). The Canary, Azores, and Portuguese currents alluded to in the text flow southward, eastward, and northerly, respectively, in the North part of the Atlantic not shown. For illustration purposes, an imaginary branch representing the course of these currents is shown in red. The most relevant water masses are also displayed, following sketches from Kinder & Bryden (1990).

The Gulf of Cadiz is a sub-basin of the North Atlantic Ocean located west of the Strait of Gibraltar. Its most prominent geographic features in the north are the Capes San Vicente and Santa María (Figure 1.4). The surface circulation patterns on the shelf are wind-driven and characterized by two cyclonic eddies (García-Lafuente et al., 2007). One gyre flanks the western side and extends from Cape San Vicente to Cape Santa María. The other, formed by the Coastal Counter Current (CCC), occupies the eastern shelf from Cape Santa María to the Guadalquivir River (Teles-Machado et al., 2007). These eddies promote the upwelling of nutrient-rich deep waters, creating highly productive zones that are exploited by mesopelagic species (Sánchez-Garrido et al., 2015). The offshore boundary of these eddies is defined by an eastward-flowing branch of the Portuguese-Canary Current. Within the Gulf, part of this current flows towards the Strait of Gibraltar,

while another recirculates anticyclonically. The central Gulf is also influenced by the eastern branch of the Azores Current, which feeds into the Portugal Current (Barton, 2001), and by the Canary Current, flowing along the northwestern coast of Africa.

### 1.3.2 The Adriatic Sea

The Adriatic Sea is a semi-enclosed basin in the northernmost Mediterranean Sea (Figure 1.3, Figure 1.5). The bathymetry is characterized by a strong asymmetry, shallow in the upperpart, gradually deepening towards the middle, and rising sharply to ~1270 meters at the lower part in the Otranto Sill (Cushman-Roisin et al., 2001). It is connected to the Ionian Sea via the Strait of Otranto, a ~75-km-wide and ~800-m-deep channel where different water masses are exchanged (Orlić et al., 1992). The surface flow circulation is generally cyclonic (Russo & Artegiani, 1996). It consists of a northwestward current along the eastern coast, the Eastern Adriatic Current (EAC), composed of Levantine Intermediate Water (LIW) and Ionian Surface Water (ISW), and a fast, coastally confined southeastward current, the Western Adriatic Current (WAC) along the western coast (Figure 1.5).

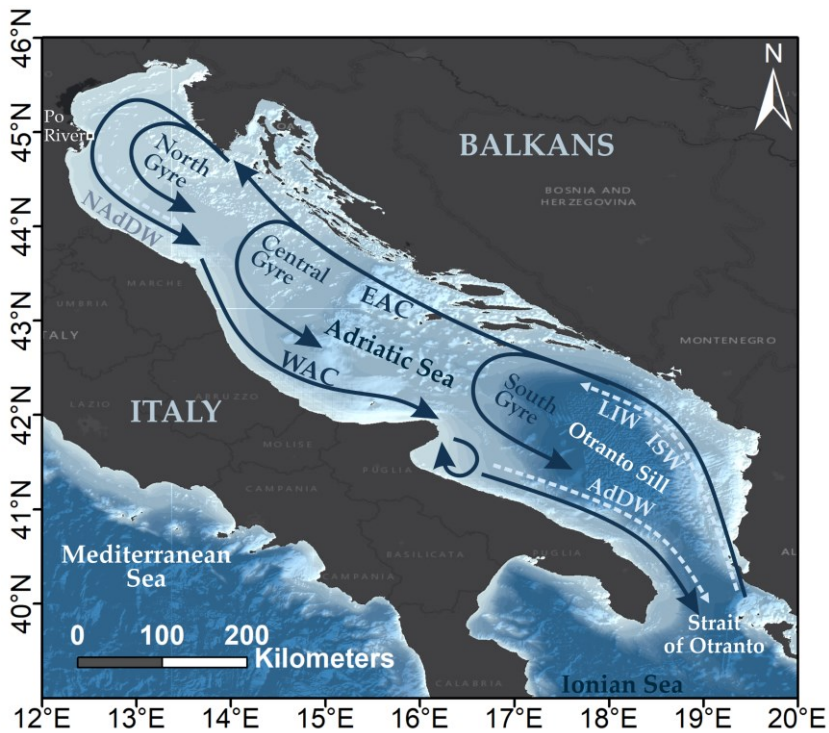


Figure 1.5. Map of the Adriatic Sea sketching its general circulation: the Western and Eastern Adriatic Currents (WAC and EAC, respectively) and the North, Central and South Cyclonic Gyres. The most relevant water masses are displayed, following sketches from Russo & Artegiani (1996). Some of the relevant locations are also displayed.

The WAC exports fresher waters in the surface layer and denser water below it to the Ionian Sea (Figure 1.5). The surface water of the WAC is formed in the northern Adriatic and is principally due to the Po River, whose mouth is located in the northwestern part of the basin and whose mean annual discharge is  $1500 \text{ m}^3/\text{s}$  (Russo & Artegiani, 1996). The bottom portion of the WAC is a density-driven current, consisting of North Adriatic Dense Water (NAdDW) which is formed during winter in the central part of the basin (Malanotte-Rizzoli et al., 1996). Another characteristic dense water, namely Adriatic Deep Water (AdDW), formed by the NAdDW contribution and by the diapycnal convection in the deep Otranto Sill (Vilibić et al., 2012), exits the Adriatic Sea at the bottom, pressed against the continental margin of the western flank of the Strait of Otranto (Russo & Artegiani, 1996).



## 2 Methodology

### 2.1 Numerical model

A cardinal element of this thesis is the outcome of general circulation models, intended to represent the time evolution of the velocity field and thermohaline properties (i.e. temperature and salinity) of the water column in a large domain encompassing the regions under study. The purpose of this section is to revise the architecture of the models employed, that will be coupled to the Lagrangian modules for the study of population dynamics in the cited nearshore environments. Specifically, two numerical models used in the following chapters are scrutinized: MITgcm (c.f. Subsection 2.1.3) and SHYFEM (c.f. Subsection 2.1.4). Some notions on the knowledge of general circulation models follow.

#### 2.1.1 Governing equations

In the field of environmental science, a numerical model is frequently described as a tool that employs numerical integration techniques to solve the fundamental governing equations of fluid dynamics (Kowalik & Murty, 1993). The governing equations for a fluid in a rotating system is a set of equations based on the Newton's second law applied to a non-inertial reference system, along with another equation for mass conservation, which for water, a fluid basically incompressible, can be transformed in another for volume conservation. The deduction of these equations, which is a classic topic of geophysical fluid dynamics, is long and somewhat complicated and is out of the scope of this dissertation. They can be found in many textbooks (Cushman-Roisin & Beckers, 2006; Gill, 1982; Kundu et al., 2012; McWilliams, 2006; Stewart, 2009). The equations, using a standard nomenclature, are written here for the sake of a better understanding of the numerical models, which is the objective of this Chapter:



$$\frac{\partial u}{\partial t} - 2\Omega \sin \varphi v + u \frac{\partial u}{\partial x} + v \frac{\partial u}{\partial y} + w \frac{\partial u}{\partial z} = -\frac{1}{\rho} \frac{\partial p}{\partial x} + F_x \quad [2.1]$$

$$\frac{\partial v}{\partial t} + 2\Omega \sin \varphi u + u \frac{\partial v}{\partial x} + v \frac{\partial v}{\partial y} + w \frac{\partial v}{\partial z} = -\frac{1}{\rho} \frac{\partial p}{\partial y} + F_y \quad [2.2]$$

$$\frac{\partial w}{\partial t} + u \frac{\partial w}{\partial x} + v \frac{\partial w}{\partial y} + w \frac{\partial w}{\partial z} = -\frac{1}{\rho} \frac{\partial p}{\partial z} - g + F_z \quad [2.3]$$

( $\rho$  the density,  $\Omega$  the rotation rate of earth,  $\varphi$  the latitude,  $g$  the acceleration of gravity,  $u$ ,  $v$  and  $w$  the velocity components in the  $x$ ,  $y$  and  $z$  dimensions, and  $F_i$  the components of frictional and any other body force as, for instance, tidal forces derived from the tidal generation potential). Additionally, these equations are complemented by the classical advection-diffusion equation that applies to variables such as temperature [2.4], salinity [2.5], or other biochemical substances (tracers), which are based on conservation laws.

$$\frac{\partial T}{\partial t} + u \frac{\partial T}{\partial x} + v \frac{\partial T}{\partial y} + w \frac{\partial T}{\partial z} = K_H \left( \frac{\partial^2 T}{\partial x^2} + \frac{\partial^2 T}{\partial y^2} \right) + K_z \frac{\partial^2 T}{\partial z^2} \quad [2.4]$$

$$\frac{\partial S}{\partial t} + u \frac{\partial S}{\partial x} + v \frac{\partial S}{\partial y} + w \frac{\partial S}{\partial z} = K_H \left( \frac{\partial^2 S}{\partial x^2} + \frac{\partial^2 S}{\partial y^2} \right) + K_z \frac{\partial^2 S}{\partial z^2} \quad [2.5]$$

( $T$  temperature,  $S$  salinity, and  $K_H$  and  $K_z$  the horizontal and vertical eddy diffusivities, respectively). Again, their deduction is somewhat cumbersome and is not provided here. It can be found in the above-referred textbooks.

### 2.1.2 General considerations on the setup of ocean models

The configuration of a numerical model for the reproduction of the hydrodynamics of specific regions involves various key steps, which are generally analogous for all models (Oke et al., 2016). These include the generation of a model grid, the preparation and interpolation of bathymetry, initial and boundary conditions, calibration, validation, and verification procedures prior to its application, which in turn are contingent on the region to be simulated. Guidance on model building procedures is widely documented in the environmental modeling community (Griffies & Adcroft, 2008; Kowalik & Murty, 1993; Rahman, 2019; J. J. Williams & Esteves, 2017) and, therefore, a detailed description of the step-by-step instructions is

unnecessary. However, general considerations are relevant to the description of the numerical tools used in this thesis, for which an overview description of general setups of ocean models is given below. A scheme of the steps involved is shown in Figure 2.1.

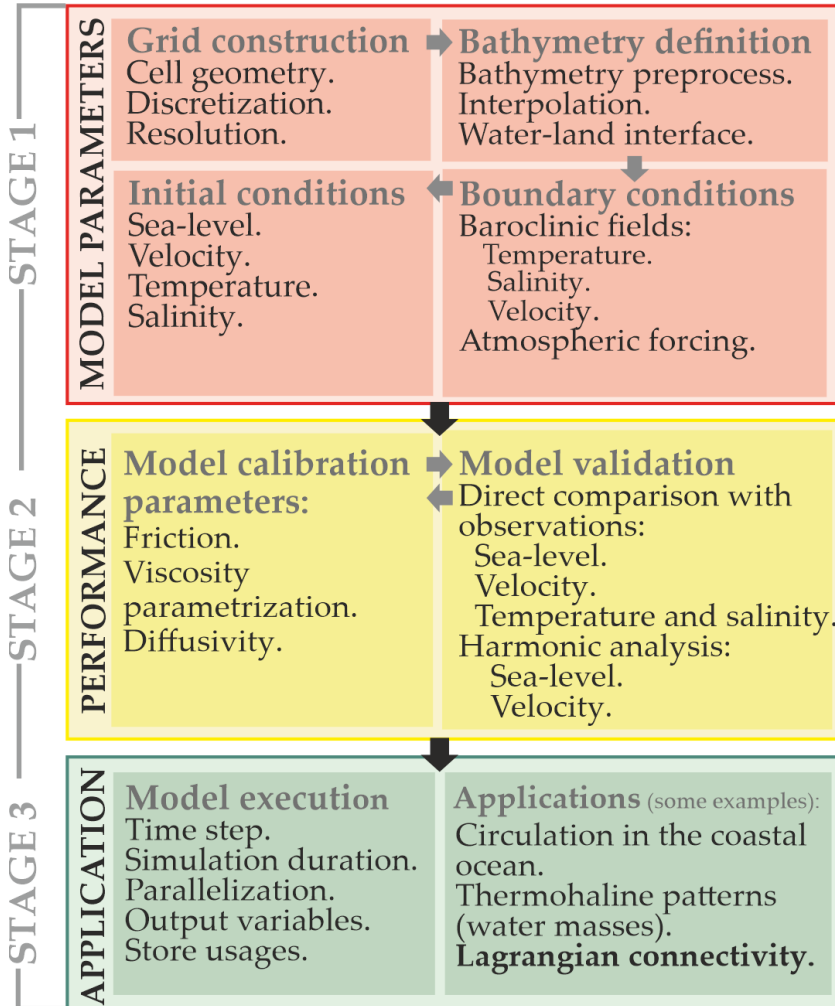


Figure 2.1. Schematic diagram of some of the typical stages required for a hydrodynamic model setup.

With a pre-determined spatial extent, the initial phase of the model construction process involves selecting and configuring the model grid and bathymetry (Stage 1, Figure 2.1). This involves deciding on the cell geometry (i.e. shape and size), the horizontal and vertical resolution, and the

discretization of cells (Bomers et al., 2019). Traditionally, structured curvilinear grids have been employed as an effective way of discretizing the model domain to provide a high density of grid points in a particular region (e.g. MITgcm model; Marshall, Hill, et al., 1997). A further prevalent approach is to configure the modeling domain as a flat plane defined by structured Cartesian coordinates, but this often results in a loss of realism, unavoidable due to distortions caused by conformal map projections (Riha, 2017). The restrictions of structured domains are particularly acute when representing nearshore environments with complex geometric features such as main channels, branches, and floodplains. In such cases, the most commonly employed approach is the use of unstructured meshes (e.g. SHYFEM model; Umgiesser et al., 2004), by dividing the model domain into triangles, a process that is relatively straightforward and allows for considerable flexibility in terms of shape (Loseille, 2017). However, they are also associated with lower numerical accuracy (Ventosa-Molina et al., 2017). The advantages and disadvantages of the fully structured and fully unstructured grids have led to a recent combination of the two grid types (e.g. Delft3D Flexible Mesh model; Mogé et al., 2019), although much effort for optimization and improvement still must be done (Bomers et al., 2019).

The use of accurate bathymetry is another critical factor in modeling studies, especially in coastal and shelf sea applications, and efforts must be made to ensure that the best and most recent bathymetric information is used. The selection of the interpolation method (e.g. linear, nearest neighbor, inverse distance weighted, or spline), is of great importance and depends on the data density and the requirements of the model (Amoroso et al., 2023). Initial and boundary conditions are also configured at this stage, including oceanic states at the model boundaries and sea-atmosphere interactions. The approach to forcing the model typically consists of a one-way nesting scheme in which the model variables (e.g. velocity, temperature, salinity) are relaxed at the open boundaries within a buffer region. In general, ocean circulation models do not incorporate tides. There are specific global ocean models developed for the purpose of forecasting the tidal sea surface elevation signal within the ocean, which typically employ sea-surface height (SSH) data

derived from satellite altimeters and coastal tide gauges. The output from these global tidal models, which consists of tidal constants (i.e., amplitude and phase for many tidal constituents) throughout the domain, is used to provide tidal forcing to regional ocean circulation models, such as those applied in this memory.

Once the geometry and spatial extent of the model have been configured, calibration and validation are the two major steps in the subsequent stage of model implementation (Stage 2, Figure 2.1). Calibration requires the adjustment of certain model parameters to achieve optimal model performance for specific locations and applications, which typically include bed roughness and friction factors, and horizontal eddy viscosity and diffusivity, among others (Zapata et al., 2019). In this step, sensitivity analyses are commonly performed to test the robustness of the model and to identify errors by finding unexpected relationships between inputs and outputs. Validation, on the other hand, involves running a model with the parameters determined during the calibration process and comparing the predictions with observations, not necessarily used in the calibration process. This is usually done by direct comparison of the observed and simulated variable time series or, for certain nearshore environments, by comparison of the tidal constants derived from observations and model output using standard harmonic analysis (Pawlowicz et al., 2002). A close agreement between model predictions and measurements indicates that the model is both calibrated and valid.

The final crucial stage is the execution and application of the model to study a particular process of interest. At this stage (Stage 3, Figure 2.1), decisions are made regarding the model's computational parameters, such as the time step (i.e., the increment of time simulated in each iteration) and the total simulation duration. Also, the configuration of the output variables to be stored is determined, typically planned ad-hoc for subsequent coupling to Lagrangian algorithms. Given the significant computational resources typically required, these simulations are often run on supercomputers with hundreds of processors located in specialized research centers (Kowalik &

Murty, 1993). In this context, parallelization, which involves dividing a task into smaller sub-tasks that are simultaneously processed across multiple processors, significantly reduces execution time by effectively distributing the workload (Lee et al., 2014). The outcome of simulations is finally represented by the model outputs, which encapsulate the variables representing the hydrodynamic temporal evolution of the studied region.

Numerous applications have been developed for representing such oceanic fluids, many of which utilize three-dimensional numerical models applied to oceans, marginal seas, coastal areas, estuaries, and rivers. Examples of these models include TELEMAC (Galland et al., 1991), DELFT3D (Roelvink & Banning, 1995), MITgcm (Marshall, Hill, et al., 1997), SHYFEM (Umgiesser et al., 2004), OpenFOAM (Nilsson & Page, 2005), ROMS (Shchepetkin & McWilliams, 2005), HYCOM (Chassignet et al., 2009), FVCOM (Wu et al., 2011), ELCOM (Leon et al., 2012), MPIOM (Jungclaus et al., 2013), NEMO (B. Jones, 2014), and SCHISM (Zhang et al., 2016), among many others. It thus seems reasonable to utilize an existing model instead of developing a new modeling system for studying a particular application. In this research, the potential of two hydrodynamic models, MITgcm (Subsection 2.1.3) and SHYFEM (Subsection 2.1.4) to accurately represent the main circulation patterns in the areas under study is explored. A detailed description of each model is provided below.

### 2.1.3 MITgcm

The first numerical model employed in this thesis is the Massachusetts Institute of Technology General Circulation Model (MITgcm), a flexible tool designed for the study of the atmosphere, ocean and climate (Marshall, Adcroft, et al., 1997; Marshall, Hill, et al., 1997). The model solves the fully non-linear, non-hydrostatic Boussinesq form of the Navier-Stokes equations with a spatial finite-volume discretization on a curvilinear grid (Marshall, Adcroft, et al., 1997; Marshall, Hill, et al., 1997). The model is written in FORTRAN, a language widely used in computational fluid dynamics and is compiled and run on UNIX/LINUX-based systems. Source code can be found on the MITgcm group web site (<http://mitgcm.org/>).

MITgcm is used by a large global research community with broad applications. For instance, it has been applied to provide an accurate prediction of sea ice in the Arctic (Yuan et al., 2024) and the Nordic Seas (Jensen et al., 2018). It has been employed to gain understanding of certain lake-dynamics (Dorostkar et al., 2022; Safin et al., 2021; Walsh, 2020). It has been applied to analyze extreme heat events occurring on the Red Sea (Sun et al., 2019), to assess mesoscale variability in the Caribbean Sea (Boog et al., 2019), and to study the dynamics of the ocean current-induced in the Green Island (Hsu et al., 2020). Yet, the primary uses for this model involve the examination of regional-to-large scale ocean dynamics. Among these, one of the most relevant and near applications to the region of interest in this thesis is the study of the fluid dynamics of the Mediterranean Sea (Sannino et al., 2009, 2022), and particularly, the Strait of Gibraltar and adjacent basins (Sánchez-Garrido et al., 2011, 2013). The latter application is the one in use in this thesis and the following description is a brief overview.

### 2.1.3.1 Setup for the Strait of Gibraltar and adjacent basins

The model is implemented on a curvilinear grid that spans the Gulf of Cadiz, starting from 9.4°W, and extends to the eastern limit of the Alboran Sea, at 1.6°E (Figure 2.2). The model's horizontal resolution and vertical discretization are unequal, being highest horizontally in the Strait of Gibraltar and near the surface in the vertical dimension. The bottom topography is derived from four bathymetric sources: (1) the multilayer bathymetric product from the EMODnet Digital Terrain Model (EMODnet Bathymetry Consortium, 2018), (2) the ecocartography campaign developed by the Spanish Ministry of Agriculture, Fisheries and Food between 2000 and 2012 for the Gulf of Cadiz (Gaide et al., 2018), (3) the high-resolution topobathymetric map of the southeastern Spanish continental shelf produced by the Spanish Oceanographic Institute and the General Secretariat of Maritime Fisheries (Acosta Yepes et al., 2006), and (4) the high-resolution coastline of the OpenStreetMap project (OpenStreetMap contributors, 2015).

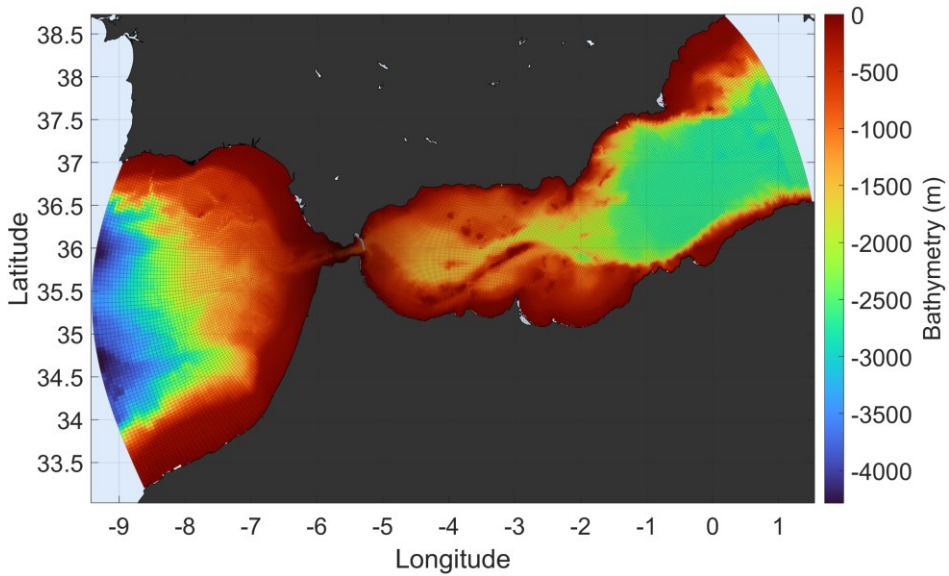


Figure 2.2. Numerical grid and bathymetry of MITgcm application in the Strait of Gibraltar and adjacent basins.

At the two lateral open boundaries (the west - Atlantic Ocean, the east - Western Mediterranean Sea), the hourly baroclinic (density varying) fields of temperature, salinity, and zonal ( $u$ ) and meridional ( $v$ ) components of velocity orthogonal to the boundary are imported from the CMEMS-IBI model for simulations up to 2021 (Sotillo et al., 2015), and from the Mediterranean Sea Physics Analysis and Forecast System (CMEMS MED-Currents, EAS6 system; Clementi et al., 2021), for simulations from 2021 onwards. The operational storm surge NIVMAR model (Álvarez-Fanjul et al., 2001) provides meteorologically-driven barotropic (vertically integrated) flows to account for the remote effect of the atmospheric forcing over the Mediterranean basin. These flows are imposed at the two open boundaries by prescribing a vertically homogeneous velocity at the grid cells of the boundary which, integrated over the whole contour, reproduces the barotropic flow from NIVMAR model. In a relatively small region strongly influenced by tidal currents such as the Strait of Gibraltar, tides must be imposed as boundary conditions in the domain contours. A barotropic tidal velocity is prescribed at the same nodes and following the same procedure as before. The barotropic tidal velocity is computed via tidal prediction using

the outputs of the MOG2D-G High Resolution barotropic model (Carrère & Lyard, 2003), developed by Legos/CNRS. Tidal constituents employed in the prediction are  $M_2$  (lunar semidiurnal),  $S_2$  (solar semidiurnal),  $N_2$  (lunar elliptical semidiurnal),  $K_2$  (luni-solar declinational semi-diurnal),  $K_1$  (luni-solar diurnal),  $O_1$  (lunar diurnal),  $P_1$  (solar diurnal), and  $Q_1$  (lunar elliptical diurnal). The atmospheric forcing at the sea surface, including wind stress, humidity, air temperature, and shortwave and longwave radiation, is computed using data from atmospheric reanalysis (Hersbach et al., 2023).

Previous applications of the implementation of MITgcm in this area have demonstrated the model's efficacy and reliability, and the results have been published in several high-scored international journals. Examples of such studies are the investigations of the dynamics of the Bay of Algeciras at tidal and subinertial scales (Sammartino, García Lafuente, et al., 2014; Sammartino et al., 2017; Sánchez-Garrido et al., 2014), including a validation of the surface fields using the Lagrangian trajectories of a set of surface drifters released in the Strait area (Sotillo et al., 2016). The MITgcm model is therefore deemed suitable for the study of Lagrangian connectivity. In particular, it will be employed in the following chapters:

- (1) In Chapter 3, the prior version of MITgcm is used to simulate the hydrodynamics of the region of interest (Strait of Gibraltar and adjacent basins) from November 2004 to April 2005 to cover the most active spawning months of the modeled species, the blackspot seabream (*Pagellus bogaraveo*).
- (2) In Chapter 6, the most recent version of MITgcm is used in a two-level nesting representation to improve its already high performance in simulating the complex hydrodynamics of this area in the year 2021, which could shed light on the causes of the expansion of the seaweed *Rugulopteryx okamurae* across the Strait of Gibraltar and the Alboran Sea.



## 2.1.4 SHYFEM

The second numerical model employed in this thesis is the Shallow water HYdrodynamic Finite Element Model (SHYFEM), developed by the Institute of Marine Science, CNR, Venice, Italy (Umgiesser et al., 2004). SHYFEM is based on the solution of the primitive equations considering an incompressible fluid and applies hydrostatic and Boussinesq approximations. It runs on an unstructured grid with a staggered horizontal discretization of the Arakawa B-grid type (Bellafiore & Umgiesser, 2010). SHYFEM is particularly well suited for solving the hydrodynamics of domains characterized by complex geometries and bathymetries, such as lagoons, coastal seas, estuaries, and lakes. In such domains, the finite element method allows local refinements of the resolution to achieve finer accuracy in regions where the physical phenomena are more complex, while saving computational resources. The source code can be accessed via the SHYFEM GitHub repository (<https://github.com/SHYFEM-model/shyfer>), which also contains illustrative examples of model configurations and detailed descriptions of the model development process.

To date, SHYFEM has been successfully applied to simulate hydrodynamics in several areas, including the Mediterranean Sea (S. Mariani et al., 2015), several coastal lagoons (De Pascalis et al., 2012; Ghezzi et al., 2015), the Po River-Delta-Sea system (Maicu et al., 2018), and the Adriatic Sea, where most applications have been developed (Bellafiore & Umgiesser, 2010; Federico et al., 2017; Ferrarin et al., 2016, 2017). The latter region is the subject of Chapter 4 of this thesis, for which a brief description is given below.

### 2.1.4.1 Setup for the Adriatic Sea

The model is implemented on an unstructured numerical grid that encompasses the Strait of Otranto and the entire Adriatic Sea (Figure 2.3). The horizontal and vertical resolutions are uneven, with the highest resolution occurring near the surface and the shoreline. The numerical grid consists in approximately 110,000 triangular elements with a resolution that varies from a few dozen kilometers in the open sea to a few hundred meters along the

coast and tens of meters in the inner lagoon channels. The bathymetry of the Adriatic Sea and its lagoons combines multiple datasets with varying spatial resolutions and measurement methods, all of which utilized the IGM42 reference datum (Ferrarin et al., 2019).

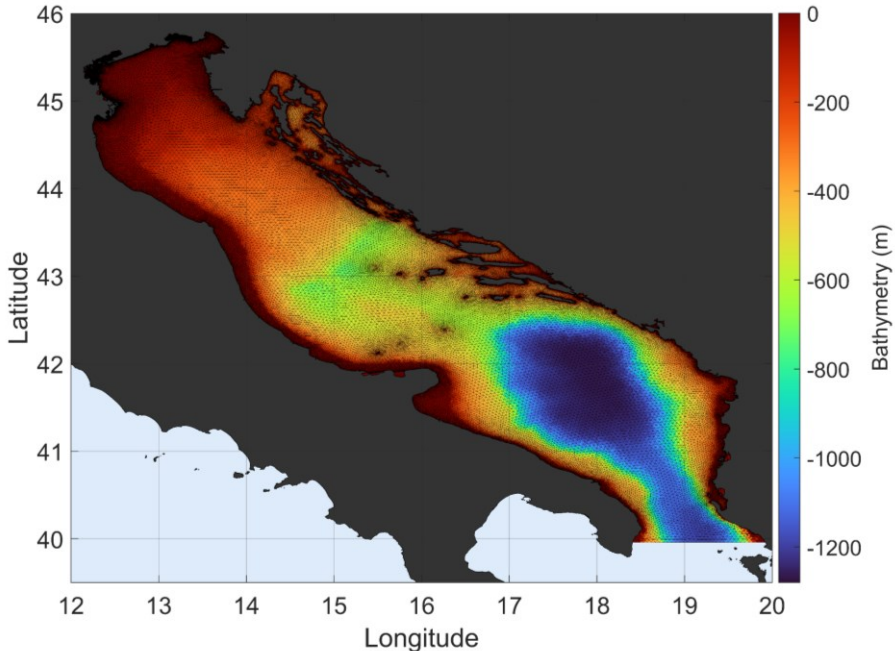


Figure 2.3. Numerical grid and bathymetry of SHYFEM application in the Adriatic Sea.

It considers five boundary conditions, including the sea level, velocity, temperature and salinity at the Strait of Otranto, and freshwater discharges from 17 tributaries (see details in Ferrarin et al., 2019). The sea level and the current velocity conditions are imposed through the hourly tidal signal provided by the FES2012 global tidal model (Carrere et al., 2013). The daily water level, baroclinic velocity, water salinity and temperature are provided by the Mediterranean Forecast System (Tonani et al., 2008), available via the Copernicus Marine Environmental Monitoring Service (<http://marine.copernicus.eu/>). Daily freshwater discharges at river boundaries are obtained, where available, from automatic hydrometric stations closest to river mouths, through calibrated stages, or from monthly and annual climatological values (Ferrarin et al., 2019 and references therein).

The atmospheric forcing, including pressure and wind, is provided by the ECMWF ERA5 atmospheric reanalysis (Hersbach et al., 2023).

The application of the SHYFEM model to the Adriatic Sea has been validated in previous works, demonstrating the ability to accurately reproduce tidal propagation, storm surge, water flows at the lagoons' inlets, and water temperature and salinity variability (Ferrarin et al., 2008, 2010; Ghezzi et al., 2011; Umgiesser et al., 2004). For this reason, it is further considered to be an appropriate tool for simulating the Lagrangian transport of virtual particles in this region. In particular, the model will be employed in Chapter 4, where the SHYFEM output from 2018 will be utilized to assess the influence of hydrodynamics on connectivity, dispersal, and retention patterns in the Adriatic Sea.

## 2.2 Lagrangian particle tracking

In terms of particle tracking, there exist basically two approaches for the numerical simulation of dispersing agents, categorized as Eulerian and Lagrangian. In computational fluid dynamics, the Lagrangian particle tracking is commonly defined as a numerical technique for tracing Lagrangian particle paths within a Eulerian frame (Schröder & Schanz, 2023). In essence, the objective of Lagrangian analysis is to describe the fluid motions by tracking the movement of individual fluid parcels based on the particle motion equations (Rühs, 2018). As the particle displaces, it follows a curve in space called the Lagrangian particle trajectory. The velocity of the Lagrangian particle is thus the time derivative of the trajectory position, and must be equal to the local Eulerian velocity at each point crossed in space and time:

$$\frac{\partial \vec{x}}{\partial t} = \vec{v}(\vec{x}, t) \quad [2.6]$$

Where  $\vec{v}$  is the vector velocity with components  $u$ ,  $v$  and  $w$  in the  $x$ ,  $y$  and  $z$  directions, and  $\vec{x}$  is the particle coordinate in the three directions. When the  $n$ th particle is located at the point  $\vec{x}(t) = x$ , its position in  $t + \Delta t$  can be updated as:

$$\vec{x}(t + \Delta t) = \vec{x}(t) + \vec{v}(\vec{x}(t), t)\Delta t \quad [2.7]$$

The time integration of the trajectory equation [2.7] can be obtained via explicit or implicit time-stepping, as well as in the form of analytical solutions. The simplest explicit time-stepping method is the so-called Euler method, for which the velocity at a given point of the trajectory in space and time is multiplied by a time step  $\Delta t$ . Better accuracy of the trajectories can be obtained by using higher-order methods for the integration of equation [2.7], such as the 4<sup>th</sup> order Runge-Kutta scheme, which involves determining the position of a passive tracer by starting from a known initial condition and applying a weighted average of four successive increments between time steps  $t_n$  and  $t_{n+1} = t_n + \Delta t$ . The solution from  $\vec{x}_n$  to  $\vec{x}_{n+1} = \vec{x} + \Delta t$  can therefore be written as:

$$\vec{x}_{n+1} = \vec{x}_n + \frac{1}{6} \Delta t (k_1 + 2k_2 + 2k_3 + k_4) \quad [2.8]$$

where,

$$k_1 = \vec{v}(\vec{x}_n, t_n) \quad [2.9]$$

$$k_2 = \vec{v}\left(\vec{x}_n + \frac{1}{2}k_1\Delta t, t_n + \frac{1}{2}\Delta t\right) \quad [2.10]$$

$$k_3 = \vec{v}\left(\vec{x}_n + \frac{1}{2}k_2\Delta t, t_n + \frac{1}{2}\Delta t\right) \quad [2.11]$$

$$k_4 = \vec{v}(\vec{x}_n + k_3\Delta t, t_n + \Delta t) \quad [2.12]$$

and  $v_j$  is the velocity delivered at each iteration  $t_j$ .

Thus, a simulated Lagrangian trajectory inherently carries information about the displacement, but also about the Lagrangian velocities of a given virtual fluid particle. In addition, it is possible to store salinity and temperature (if simulated) values along the trajectory by interpolating spatially and temporally the respective gridded simulated Eulerian fields onto the particle positions.

### 2.2.1 Applications

Aiming at describing the flushing patterns in the Bay of Algeciras, Sammartino et al. (2017) employed virtual Lagrangian drifters and a tracking algorithm specifically adapted to the curvilinear grid of the numerical model MITgcm implemented in the region. The three-dimensional velocity field provided by the numerical hydrodynamic model was used to determine the trajectory that a virtual particle at a given horizontal position, depth and time, would follow when subjected to these currents.

In addition, many third-part particle tracking software packages have been developed, each offering unique capabilities tailored to specific scientific needs, ranging from broad ocean circulation studies to focused biological and environmental applications. The packages OceanParcels (Lange & Van Sebille, 2017), and OpenDrift (Dagestad et al., 2018) are amongst the most common applications, which are versatile modules to simulate the transport of diverse type of elements, such as plastics, pollutants, and water parcels. Other models, such as Ichthyop (Lett et al., 2008) or PaTATO (Fredj et al., 2016), are specifically designed for marine propagule dispersal and simulate the transport and behavior of larvae, incorporating biological processes such as vertical migration and mortality. Other tools, such as TrackMPD (Jalón-Rojas et al., 2019), and TRACMASS (Döös et al., 2013), are designed to analyze the transport and transformation of water masses, focusing on pathways and transformations that involve changes in heat and salinity. Finally, models such as Ariane (Muller et al., 2009) and Deft3D-PART (Mogé et al., 2019) are used for general particle tracking in three-dimensional oceanographic contexts, helping to study complex flow patterns and particle dynamics in the marine environment. In this research, the potential of two Lagrangian algorithms to accurately represent the dispersal patterns of certain target individuals under study is explored:

- (1) In Chapter 3, the two-dimensional algorithm developed by Sammartino et al. (2017) is utilized as the numerical tool to investigate the hydrodynamics that influence the connectivity of the blackspot

seabream (*Pagellus bogaraveo*), which is an exploited fishery species in both Spanish and Moroccan waters.

- (2) In Chapter 4, the software OpenDrift is employed as the numerical tool to examine the hydrodynamics that regulate connectivity in the Adriatic Sea. Lagrangian particles, representing eggs and larvae with typical biological characteristics of generic marine organisms inhabiting the region, are released throughout the basin at different times during a test year to identify the most likely pathways of individual dispersal.
- (3) In Chapter 6, OpenDrift is again used to assess the environmental impact of the alien macroalga *Rugulopteryx okamurae* over the Strait of Gibraltar, the Gulf of Cadiz and the Alboran Sea. Particles are released in different scenarios consisting of a combination of environmental conditions.

#### 2.2.1.1 OpenDrift

OpenDrift is an open-source python-based software application developed by the Norwegian Meteorological Institute (Dagestad et al., 2018). It consists of several particle-based sub-models used to predict the transport and destination of different types of objects or substances drifting in the ocean (Dagestad et al., 2018). The sub-models incorporate environmental variables to compute the advection of the seeded particles, including eastward and northward velocities, waves and winds, among other variables, which are loaded as objects called "readers". The basic sub-module, OceanDrift, considers the particles as passive, i.e. the transport is determined by the time the particles spend drifting in the ocean. Bioecological properties such as motility, migration, and birth and death rates are not considered.

Multiple parameters can be configured when running a simulation, including the number and distribution of seeded particles (or drifters), the size and shape of the seeding area, the simulation time step, and the integration method (e.g., Euler or Runge-Kutta), among others. Once all parameters are set and the simulation is run, OpenDrift generates output files in NetCDF format containing information on particle trajectories, including

geographic coordinates (latitude and longitude) over time, and environmental properties such as velocities and thermohaline (if simulated) values along the trajectory.

### 2.3 Connectivity computation

A key quantitative measure of population connectivity is the source distribution matrix, where each cell is the number of particles ( $p$ ) released from a certain source  $i$  (along the vertical axis) and collected in a certain destination  $j$  (along the horizontal axis), so  $C_{i,j}$  is the probability that an individual or group of individuals of population  $i$  will move to population  $j$  after a certain tracking time:

$$C(i, j) = \frac{p_j}{p_i} \quad [2.13]$$

The diagonal cells of this matrix (where  $i = j$ ) represent the local retention, which is the number of individuals that remain in the region where they were originally released, including those individuals that leave and eventually return to their source area (Cowen et al., 2007). Therefore, connectivity ratios ( $C$ ), ranging from 0 to 1, quantify the strength of connectivity between different sites, with higher (lower) values indicating stronger (weaker) or more (less) favorable connections between subsites. This approach provides only a partial representation of connectivity, neglecting crucial temporal information, such as the identification of areas with different individual retention characteristics over time (e.g. boxes that rapidly disperse, both disperse and recruit, or recruit only). To overcome this limitation, three different approaches are defined:

In Chapter 3, an alternative definition of connectivity is adopted by calculating the maximum percentage of particles collected in each landing area, together with the time at which it occurs, throughout the entire duration of the simulation, which is 60 days, corresponding to the maximum PLD estimated for blackspot seabream (Peleteiro-Alonso et al., 1997):

$$C(i, j) = \max\left(\frac{p_j(t)}{p_i}\right) \quad [2.14]$$

In Chapter 4, a more-recent approach consisting of a “retention clock matrix” is used to track the temporal changes in source-sink connections, where the release event is described as a circular clock that tracks the number of particles ( $p$ ) over the entire time scale of interest (Defne et al., 2016):

$$C(i, j, t_n) = \frac{p_j(t_n)}{p_i(t_0)} \quad [2.15]$$

In Chapter 6, connectivity is assessed as the probability of algal accumulation for the affected coastlines. To estimate these accumulation rates along the coastal zone, the coastline is divided into 630 segments ( $n$ ), each ~1000 m long and ~100 m wide. For each simulated period, the accumulation per segment ( $A_n$ ) and the total accumulation for all segments ( $A_T = \sum_1^n A_n$ ) are obtained. The relative percentage of accumulation for each region is then calculated by dividing the amount of settled particles in each segment by the total accumulation as:

$$\%RA = \frac{A_n}{A_T} \cdot 100 \quad [2.16]$$

Further details on the development of these methodologies and sensitivity analysis of each quantification measure will be provided in subsequent chapters.





# 3 Hydrodynamic connectivity and dispersal patterns of a transboundary species (*Pagellus bogaraveo*) in the Strait of Gibraltar and adjacent basins<sup>1</sup>

## 3.1 Abstract

The blackspot seabream (*Pagellus bogaraveo*) is a benthopelagic fish species highly appreciated by consumers and an important target of the Spanish and Moroccan fisheries in the transcontinental waters of the Strait of Gibraltar area. It is also one of the most exploited resources of the region, which has led to a situation of overexploitation and a notable drop of catches. To gain insight into the sustainability of this resource and certain patterns of the spatial adaptation of the species, a high-resolution circulation model coupled to a Lagrangian tracking module has been employed to investigate the dispersal pathways of blackspot seabream, using eggs and larvae (early-life-stages, ELS) as purely passive particles advected by currents. Several spawning scenarios consisting of different spatial (depths and sites) and temporal (tidal phase and strength) initial conditions have been analyzed to identify the most likely pathways of ELS dispersion. Eastward transport by the Atlantic Jet exiting the Strait of Gibraltar is the most influencing process

---

<sup>1</sup> The contents of this chapter are open-access published in:

**Nadal, I.,** Sammartino, S., García-Lafuente, J., Sánchez Garrido, J. C., Gil-Herrera, J., Hidalgo, M., & Hernández, P. (2022). Hydrodynamic connectivity and dispersal patterns of a transboundary species (*Pagellus bogaraveo*) in the Strait of Gibraltar and adjacent basins. *Fisheries Oceanography*, 31(4), 384-401. <https://doi.org/10.1111/fog.12583>.

in that dispersion. Regarding temporal fluctuations, fortnightly tidal modulation is the prevailing factor to determine the horizontal paths of the ELS, spring tides being the cause of the greatest scattering of propagules. Spawning depth in the Strait of Gibraltar is a critical condition, as revealed by the model sensitivity tests. Potential implications of the results of the study to improve the assessment and management of this species are discussed.

## 3.2 Introduction

Oceanographic features largely control the dispersal of fish eggs and larvae and thereby the dynamic connectivity of geographically separated fish subpopulations (Cowen & Sponaugle, 2009). Such control is particularly tight in highly energetic areas influenced by tides, wind-driven currents and small-scale turbulence (Cowen et al., 2006; Ayata et al., 2010). Dynamic connectivity concerns to those interactions between the life cycle of the fish species in question and the physical processes that drive the dispersal of early life stage individuals (ELS, hereinafter) at different spatial and temporal scales.

Understanding the processes and scales controlling ELS dispersal and how connectivity influences the dynamics of the affected populations is a major challenge of special interest for vulnerable species (Cowen et al., 2006; Pineda et al., 2007), particularly relevant for species inhabiting across jurisdictional waters of different countries (Hidalgo, Rossi, et al., 2019; Palacios-Abrantes et al., 2020; Pinsky et al., 2018). Resolving the mechanisms controlling ELS dispersal entails the understanding of the relevant physical processes and how the species mediate the physical outcome (García-Lafuente, Sanchez-Garrido, et al., 2021). Currently, studies of dispersal dynamics and larval connectivity are being used to provide an approach to improve fisheries management and assessment (Fogarty & Botsford, 2007; Hidalgo, Rossi, et al., 2019). Focusing on fisheries health in the Strait of Gibraltar (SoG hereinafter, see Figure 3.1), the blackspot seabream [*Pagellus bogaraveo* (Brünnich, 1768)] is one of the most affected stocks (Gil Herrera, 2006, 2010). It is targeted by local fishermen from Spain and Morocco using a special longline gear, known as *voracera*.

Landings from this shared fishery exhibit a clear decreasing trend since 2009, which shows up a vulnerability that is raising serious concerns at local and international levels in a socioeconomic context (Báez et al., 2014). In 1998, the Spanish Government introduced technical measures to manage this fishery, and few years later, the Andalusian Regional Government developed a specific fishing plan that included a biological rest period and the limitation of the number of hooks per *voracera* (Burgos et al., 2013). Transitional measures for the management of blackspot seabream in the Alboran Sea (AS, hereinafter) were primarily set out by the General Fisheries Commission for the Mediterranean (GFCM) in 2017 (Recommendation GFCM/41/2017/2). Later on, the Recommendation GFCM/43/2019/2 establishes an adaptive multiannual management plan for its sustainable exploitation in the AS. Last GFCM stock assessment indicated that the SoG and population (geographical subareas, hereafter GSAs, 1 and 3; see Figure 3.1) is overexploited and in overexploited status and, consequently, a reduction of fishing mortality towards sustainability levels was recommended (GFCM, 2021b). Even so, the sustainability of blackspot seabream fisheries requires more efforts (Gil-Herrera et al., 2021).

The optimization of the fishery stock and the curbing of the over-exploitation of the resource require further studies of population dynamics and hydrodynamic and demographic connectivity, especially during larval stages. They should address the consequences of the connectivity on the production of the stocks and other characteristics at interannual time-scales. Trying to fill these gaps, the Regional Cooperation Project for Fisheries in Western Mediterranean (CopeMed) and the GFCM of the Food and Agriculture Organization (FAO) developed the EU-funded project “Transboundary population structure of Sardine, European hake and blackspot seabream in the Alboran Sea and adjacent waters: a multidisciplinary approach” (TRANSBORAN; CopeMed II, 2017, 2019), which focused on the management of the fishery stocks of these species in the AS and adjacent waters. One of the main objectives of the project was to understand and identify the mechanisms of larval dispersal in the area, which

is crucial to determine the populations structure and to optimize the fisheries functioning (Pineda et al., 2007; Virtanen et al., 2020).

From a hydrodynamic point of view, ELS dispersal is usually investigated by means of tracking algorithms fed by hydrodynamic numerical models (e.g., Dubois et al., 2016; Rossi et al., 2014). Some studies suggest that ELS information concerning larval behavior, egg buoyancy or diel vertical cycles is critical (Fiksen et al., 2007; Sundelöf & Jonsson, 2012), whereas others show that active swimming during ELS is negligible when compared with the effect of the drifting by the ocean currents (Hidalgo, Rossi, et al., 2019). This biological aspect has not been elucidated yet for the blackspot seabream. Nevertheless, the high dynamics of the area strongly supports the second hypothesis. Consequently, the present study considers the ELS as passive tracers advected by the currents and investigates their dispersion and connectivity patterns using a high-resolution ( $\approx 1$  km) circulation model of the SoG, the spawning area of the species (Gil Herrera, 2006, 2010), and the AS. Different scenarios have been considered in order to assess the sensitivity of the resulting patterns against the initial conditions. The scenarios include diverse spawning grounds and depths in the SoG as well as distinct hydrodynamic initial conditions associated to the tidal phase and strength (spring-neap tidal cycle) of the currents at the moment of the spawning.

The paper is organized as follows: next subsections present the main traits of the biology of the blackspot seabream and of the hydrodynamic features of the area of study. Section 3.3 describes the numerical model and the Lagrangian approach and provides details about the experimental procedure. Section 3.4 reviews and discusses the results of the numerical experiments. It has been organized into seven subsections addressing different aspects of the dependency of the specific spatial and temporal initial conditions on the ELS dispersal paths and the potential implications for fishery management of the species. Section 3.5 includes a summary of the results and conclusions of this work.

### 3.2.1 Life cycle of blackspot seabream

As other Sparidae species, the blackspot seabream is a sequential protandric hermaphrodite, starting as males and then changing into females at 30-35 cm length and around 4 to 6 years age (Alcaraz & Estrada, 2022; Gil Herrera, 2006; Krug, 1994). It grows relatively slow to a maximum size of 70 cm, weight of 4 kg and about 15 years age (Gil Herrera, 2006; Krug, 1994; Sánchez, 1983). Juveniles inhabit inshore areas while adults have deeper distribution (Desbrosses, 1932; Olivier, 1928). Olivier (1928) and Desbrosses (1932) report species vertical movements during the night and in certain seasons, related to daylight and spawning. However, this has not been already demonstrated for the case of the SoG population. Fish populations are potentially able to adapt to the mean horizontal transport and dispersion pattern of its ELS by influencing the vertical position of their planktonic offspring either by its spawning behavior (fish selection of spawning area and depth) or by producing eggs of certain specific gravity (Sundby & Kristiansen, 2015). The ontogeny of the species ELS is only available from aquaculture experiments estimating a pelagic larval duration (PLD) from 40 to 60 days (Peleteiro-Alonso et al., 1997).

The AS might be considered as a hatchery and nursery area of the species (Gil et al., 2001): Juveniles are mostly caught close to the shore by recreational angling fishery, following similar patterns seen in other places like the Bay of Biscay (Lorance, 2011), the Azores Islands (Pinho et al., 2014), and the Mediterranean Sea (Biagi et al., 1998). Adults, targeted by the Spain and Morocco *voracera* fishing fleets, spawn during the first quarter of the year in the SoG (Gil Herrera, 2006, 2010). Interconnected cycles of recruitment in both sides of the nearby coastal areas of the SoG followed by juveniles returning to the grounds where the fishery takes place were suggested by Gil et al. (2001)

### 3.2.2 Relevant hydrodynamic features of the area

The SoG connects the North Atlantic Ocean and the Mediterranean Sea and is one of the most energetic spots in the world ocean. The net freshwater

deficit of the Mediterranean basin drives an archetypical baroclinic exchange that involves very large currents. Lighter Atlantic water flows into the Mediterranean basin invading the AS in the form of a swift Atlantic Jet (AJ hereinafter), while denser Mediterranean water flows underneath toward the Atlantic Ocean (García Lafuente et al., 2013). On average, each of these flows are slightly less than 1 Sv ( $1 \text{ Sv} = 10^6 \text{ m}^3 \text{ s}^{-1}$ ; García-Lafuente, Sammartino, et al., 2021; Sammartino et al., 2015), but they can quadruple the values during certain moments of the tidal cycle due to the strength of the tidal currents (García-Lafuente et al., 2000). Actually, the tide-topography interaction in the area gives rise to one of the most noticeable internal tides in the world ocean (Sánchez-Garrido et al., 2011), which displaces vertically the interface between Atlantic and Mediterranean waters by more than 100 m periodically. Also, forced barotropic flow through the SoG driven by the changing atmospheric pressure field over the Mediterranean basin modifies the baroclinic exchange by significant fractions of their average values at few-days' timescale (García Lafuente, Alvarez Fanjul, et al., 2002).

The general circulation of the AS is determined by the mentioned AJ (see the pioneer paper by Lanoix, 1974, or the extensive review by Parrilla & Kinder, 1987, for details). The AJ sets up two anticyclonic structures: the Western and the Eastern Alboran Gyre (WAG and EAG, respectively; see sketch of Figure 3.1), which exhibit seasonal and shorter time-scale variability. In winter, the WAG tends to be replaced by a coastal jet attached to the African coast (Flexas et al., 2006; Vargas-Yáñez et al., 2002). Surface variability is reduced during summer, when the atmospheric forcing is less variable (Sánchez-Garrido et al., 2013). Smaller scale processes such as tidally driven relative vorticity imported from the SoG, westerly winds and occasional AJ drifts, propitiate the formation of cyclonic eddies along the northern side of the jet in the western Alboran basin (Sánchez-Garrido et al., 2013; Sarhan et al., 2000) and also in the southern coast (Mason et al., 2019). These eddies induce upward pumping of deep waters, entailing high productivity areas favorable for mesopelagic species development (Sánchez-Garrido et al., 2015).

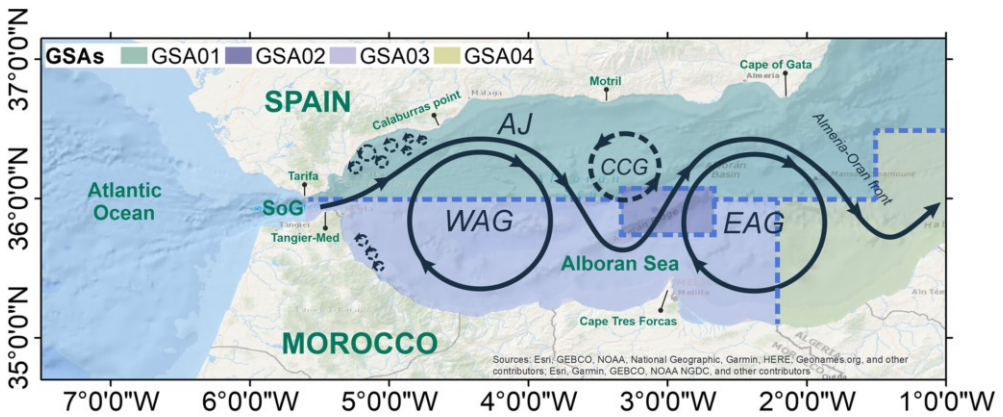


Figure 3.1. Map of the Alboran Sea showing the Strait of Gibraltar (SoG) and sketching its general surface circulation: the Atlantic Jet (AJ) and the western and eastern Alboran Gyres (WAG and EAG, respectively). CCG stands for Central Cyclonic Gyre, a weaker structure that normally develops whenever the WAG and EAG are fully developed (adapted from Sánchez-Garrido et al., 2013). Smaller cyclonic eddies, represented by dashed lines, are often found rightwards and leftwards of the AJ main path. Some relevant locations are displayed and the GSAs (1-4), defined by the GFCM (2021) are patched.

### 3.3 Numerical data and methods

#### 3.3.1 The hydrodynamic model

The numerical model used to simulate the hydrodynamics of the studied area is based on the MITgcm code (Marshall, Adcroft, et al., 1997; Marshall, Hill, et al., 1997), which has been already used in previous studies of this particular region (Sammartino, Sánchez-Garrido, et al., 2014; Sánchez-Garrido et al., 2011, 2013). The general configuration of the model, its advection scheme, and other technical details are provided in these works. It has been implemented on a curvilinear grid that covers the Gulf of Cadiz (from 9.4°W) and the AS to its eastern limit (around 1.6°E). The horizontal resolution and vertical discretization are uneven, being maximal in the SoG area and near the surface in the vertical (see Figure S3.1). At the two open lateral boundaries, the model is forced with baroclinic horizontal velocities, temperature, and salinity fields imported from CMEMS-IBI model (Sotillo et al., 2015).



Tides are also prescribed in these open boundaries using the harmonic constants of the eight most important tidal constituents (the main semidiurnal:  $M_2$ ,  $S_2$ ,  $N_2$ ,  $K_2$ , and diurnal:  $K_1$ ,  $O_1$ ,  $Q_1$ ,  $P_1$ ). The meteorologically driven barotropic flow prescribed at the SoG by the NIVMAR storm surge model (Álvarez Fanjul et al., 2001) is distributed throughout these boundaries to incorporate the meteorological forcing into the model. At surface, the model is forced with atmospheric conditions provided by the MED-Cordex model (Ruti et al., 2016). The model has been run from November 2004 to April 2005 in order to cover the most active spawning months of the blackspot seabream (Gil Herrera, 2006, 2010), and the 3D velocity field has been stored every 30 min.

In the vicinity of the SoG, but yet inside the AS, the highest variability of the velocity field is associated with the tidal dynamics of the Strait (García-Lafuente et al., 2000). Figure 3.2 shows the surface velocity and the kinetic energy per unit of mass (computed as  $K_E = \frac{1}{2} \cdot (U^2 + V^2)$ , U and V the zonal and meridional surface velocity components, respectively) over two different periods. The panel on the left corresponds to neap tide and illustrates a surface pattern with diminished velocities. Right panel is for spring tide and presents the characteristic average circulation that uses to prevail: the AJ flowing into the AS, the WAG and EAG, a small CCG in between, and the Almeria-Oran (AO) front in the eastern limit of the AS. Both panels show similar circulation patterns, although velocity field is noticeably larger during spring than in neap tides. In fact, spring tides not only generate stronger currents and inject more energy, but also induce higher variability and, expectedly, rates of dispersion all over the basin. Even though the simulated period does not cover a seasonal cycle, some hints of seasonal variability are reflected in the monthly averaged velocity at the surface and the sea surface height (SSH) during the simulation months (Figure S3.2).

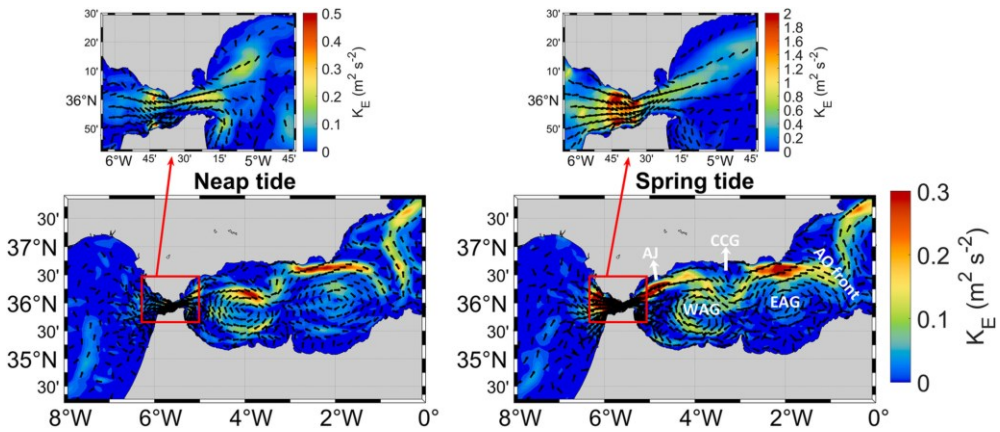


Figure 3.2. Surface current direction and kinetic energy per unit of mass ( $m^2 \cdot s^{-2}$ ) in the AS (lower panels) and in the SoG region (upper panels) during neap (left side) and spring tide (right side). The main surface structures sketched in Figure 3.1 have been tagged in the lower right panel using the same acronyms.

### 3.3.2 Releasing boxes and landing areas selection

To investigate the dispersion of blackspot seabream ELS in the area, a set of numerical experiments have been run and their outputs subsequently analyzed. All of them make use of what has been named “releasing boxes” and “landing areas” in this study. Releasing boxes embrace the most probable spawning areas of blackspot seabream. Three boxes have been established, two along the north and south shores of the SoG, labeled Tarifa and Tangier-Med, respectively (see inset in Figure 3.3), and a third one in between occupying the center-west area of the SoG (Tangier box). The three boxes not only cover what is currently thought to be the main spawning grounds of the species (Gil et al., 2001) but also address the geographical differentiation of the spawning area, which will have consequences on the spreading of the ELSs of blackspot seabream.

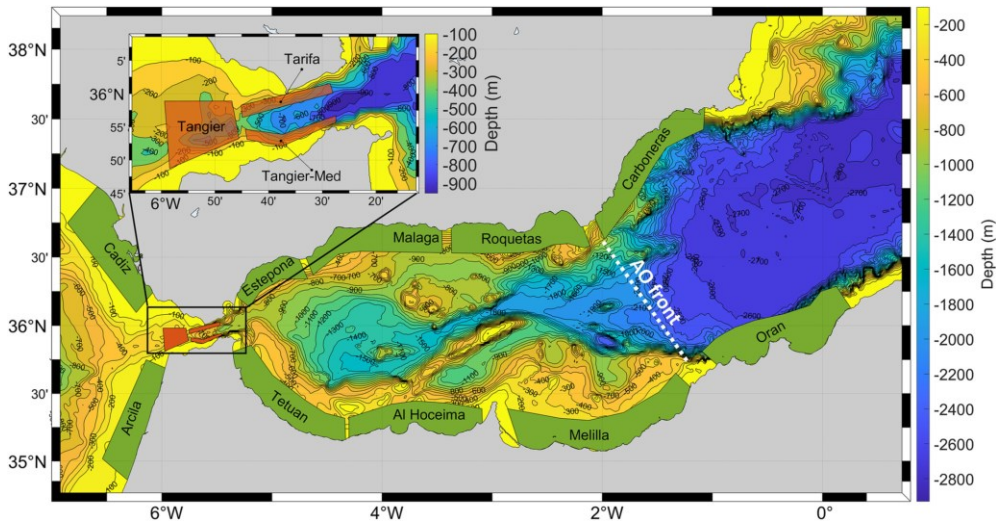


Figure 3.3. Map of the study area showing the releasing boxes of Tarifa, Tanger and Tanger-Med (brown polygons in the inset) and the landing areas of Cadiz, Estepona, Malaga, Roquetas, Carboneras, Oran, Melilla, Al Hoceima, Tetuan, and Arcila (green polygons). Adapted from CopeMed II, 2019.

These spawning products are then transported by the currents and their fate is interpreted in terms of concentration within landing areas, which are understood as potential coastal nursery grounds. In a broad sense, a strip few kilometers wide along the coasts of the whole region should be considered as such. However, the remarkable spatial variability of the hydrodynamics of the region recommends the splitting of the strip into more reduced landing areas. The presence of notable topographic features such as Cape Tres Forcas, or Calaburras Point or Cape of Gata (see Figure 3.1) also favors this division. On the other hand, the zonal orientation of the AS suggests a mirror-like correspondence of landing areas in the north and south shores. According to these premises, a total of ten areas have been defined, five in each shore (Figure 3.3). Two of them are in the Gulf of Cadiz (Cadiz and Arcila) to check eventual westward transport of ELS, and other two in the opposite end of the region to the east of the AO front, out of the AS (Carboneras and Oran). The remaining six are located in the AS, two in the vicinity of the SoG (Estepona, Tetuan), which leaves them exposed to high-energy dynamics, two (Malaga, Al Hoceima) in the western Alboran basin under the influence of the WAG and the last two (Roquetas, Melilla) in the eastern basin under the influence

of the EAG. All the landing areas are attached to the shore and subjected to different oceanographic regimes.

### 3.3.3 Lagrangian particle tracking and experimental setup

A Lagrangian particle tracking algorithm (LaCasce, 2008; Nicolle et al., 2013, 2017) has been used to study the transport and dispersion of blackspot seabream ELS. A detailed description of the procedure can be consulted in Sammartino et al. (2017). In this Lagrangian approach, eggs and larvae are virtual passive tracers during the PLD phase. Larvae swimming capability, although barely known, appears to be insufficient to overcome the strong currents of this region and has not been considered. Therefore, ELSs are just advected by the model horizontal velocity. The horizontal trajectories have been computed by integrating the bilinearly interpolated horizontal velocity field at every grid point of the domain using a Runge-Kutta fourth-order scheme (Rossi et al., 2014). Vertical larvae migration is a sensitive information that is not yet demonstrated for the studied species, so it has been neglected for simplicity (Rodríguez et al., 2001).

In order to investigate the influence of the depth on the dispersion patterns, five different vertical spawning layers have been selected: surface (from 0 to 3 m), 12 m (from 10 to 14 m), 25 m (from 23 to 28 m), 52 m (from 48 to 56 m), and 81 m (from 76 to 87 m). To account for the effects of the time variability associated with tides, releasing times have been selected with the aim of covering a wide variety of tidal conditions that combine semidiurnal phase during four fortnightly cycles. This approach allows for replicating four times every tidal condition. Figure 3.4 gives information on the tidal conditions at the moment of the release for all the experiments. Lagrangian particle tracking simulations have then been run starting from every releasing time during a period of 60 days, which is the maximum PLD estimated for the blackspot seabream (Peleteiro-Alonso et al., 1997).

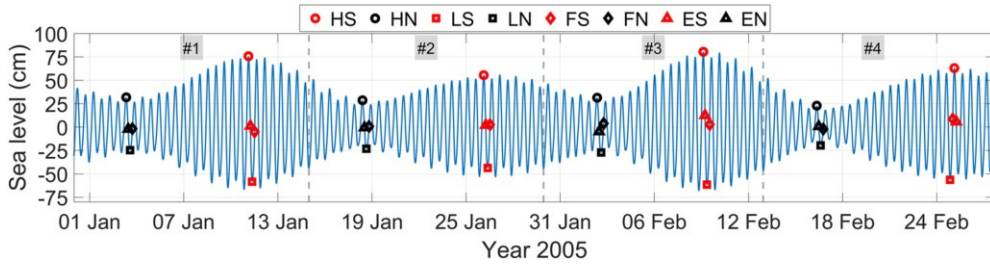


Figure 3.4. Sea level in Tarifa (blue line) during the period used for ELS release. Releasing times are shown by symbols whose meaning is indicated in the legend. It makes use of the following code to specify tidal conditions: first letter refers to tidal phase according to: H, high water; L, low water; F, maximum flood (westward) tidal current; E, maximum ebb (eastward) tidal current. Second letter specifies the fortnightly cycle according to: S, spring; N, neap tides. The gray vertical lines divide the series into four pieces that correspond to each replica.

### 3.3.4 Pool of experiments and connectivity computation

The combination of spatial and temporal conditions gives a total of 160 numerical runs per releasing box (4 tidal phase  $\times$  2 tidal strength  $\times$  4 replicas  $\times$  5 depths), or a grand total of 480 experiments for the three boxes. The following table (Table 3.1) summarizes the set of numerical batches combination that has been performed with the numerical model.

Table 3.1. Summary of the different spatial and temporal conditions configured in each numerical experiment.

Releasing area	Spawning depth	Tidal phase	Tidal strength	Releasing times	Total
Tarifa	[1,12,25,52,81]	[High, Low, Ebb, Flood]	[Spring, Neap]	[#1, #2, #3, #4]	160
	[120,150]	[Flood, Ebb]	[Spring, Neap]	[#2, #4]	16
Tangier-Med	[1,12,25,52,81]	[High, Low, Ebb, Flood]	[Spring, Neap]	[#1, #2, #3, #4]	160
	[120, 150]	[Flood, Ebb]	[Spring, Neap]	[#2, #4]	16
Tangier	[1,12,25,52,81]	[High, Low, Ebb, Flood]	[Spring, Neap]	[#1, #2, #3, #4]	160
<b>Total</b>					512

*Note: From left to right: Releasing area refers to the assumed spawning zones of blackspot seabream. Spawning depth represent the depth of the spawning layers; the five depths in the range [1–81]m corresponds to the main analysis (black text), and depths 120 m and 150 m, to the tests carried out in the boxes of Tarifa and Tangier-Med to assess depth sensitivity (gray text; see Section 2.2 for details). Tidal phase refers to tidal conditions within the semidiurnal cycle (see also Figure 4): High and low correspond to high and low water, ebb is the time of maximum eastward tidal current, which happens mid-time from high-to-low water and flood is the time of maximum westward tidal flow (from low to high water). Tidal strength denotes spring and neap tides within the fortnightly cycle. Releasing times refer to the four replicas of every single experiment carried out in different times, as indicated by the numbered boxes in Figure 4. Last column is the total batch of experiments for the main analyses and the sensitivity tests.*

As the analysis searches for ELS within each of the 10 landing areas in each experiment, a total of 4800 cases have been handled for the main analysis (to which 320 more from the depth-sensitivity study must be added). For each experiment, ~1000 particles have been released, and the position of each particle has been computed every 5 min. The huge amount of information needs to be processed and summarized in order to depict a relatively straightforward pattern of the ELS dispersal pathways. From an ecological point of view, dynamic connectivity is usually assessed as the percentage of particles (ELS) collected in a landing area  $b$  at a time  $t(p_b(t))$  compared with those released in box  $a$  (Cowen et al., 2006; Crochelet et al., 2016; Gamoyo et al., 2019; Nicolle et al., 2017), where  $t$  corresponds to a certain PLD, or to a fraction of it, which is fixed *a-priori*:

$$C_{a \rightarrow b}(t) = \frac{p_b(t)}{p_a} \cdot 100$$

In these works, the output usually consists of a connectivity squared matrix in which each cell is the probability of exchange of individuals between regions (row and column of the matrix), and the diagonal stands for the local-retention that is, the percentage of ELS released and settled in the same box (Cowen et al., 2006). However, this approach is inappropriate in this study for two reasons. First, releasing boxes are different from landing

areas because of the biological habits of the blackspot seabream, which has its only spawning area in the SoG. Hence, a reciprocal connectivity matrix is not feasible. Second, the strong and highly variable dynamics of the region makes the propagules to be swiftly advected away shortly after the release, hampering larval retention (Gil Herrera, 2006, 2010).

Figure 3.5 illustrates the shortcomings of this standard approach when it is applied to this study. It shows the time evolution during the first 12 days of simulation of the percentage of particles collected in Estepona landing area that were released at the surface in Tarifa releasing box (see Figure 3.3) under high-spring tidal conditions. The percentage may change from 10% to 90% in few hours (also the reciprocal), which makes meaningless the computation of the connectivity at a given time because of its strong dependence on the selected instant: the resulting value will not be representative.

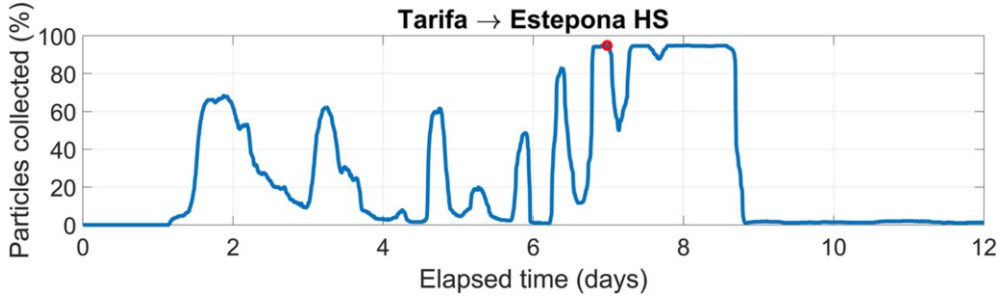


Figure 3.5. Time series of the percentage of ELS released in Tarifa box at the surface that were found in Estepona landing area as a function of time, in a high-spring (HS) tide scenario. Red dot indicates the maximum value of 94.85% on day 7.

In order to cope with this limitation, an alternative connectivity definition is adopted as the maximum percentage of particles (MPoP hereinafter) collected in each landing area throughout the total duration of simulation (60 days; see Section 3.3.3):

$$C_{a \rightarrow b} = \max \left( \frac{p_b(t)}{p_a} \right) \cdot 100$$

Associated with this maximum percentage is the time at which it is achieved (time of maximum connectivity; ToMC hereinafter). This time is of



concern as far as it must be compared with the actual PLD. Notice that contrary to the fixed time interval, the ToMC is not imposed or prescribed a-priori, but it is deduced from the analysis.

### 3.4 Results and discussion

#### 3.4.1 MPoP and ToMC averages

Table 3.2 shows the MPoP released at the three boxes that were found in the different landing areas and the ToMC when this percentage is attained. They are averaged over the whole combination of spatial and temporal releasing conditions and provide global connectivity values that summarize the huge amount of information generated in the study. Table 3.2 highlights the fundamental role of the eastward flowing AJ, which is responsible for the direct spread of the ELS released in the SoG toward the AS and the nearly null abundance of particles in the Atlantic landing areas of Cadiz and Arcila.

Table 3.2. Maximum percentage of particles (MPoP column) and time of maximum connectivity (ToMC column) of ELS with their corresponding standard deviations for all landing areas and releasing boxes, averaged for all scenarios of initial conditions.

Landing area		Tarifa		Tangier-Med		Tangier	
		MPoP (%)	ToMC (days)	MPoP (%)	ToMC (days)	MPoP (%)	ToMC (days)
Northern coast	Cadiz	0 ± 0*	1 ± 3	0	-	0 ± 0*	1 ± 4
	Estepona	38 ± 11	4 ± 3	8 ± 8	21 ± 9	10 ± 6	13 ± 6
	Malaga	45 ± 12	7 ± 3	11 ± 8	22 ± 9	15 ± 7	11 ± 6
	Roquetas	17 ± 8	22 ± 8	5 ± 4	32 ± 6	5 ± 4	26 ± 7
	Carboneras	6 ± 4	31 ± 7	2 ± 3	33 ± 6	2 ± 2	35 ± 6
Southern coast	Arcila	0	-	0 ± 0*	1 ± 2	1 ± 2	5 ± 5
	Tetuan	8 ± 5	30 ± 13	45 ± 19	25 ± 9	33 ± 17	25 ± 7
	Al Hoceima	8 ± 5	34 ± 8	17 ± 18	40 ± 9	14 ± 13	41 ± 11
	Melilla	6 ± 3	41 ± 10	4 ± 3	46 ± 8	3 ± 2	47 ± 9
	Oran	14 ± 4	36 ± 7	5 ± 3	42 ± 6	6 ± 4	38 ± 8



*Note: Landing areas have been grouped according to its geographical location. Asterisks indicate values of MPoP very close to zero (that round to zero), but not strictly null. In such situation, the ToMC is meaningless, and these cases are ignored and not discussed in the text. The two special cases of Tarifa–Arcila and Tangier–Med–Cadiz in which MPoP is strictly null; the ToMC is not defined.*

A high connectivity (i.e., high value of MPoP) for Tarifa releasing box is observed in Malaga, Estepona, and Roquetas landing areas (45%, 38%, and 17%, respectively), followed by Oran (14%). This spatial pattern is to be expected as the AJ acts as the main advection mechanism (see Figure 3.1). Carboneras landing area, located outside of the AS on the northern shore, stands apart from the path of this stream and, consequently, the MPoP falls well below the previous values. A weak north-to-south connectivity is inferred from the non-null MPoP of 8% computed in Tetuan and Al Hoceima. This spatial distribution is consistent with results of larvae distribution obtained from samples collected during a scientific survey carried out in the area in the late winter 2020: a considerable number of larvae (~8 mm length) of *P. bogaraveo* were collected in the AS, the greatest abundance (from 10 to 14.96 larvae 10 m<sup>-2</sup>) having been found in Estepona and Malaga coasts (TRANSBORAN survey; J.M. Rodríguez, Pers. Comm.).

Similar zonal spread is found in the case of Tangier-Med releasing box, the southern counterpart of Tarifa box. Highest connectivity is reached in Tetuan and Al Hoceima in the south shore (MPoP of 45% and 17%, respectively). Again, a south-to-north connection is suggested by the significant MPoP of 11% and 8% in Malaga and Estepona, respectively, though the associated standard deviation, which is comparable to the mean, sheds uncertainty on the result. Roquetas and Oran areas have values of 5%, compatible with the isolation effect of the eastern rim of the WAG and the own EAG. This effect would also explain the very low values in Melilla and Carboneras (4% and 2%, respectively). Results for Tangier releasing box are similar to those of Tangier-Med. The reason is the Coriolis force that deflects particles to the south within the limits of the very SoG before the AJ spreads into the AS (Albérola et al., 1995). Therefore, once the ELSs enter the AS, their trajectories

should not be much different regardless the particles were released in one box or the other.

ToMCs in Table 3.2 are consistent with the ELS dispersal inferred from the MPoP analysis. Shorter ToMCs are found in the landing areas closer to the releasing boxes. For particles released in Tarifa box, the shortest time is found in Estepona area (4 days). The result applies for Tangier-Med and Tangier boxes and Tetuan landing area in the southern coast (3 and 4 days, respectively). A shorter ToMC is obtained for Tangier box and Arcila area (1 day), but the very low MPoP of 1% in the area makes it not worth discussing. As distances increase, ToMC also does. In the case of Tarifa box and for northern landing areas, the greatest ToMC is found in Carboneras, the easternmost area (31 days). The same applies in the south coast, where the easternmost area (Oran) shows ToMC of 46 and 47 days with Tangier-Med and Tangier boxes, respectively. A curious case that deserves comment is that the northern landing areas have shorter ToMC with these two releasing boxes than the areas in the south (except for Tetuan). The interpretation of this somewhat anti-intuitive result is the advection of ELS by the western rim of the WAG towards the north shore. Once there, the products follow similar trajectories as the particles released in Tarifa box.

These scenario-averaged values reflect the prevailing role of the main dynamic structures of the SoG-AS system on the ELS dispersion and provide foreseeable connectivity patterns. Nonetheless, the large standard deviations (uncertainties) associated to the mean values reveal high variability related to the temporal and spatial variability of the SoG hydrodynamics as well as to the very location of the releasing boxes. These issues are addressed next for Tarifa (Section 3.4.2.1) and Tangier-Med (Section 3.4.2.2) boxes. Tangier box is presented in Figure S3.3 due to the aforementioned similitude with Tangier-Med, and it is not discussed here.

### 3.4.2 Release area dependency

#### 3.4.2.1 Tarifa releasing box

Table 3.2 shows that, as a result of the advection by the AJ, the main connections of ELS released at the surface in Tarifa box take place with the northwestern areas of the AS. However, some differences appear when specific tidal conditions and depths are considered (Figure 3.6). (Figure 3.6a shows that the highest connectivity in Estepona for surface release is achieved under ebb (E) condition in spring (S) tide (~60%), when the eastward flow in the SoG is boosted by the strong ebb current of spring tides. The same applies for near-surface releases, 12 and 25 m, which give MPoP values of ~63% and ~61%, respectively. In Malaga, MPoP is consistently greater and, somewhat paradoxically, ToMC is smaller in neap than in spring tides (Figure 3.6b). The behavior is reproduced by the remaining landing areas of the northern coast. As the distance of the landing area increases, however, the ratio of MPoP neap/spring increases until it reaches the highest value in the farthest landing area of Carboneras (Figure 3.6a).

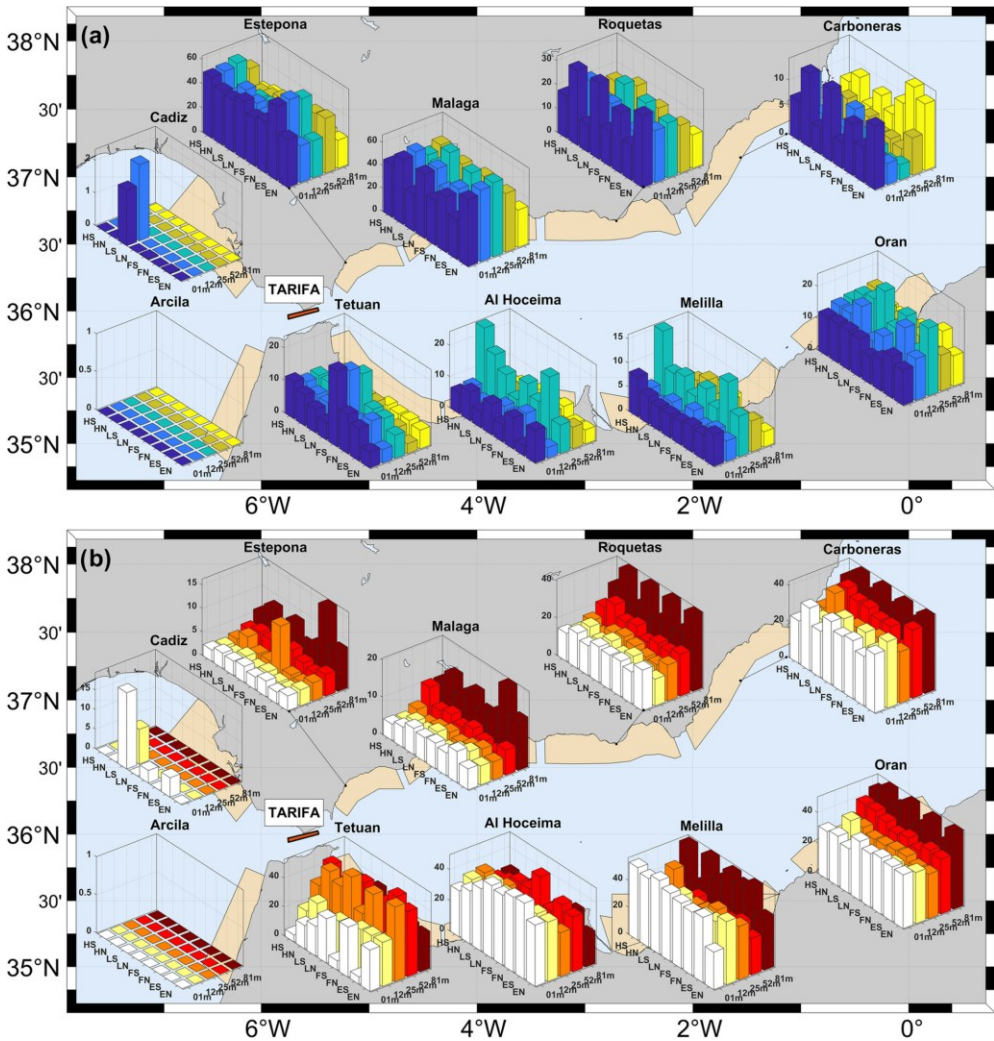


Figure 3.6. (a) Diagrams of MPoP (%) in each landing area, averaged over the four replicas of the ELS released at Tarifa box (red rectangle) for the 40 combinations of spatial (5 depths, Y-axis) and temporal (8 tidal conditions, X-axis; see acronym code in Figure 3.4) conditions. (b) Same as panel (a) for ToMC (days). Notice the changing Z-axis scale in the different diagrams of both panels.

The effect that initial conditions in Tarifa box has on the dispersal patterns is less defined in the southern landing areas. MPoPs are systematically inferior to their mirror area in the northern shore except for the two easternmost areas, with Oran showing a slightly higher MPoP than Carboneras. Such structure emphasizes the fact that north-to-south connectivity is less achievable than west-to-east connectivity due to the role

of hydrodynamic barrier played by the AJ for meridional exchange. ToMCs are consequently greater than in the northern areas, except for Tetuan in spring tides, where they are similar to those found in Estepona in the north (Figure 3.6b).

The behavior in Tetuan contrasts with the much larger ToMCs in the other southern landing areas, which are rather independent of the tidal variability. Two different mechanisms seem to be at work. Particle scattering promoted by the intensified inflow would be the reason for the reduced ToMC in Tetuan during spring tides (Figure 3.6b) and for the relatively large MPoP of 23% under FS conditions in particular (Figure 3.6a). ToMCs in the three other areas, on the contrary, are rather independent of tidal conditions (Figure 3.6b). The interpretation given to this different response is that Tetuan area is directly reachable by southeastward trajectories scattered from Tarifa releasing box during the spring tide periods of enhanced currents. This process is unfeasible for the three other areas where particles will most likely arrive after completing one WAG turn around at least. It requires a time long enough to smooth out the effects of the SoG tide and the particles end up being transported by a tidal-free large-scale circulation that propitiates ToMC as large as 40 days in Al Hoceima, in sharp contrast with the scarce 6 days of Tetuan in spring tides (Figure 3.6b).

#### 3.4.2.2 Tangier-Med releasing box

The most obvious feature is the high MPoP in the nearest eastward landing area of Tetuan, increased during spring tides to values of  $\sim 60\%$  (Figure 3.7a). The behavior resembles the east-to-west connectivity between Tarifa and Estepona area in the northern shore. Both would have the same cause, which is the zonal advection by the AJ. But the similitude Tarifa-northern areas versus Tangier-Med-southern areas finishes just here. Whereas in the first case MPoPs were clearly higher in all northern areas of the AS, in the case of Tangier-Med releasing box, south areas of Al Hoceima and Melilla have MPoP of the same magnitude, if not less, than in the north areas. In other words, zonal connectivity in the south is not as efficient as in the north, except for Tetuan area.

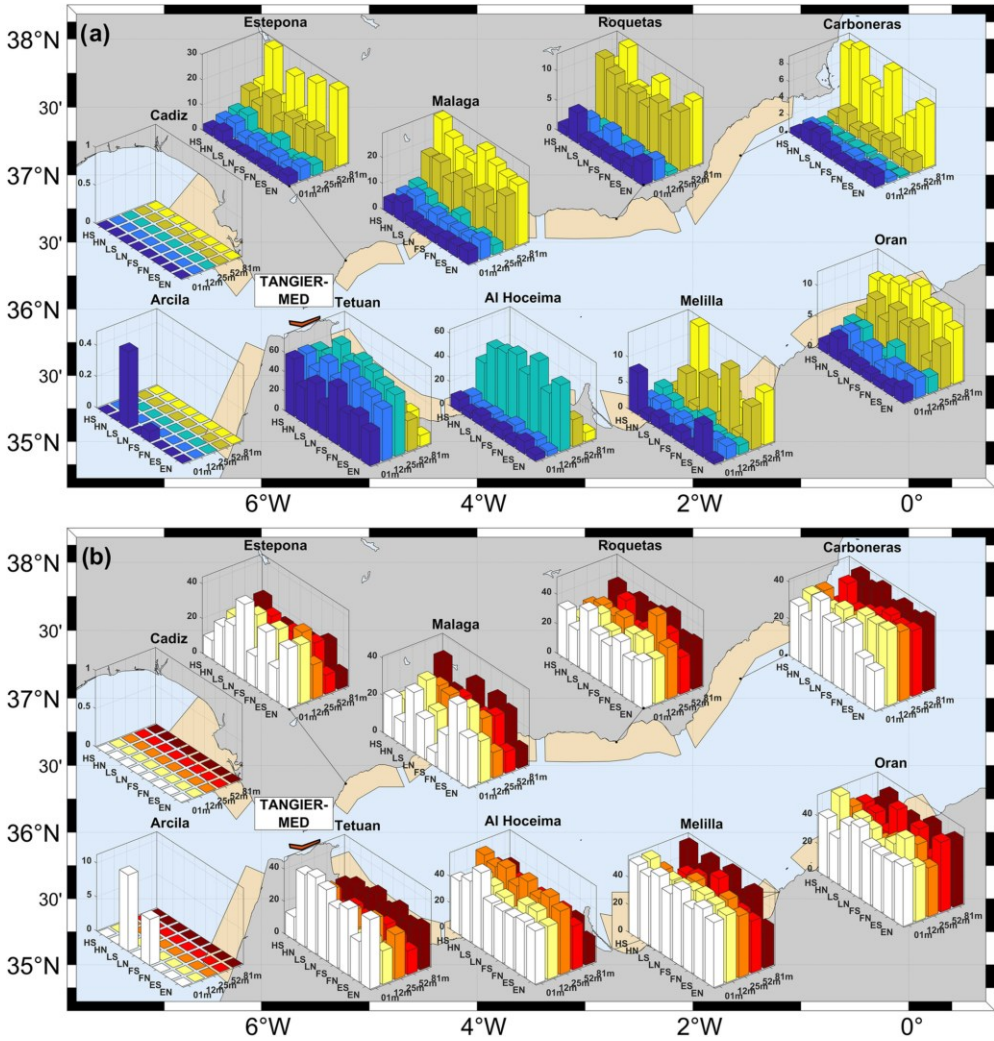


Figure 3.7. Same as Figure 3.6 for Tangier-Med releasing box, indicated by the red polygon.

The explanation provided for this unexpected behavior is that the coastal eddy that usually forms south of the AJ and close to the African shore at the exit of the SoG (Sánchez-Garrido et al., 2013; see Figure 3.1 and Figure 3.2) favors high MPOps in the Tetuan area. This structure propitiates ELS retention. The trapped propagules can be eventually transferred to the western rim of the WAG and advected to the northern coast, making south-to-north connectivity feasible, and hampering west-to-east transport. The rather low values of MPOp in the upper layers of the northern areas indicate

that the connection is weak. However, and this is an intriguing question, the connectivity increases with depth (Figure 3.7a, yellow bars), a behavior not shared so clearly by the southern areas. Such increase raises new questions because, intuitively, connectivity should be greater at the surface, where the WAG and EAG hold stronger currents. But high velocities also entail more instabilities and turbulence that increase ELS scattering toward the interior of the Alboran basin. Velocity reduction with depth would diminish the scattering and improve the chances for ELS to arrive to farther landing areas. Consistent with this conceptual model is the fact that MPoPs at 81 m depth tend to reach absolute maxima during neap tides in Estepona area (Figure 3.7a).

ToMC also shows unexpected behavior. The most striking one is the large values in Tetuan area considering its proximity to the releasing box. ToMCs are even noticeably larger than those obtained for the Tarifa releasing box, particularly during spring tides (compare Figure 3.6b and Figure 3.7b). Particles released in Tarifa box reach Tetuan area much faster than those released in Tangier-Med under the same initial conditions. It is particularly true during spring tides. But the number of particles that reaches the area is appreciably less when they come from Tarifa box (Figure 3.6a,b). Same conclusions apply to the other areas, the northern ones showing less ToMC than the southern ones systematically. This would confirm the aforementioned slightly better connectivity that this releasing box establishes with the north part of the AS.

Regarding the areas in the Gulf of Cadiz, Figure 3.6 and Figure 3.7 show very poor connectivity for both releasing boxes that only occurs in zonal direction (Tarifa-Cadiz, Tangier-Med-Arcila), not north-to-south (Tarifa-Arcila, Tangier-Med-Cadiz). It is almost uniquely met under LS initial conditions, that is, particles released at low water in spring tides. They are the most favorable conditions, as low water is the moment when barotropic tidal current reverses towards the Atlantic and spring tide enhances its intensity. The low-to-high semicycle that follows maintain relatively



favorable conditions for westward transport, which causes the very low, though not null, MPoP found in those areas.

Previous discussion indicates that the dispersal of ELS is highly sensitive to the tidal phase and depth. Tidal phase and, more specifically, tidal strength related to the fortnightly spring-neap cycle is relevant for Tarifa releasing box (Figure 3.6) while spawning depth causes higher variability in the Tangier-Med case (Figure 3.7). Both initial conditions are examined in more detail for selected cases of study in the following sections.

### 3.4.3 Tide dependence: A case study in the northern shore

In addition to the tidal variability that can be inferred from the abundant information in the diagrams of Figure 3.6 and Figure 3.7, part of which has been already commented, this section addresses an illustrative case of study to assess the tidal influence. The specific instant of spawning in a given semidiurnal cycle (tidal phase) affects the initial ELS dispersion trajectories at the very beginning of the experiment, as it depends on the direction of the instantaneous velocity at that time. Its importance, however, fades out shortly after because of its short time scale that implies reduced Lagrangian correlation scales (G. I. Taylor, 1922), leaving only the effect of the spring-neap intensity. It mostly determines the final evolution of ELS dispersion in the middle-long term, as it is demonstrated in the following case of study that involves Tarifa box and Estepona and Malaga landing areas in the north coast.

Figure 3.8 shows that the dispersion of ELSs released in Tarifa that induces the AJ in spring tide is greater than in neap tide (see inset) because of stronger tidal currents. When ELSs enter the AS in spring tide, the augmented scattering allows particles to reach the nearer landing areas directly, whereas particles follow the farther-from-shore AJ trajectory in neap tides (inset of Figure 3.8). As a result, particle concentration in Estepona is much higher in spring tide (Figure 3.8, solid lines). The deflection to the south of blue lines in the inset also illustrates the already discussed result of enhanced MPoP in Tetuan area in spring tides (Figure 3.6a). The progressive decrease of



connectivity from HS to FS in spring-tide experiments (solid lines in left panel of Figure 3.8) follows the fact that eastward velocity reaches larger values during ebb tide (from HS to LS, peaking at ES) and a minimum at FS. Notice, however, that these differences are less than the ones observed between spring and neap tides (compare solid and dashed lines in this panel). It confirms the fact that tidal strength is more influential than tidal phase, what is further supported by the fortnightly modulation of ToMC in this area, with systematically shorter times in spring tides (Figure 3.6b).

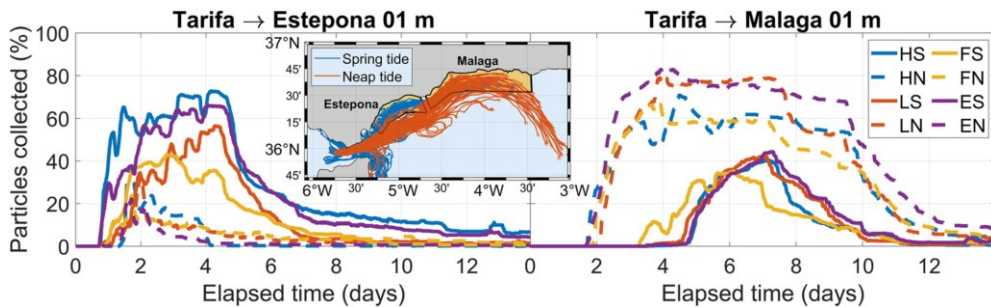


Figure 3.8. Time series of percentage of particles released at the surface in Tarifa releasing box collected in Estepona (left panel) and Malaga (right panel) for all tidal combinations discussed in text (see legend). The inset shows trajectories for the whole combination of phases in spring (blue lines) and neap (red lines) tides during the first 6 days after the release.

The opposite situation is seen in Malaga area (Figure 3.8, right panel), where particle percentages in neap tides is almost twice than in spring tides. Moreover, as mentioned previously, ToMCs are greater in spring tides (Figure 3.6b). Inset in Figure 3.8 helps to explain these facts: during neap tides, a good fraction of trajectories invades directly the landing area (red lines), with reduced dispersion seaward. In spring tide, many particles arrive after having undergone some recirculation, a process that takes longer and results in greater ToMC, as discussed in Section 3.4.2.1. Also, more particles are scattered seaward, reducing the number of particles that reach the area. This behavior is shared by Roquetas and Carboneras landing areas to the east, confirming the better connectivity efficiency during neap tides (Figure 3.6).

### 3.4.4 Depth dependence

Figure 3.6 and Figure 3.7 show that, on average, MPoP tends to increase with depth in all landing areas and for all releasing boxes and, simultaneously, ToMC tends to be shorter. On the other hand, the present uncertainty on the actual spawning depth of the blackspot seabream along with the marked baroclinity of the exchange through the SoG raises the question of whether the so far ignored westward connectivity gains prominence for hypothetical deeper layers of spawning. Both questions are addressed next:

#### 3.4.4.1 A case study of south-to-north connectivity as a function of depth

Figure 3.7a shows a rather clear increase of MPoP with depth in all landing areas of the north coast for particles released in Tangier-Med box. For Estepona area, this depth dependence is concomitant with the spring-neap fortnightly modulation. Overall, the influence of depth on the connectivity is less marked than that associated to tides and does not exhibit a regular pattern. Nevertheless, the diminution of the AJ intensity with depth allows for establishing a rough analogy between releasing depth and strength of the tide. For a given tidal condition, the patterns associated with releasing at the surface would differ from those at depth in a similar way to how patterns produced during spring tides differ from neap tides for a given depth.

Figure 3.9 illustrates the connectivity between Tangier-Med box and Estepona landing area under HN initial conditions (release at high water in neap tides). The larger surface current scatters more particles than the diminished current at 81 m depth, resembling the pattern observed in the case of spring against neap tides in the previous discussion. As a result, arrival time of particles released at surface levels ( $z \leq 25$  m) in Tangier-Med box is noticeably shorter ( $\sim 4$  days) than that of particles released at 25 m (ToMC  $\sim 7$  days) or 81 m (ToMC  $\sim 15$  days), and the chance of arrival is notoriously reduced (MPoP of 17% for 25 m, which increases to 32% at 52 m and to 78% at 81 m, see also Figure 3.7a). As the depth increases, ELSs follow smoothed trajectories with reduced dispersion, which improves not only the chance for more particles to arrive but also for them to arrive further. The behavior,

which can be applied to the other areas in the north coast, is similar to that described in neap tides for the connectivity Tarifa-Malaga.

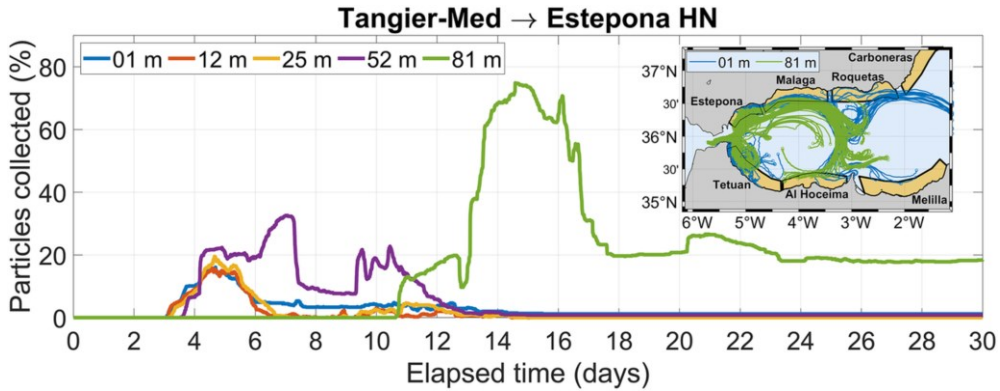


Figure 3.9. Time series of percentage of particles released in Tangier-Med releasing box under HN conditions and collected in Estepona landing area for the five depths considered (1, 12, 25, 52, and 81 m). Inset map shows trajectories for surface and 81 m depth spawning levels after 30 days of simulation using the same color code as in the main panel.

#### 3.4.4.2 A sensitivity analysis on spawning depth

The effect of depth on connectivity patterns, and its interaction with tide in the case of this species, raises the question of whether or not the species has adapted its life cycle to optimize the reproductive success. For instance, blackspot seabream should spawn at greater depths if the survival success relies on chances of reaching further landing areas (see previous section) with suitable nursery conditions. It represents a plausible method of colonization, which maximizes the population survival (Krueck et al., 2020). Selecting the highly dispersive environment of the SoG as spawning grounds almost rejects the hypothesis that this species attempts to maximize self-recruitment as observed in other species (e.g., European hake; Hidalgo et al., 2019). Since the SoG holds a permanent two-way exchange, depth results are critical to determine the direction of the ELS dispersion. At greater depths than those considered so far in the main study, eggs would be advected toward the Atlantic Ocean by the Mediterranean undercurrent and the connectivity with landing areas of the AS be drastically reduced.

Given the degree of uncertainty about the range of plausible spawning depths, it is worth exploring that possibility with the model. To this aim, a spawning depth of 150 m has been selected in Tarifa and Tangier-Med boxes and initial conditions of ES, EN, FS, and FN have been then applied. Figure 3.10 shows the trajectories of particles released at 52 and 150 m under identical initial conditions of maximum westward tidal current at spring (FS) and neap (FN) tides. In the case of 52 m depth, particles make small incursions to the west transported by the flood, west-going tidal current that overcomes the average eastward inflow during short intervals. After this otherwise brief current reversal, particles enter the AS and remain there following trajectories similar to those depicted in the previous section. At the deeper layer of 150 m, however, flood tidal current increases the Mediterranean undercurrent extant at this depth and ELSs will spread westwards, with no particles entering the AS. Therefore, Atlantic (Cadiz and Arcila) landing areas are accessible as far as the direction of propagation is concerned. However, both landing areas are shallower than 100 m, whereas ELS propagates at 150 m. Unless vertical and onshore motions occur, the connectivity with the selected Atlantic landing areas is unfeasible.

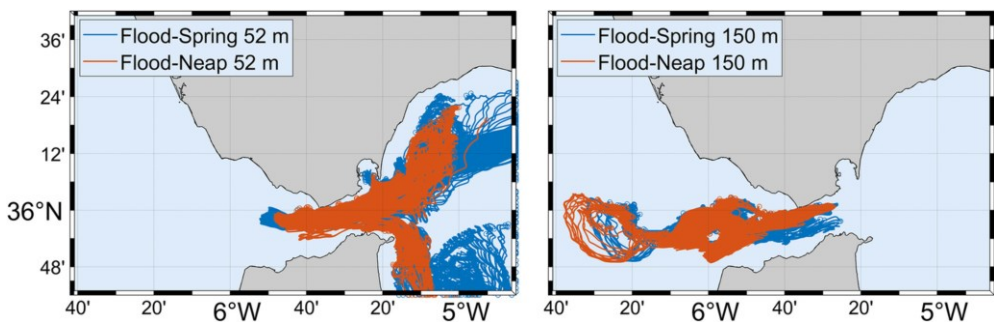


Figure 3.10. ELS trajectories after 3.5 days of simulation for particles released in Tarifa box at 52 m (left panel) and 150 m (right panel) in case of FS (blue lines) and FN (orange lines) initial conditions.

The western half of the SoG is a well-known mixing area with large vertical motions driven by the amazing internal tide generated by topographic interaction (García Lafuente et al., 2013; García-Lafuente et al., 2000; Wesson & Gregg, 1994). Such turbulent mixing is a potential

mechanism to bring particles to shallower layers, in a similar manner as it does the westerly inducing upwelling and turbulence in the Gulf of Cadiz (Navarro et al., 2011; Sánchez-Garrido et al., 2015). All of them can modify the horizontal depth of ELS advection but does not necessarily imply shoreward advection, which should be achieved by other concomitant processes.

Recent scientific surveys have detected ELSs of the species in the Atlantic region, but their relative abundances are noticeably lower than those reported in the Alboran basin: 0.46 larvae  $10 \text{ m}^{-2}$  ( $\pm 1.39$  SD) in the Atlantic region versus 2.03 larvae  $10 \text{ m}^{-2}$  (4.86 SD) in the northwest Alboran areas (maximum abundances of 5 and 15 larvae  $10 \text{ m}^{-2}$ , respectively; J.M. Rodríguez, Pers. Comm.). These observational and numerical results keep open the feasibility of the Atlantic connectivity, which requires further studies to give an adequate answer. Observational research on the spawning behavior is also needed to elucidate the question of the spawning depth range of the species. From a modeling perspective, new experiments are necessary to assess how different larval behavior (vertical migration) and hydrodynamic secondary patterns (vertical velocity ignored in this study) affect the dispersion patterns and survival probabilities of ELS under different scenarios.

### 3.4.5 A sensitivity analysis on PLD

From a biological point of view, time of arrival of ELS at a given landing area only makes sense if it is less than the assumed PLD of the species (Shanks, 2009). In order to investigate the dependence of connectivity on PLD, MPoPs between releasing boxes and landing areas have been recalculated for PLD windows of 15 and 30 days. The new values of MPoP (denoted by  $C_n$ ,  $n = 15, 30$ , in the following discussion), have been compared with those of the original PLD window of 60 days ( $C_{60}$ ), to obtain a metric  $\Delta_n$ , defined as the ratio:

$$\Delta_n = \frac{C_n}{C_{60}} \cdot 100$$

in order to assess the differences.

Table 3.3 summarizes the results of this analysis and confirms the fact that the MPoP is constrained by the available time of arrival, that is, the assumed PLD. In the landing areas nearest to the releasing boxes (i.e., Tangier-Med/Tangier – Tetuan, Tarifa – Estepona) arrival times keep on being short and maximum ratios obtained with different PLDs (15, 30, 60 days) are little altered (high values of  $\Delta_n$ ,  $n = 15,30$ ). On the contrary, in the furthest landing areas (Carboneras, Melilla, or Oran), large MPoPs are only obtained after completing a long path that requires dilated elapsed times, which makes the result sensitive to the assumed PLD. It results in substantial discrepancies (low ratio values). Extreme cases are provided by Tarifa-Carboneras or Tangier-Med/Tangier-Melilla, which shows ratios of  $\Delta_{15}$  less than 1%. The range of variation of the MPoPs recalls the need of improving the knowledge about the blackspot seabream life cycle, particularly PLD.

Table 3.3. Differences of MPoP computed using PLD windows of 60 and 30 days ( $\Delta_{30}$  column) and 60 and 15 days ( $\Delta_{15}$  column) for the three releasing boxes and the Alboran Sea landing areas.

Landing area		MPoP differences (%)					
		Tarifa		Tangier-Med		Tangier	
		$\Delta_{15}$	$\Delta_{30}$	$\Delta_{15}$	$\Delta_{30}$	$\Delta_{15}$	$\Delta_{30}$
Northern Alboran	Estepona	77.69	92.79	49.65	83.79	50.22	84.40
	Malaga	62.02	94.37	62.49	94.20	63.20	95.60
	Roquetas	27.16	72.97	40.35	80.40	37.96	79.02
	Carboneras	0.92	36.55	2.290	31.31	1.610	26.19
Southern Alboran	Tetuan	89.90	95.92	96.10	98.60	95.56	99.16
	Al Hoceima	68.57	89.70	74.89	88.01	74.14	84.50
	Melilla	2.77	41.34	0.56	28.40	0.41	34.30
	Oran	7.44	55.11	3.59	61.64	1.47	60.07

*Note: Cadiz and Arcila have been excluded because of its low representativeness.*

### 3.4.6 Release time dependency (replicas)

To prove the representativeness and reliability of the Lagrangian particle tracking experiments, the uncertainty of each single run has been assessed by means of four replicas of the same combinations of semidiurnal tide and depth conditions during four fortnightly cycles. Despite the same initial conditions with respect to the releasing time, the overall situation is not exactly the same in the replicas. This is so because the four spring-neap tidal cycles considered comprises the monthly cycle arising from the modulation of the semidiurnal constituents  $M_2$  and  $N_2$ , responsible for the greater similarity of alternate than contiguous spring cycles. In addition, subinertial meteorologically induced fluctuations due to atmospheric pressure and wind variations change from one replica to the other.

The unavoidably, yet small, difference of the initial conditions of the replicas lead to concomitant differences in the outputs (not shown for the sake of clarity) and allows for assessing the variability of each experiment by means of the standard deviation of the four replicas. The averaged standard deviation of the whole pool of experiments is  $\sim 8\%$ , which is approximately the same value obtained by comparing scenarios of different tidal phases but the same tidal strength. If the metric is used to compare spring and neap tidal scenarios (different tidal strength), the averaged standard deviation is  $\sim 30\%$ . Therefore, subinertial variability and lower frequency tidal modulations could account for approximately one quarter of the variability of the fortnightly tidal cycle, which has been shown to be the prevailing factor for connectivity.

### 3.4.7 Implications for the species assessment and management

Transboundary fish stock management is based in the cooperation and collaboration among countries to assess shared resources status and regulate harvest according to common measures and controls or joint decision-making. However, to build an effective management framework, a solid scientific basis is required. The present study provides this basis to potentially improve the assessment and management of this species



harvested by Moroccan and Spanish fleets, while we acknowledge that further work is needed. First, it provides evidence of the differential role of different spawning grounds in the AS, which could be useful in the future if the spatial dynamics is implemented in the stock assessment models and procedures (e.g., (Goethel & Berger, 2017; Punt, 2019)). While the results of the study point at independent dispersal and connectivity patterns of north and south Strait spawning grounds due to the role of the AJ, they do not imply stock differentiation consistent with recent genetic studies (Spiga, 2020), but different spawning locations, which is an important element to be considered in spatial stock structure approaches. Second, in terms of spatial management and potential spatio-temporal closures already applied to other Mediterranean species (Regulation [EU] 2019/1022 of the European Parliament and of the Council of June 20, 2019, OJEU L172/1 and GFCM Recomm. GFCM/42/2018/5), the study facilitates information of the role of the spawning sites investigated, and also the interaction with depth and tidal regime that could potentially lead to seasonal or, even, short term (i.e., attending to tidal phase) fisheries closure. The information made available here is relevant for the ongoing process for the establishment of a specific joint (Spain and Morocco) management plan for blackspot seabream in the SoG within the framework of GFCM (2021). Notwithstanding, further studies are needed as it is not yet clear whether the spawning strategy of the species attempts to minimize dispersal time, maximize dispersal distance, or even a more complex trade-off between both. The interpretation and implications of the results presented in this study can be certainly different attending to the species strategy. The role of other important larval traits not included in this study requires also further research.

### 3.5 Summary and future works

The differences observed in the ELS connectivity patterns are mainly caused by the geographical location of the spawning areas in the SoG (north shore versus south shore). From a hydrodynamic perspective, the mean circulation patterns favor the zonal (west-to-east) connectivity: Particles released in the northern margin of the Strait are mostly registered in the



northern areas of the AS, while particles released in the south are collected in the southern shores of the AS. Thus, the eastward transport linked to the AJ entering the Alboran basin appears as the main mechanism of connectivity. On the other hand, meridional connectivity (north-to-south, south-to-north) is hampered by the very AJ that is a potential hydrodynamic barrier (García-Lafuente, Sanchez-Garrido, et al., 2021). Overcoming this obstacle depends on the stability of the mean patterns of circulation of the SoG-AS system and its evolution. Non-geostrophic motions, instabilities associated with the WAG-AJ collapse (García Lafuente et al., 1998; García-Lafuente, Sanchez-Garrido, et al., 2021; Sánchez-Garrido et al., 2013) or the AJ meandering (García Lafuente & Delgado, 2004) or, even, the WAG or EAG themselves can entail occasional meridional ELS transports. For instance, the study shows that ELSs released in Tangier-Med box are more susceptible to latitudinal (south-to-north) migration. Apparently, Tetuan area in the south exhibits characteristics of particle concentration/retention zone related to the existence of a small cyclonic eddy between the African coast and the WAG (Figure 3.1). Particle transfer from the eddy to the north-flowing western rim of gyre is practicable, after which particles reach the northern areas without impediment. This process impairs west-to-east connectivity in the south coast, which is therefore less efficient than in the north coast (compare Figure 3.6a and Figure 3.7a). Another example is provided by the EAG, whose eastern edge can transport particles from the north to the south. This process makes Oran landing area be connected with Tarifa releasing box in the north better than with Tangier-Med in the south, despite being in the same coast (Table 3.2).

Atlantic, that is, east-to-west, connectivity at surface layers is prevented by the AJ. But it does not have to be so at greater depths where the Mediterranean undercurrent flows. In a hypothetical situation of deeper spawning (150 m), the model shows ELS transport towards the Atlantic Ocean exclusively, which opens the possibility of connection with landing areas in the Gulf of Cadiz (Cadiz, Arcila). However, achieving a successful connectivity with Atlantic landing areas requires additional processes to carry the ELS to shallower levels. Enhanced tidal mixing and turbulence occurring

in the western part of the SoG, or wind-inducing upwelling in the Gulf of Cadiz are candidate processes.

Tides in the neighborhood of the SoG are influential. Variability due to tidal forcing is especially noticeable in terms of fortnightly modulation. In the landing areas closer to the spawning boxes (Estepona in the north, Tetuan in the south), connectivity is more efficient in spring tides. In these conditions, north-to-south connectivity is achieved by direct advection of ELSs from the releasing box of Tarifa to Tetuan landing area (Figure 3.6; see also inset in Figure 3.8). During neap tide, on the contrary, particles suffer less scattering and increase chances of reaching further landing areas. Overall, tidal conditions depict two different mechanisms: spring tides tend to favor connectivity (increase MPoP) by the direct advection promoted by the increased energy of the flows. It applies to landing areas adjacent to the releasing boxes in both, west-to-east and north-to-south, directions and yields relatively small ToMC. On the contrary, in neap tides connectivity is mainly achieved by the mean circulation of the AS, connecting far away landing areas with releasing boxes after considerably large ToMC (Figure 3.6 and Figure 3.7). This pattern is consistent with previous studies on connectivity analysis in the region (Muñoz et al., 2015), who used altimetry-derived geostrophic currents, a product that removes tidal contribution during the data-processing. The circulation emerging from such an approach would be more similar to the pattern of neap tides (less tidal variability) inferred from the numerical outputs.

The depth of spawning also results in different patterns of conductivity. Obviously, the greatest differences arise when comparing patterns associated with spawning at depths immersed in one or another layer of the baroclinic exchange, as illustrated by the case of 150 m releasing depth already discussed. But there are still differences even if spawning takes place at different depths within the very surface layer (Figure 3.6a and Figure 3.7a). The origin of the differences has been ascribed to the diminution of the velocity of the current with depth. At shallow depths, ELSs are scattered more actively by the more energetic current, recalling the effect of the spring tide. At deeper layers, the main circulation weakens and allows ELS to move less

chaotically and reach greater distances. The behavior resembles the pattern observed during neap tides, when far away areas are connected to the releasing boxes. Such connection may demand high ToMCs (Table 3.2, Figure 3.6b and Figure 3.7b), which represent a potential constrain for connectivity, since the time must be less than PLD for obvious reasons. The need of improving the knowledge of blackspot seabream ontogeny, particularly the possible range of variation of its PLD, becomes crucial to achieve an optimization of the fishery management. As indicated in Faillettaz et al. (2018), this factor strongly influences the larval dispersal patterns and connectivity among adult subpopulations whose calculation is fully based in passive drifting larvae.

Larval dispersal studies rely on the dependence of numerous biological and physical key factors, which must be considered to determine broad-scale ecological connectivity. Egg buoyancy, vertical migrations, and the possible influences on the ELS fate of other biogeochemical features (Wor et al., 2018) are sensible information that is not yet well determined for the studied species (Gil Herrera, 2006), nor incorporated to the model. The 150 m depth case study addressed in this study illustrates how drastically different the results of connectivity can be. Even in the case that depths were restrict to the upper 100 m, the depth range mainly explored in this study (which results in connectivity patterns involving the AS exclusively), vertical motions in the SoG as well as other processes not considered, such as the egg buoyancy or the diel vertical cycle, can displace ELSs to greater depths. If so, part of the spawning products will go beyond the critical depth for which Atlantic connectivity is feasible. Covering these complexities is crucial to be able to implement fully 3D approaches, and, consequently, attain a more reliable vision of population dynamics of blackspot seabream and ultimately transfer this new knowledge to improve the management of this overexploited species. Further studies are needed as it is not yet clear whether the spawning strategy of the species attempts to minimize dispersal time, maximize dispersal distance, or even a more complex trade-off between both. The interpretation and implications of the results presented in this study can be certainly different attending to the species strategy. The role of other

important larval traits not included in this study requires also further research that may help decision-makers to establish biological rest periods that lead to maximize connectivity and sustainability. All in all, improving our knowledge on the interaction of this species with its physical environment is a key issue in the efforts towards rebuilding the fishery target population until its maximum sustainable yield.



### 3.6 Supplementary material

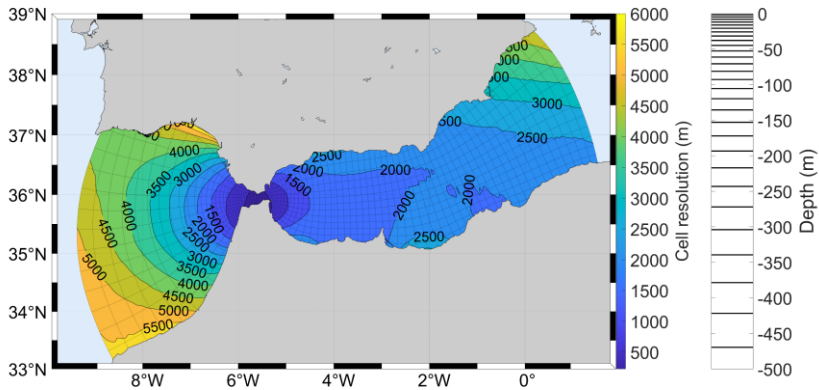


Figure S3.1. Domain, horizontal grid and vertical discretization of the model used to carry out the numerical experiments.

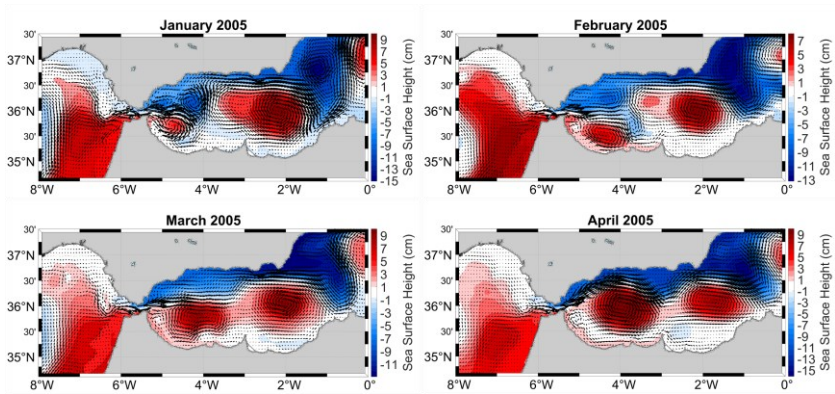


Figure S3.2. Monthly averages of Sea Surface Height (SSH), in cm (color scale on the right) and surface velocities, indicated by vectors, simulated by the numerical model during the simulation months: January (top left), February (top right), March (bottom left) and April (bottom right) 2005.

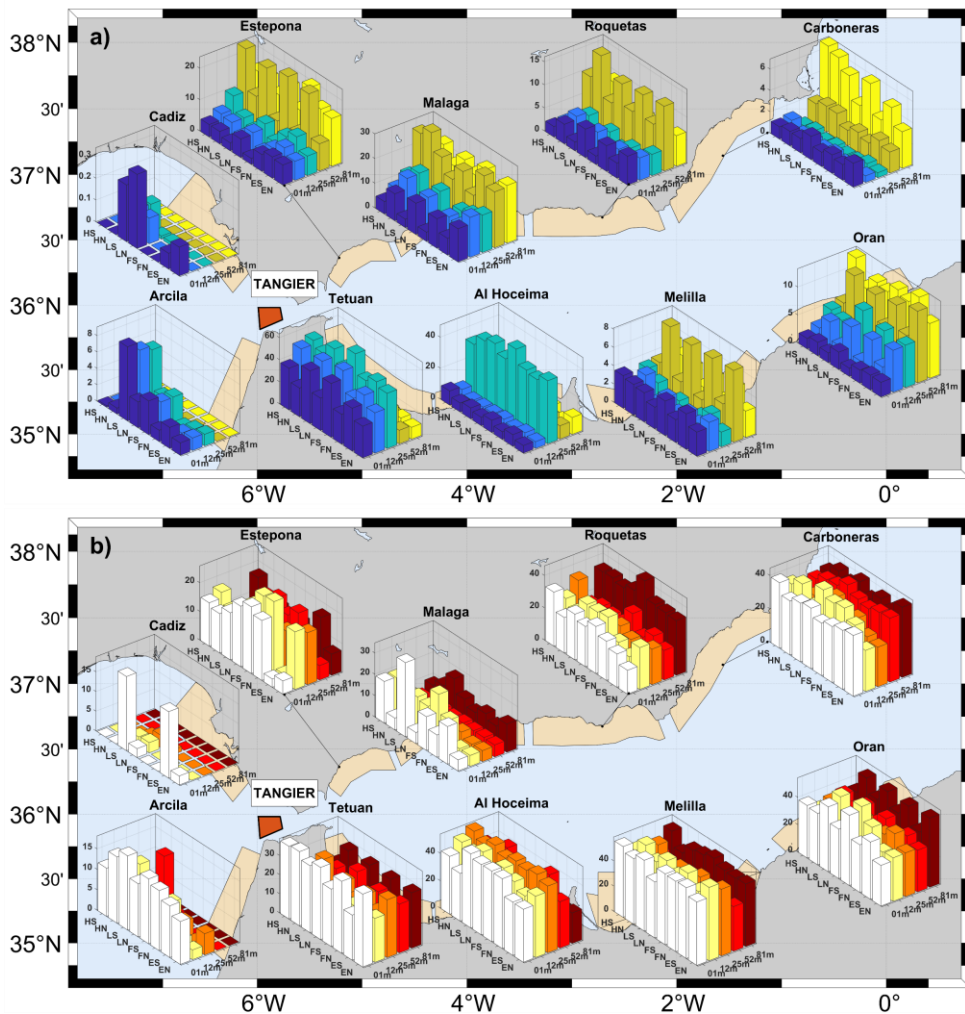


Figure S3.3. As Figure 3.6 and Figure 3.7 for Tangier case.

# 4 Spatio-temporal connectivity and dispersal seasonal patterns in the Adriatic Sea using a retention clock approach<sup>2</sup>

## 4.1 Abstract

Hydrodynamic features play a key role in determining the dispersal and connectivity of fish populations, especially in highly energetic areas determined by currents, river flow, and meteorologically induced fluctuations. Understanding how species interact with these physical processes is essential for managing vulnerable populations and identifying areas that require effective conservation efforts. This study examines the hydrodynamics that regulate connectivity in the Adriatic Sea, a shallow and semi-enclosed basin that is widely recognized as one of the most important areas in the Mediterranean Sea for protection. A high-resolution hydrodynamic model coupled with a Lagrangian tracking module serves as the numerical tool. Lagrangian particles, representing eggs and larvae with typical biological characteristics of generic marine organisms inhabiting the region, are released throughout the basin at different times during a test year to identify the most likely pathways of individual dispersal. The temporal component of connectivity is highlighted using a previously developed retention clock matrix over different larval durations. Seasonality is a critical

---

<sup>2</sup>The contents of this chapter are open-access published in:

**Nadal, I.,** Picciulin, M., Falcieri, F. M., García-Lafuente, J., Sammartino, S., & Ghezzi, M. (2024) Spatio-temporal connectivity and dispersal seasonal patterns in the Adriatic Sea using a retention clock approach. *Frontiers in Marine Science*, 11:1360077. <https://doi.org/10.3389/fmars.2024.1360077>.



factor in dispersal, with greater variability and reduced efficiency in winter compared to summer. The potential implications of the results for improved assessment and management of high value marine species in the basin are discussed.

## 4.2 Introduction

In marine systems, the persistence and recovery of a population are influenced by the dispersal and transport processes of individuals within it, which are controlled by the hydrodynamic circulation of a given study area (P. D. Williams & Hastings, 2013). When complemented by favorable environmental conditions that support the survival of the dispersed organisms, this dynamic process gives rise to the concept of population connectivity, a phenomenon that encompasses the exchange of individuals within and between geographical subregions through the transport of water bodies (Cowen & Sponaugle, 2009; García-Lafuente, Sammartino, et al., 2021). For most marine species, exchanges occur through the pelagic dispersal of early life stages, when eggs and developing larvae can be treated, at least to some degree, as plankton (Largier, 2003). However, circulation can still play a key role in the success of organisms at advanced developmental stages, by conditioning their settlement and dispersal in particular locations, or by influencing the reproductive stock, e. g., altering the spawning location and time (Ciannelli et al., 2015). Estimating these transport pathways is a necessary step towards understanding the regional functioning of pelagic ecosystems, as well as for marine ecosystem management, the design of marine protected areas (Lester et al., 2007; D'Agostini et al., 2015) and the optimization of vulnerable fisheries resources (Fogarty & Botsford, 2007; Gaines et al., 2010; Nadal et al., 2022), among others.

A key component to estimate hydrodynamic connectivity, this understood as the potential of a hydrodynamic field to connect different sub-areas through the exchange of its individuals (García-Lafuente, Sanchez-Garrido, et al., 2021), is the spatio-temporal context in which subpopulations are connected (Trembl et al., 2012) To this aim, hydrodynamic numerical models have become robust tools capable of representing circulation features and,

when coupled with appropriate mathematical approaches, effectively analyzing dispersal pathways by simulating the Lagrangian transport of virtual particles (van Sebille et al., 2018). This is particularly relevant for coastal environments, which normally are highly dynamic regions dominated by tides, upwelling or small-scale turbulence processes, harsh to study via observational methodologies (Pineda, 1991). Ideally, a numerical model of a continental shelf should capture these small-scale coastal features on a high-resolution grid (at least, 0.5-1 km horizontally), with accurate near-shore tidal and meteorological forcing implementation and satisfactory calibration and validation.

An example of such complex application with a strong linkage to its coastal system is found in the Adriatic Sea (AS hereafter), a marginal water body characterized by a peculiar topography, having a very shallow northern area gradually deepening towards the southeast, and by a large number of freshwater sources (Russo & Artegiani, 1996). This paper explores the role of AS hydrodynamic circulation in governing population connectivity and entails the understanding of key physical processes and temporal-scales controlling the drifting of individuals, including spawning, dispersal and final settlement. The relevance of each species-specific behavior within the hydrodynamic circulation of the area makes every specific case study challenging.

Thus, this study did not aim to replicate the behavior of any specific species, but rather focused on resolving the physical mechanisms controlling dispersal of passive elements, representing propagules of generic abundant species within the specified region. A high-resolution circulation model, already used in previous studies of this particular region, coupled to a lagrangian tracking module, is used as a numerical tool for the estimation of population connectivity and dispersal. A sophisticated concept introduced by (Defne et al., 2016), consisting of a “retention clock” that highlights the evolution of source-sink connections through time, is employed to compare simultaneous spatio-temporal analysis of connectivity. The proposed methodological approach is applied on a tested year as a case of study.

The paper is organized as follows: Section 4.3 presents the hydrodynamic characteristics of the study area and the biodiversity of the region, including a list of ichthyofauna inhabiting the basin to which the results of our research may apply. The model framework used to represent the main circulation features of the AS and the lagrangian approach used to study the transport of virtual tracers, as well as the methods used to estimate connectivity from model results, are described in Section 4.4. The results of the lagrangian experiments on the tested year are discussed in Section 4.5, which includes subsections examining the influence of seasonality on virtual particle dispersal pathways and factors related to developmental aspects of abundant fish species in the AS, with a particular focus on pelagic larval duration. Finally, Section 4.6 contains the concluding remarks of this work.

### 4.3 Study area

The AS is a semi-enclosed basin in the northernmost Mediterranean (Figure 4.1). It is narrow and elongated in a NW-SE direction, with a length of ~800 km and a maximum width of ~200 km. It is bounded by an extremely complex rocky coast along the Balkans peninsula and by a sandy and regularly shaped shore along the Italian coastline (Ružić et al., 2019). It is divided into three main sub-basins, explained by the diverse bathymetric profiles (Russo & Artegiani, 1996). The Northern Adriatic (“NA” in Figure 4.1), extending from the Gulf of Venice and Trieste to the 100 m isobath, is characterized by an extremely shallow mean depth (~30 m) with a very weak bathymetric gradient, and occupies the flooded seaward extension of the Po Delta. The Middle Adriatic (“MA” in Figure 4.1) still has relatively shallow waters and constitutes the transition between the northern and southern subbasins. MA is characterized by two depressions, the Pelagosa Sill and the Pomo (or Jabuka) Pit, with depths of ~170 m and ~270 m, respectively. The southern part (“SA” in Figure 4.1) extends to the Strait of Otranto, the channel connecting the Adriatic with the Ionian Sea, and is characterized by the depression of the Otranto Basin, with a maximum depth of ~1270 m. The Otranto Channel, which is ~75 km wide and ~800 m deep, acts as an

exchange area for water masses, and export of nutrients from the AS (Civitarese et al., 1998; Fanelli et al., 2023).

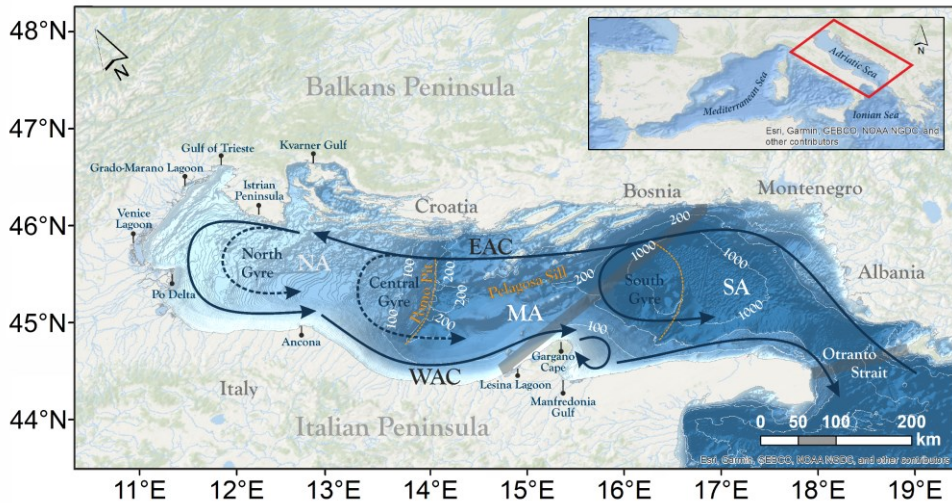


Figure 4.1. Map of the AS showing bathymetry from EMODnet, and sketching its general surface circulation: the Western and Eastern Adriatic Currents (WAC and EAC, respectively) and the North, Central and South Cyclonic Gyres. Orange dashed lines show the virtual boundaries of the three sub-basins, Northern, Middle and Southern Adriatic (NA, MA, SA, respectively), while semitransparent gray bands show the limits of the two Geographical Subareas (GSA17 in the north and GSA18 in the south; see Section 4.3.2). Maps were created using ArcGIS® 10.8 software from ESRI.

#### 4.3.1 Relevant hydrologic features

The surface flow dynamics of the AS are characterized, with a certain seasonal variability, by a general cyclonic circulation (Russo & Artegiani, 1996). Levantine intermediate waters and Ionian surface waters flow northward from the Otranto Channel along the Balkans coast within the Eastern Adriatic Current (EAC), and return southward with the Western Adriatic Current (WAC) along the Italian peninsula (Orlić et al., 1994). Coastal currents exhibit seasonal variability, with the WAC generally stronger in summer, and the EAC stronger in winter (Zore, 1956; Poulain, 2001). Prevalently during winter, part of the EAC recirculates, shaping the nearly-

permanent Southern Adriatic Gyre in the southern sub-basin (López-Márquez et al., 2019), and less frequently, the Northern and Central Adriatic gyres (Martin et al., 2009) in the upper and middle sub-basins. These eddies partially favor the cross-basin (east-to-west) transport via their northern rims (López-Márquez et al., 2019), and also result in the pumping of highly productive waters that entail rich areas favorable for mesopelagic spawners (Specchiulli et al., 2016).

Tides in the AS are amplified northwesterly (from the Strait of Otranto to the northernmost Adriatic), reaching amplitudes up to 1 m in the Venice shoreline, an exceptionally large value in the Mediterranean basin (Medvedev et al., 2020). The influence of tides and local winds, namely Bora and Sirocco, induce an important variability in the main circulation pattern (Orlić et al., 1994). The dry, cold and strong northeasterly Bora, more frequent in winter storms, provokes a double gyre response in the North Adriatic circulation, consisting of a cyclonic loop drifting northward and an anticyclonic drifting southward (Kuzmić et al., 2006). Otherwise, the wetter and warmer southeasterly Sirocco, typical from late autumn to early spring, tends to accumulate water near the northernmost coasts (Pasarić et al., 2007; Molinaroli et al., 2023), usually strengthening the EAC (Book et al., 2007) and weakening or even reversing the WAC (Bignami et al., 2007). Summer winds (e.g. the northwesterly Mistral) are weaker and more stable, which favors a slower and steadier circulation during this period (Pasarić et al., 2009).

#### 4.3.2 Ichthyo-biodiversity in the AS

The AS is a recognized biodiversity hotspot in the Mediterranean, driven by the nutrient transport and runoff by rivers and the consequent phytoplankton primary production, and marked by the strong seasonality of the Po River discharges (Cozzi & Giani, 2011). It is a highly productive fishing ground (Cavrarò et al., 2023), grouped into two Geographical Subareas (GSA17 in the north, and GSA18 in the south, as shown in Figure 4.1) according to the General Fisheries Commission for the Mediterranean (GFCM, 2009). GSA17 has a wide variety of seabed habitats, from shallow and muddy bottoms in the east to steep and rocky bottoms in the west,

whereas GSA18 is predominantly deep, steep, and rocky, supporting sensitive marine habitats that are under high fishing pressure (Grati et al., 2018). Despite the differences, both GSAs share important fish stocks (UNEP/MAP-RAC/SPA, 2015), which has led to the proposal of a large transboundary marine protected area (Bastari et al., 2016).

Particularly, the AS supports regionally important fisheries of small pelagic stocks such as sardine (*Sardina pilchardus*) and anchovy (*Engraulis encrasicolus*) (Morello & Arneri, 2009), which are widely distributed throughout the whole AS. Over the last two decades, sardine specimens in the AS have tended to spawn from early autumn until late spring (Zorica et al., 2020). The peak of reproductive activity occurs between November and February, primarily depending on environmental parameters such as temperature (Zorica et al., 2019). In contrast to the AS, the spawning period for *S. pilchardus* appears to end earlier in other Mediterranean areas (Tsikliras et al., 2010; Basilone et al., 2021). The Adriatic anchovy spawns from the end of March (winter) to October (autumn), with its peak spawning season occurring in July (Zorica et al., 2020). According to Somarakis et al. (2004) and Basilone et al. (2006), the species' reproductive peak is in the summer in the central Mediterranean. In the Bay of Biscay, anchovy spawn earlier and for a shorter period, peaking in May and June (Motos, 1996).

As for the bottom trawl fishery, the European hake (*Merluccius merluccius*) is the most important target species in terms of both landed weight and value for the fleets involved (Arneri & Morales-Nin, 2000). Unlike the other demersal species, it has two recognized spawning phases in the AS: the first occurring in winter in deeper waters, and then, a second occurring in summer after an adult migration to shallower waters (Ungaro et al., 1993; Vrgoč et al., 2004). Based on a recent study conducted on specimens sampled from the GSA17 (Candelma et al., 2021), the hake reproductive season peaks from April to July. However, spawning females can be found throughout the year, indicating a protracted spawning period (Zorica et al., 2019). It should be noted that the reproductive peak of *M. merluccius* varies in different geographical areas. Along the Tunisian coasts, the main peak is recorded from

June to October, with minor peaks in January and April (Khoufi et al., 2014). In the Gulf of Lion, spawning is highlighted in autumn (Morales-Nin & Moranta, 2004). Along the Portuguese coast, spawning peaks are observed in March, May, and August (Costa, 2013). In North Atlantic waters, the spawning peak lasts from January to April (Alvarez et al., 2004; Murua & Motos, 2006).

Medium-sized pelagic fish species such as the Atlantic mackerel (*Scomber scombrus*), horse mackerel (*Trachurus trachurus*) and Mediterranean horse mackerel (*Trachurus mediterraneus*), despite their relatively lower commercial value compared to other pelagic fish species, play also a key trophic role as mesopredators in the basin (Da Ros et al., 2023), with their reproductive activity peaking in winter, late winter and summer, respectively (Jardas et al., 2004; Zardoya et al., 2004). High variability in range and peak spawning season is associated with latitude, with *T. trachurus* spawning season extending up to 8 months, with a peak in spring, in both the Atlantic and the Mediterranean (Abaunza et al., 2003). Other relevant fish stocks targeted by the bottom fleet are the red mullet (*Mullus barbatus*) and the common pandora (*Pagellus erythrinus*), with a spawning peak during summer (Carbonara et al., 2015; Muntoni, 2015; Zorica et al., 2020), as well as flatfish species such as the common sole (*Solea solea*), with a spawning peak in winter (Fanelli et al., 2022).

Some of the authors previously cited in their works indicate that some of the most important spawning and nursery grounds on the AS for these species are the Gulf of Trieste, Po Delta, Gargano Cape, Manfredonia Gulf, Kvarner Gulf, and the northern and the central Italian coastlines (see locations in Figure 4.1). Management measures intended to protect marine resources in the AS were additionally set out by the GFCM (2021) in the Pomo Pit (Figure 4.1), an area recognized as a critical habitat for demersal species and identified as an Ecologically or Biologically Significant Area (EBSA) under the 1992 Convention on Biological Diversity.

## 4.4 Experimental procedure

### 4.4.1 Hydrodynamic model

Modeling the hydrodynamic processes of the Adriatic is challenging due to the large number of spatial scales involved and the extremely intricate coastal morphology (McKiver et al., 2016). Such complex application was carried out with a high-resolution numerical model, whose code is based on the Shallow Water Hydrodynamic Finite Element Model (hereafter SHYFEM; Umgiesser et al., 2004). SHYFEM solves the shallow water equations of motion for complex morphology and wide bathymetric gradients on unstructured grids. The effectiveness of SHYFEM is well-documented in various applications in Europe (Bajo et al., 2014; Umgiesser et al., 2014; among others) and in the Adriatic basin (Bellafiore & Umgiesser, 2010; Ghezzi et al., 2015, 2018; Umgiesser et al., 2022 and citations therein). The version used in this study (SHYFEM-Tiresias, Ferrarin et al., 2019) covers the entire AS, from 12.05° E to 19.92° E and from 39.95° N to 45.80° N, including the small lagoons of Grado-Marano, Lesina and Venice and the Po Delta (Figure 4.1).

The full numerical grid consists of 96,392 triangular elements with horizontal resolution varying from 5 km in the open-sea to a few dozens of meters along the coastlines (Figure 4.2A), and 72 vertical Z-layers of uneven discretization (Ferrarin et al., 2019). It includes the contribution of five boundary conditions, namely, the sea level, current velocity, temperature and salinity fluxes at the Strait of Otranto, and the freshwater discharges from 17 tributaries. Temperature and salinity fluxes were provided by the oceanographic fields of Mediterranean Forecast System (Tonani et al., 2008), and the freshwater discharges were obtained from monthly and annual climatological values at the river boundaries (for the location of tributaries, see Ferrarin et al., 2019 and references therein). Atmospheric forcing, i.e., pressure and wind, is given by the ECMWF ERA5 atmospheric reanalysis (Hersbach et al., 2023).

The model outputs in this study are hourly surface values of zonal ( $u$ ) and meridional ( $v$ ) components of drift velocity, sea level, temperature, and



salinity for the year 2018. The selected year is as a representative scenario for the general hydrographic conditions of the AS and is accessible in NetCDF through the Institute of Marine Sciences of the National Research Council of Italy (CNR-ISMAR) OpenDAP catalog (<https://iws.ismar.cnr.it/thredds/catalog/emerge/catalog.html>). It serves as a case study, examining spawning areas and intra-annual connectivity patterns, rather than assessing interannual variability, which is currently being investigated but not shown for simplicity in this first application. Supplementary Figure S4.1 displays the monthly averaged surface velocity data from SHYFEM and the ECMWF ERA5 wind fields for the simulated months (January to December 2018). Winter and summer averaged surface circulation is presented in Figure 4.2B and Figure 4.2C, respectively.

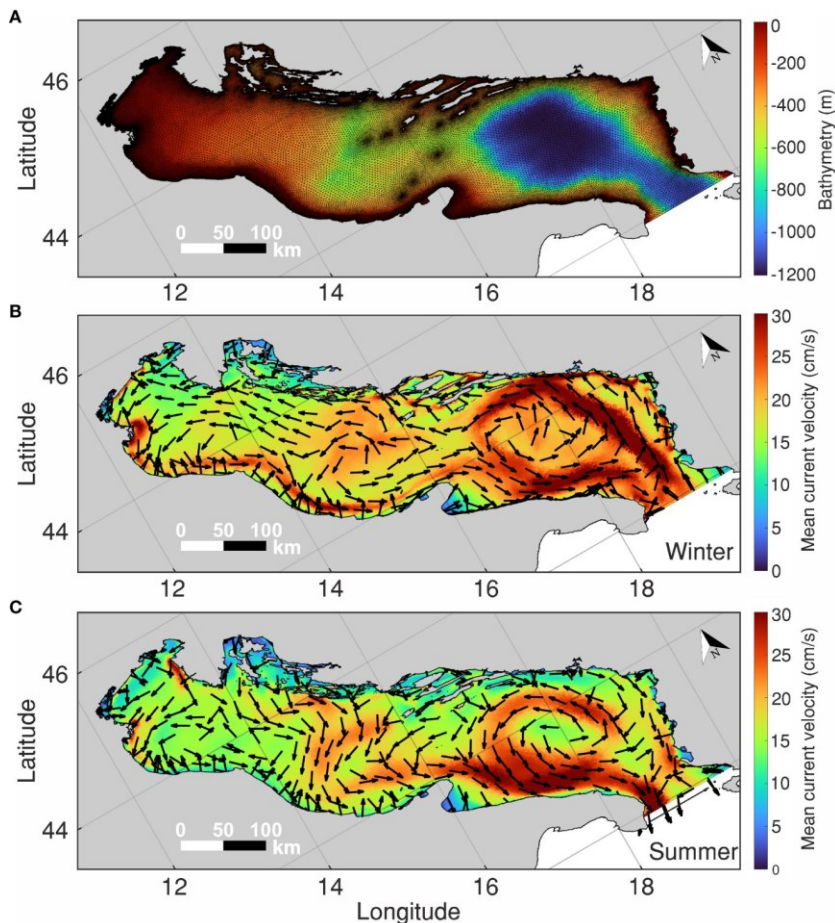


Figure 4.2. (a) Numerical grid and bathymetry of SHYFEM-Tiresias (i.e., the SHYFEM application in the AS; Ferrarin et al., 2019). (b) Modeled surface velocity (color scale) and direction (arrows), in  $\text{cm}\cdot\text{s}^{-1}$ , in winter (January-March). (c) Same as panel (b) for summer (July-September).

The synoptic fields in Figure 4.2 reveal similar circulation patterns, with the velocity field exhibiting greater variability in winter than in summer. The winter mean (Figure 4.2B) shows a more prevalent WAC in the northern sub-basin, and a stronger EAC along the north-flowing eastern rim of the southern gyre. The circulation is weaker in summer (Figure 4.2C), although the WAC is stronger along the south-flowing rim of the southern gyre in this season. Despite not being the most typical configuration reported in the AS, which is characterized by the presence of the EAC and the WAC and the three reported cyclonic gyres, the slight weakening of the currents during summer is not unusual. The prevailing northwesterly Mistral winds during summer intensify the east-to west cross-basin transport, leading to stronger southeastward coastal currents and increased export to the northern Ionian Sea. During winter, the effect of both easterly and southeasterly winds disrupts the unidirectional shore transport, resulting in a more dispersed and irregular pattern within the basin.

#### 4.4.2 Particle tracking module

Dispersal and connectivity were assessed by implementing a lagrangian particle tracking algorithm based on the open-source software OpenDrift (version 1.10.6, Dagestad et al., 2018). OpenDrift consists of several particle-based sub-models that can be used to predict the transport and fate of different types of elements. This study applies the main sub-model, OceanDrift, that uses neutral buoyant particles as tracers. Virtual particles represent propagules (i.e., eggs and larvae) with the typical biological traits of generic marine organisms (Table 4.1). The analysis focuses on basin-scale larval connectivity from an ecosystem perspective, rather than on specific target species.

Horizontal trajectories were simulated by integrating the zonal and meridional velocity field using a 4<sup>th</sup> order Runge-Kutta advection scheme,

where particle positions are bilinearly interpolated using the model output data in the hydrodynamic grid. Vertical velocities, mainly associated with wind-driven upwelling /downwelling in certain AS areas, are of small magnitude (less than  $\text{mm}\cdot\text{s}^{-1}$  to  $\text{cm}\cdot\text{s}^{-1}$ ) compared to horizontal velocities ( $\text{cm}\cdot\text{s}^{-1}$  to  $\text{dm}\cdot\text{s}^{-1}$ ). Vertical motions are influenced by other phenomena such as diel cycles, feeding patterns, egg buoyancy or settlement due to changes in fat content, diurnal temperature variations affecting buoyancy, etc. As a result, the vertical velocity is poorly determined, with an uncertainty in its value that could even change its sign, for which it has not been considered in the advection module.

Another simplification adopted in our method is that the tracers are fully-passive, meaning that complex larval traits, such as swimming capability, migrations, and natality and mortality rates are not considered in the approach. Under these assumptions, transport of eggs and developing larvae is determined by the PLD (i.e., the time propagules spend drifting with currents), the duration of spawning, and the time-varying horizontal velocity. To prevent particle stranding near the release site, a strategy of relocating particles to the open sea was implemented upon encountering the continental coastline or islands when oceanographic conditions allowed. The coastline was represented using the Global Self-consistent Hierarchical High-Resolution Geography in its full resolution version (GSHHG\_F, version 2.3.7). A 30-minute time step with non-additional diffusion nor wind field were added to the trajectories, as they were already included in the hydrodynamic simulation run of SHYFEM-Tiresias.

To investigate the spatial connectivity patterns, the AS basin was divided into 40 sub-zones, 21 along the coastlines and 19 distributed by the open sea (Figure 4.3). These areas were partially selected based on the experience gained from studies on the circulation and ecological characteristics of the region of interest (Coll et al., 2010; Lipizer et al., 2014; UNEP/MAP-RAC/SPA, 2015; Bastari et al., 2016). Each area played, simultaneously, the role of source and destination of particles. Two hundred Lagrangian particles as a representative number of propagules are seeded in each box randomly distributed in the surface layer, so each release allocates 8,000 new particles

in the AS, and their position is computed every 30 min. To avoid any potential bias that could be introduced in trajectories if particles were only released at a single time of the day, particles are released four times per day for 14 days (56 releases, 448,000 particles in total). All the particle tracks were stored in netCDF format and the post-processing and visualization of the simulations were performed in Matlab (version 2023a).

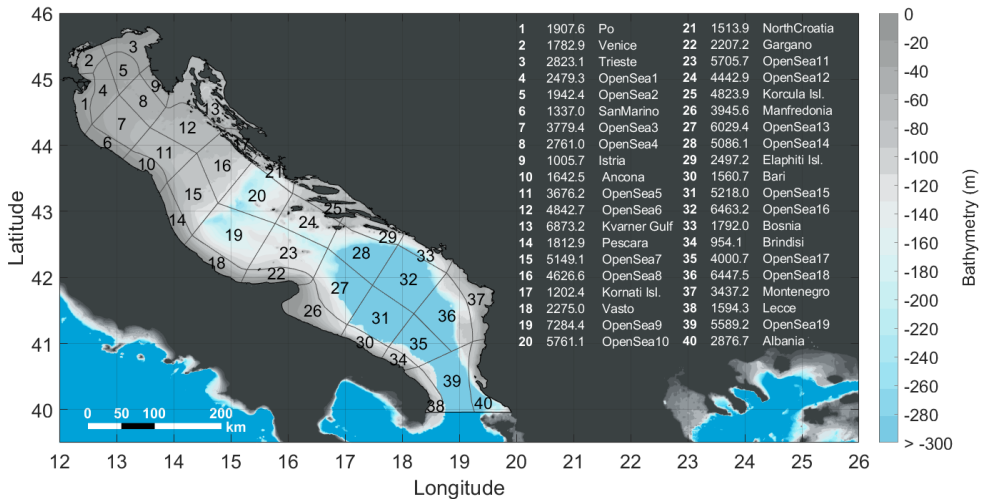


Figure 4.3. Map of the study area with the subareas of source and destination of particles and bathymetric features. A summarizing table that illustrates the code numbers, associated names and surface areas in km<sup>2</sup> of each box is included.

In addition to the spatio-temporal analysis of the trajectories of eggs and larvae, several factors related to the biology and development of common fish stocks in the AS with influence on the dispersal pathways of particles were tested. Table 4.1 provides the biological parameters considered in the Lagrangian experiments. The first one is the spawning time, understood as the time of particle release. Simulations were run for winter and summer, representing the most active spawning periods of the abundant species inhabiting the region. The second parameter being tested is the pelagic larval duration (PLD), which is the time between when a pelagic propagule leaves the spawning site and when it finally settles. In practice, the duration of egg and larval drift of marine organisms varies from weeks to months, depending on the ontogeny of fish larvae. The value of this parameter per species has

been inferred from the literature cited in Table 4.1. Overall, given the uncertainties in determining the transition from passive to active behavior, we considered a wide PLD of 60 days as a good compromise between a stable value for connectivity in the AS and an affordable computational time. To test the sensitivity to PLD, connectivity was recalculated for time windows ranging from 15 to 90 days (Section 4.5.4).

Table 4.1. Literature review of biological traits for some emblematic species relevant for modeling in relation to the AS oceanographic conditions.

<b>Marine species (habitat)</b> Common name Scientific name	<b>Spawning season</b>	<b>PLD</b> [days]	<b>Bibliography</b>
Sardine (P) <i>Sardina pilchardus</i>	Winter	40-60	Sciascia et al., 2018; Zorica et al., 2019, 2020
Anchovy (P) <i>Engraulis encrasicolus</i>	Early summer	30-40	Morello & Arneri, 2009; Patti et al., 2020; Zorica et al., 2020
Atlantic mackerel (P) <i>Scomber scombrus</i>	Winter	n.f.	Zardoya et al., 2004
Horse mackerel (P) <i>Trachurus trachurus</i>	Late winter	21-30	Jardas et al., 2004; Van Beveren, 2012
Mediterranean horse mackerel (P) <i>Trachurus mediterraneus</i>	Summer	n.f.	Viette, 1997
European hake (D) <i>Merluccius merluccius</i>	Winter, Summer	40	Arneri & Morales-Nin, 2000; Hidalgo et al., 2019
Red mullet (D) <i>Mullus barbatus</i>	Summer	22-37	Carbonara et al., 2015; Muntoni, 2015
Common pandora (D) <i>Pagellus erythrinus</i>	Summer	44	Vrgoč et al., 2004
Common sole (B) <i>Solea solea</i>	Winter	31-38	Fanelli et al., 2022; Paoletti et al., 2021

**Note:** From left to right: Marine species are the organisms to which the results of this work may apply, with a code that indicates their corresponding habitats (P: Pelagic, D: Demersal, B: Benthonic); spawning period is the average reproductive season; PLD is the length of time the propagule is pelagic; bibliography indicates the source(s)

where information was obtained. Abbreviation: *n.f.* (not found/not reported) in the AS.

#### 4.4.3 Construction and analysis of connectivity

Two different methods were followed to address hydrodynamic connectivity (Figure 4.4). First approach consisted in the so-called “connectivity matrix” (Figure 4.4A), which represents the probability of larval exchange among geographically separated sites (Cowen & Sponaugle, 2009). In this matrix, each cell is the number of particles ( $p$ ) released from a certain source  $i$  (along the vertical axis) and collected in a certain destination  $j$  (along the horizontal axis), so  $C_{i,j}$  is the probability that an individual or group of individuals of population  $i$  will move to population  $j$  after a certain tracking time ( $C(i,j) = \frac{p(j)}{p(i)}$ ). Diagonal cells of this matrix (where  $i = j$ ) stand for the self-recruitment, i.e., the number of individuals that remain in the same region from which they were originally released, including particles that eventually return to the sourcing area (Cowen et al., 2006).

Connectivity ratios ( $C$ , with values ranging from 0 to 1), therefore, quantify the strength of connectivity between different sites, with higher values indicating more favorable connections. Source-sink dynamics of larval dispersal can be elucidated with this approach, revealing the direction and intensity of connections. It further enables to estimate the potential and effectiveness of a given area as a nursery ground for developing larvae. Despite this, connectivity matrices only offer a partial depiction of larval connectivity complexity, neglecting crucial information such as the identification of areas that are rapidly dispersing, both dispersing and recruiting, or only recruiting for individuals through time.

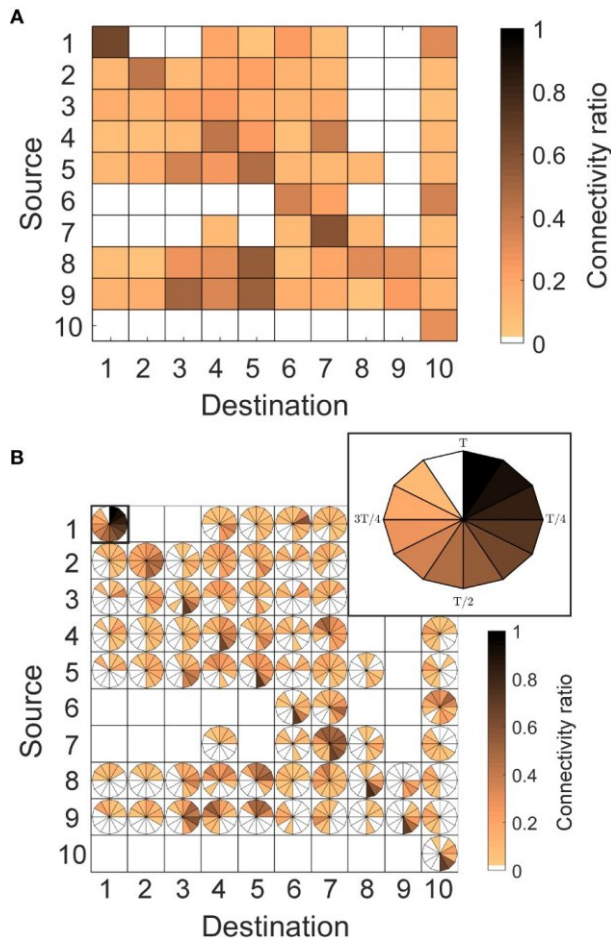


Figure 4.4. (a) An example of a connectivity matrix estimated in ten artificial subareas with fictitious ratios of connectivity varying from 0 (blank cells, null connectivity) to 1 (brownest colored cells, maximum connectivity). Rows correspond to the release zones of virtual larvae, whilst columns correspond to the destination areas of the released larvae. Diagonal stands for self-recruitment, which is the number of virtual larvae retained within the area from which they were released. (b) RCM applied to the same example, with an inset that zooms an example of a box connection with itself. In the inset, time progresses clockwise from 0 to a time scale  $T$  (e.g. 60 days) as concentration of particles decreases from 1 to 0, with a given temporal resolution of  $\Delta t$  (e.g. 12 slices of 5 days each).

Prompted by this lack of temporal information in the network, the second method used a more-recent approach developed by Defne et al. (2016). The method, called a “retention clock matrix” (RCM, hereafter), uses a clock in



each cell to track the temporal changes in source-sink connections, evaluating the time-dependent connectivity (see Figure 4.4B). Specifically, each retention clock describes the release event as a circular clock that tracks the number of particles ( $p$ ) over the entire time scale of interest ( $T$ ) (see inset of Figure 4.4B). The time scale is discretized into slices with a temporal resolution of  $\Delta t_n$  ( $C(i, j, t_n) = \frac{p(j, t_n)}{p(i, t_0)}$ ).

As in the conventional connectivity matrix, in all RCMs, the horizontal axis represents the boxes from which particles are released, and the vertical one is where the particles end up. The strength of connectivity between each possible combination of source-destination is depicted with a color scale, in which slices with the darkest color intensity indicate the larger fraction of particles moving from their origin to the destination. Naturally, domains with different retention characteristics have unique retention clocks, which reflect the rate at which particles are retained or lost within a domain through time. In slowly dissipating environments, the particle concentration, hence the clock, would gradually approach zero, indicating that individuals are being spawned at a slower rate than they are being dispersed. In rapidly dispersing domains, the clock would approach zero faster and a larger portion of it would remain at null values, suggesting that tracers are subjected to strong currents that result in direct connections to other domains. The opposite behavior is depicted by retentive domains, identified by clocks with connectivity values close to 1 at all-time scales, which indicate that spawned individuals are effectively retained due to physical or biological features that prevent their advection.

To account for the discrepancy in sizes and shapes of source and destination polygons (see Figure 4.3), the estimated connectivity in both cases was normalized by the areas ( $a$ ) of each cell involved in the connection  $C = C \cdot \left[ \frac{a(i)}{a(j)} \right]$ , so that the maximum value of the matrix is 1. In both methods, connectivity was only considered significant if the ratio  $C$  satisfied a minimum threshold of 0.01, meaning that at least 1% of the particles released from the source reached the destination polygon. Thus, the presence of either colored cells (in method 1) or clocks (in method 2) indicate a connection



between the source and destination polygon, while a blank cell indicates that the connection is zero or less than 1%, and thus, negligible. The connectivity ratios  $C$  are hereinafter interpreted in the text as  $S\# - D\#$ , indicating particle transport from source (row number) to destination (column number), respectively. A numerical code made available to the scientific community by Defne et al. (2016) was adapted to calculate the RCMs in this study.

## 4.5 Results and discussion

### 4.5.1 Connectivity matrix

The mean connectivity matrix estimated at winter and summer for the year 2018 is illustrated in Figure 4.5A and Figure 4.5B respectively, and the result of its difference (summer minus winter) is provided separately in Supplementary Figure S4.2.

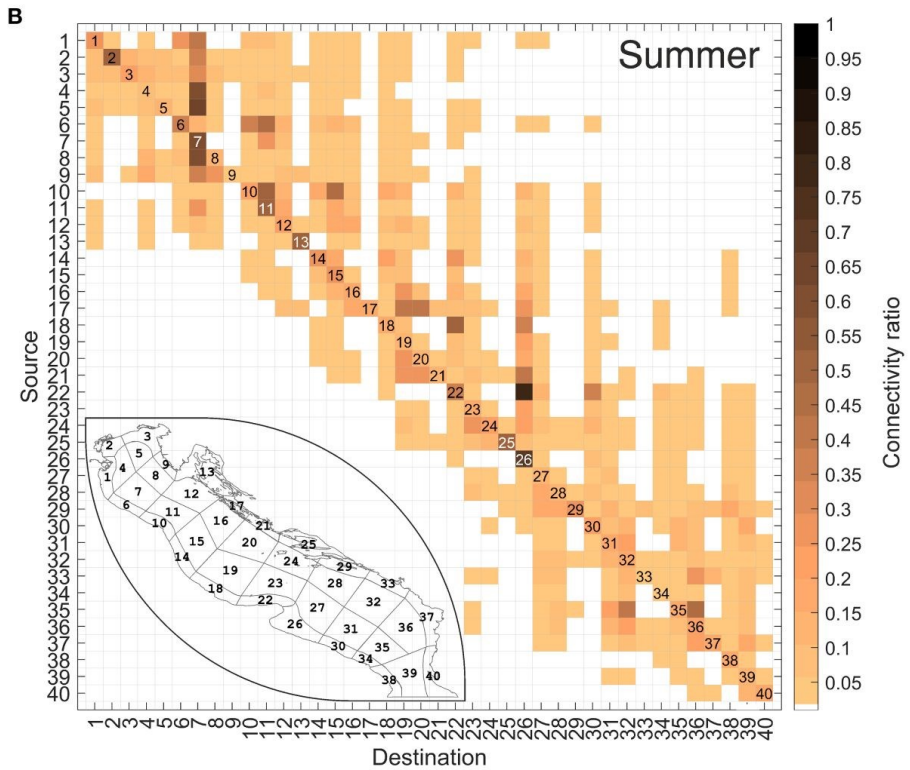
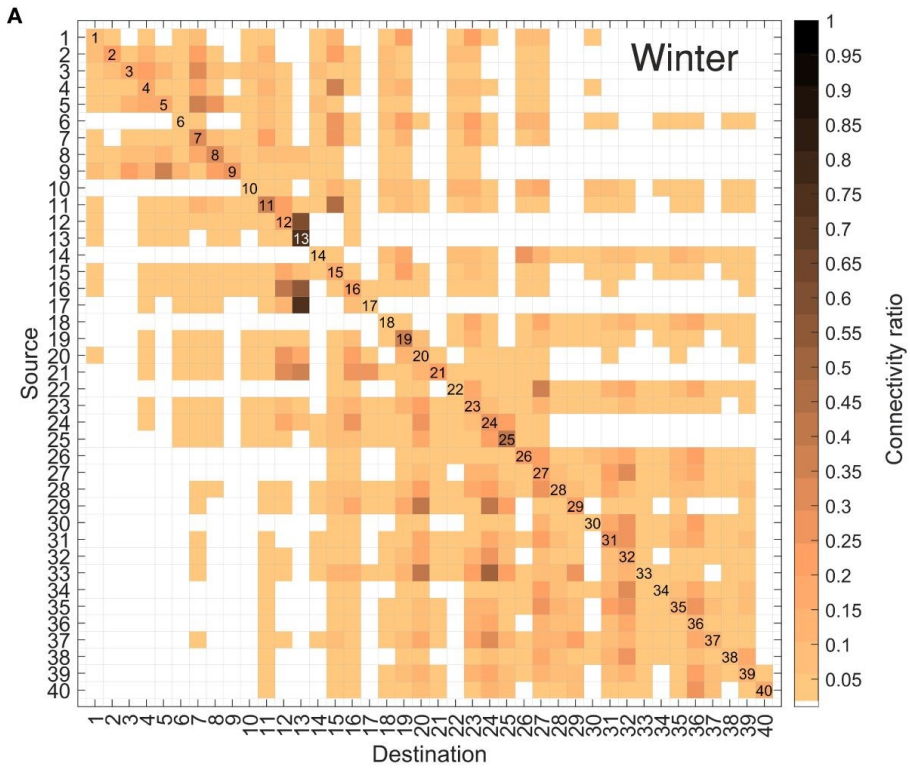


Figure 4.5. Average connectivity matrices representing the mean exchange of particles between sub-zones in winter (A) and summer (B). The color scale represents the particle concentration at the selected time scale. A small map of the study area showing the sub-areas is displayed in the summer scenario to facilitate interpretation.

A characteristic feature of both winter and summer scenarios is the prevalence of high connectivity rates along the diagonal of the matrix. This indicates that these regions are characterized by a certain level of auto-retention of propagules. Self-retention probability differs greatly between the distinct boxes, ranging from 60% in the Kvarner Gulf (S13-D13) to 5% in Bosnia (S33-D33) for winter (Figure 4.5A), and from 55% in Manfredonia (S26-D26) to 4% in Brindisi (S34-D34) for summer (Figure 4.5B). This spatial difference is foreseeable, as the complex system of islands in the Kvarner Gulf, and the existence of a small cyclonic eddy in the Gulf of Manfredonia (see Figure 4.1) act as trap of propagules (Sciascia et al., 2018; Specchiulli et al., 2016), whilst Brindisi and Bosnia coasts, nearby the Strait of Otranto, are subjected to stronger advection by the EAC-WAC circulation system. Overall, self-retention in the northern and middle Adriatic sub-basins (areas 125) is more likely than in southern Adriatic sub-basin (areas 26-40), denoted by the darker color intensity of the former diagonal cells compared with the latter elements (~28% in areas 1-25, compared to ~13% in areas 26-40, in both winter and summer scenarios).

Considering also the connectivity values out of the diagonal, Gargano (D22) and Manfredonia (D26) during summer (Figure 4.5B), display a large fraction of particles arriving from S14-20 and S18-22, with mean connectivity values of 10% and 20%, respectively, and maximum reaching 50% (S18-D22) and 70% (S22-D26). This spatial pattern is to be expected, since the WAC acts as the main advection process along the Italian shelf, although it is also subject to seasonal fluctuations (Supplementary Figure S4.1). Contrastingly, Istria (D9), Kvarner Gulf (D13), and the Kornati (D17), Korcula (D25), and Elaphiti (D29) Islands, exhibit external particle reception rates less than 5%. Extreme case is provided by D17 (Figure 4.5B), which shows zero reception of individuals from external boxes. These areas harbor relatively closed

populations, receiving particles from a limited number of grounds, but suggest their potential as self-sustaining areas. During winter (Figure 4.5A), isolated self-sustaining areas are less obvious, although the shielding capacity of the Kornati Islands (D17), northern Croatia (D21) and the Korcula Islands (D25) is noteworthy, as they receive nearly null abundance of particles from the northern part of the basin. Areas D2 (Venice), D3 (Trieste), D5 (OpenSea2) and D9 (Istria) only receive particles from a small part of the southern sub-basin, while source areas S12 (OpenSea6), S13 (Kvarner Gulf), S17 (Kornati Islands), S21 (North Croatia), S24 (OpenSea12) and S25 (Korcula Islands) do not send any particles to the southern sub-basin. A striking example is the Kvarner Gulf (D13), which paradoxically shows minimal external particle receptions in summer, but high external particle exchange in winter, while remaining self-retaining (elevate connection with itself). This suggests that this area may play a hatchery and nursery role for marine species, as suggested by the previously cited authors (Zorica et al., 2020), and suggest the existence of physical processes determining the temporal evolution of the particles in the basin.

Based on the averaged result, we can derive macro-regions as combinations of boxes of our network. For instance, more evident in summer than in winter, areas 1-9 and 26-40 may be identified as two isolated regions with a slight or null inter-connection. A third area can be identified in 10-25 (central Adriatic), where the particle reception is mainly limited to the upper part of the connectivity matrix (northern and central Adriatic), with limited or no exchange with the southern sub-basin during summer. During winter, the prevailing currents over the AS inject more energy in the basin, leading to a wider dispersion of particles and a less distinct delineation of macro-regions. The seasonality is also evident by the significantly higher number of valid elements, i.e., cells with connectivity probabilities higher than 1%, in winter (~900 out of 1600, Figure 4.5A) compared to summer (~600 out of 1600, Figure 4.5B). The likely reason is the atmospheric forcing, which is less variable and more stable in summer, resulting in diminished velocities and consequently shorter drifter paths in this period. The much more dispersed

transport because of the more variable atmospheric forcing during winter may create otherwise less structured connectivity patterns within the basin.

#### 4.5.2 Time-dependent connectivity

Temporally averaged connectivity matrices (Figure 4.5; Supplementary Figure S4.2) highlight the role of circulation structures on particle dispersion and provide predictable connectivity patterns that show seasonal variability. However, it also shows that the selection of a temporal snapshot is subjective and can limit the analysis due to loss of information. It is more adequate to preserve the temporal information of connectivity, while benefiting from the simplicity of a connectivity matrix (Defne et al., 2016). To this end, the RCM for all source-destination pairs in the AS basin has been estimated for the same temporal configurations (winter and summer, and their difference Figure S4.3). A maximum time scale of 60 days is used for all model scenarios. Each slice on all retention clocks represents 5 days. The color scale in each clock represents the particle concentration at the selected time slice, with darker colors indicating larger fraction of particles moving from source to destination.

#### 4.5.3 Auto-connectivity

Auto-connectivity, the ability of a system to receive and retain particles from and within itself, is a pivotal determinant of population persistence. It represents the self-sustaining capacity of a population structure, a factor intricately influenced by the physical processes that mediate the propagules transport (Cowen et al., 2006). The quantification of self-recruitment probability, a direct metric of auto-connectivity, is made by evaluating the diagonal cells of the connectivity matrix (where  $i = j$ ), with higher values signifying a more robust tendency for particles to remain within the area from which they were initially released. The cells corresponding to these diagonal matrices are extracted from the estimated RCMs and depicted in Figure 4.6, illustrating the time dependent self-recruitment probabilities for both winter and summer seasons.

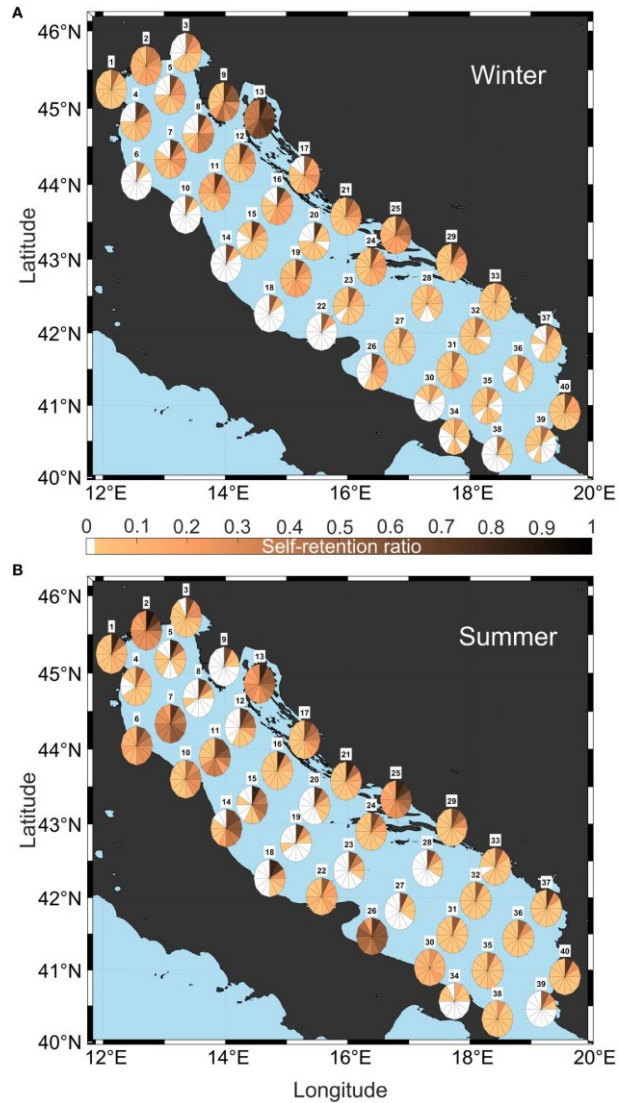


Figure 4.6. Clocks of auto-connectivity extracted from the diagonal of RCMs estimated at winter (A) and summer (B) and displayed spatially in the centered positions of the 40 defined subareas.

In the winter experimental configuration (Figure 4.6A), a low self-sustained clock pattern is evident along the Italian coast, indicating rapid southward transport within the western Adriatic shelf, with particles leaving the source area within a maximum of 10 days. This is consistent with the winter WAC pattern shown in Figure 4.6B. Regions located above the northern Adriatic gyre show retentive characteristics, as indicated by elevated clock values in

both intensity and duration, particularly observed in Po (1), Venice (2), OpenSea5 (11), and OpenSea6 (12). The summer scenario (Figure 4.6B) presents a stark contrast, with the exception of the Croatian coast, which shows similar auto-retention characteristics. Specifically, the Kornati Islands (17) and northern Croatia (21) retain their winter characteristics for an extended period of up to 50 days, and the Gulf of Kvarner (13), along with the islands of Korcula (25) and Elaphiti (29), exhibit clock patterns almost identical to the winter configuration throughout the 60-day tracking period. This suggests that the coastal topography of the eastern Adriatic coast, rather than the seasonal regime, plays the primary role in influencing its autoretention behavior. Po (1) and Venice (2), which contain complex lagoon systems, also maintain their behavior in both seasons due to their topographic conformation. Conversely, the coastal areas of Gargano (22) and Manfredonia (26) along the Italian shelf, exhibit higher auto-retention values in summer than in winter, in both intensity and duration, which persist for almost the entire 60-day period. Similarly, the onshore regions along the western Italian coast south of the Po estuary (6, 7, 10, 11) show high retention rates, in agreement with previous findings in this region (Revelante & Gilmartin, 1992; Bray et al., 2017).

#### 4.5.3.1 Winter connectivity

When the RCM estimated in winter (Figure 4.7) is analyzed, more granular temporal information becomes available with respect to the time-averaged analysis. For instance, among the previously identified macro-regions, the one corresponding to the northern Adriatic Sea (boxes 1-9), not only shows low ratios but also exhibits poor retention capacity with decreased persistence of connectivity over time. This is especially noticeable in the OpenSea3 (S7), which exhibits high average connectivity ratios (~40%, Figure 4.5A) but, when evaluated temporally, reveals consistently short and variable durations, with peak rates occurring at 40 days of tracking for particles originating from Trieste (S3-D7) and OpenSea2 (S5-D7).



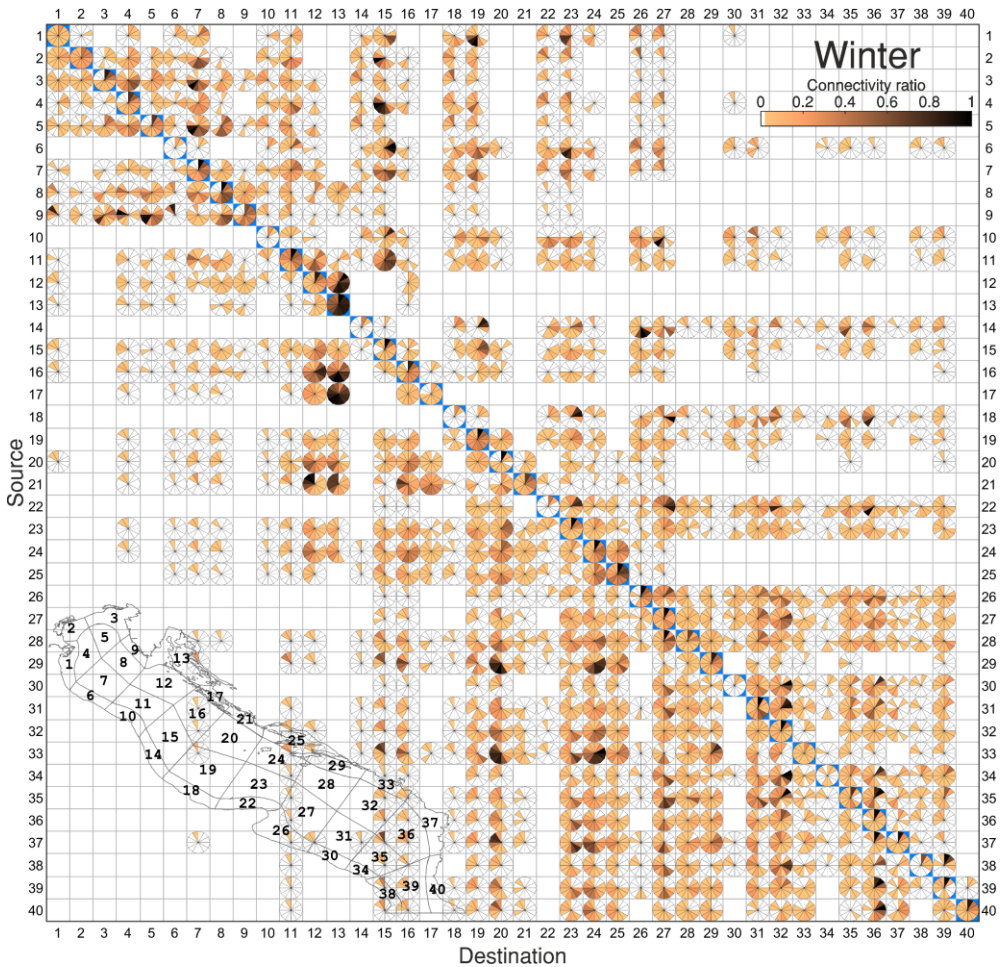


Figure 4.7. RCM representing the time-dependent exchange of particles between sub-zones in winter, with the diagonal cells highlighted in blue color. A small map of the study area showing the 40 sub-areas and their corresponding codes is displayed to facilitate the interpretation of results.

The central macro-region (10-25) shows a more extensive distribution of connections, encompassing both the northern and southern sub-basins, with particle transfers to the southern Adriatic being significantly stronger and more persistent throughout the tracking period. Retention areas in this part of the basin occur in the Kvarner Gulf (D13), OpenSea10 (D20), OpenSea12 (D24) and the Korcula Islands (D25). It is particularly noteworthy in the case of the Kvarner Gulf (D13), which, despite the extremely complex rocky coastline, shows the highest connectivity receptions within the RCM (S16-



D13, S15-D13, S12-D13 with a ratio of >60% sustained over longer periods). This pattern is likely due to enhanced atmospheric variability during winter, which induces rapid and direct transport of particles into these coastal areas. A strong and persistent rate of particle reception is further in the OpenSea6 (D12), which maintain a strong connectivity throughout the 60-day tracking period with the OpenSea8 (S16-D12), the Kornati Islands (S17-D12), the OpenSea10 (S20-D12) and North Croatia (S21-D12).

These four areas shape a continuously well-connected water parcel compatible with the effect of the central Adriatic gyre, and likely identify one of the most productive areas for fish and important spawning and nursery grounds for commercially valuable fish species. Other important connections with the southern subbasin occur in the OpenSea9 (D19) and in the OpenSea10 (D20), which receives particles from Gargano (S22), OpenSea11 (S23), OpenSea12 (S24), and Korcula Islands (S25). These areas build a corridor of connection south of the Pelagosa Sill, with connectivity percentages of 45% throughout the 60-day clock period. The area D20 receives particles secondarily from S26-40, with special intensity in a period from 25 to 45 days from areas S29, S33, S37 which represent the pattern of the EAC. The connection of the central Adriatic with the northern is relatively weak and variable, as evidenced by the low (<30%) and delayed (>40 days) ratios in the upper portion of the matrix, attributed to the northward transport of currents towards the end of the tracking period. A relevant connection in this part of the basin occur in the OpenSea7 (D15) for particles arriving from the northernmost Adriatic (S1-D15, S2-D15, S4-D15, S5-D15, S7-D15, S10-D15 and S11-D15), indicating a particularly retentive area south of the Po River, corroborating previous findings in the region (Bray et al., 2017).

Among the three identified macro-regions, the southern one (26-40) emerges as the most retentive. It maintains a generally persistent connectivity, being particularly significant in specific regions of the central macro-region (S28-D24, S33-D24), with a high rate of connections (>70%) persisting 35 days. Additionally, it exhibits a high degree of inter-connectivity, with the most extensive and enduring connection occurring between areas 31, 32 and 35, 36. This pattern is likely attributable to the

presence of the south gyre, which is particularly prominent during winter (Figure 4.2B; Supplementary Figure S4.1).

#### 4.5.3.2 Summer connectivity

The rather scattered and variable connections seen in winter contrast with the much more unidirectional connectivity pathways in summer (Figure 4.8). This becomes apparent in the less heightened variability observed in both direction and duration of connections compared to the winter RCM. The northern macro-region (boxes 1-9), which showed a reduced ratio and persistence over time in winter, shows not only the highest but also the most persistent connectivity percentages in summer, denoted by the clocks with probabilities above 20% on all time scales (S2-D1, S3-D2, S4-D2, S5-D2, S4-D3, S2-D3, S2-D4, S3-D4, S3-D5). The darker color intensity in the matrix indicates a significant influx of individuals into destination 7 (OpenSea3), with a concentration of elements ranging from 20% to 60% between S1-D7 (Po-OpenSea3) and from 30% to 90% between S8-D7 (OpenSea4-OpenSea3) during the tracking time. Within the same box, particles originating from source boxes 3 (Trieste), 4 (OpenSea1), and 5 (OpenSea2), once arriving, maintain connectivity percentages above 70% for the rest of the tracking period. The particles reaching these areas exhibit rapid travel times (5 to 15 days), which is within the range of the PLD of the relevant species (Table 4.1) and indicates their potential for retention. Overall, the entire northern macro-region requires a longer time (approximately 30-60 days) to establish a connection with the central part of the basin (D10-25), with slight or null transport towards the southern macro-region (D26-40). This pattern is consistent with the slower flow conditions seen during summer (Figure 4.2C), but also provides important information regarding species strategy, as individuals arrive in that region at advanced developmental stages.

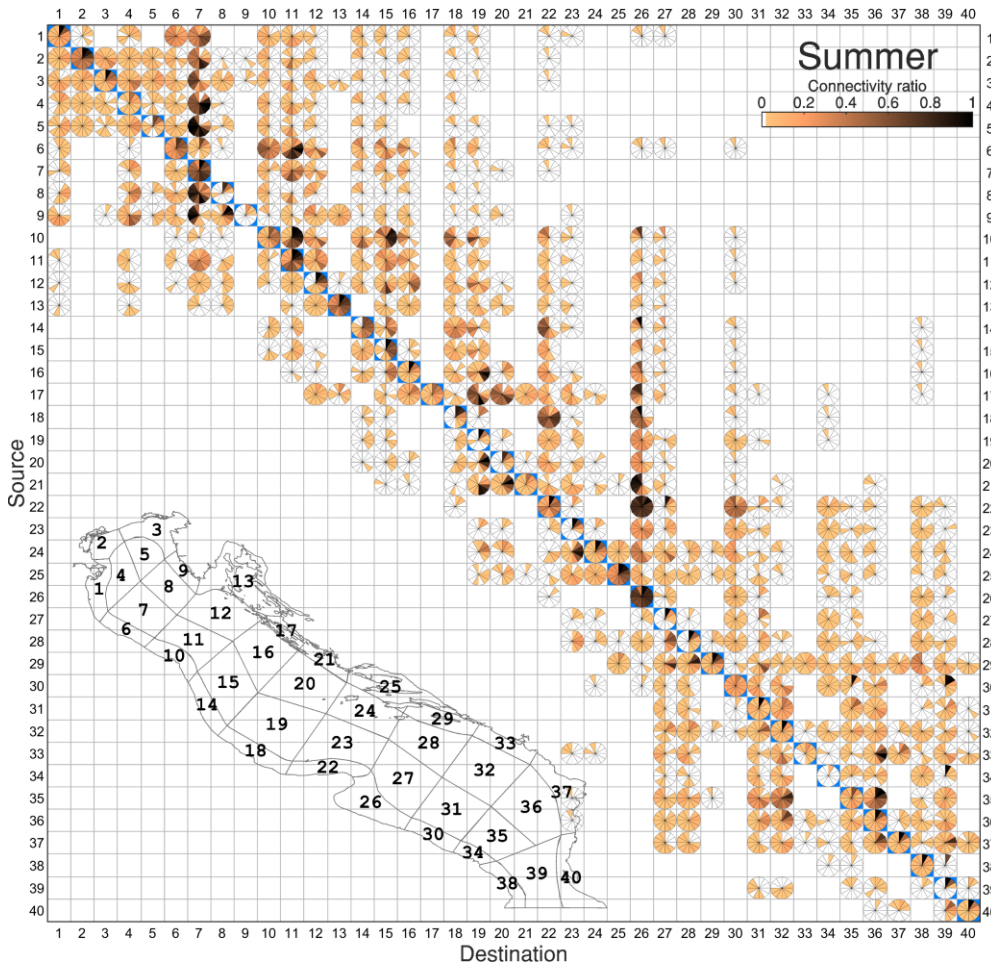


Figure 4.8. Same as Figure 4.7 for the summer experimental configuration.

Regarding temporarily sustained connectivity, the southern macro-region 26-40 follows, with the highest and longest connectivity observed between the boxes 35 and 36 (OpenSea17 and OpenSea18). These two sites also exhibit strong connectivity for the entire 60-day tracking period to boxes 31 and 32 (OpenSea15 and OpenSea16), forming a well-connected water parcel consistent with the isolation effect of the southern Adriatic gyre. Paradoxically, a notable connectivity is observed between Bosnia (S33) and Montenegro (D37), with 67% of particles flowing in the opposite direction of the EAC. This unexpected behavior is attributed to the reversal of currents very close to the shore due to instability created by the weakening of the coastal current during summer. In the southern macro-region, a mirrored

relationship emerges in comparison to the northern counterpart along the south shore, characterized by a limited number of connections with the northern areas at longer times of arrival (>45 days). This pattern confirms that the northern and southern Adriatic, while internally connected, act as isolated water bodies within the region, which maximizes their potential as unique nursery environments. The opposite situation is seen in the areas of the central macroregion 10-25, which reveal connections with a wider portion of the AS and demonstrates both retention and dispersal traits.

Destination areas D10-12,14-16,18-19 consistently exhibit longer arrival times (>45 days) and poor retaining capacity for particles originating from the northern sub-basin compared to other boxes. In contrast, Gargano (D22) and Manfredonia (D26) are identified as top retaining areas, with connectivity consistently exceeding that of other destinations throughout all time slices. The majority of particles observed in the Manfredonia Gulf (D26), previously identified as a recruiting area in the averaged analysis (Figure 4.5B), are primarily and nearly continuously transported from the adjacent Gargano (S22) during the simulation period, with secondary and slightly delayed contributions from S23 and S24 (>15 days). This pattern arises from east-to-west shore transport, particularly noticeable during summer due to the displacement of the Adriatic central gyre (see Figure 4.2C). In the same area, particles require more than 30 days to arrive both from North Croatia (S21) and the Kornati Islands (S17), and more than 40 days from Ancona (S10) and the OpenSea areas of the northern Adriatic (S11, S12, S15, S16). This temporal pattern is to be expected: as the distance increases, the time of arrival of particles also does. But the point to note here is that the high rate of particles reaching Manfredonia stays and recirculates nearly continuously within the same box for the rest of the simulation period. This observation confirms the Gulf's role as a particle receptor during the summer and subsequently as a nursery ground for larvae, a finding that could not be obtained in the time-averaged analysis (Figure 4.5B).

The spatial pattern observed between Gargano and Manfredonia (S22-D26) is consistent with patterns observed between San Marino and Ancona (S6-D10), and similarly with Pescara (S10-D14), and Vasto (S14-D18). This is

likely attributable to the WAC, the primary advection mechanism transporting particles southward along the Italian shelf. Particularly during this season, the wind regime indicated a Mistral event blowing northeasterly (Supplementary Figure S4.1, July-August), which further supports the local displacement of particles onshore, despite the usual tendency of the coastal current to be detached from the shore during summer (Vilibić et al., 2012).

#### 4.5.4 Effects of PLD on connectivity

The temporal component of connectivity between specific areas must be directly related to the species-specific PLD to ensure the practical application of the research. Determining the time that propagules spend drifting with currents is a key issue in shaping the dispersal potential and population connectivity of a given area. As mentioned in Section 4.4.2, the range of plausible durations is broad and uncertain (Table 4.1). While continuing to use the numerical model as a tool, it is worth exploring the dependence of connectivity on PLDs. To address this, we investigated the rate of particle reception in each area across a range of PLD windows from 15 days to 90 days, with intervals of 15 days (Figure 4.9).

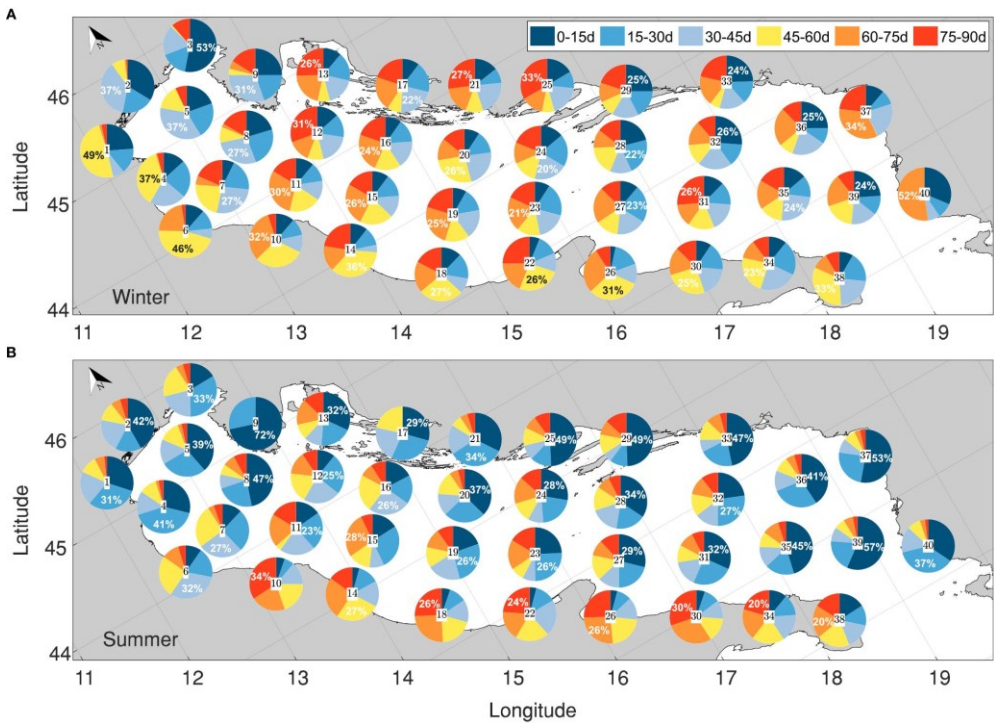


Figure 4.9. Pie charts showing the proportions of connectivity at each area at the distinct temporal bands of PLD (see legend for interpretation) for the winter (A) and summer (B) experimental configurations.

In the winter configuration (Figure 4.9A), subareas show particle receptions evenly distributed across the PLD windows, with the most significant connections forming after at least 30 days of simulation. This is particularly noticeable along the Italian shelf (areas 6, 10, 14, 18, 22, 26, 30, 34), where the probability of receiving particles is less than 5% within the initial 15 days and remains below 20% within the first 30 days. This hinders the possibility of early life stages persisting in these areas, but suggests the eventual occurrence of individuals at more-advanced developmental stages, a phenomenon partially supported by works reporting the Gulf of Manfredonia's role as a nursery ground (Sciascia et al., 2018). An exception to this trend is evident in the northernmost Adriatic, specifically in Venice (1) and Trieste (2), where the highest rate of particle reception occurs within the initial 15 days (35% and 53%, respectively), indicating a higher probability of occurrence of early life stages in these regions.

During the summer (Figure 4.9B), the arrival times are remarkably short, characterized by an average probability of reception of 30% and a maximum of 70% within the first PLD window (0-15 days). The most favorable scenario is observed in Istria (9), where the highest probability of receipt is concentrated in the first 15 days, with no further particle arrivals after 30 days of tracking. This observation indicates a prevalence of individuals in early life stages in this subarea, aligning with prior research highlighting Istria's role as a spawning ground (Zorica et al., 2020). Other potential spawning grounds are discerned in the southeastern Adriatic, specifically in OpenSea17 (35), Montenegro (37), and OpenSea19 (39). Favorable scenarios are also evident along the northern edges of the Adriatic gyres, favoring cross-shore connections, with peak reception occurring between 15 and 30 days of individual tracking.

From a biological perspective, these findings offer valuable insights into spawning strategies. According to our results, species with shorter PLD, such as the red mullet or anchovy (<40 days), would likely thrive along the Croatian coast in the summer, benefiting from the shorter arrival times and the more favorable oceanographic conditions. Conversely, species with longer PLD, such as sardine or hake (>40 days), would find the northern Adriatic and Italian shelf during winter advantageous.

#### 4.5.5 Implications for the species inhabiting the AS

Identifying the unique retentive characteristics of different areas in the AS is a crucial step in comprehending the distribution of marine species and designing effective conservation strategies in the basin. Our results indicate that particles exhibit a strong preferential direction along the coasts. The behavior in the Italian shelf was notably diverse, with some areas maintaining high self-sustaining ability during the summer and values shifting offshore in the winter. The Istrian coast (Figure 4.1) is identified as a crucial habitat for species spawning success, particularly in the summer, where arrival times fall within the ranges of PLD estimated for abundant species in the basin, such as anchovy, red mullet, and common pandora (Table 4.1).



Areas distributed along the Italian shelf can be identified as essential nursery grounds, particularly when the region's productivity is influenced by wind-induced upwelling and river discharges, creating favorable environmental conditions for larvae. During the summer, when the velocity is reduced, retention is promoted, coinciding with the spawning period of anchovy, Mediterranean horse mackerel, and hake (Table 4.1). The variability observed during winter is attributed to environmental fluctuations, specifically the prevalence of strong winds that significantly affect the displacement of drifters. This phenomenon provides advantageous opportunities for marine species with longer PLD and spawning periods concentrated in winter, such as sardines and common soles (refer to Table 4.1). Many particles arrive after undergoing recirculation, a process that requires longer times and results in extended arrival durations.

#### 4.6 Conclusions

In this study, a hydrodynamic model integrated into the AS, coupled with a Lagrangian module, was employed to systematically identify and evaluate sub-areas with distinct particle retention characteristics. While traditional connectivity matrices offer a valuable visualization tool for assessing the probability of individual exchange between zones, the challenge lies in extending this analysis across multiple time scales, often overlooked in existing approaches (Cowen et al., 2006; Crochelet et al., 2016; Gamoyo et al., 2019). To overcome this limitation, our study introduces an innovative application of the "retention clock" methodology, originally developed by Defne et al. (2016), and previously applied only in a few back-barrier estuaries (Barnegat Bay, in New Jersey, USA; Defne et al., 2016; Goodwin et al., 2019 and Chincoteague Bay, in Maryland/Virginia, USA; Beudin et al., 2017). Therefore, our research represents a pioneering effort and the first large-scale application of the temporal approach in the AS and, to our knowledge, in Europe.

The proposed methodology was tested in 2018 as a case study with representative hydrographic patterns of the AS, and in areas with known ecological characteristics. This allowed the verification of the distribution



patterns of specific areas in the AS with the existing scientific literature (Morello & Arneri, 2009; Coll et al., 2010; UNEP/MAP-RAC/SPA, 2015; Fanelli et al., 2022). It also established a correlation between the findings and the life cycle traits of different organisms. Future research should aim to improve the coupling of connectivity and biological knowledge at larger spatio-temporal scales. The spatial discretization, as shown in Figure 4.3, followed a logical subdivision of the domain into a limited number of releasing sub-regions. A more detailed subdivision of space may be necessary in future applications, especially in areas where prior knowledge is lacking. This will require significant computational effort, which can be reduced by using computer clusters. Similarly, the analysis of connectivity over multiple years requires the development of an algorithm-based method to synthesize information and highlight the most relevant aspects. Such a study is currently in progress. All in all, the tool will improve the accuracy of the AS connectivity estimates which could, for example, inform the design of networks of marine protected areas (MPAs), fisheries assessment tools, and management policies.

## 4.7 Supplementary material

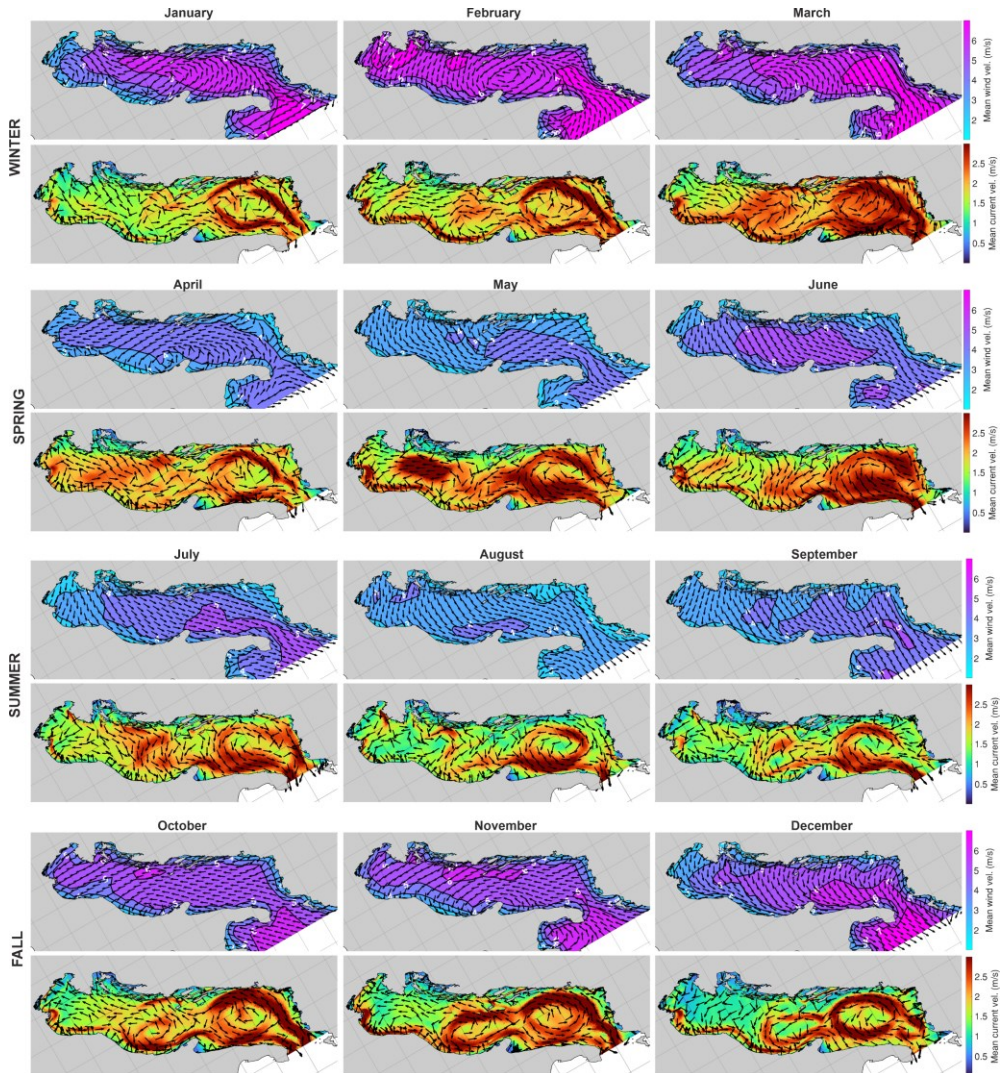


Figure S4.1. Wind fields provided by the ECMWF ERA5 atmospheric reanalysis and retrieved from the Climate Data Store of the Copernicus Climate Change Service, intercalated with the monthly averaged surface velocity data from SHYFEM for the tested year (January to December 2018).

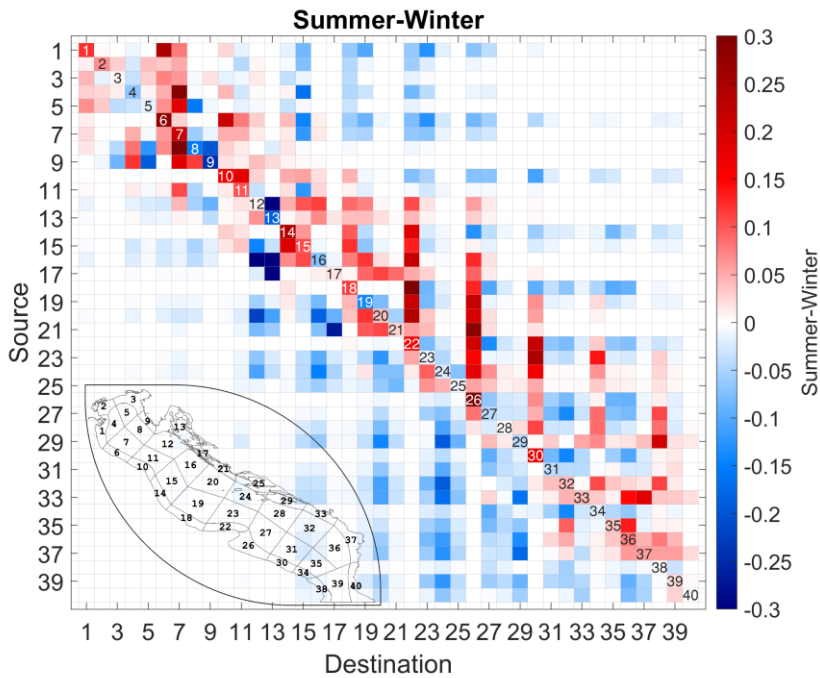


Figure S4.2. Difference between summer (Figure 4.5B) and winter (Figure 4.5A) average connectivity matrices. Positive values (shown in red) represent stronger connectivity during summer, while negative values (shown in blue) indicate greater connectivity during winter. White cells represent null connectivity, or no difference between summer and winter cases.

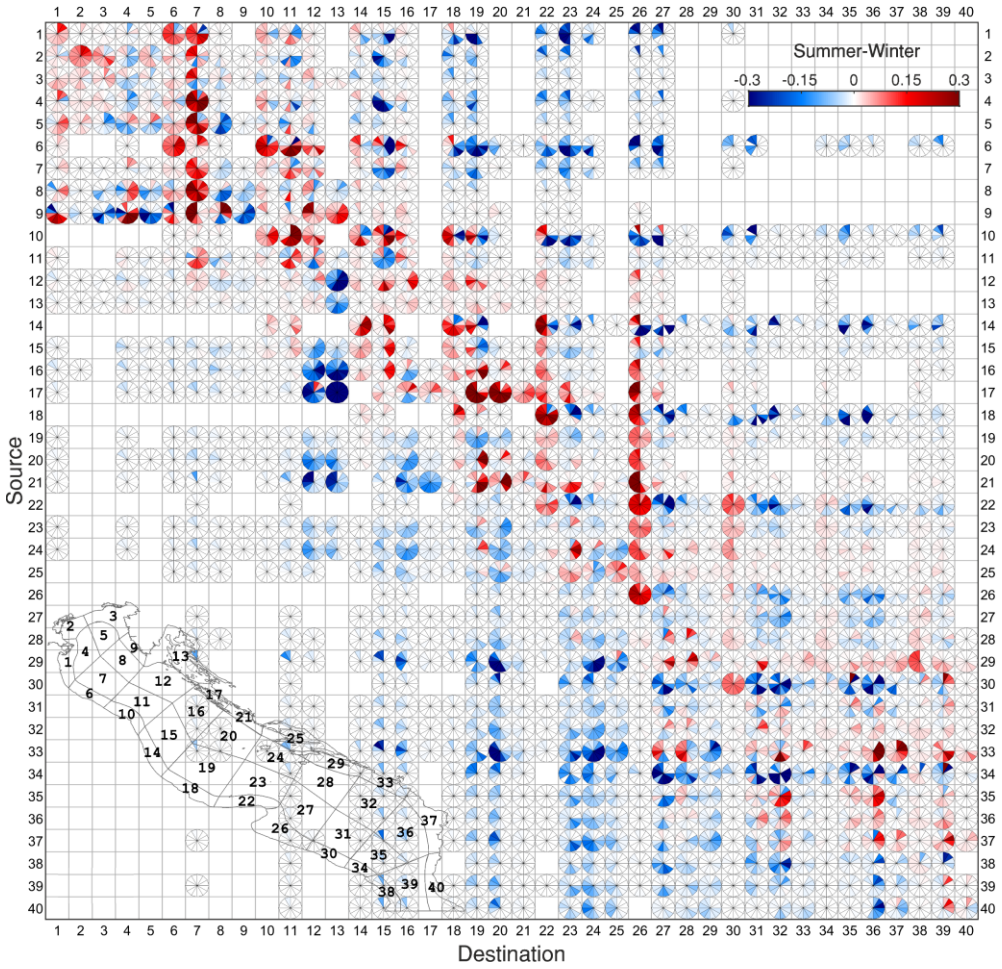


Figure S4.3. Same as Figure S4.2 for the RCM approach (RCMsummer - RCMwinter).



# 5 Could secondary flows have made possible the cross-strait transport and explosive invasion of *Rugulopteryx okamurae* algae in the Strait of Gibraltar?<sup>3</sup>

## 5.1 Abstract

Presently, the Strait of Gibraltar is undergoing an unprecedented invasion of the alien alga *Rugulopteryx okamurae* of North Pacific origin. According to the scarce literature, the algae first settled in the south shore, probably following commercial exchanges with French ports where it was accidentally introduced together with Japanese oysters imported for mariculture. There is no certainty, however, that the algae first colonized the south shore of the Strait and, from there, spread to the north. It could well have been the opposite. Whatever the case, it spread all over the Strait and surrounding areas with amazing rapidity. Human-mediated vectors (algae attached to ship hulls or fishing nets, for example) can be behind the spread from the shore initially settled to the algae-free shore on the opposite side. But it could also have happened by means of hydrodynamic processes without direct human intervention. This possibility is assessed in this paper by revisiting

---

<sup>3</sup>The contents of this chapter are open-access published in:

García-Lafuente, J., Nadal, I., Sammartino, S., Korbee, N., & Figueroa, F. L. (2023). Could secondary flows have made possible the cross-strait transport and explosive invasion of *Rugulopteryx okamurae* algae in the Strait of Gibraltar? *PLOS ONE*, 18(5), e0285470. <https://doi.org/10.1371/journal.pone.0285470>.



historical current meter profiles collected in the Strait of Gibraltar searching for secondary cross-strait flows. All the stations present an intermediate layer of northward cross-strait velocity near the interface of the mean baroclinic exchange along with a surface layer above of southward velocity, whose lower part also overlaps the interface zone. The first one would back the south-to-north transport of algal fragments, the second one, the north-to-south. In both cases, algae must reach the depth of the interface. The vertical velocity field in the area, which far exceeds the small sedimentation velocity of the algae, allows their vertical displacements throughout the water column. Its endurance to survive under the weak or no light conditions that will prevail during the cross-strait transport and its capability of reactivating the metabolism after this unfavorable period, offers chances for colonizing the opposite shore. Therefore, the propagation of the algae by hydrodynamic processes, without human intervention, cannot be ruled out.

## 5.2 Introduction

Since the mid-2010s, the coasts around the Strait of Gibraltar (SoG, hereinafter) and neighboring basins (Figure 5.1) are suffering from a drastic invasion of the algae *Rugulopteryx okamurae* (García-Gómez et al., 2020) a brown macroalga belonging to the Dictyotaceae family (Dictyotales order), original from the northwestern Pacific Ocean (Huang, 1994). The alga was detected in the small Mediterranean lagoon of Thau, southwest of France, in year 2002 for the first time in Europe (Verlaque et al., 2009) where, according to these authors, it was probably introduced along with Japanese oysters imported for mariculture purposes. In year 2015 the alga was found off Ceuta in the south coasts of the SoG (Altamirano-Jeschke et al., 2016; Aamri et al., 2018; Navarro-Barranco et al., 2019; Katsanevakis et al., 2020) where it could have arrived following commercial exchanges with Tangier-Med port (Figure 5.1).

Leisure boats and their marinas have been also shown to be important components of the hub-and-spoke model of invasion in coastal systems (Ashton et al., 2022). On the other hand, algae could have already been

present on the north coast at that time and not have been identified due to its resemblance to other algae already established in the area, although a benthic community monitoring program at some fixed sentinel stations established on the north coast did not detect algae up until 2016 (García-Gómez et al., 2020). In spite of this fact, which gives weak support to the southern pathway, the precise route of entry still remains uncertain. Regardless this uncertainty, the point is that, in few years, the alga has occupied the illuminated rocky seafloor of large extended coastal areas in both shores of the SoG and adjacent basins (García-Gómez et al., 2020), featuring an aggressive invasion with no precedents in European coastal waters (Figure 5.2A and Figure 5.2B). Northern Africa and the southern Iberian Peninsula are the most intensely affected area, but it continues expanding towards the west and east with the threat of monopolizing the sea rocky bottom to the detriment of photophilous resident biota (García-Gómez et al., 2020, 2021). Currently, the exotic alga has colonized the Marsella coast (Ruitton et al., 2021) and even the Azores islands (Faria et al., 2022). More worrisome is the risk pointed out by (Muñoz, A.R. et al., 2019) that it could cover the whole Mediterranean coasts.

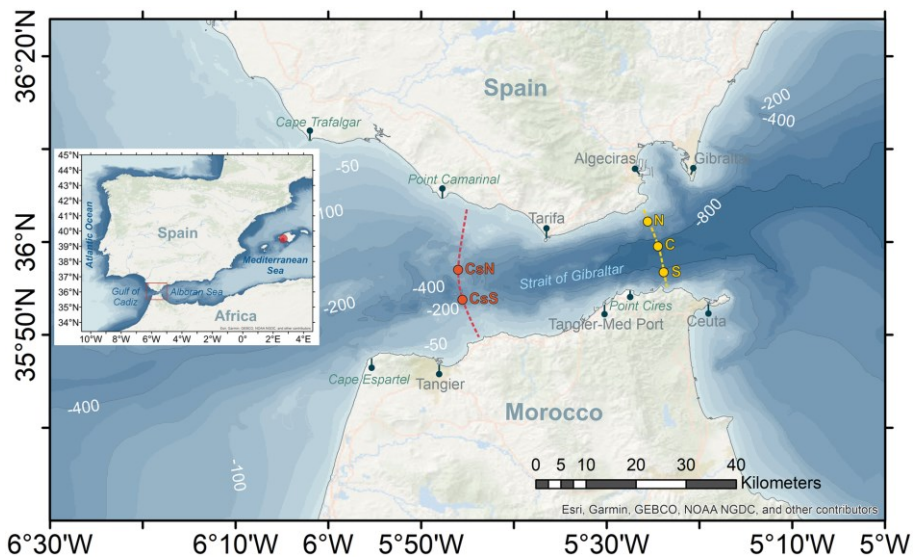


Figure 5.1. Map of the Strait of Gibraltar showing bathymetric features and locations and geographic sites mentioned in the text. Dots labelled N, C, and S in the eastern part and CsN and CsS in Camarinal section are the stations where current meter data



used in this study come from. Red dot in the inset indicates Palma de Mallorca in the Balearic Islands. Sources: Esri, GEBCO, NOAA, National Geographic, DeLorme, Geonames.org, and other contributors. Maps were created using ArcGIS® software by Esri. ArcGIS® and ArcMap™ are the intellectual property of Esri and are used herein under license. Copyright Esri. All rights reserved. For more information about Esri® software, please visit [www.esri.com](http://www.esri.com).

The explosive spreading would be linked to favorable environmental conditions, since the photic zone in the area gathers suitable year-round temperature for growth and reproduction of this subtropical species (García-Gómez et al., 2020; Mercado et al., 2022), but also to the fact that broken thalli serve as seeding population, since their specimens present vegetative (Altamirano-Jeschke et al., 2016; Hwang et al., 2009) remarkable fact to this regard is that thalli and propagules are actually found drifting not only in the illuminated zone where they are also fixed to the bottom but also at practically any depth of the SoG (Figure 5.2C–E).

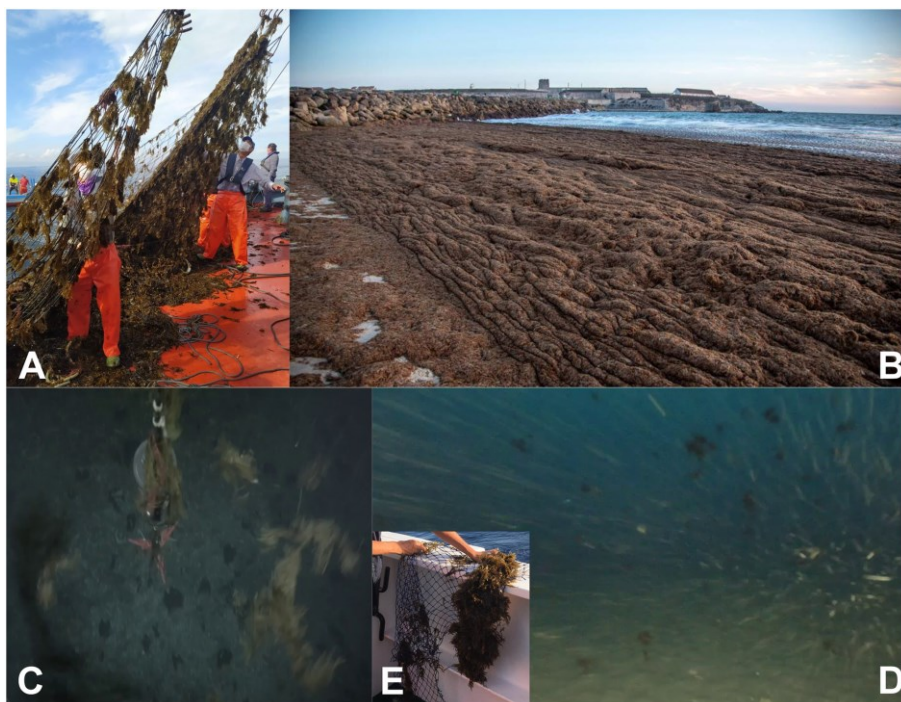


Figure 5.2. A) Tuna fishing net (Almadraba) pulled from the sea in Tarifa nearly covered with *Rugulopteryx okamurae*. B) Massive *Rugulopteryx okamurae* beaching nearby Tarifa. C) Frame taken from a video recorded by a Remotely Operated Vehicle during a rescue operation of a mooring line off Cape Espartel (see Figure 5.1) showing thalli of *Rugulopteryx okamurae* drifted by the Mediterranean outflow. Sea floor (identified by the grey spots in the background) is at 360m depth. D) Frame taken from a video recorded by a camera attached to a trawling net showing several fragments of *Rugulopteryx okamurae*. The fishing vessel was working to the northeast, but near of, the eastern limit of the SoG and the videocamera was at 120m depth. E) Fragments of *Rugulopteryx okamurae* attached to scientific equipment deployed at 350m depth off Espartel which were collected when the instruments were brought to the surface for maintenance.

The plausible hypothesis that algae first settled in a shore of the SoG, likely the south one according to the scarce available literature, poses the question of how did it spread to the other shore. Different mechanisms could be behind the spreading. The first and more plausible one is linked to the heavy ship traffic in the area, which includes continuous north-to-south ferry and other commercial ships crossing the Strait. The alga shows huge capability to colonize any type of hard substrates, not only rocky seafloor but glass, ceramic, iron, tires, etc. (García-Gómez et al., 2018), so the eventual crossing attached to ship hulls, fishing nets, including scientific sampling nets (Wejnerowski et al., 2022), or other human-mediated vectors as the mentioned recreational boats (Ashton et al., 2022) cannot be ruled out. Neither ballast waters from remote shipments can be discarded (Hyun et al., 2015; Rosas-Guerrero et al., 2018). Another possibility, however, is that the algae managed to cross the SoG taking advantage of hydrodynamic processes without human intervention. Such possibility is revised in this paper. Interestingly, it would be also applicable to pelagic larvae and propagule of other marine species that last for weeks in the pelagic realm. This opens new hypothesis about transport mechanisms between Lusitanian and Mauritanian biogeographical regions, which could eventually be testable by applying molecular techniques among populations.

### 5.3 Possible mechanisms for cross-strait connection

The SoG holds a well-known two-way (baroclinic) exchange necessary to compensate for the freshwater and buoyancy losses in the Mediterranean basin. It results in intense, zonal-oriented currents: an eastward Atlantic inflow into the Mediterranean Sea at the surface, and a subsurface Mediterranean outflow towards the Atlantic Ocean beneath (see Bryden et al. (1994) or García-Lafuente et al. (2000), for instance). Under such a system of currents, the spreading of alga and further substrate colonization in west-east direction would be achievable relatively easily, but it will not be that easy in the cross-strait direction. The intense along-strait currents behave as hydrodynamic barriers for cross-strait transport (García-Lafuente, Sanchez-Garrido, et al., 2021) that, moreover, would carry propagules out of the dimensions of the SoG well before they have chances to get to the opposite shore.

There is, however, a loophole for this dynamic constriction, which is the necessary vanishing of the along-strait current at the depth of the interface between the Atlantic and Mediterranean layers. Should exist a cross-strait secondary flow at this depth, even if weak, the chances to successfully cross the Strait would be no null. Secondary flows are linked to rotation and friction with the solid boundaries, which are the ingredients of Ekman boundary layers (Gill, 1982; Garrett et al., 1993). The along-strait inflow and outflow are density driven flows, as there is no geostrophic balance (pressure gradients balanced by Coriolis force) in the along-strait equation. However, the earth rotation acting upon them, forces a pressure gradient that leads to geostrophic cross-strait balance (Bryden et al., 1994; García-Lafuente et al., 2000; Candela et al., 1989) a pattern known as semi-geostrophy or semi-geostrophic flows. Figure 5.3 shows the good agreement between that pressure gradient, as given by the sea level difference between south and north shores, and the along-strait velocity in the Atlantic layer at the eastern SoG.

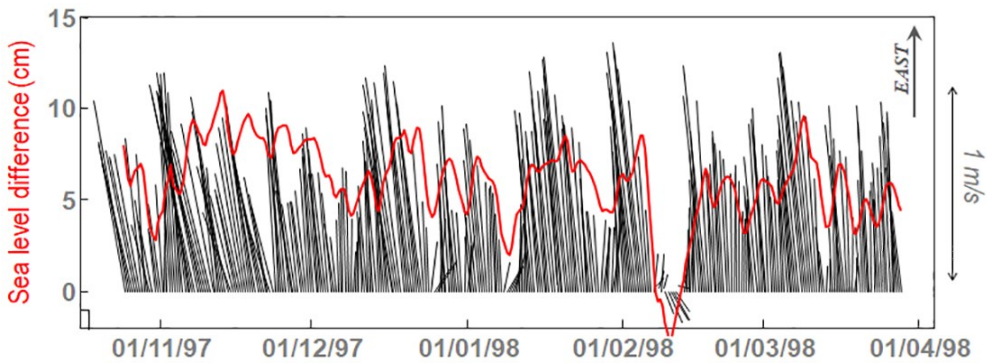


Figure 5.3. Black lines: Stick diagram of the velocity (scale on the right) recorded at 50m depth in site “C”, station C2 (Figure 5.1, Table 5.1 in Annex 5A). Vectors are oriented with reference to the East, indicated in the upper-right corner. Red line is the sea level difference between south (Ceuta, see Figure 5.1) and north (Algeciras) shores. Positive values indicate northward sea surface downslope (higher sea level in the south) as predicted by the geostrophic adjustment of an eastward surface current. (Adapted from García Lafuente, Delgado, et al., 2002).

The semi-geostrophic balance tends to accumulate water of the surface layer in the south coast of the SoG to build up the pressure gradient, a process that favors the north-to-south transport within this layer. Near the lateral boundary the geostrophically-balanced current is reduced by friction, so that the pressure gradient is able to drive cross-isobar ageostrophic flows (see Figure 5.4 and caption there) and generate a secondary cross-strait circulation (Garrett, 2004; Pratt & Whitehead, 2007). Laboratory experiments of two-layer exchange through channels of half-circular cross section (Johnson & Ohlsen, 1994) suggest that this flow is partially driven by the dynamics of Ekman boundary layers, where the net Ekman transport is to the left of the jet that induces the layer, looking downstream (Figure 5.4A). These authors suggest the existence of robust interfacial Ekman layers contributing to the secondary flow, although the behavior of these layers in the laboratory experiments was more complicated than expected as they did not extend all the way to the lateral boundaries, but apparently converged somewhere by the central part.

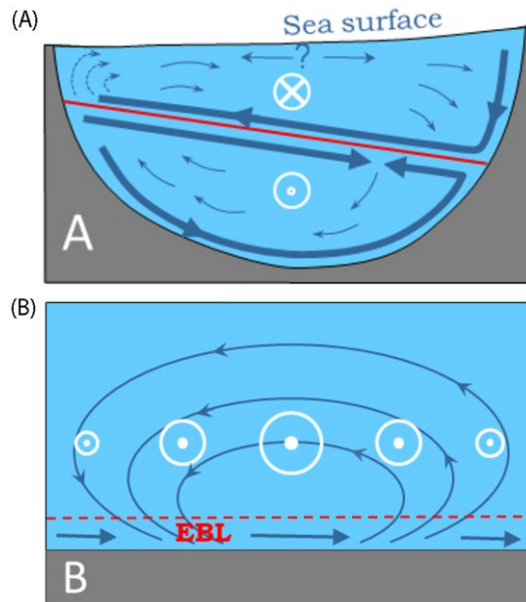


Figure 5.4. A) Schematic of a two-layer exchange through a channel of half-circular geometry, adapted from Johnson & Ohlsen (1994). Encircled white cross (dot) indicates flow into (out of) the page, thus resembling the exchange through the SoG as observed from the Atlantic looking to the Mediterranean, with the north (south) shore in the left (right). Northward downslope of the free surface and southward downslope of the interface (solid red line) are disclosed. Thick arrows indicate the solid boundary and interfacial boundary Ekman layers, whereas thin arrows illustrate the return flow in the interior (secondary circulation). B) Sketch of the interior ageostrophic circulation (thin arrows) driven by the convergence and divergence of the Ekman transport (horizontal thicker arrows) in the Ekman boundary layer (EBL, dashed red line) beneath a spatially-variable jet, represented by the (size) of the white encircled dots. Since outside of the EBL the flow is geostrophic (water moves along isobars) the secondary circulation represented by the thin arrows crosses the isobars and is therefore ageostrophic or out of geostrophic balance.

On the other hand, a spatially-variable jet flowing over the seafloor causes convergence and/or divergence in the bottom Ekman boundary layer (Figure 5.4B), in the same manner as a spatially-changing wind stress over the sea surface drives downwelling/upwelling in the open ocean. The jet forces an interior across-jet flow, sketched by the thin blue lines in Figure 5.4B that, in addition to slightly diminishing the jet strength via the Coriolis force (spin-

down process; Garrett et al., 1993, it facilitates across-jet transport of particles. Near-bottom Mediterranean outflow in the SoG shares spatial characteristics with this idealized jet (Baschek et al., 2001) for which it would provide chances for south-to-north connections in the present case.

The previous discussion has assumed a steady state exchange, which is far from being the case in the SoG. Tidal currents are strong enough to reverse the mean currents at semidiurnal time-scales (Bryden et al., 1994; Baschek et al., 2001; Sammartino et al., 2015) and, therefore, to cancel the intense flows during short time intervals. A first question is whether tidal dynamics could offer opportunity windows of diminished east-west flows for achieving north-south transport in a complete way. Tidal ellipses (over a tidal cycle, the tips of the tidal velocity vector trace out an ellipse called tidal ellipse) tend to have its major axis aligned with the shoreline and, therefore, its minor axis characterizes the cross-strait tidal velocity. Ellipses are highly polarized (García Lafuente et al., 2019) with minor axis less than  $10 \text{ cm}\cdot\text{s}^{-1}$  in all cases. A periodic velocity of this size causes periodic displacements of 1.4 km at semidiurnal frequencies, twice this value at diurnal ones, which are clearly insufficient to achieve a successful crossing. However, the shoreline orientation of the SoG changes noticeably from place to place. In the north, the shore veers almost  $90^\circ$  around Tarifa, changing orientation from NW-SE in the west to SW-NE in the east (Figure 5.1). Something alike happens in the south around Punta Cires (Figure 5.1). These important changes of orientation cause local misalignments of the ellipses that leave them partially oriented in the cross-strait direction (García Lafuente et al., 2013). Tidal currents around such singular sites would then contribute to eventual cross-strait transport more efficiently.

Another potential mechanism is the interaction of the total current with the lateral boundaries. It mainly entails the surface layer, which experiences the effect of abrupt changes of the shoreline orientation more than the Mediterranean layer, where bathymetry hardly changes orientation (Figure 5.1). García Lafuente et al. (2013) or Nadal et al. (2022), using Lagrangian trajectories of passive tracers computed from the output of a numerical model, show cross-strait intrusions of the tracer in the neighborhood of these



particular sites, opening new chances for a successful north-south connection. The mechanism is similar to the previous one, except for the fact that it deals with total current, not only tidal ones.

A detailed investigation of whether these processes can eventually lead to a successful hydrodynamic connection between the opposite shores of the SoG should be carried out by means of high spatial resolution advection schemes coupled to fully 3D, non-hydrostatic numerical models. Previously to such numerical effort, however, searching for observational evidences of cross-strait flows in existing records is an interesting exercise that can assist in future research. This is the objective of this work, which analyses different current meter data collected in the SoG to assess the potential of the recorded currents as vectors for the cross-strait spreading of the *Rugulopteryx okamurae* algae in the area.

#### 5.4 Summary of current meter observations and other data sets

Velocity observations come from three different sources: i) point-wise current meter data collected at points N, C, and S in the eastern SoG (see Figure 5.1) in the second half of 1990's decade within the frame of CANIGO project, which have been already employed in several publications (e.g. García-Lafuente et al., 2000, (García Lafuente, Alvarez Fanjul, et al., 2002; García Lafuente, Delgado, et al., 2002; Vargas et al., 2006), ii) Acoustic Doppler Current Profiles (ADCP) collected in year 2013 in the main sill of Camarinal (points CsS and CsN in Figure 5.1) used to investigate high frequency phenomena caused by flow-topography interaction (García-Lafuente et al., 2018), and iii) recent ADCP collected at point CsS (Figure 5.1) in years 2020-2021, which have not been used yet. Annex 5A provides more information about locations, time coverage and depths of all these observations.

Atmospheric pressure is provided by Puertos del Estado, Spain, (<https://portus.puertos.es>) for the period August 2020-July 2021 at a 1-minute sampling rate in the buoy of Palma de Mallorca (see Figure 5.1), taken as a representative of the Western Mediterranean basin. Wind data in the sub-

region of the SoG during the same time period have been retrieved from the ECMWF ERA5 reanalysis model (Hersbach et al., 2023), which is provided by the Copernicus Climate Change Service (C3S) (<https://climate.copernicus.eu>) with 1-hour temporal and  $\sim 25$  km spatial resolutions.

The available current meter time-series have been projected into a rotated Cartesian system aligned with the axis of the SoG (rotated  $20^\circ$  anticlockwise respect the east-north reference system). The y-component of the velocity in the new system is the cross-strait velocity, positive northwards, and the x-component is the along-strait velocity, positive to the east. The time-average of both velocity components as a function of depth is plotted in Figure 5.5 for the velocity series collected at the eastern section and in Figure 5.6 for the series collected at Camarinal sill.

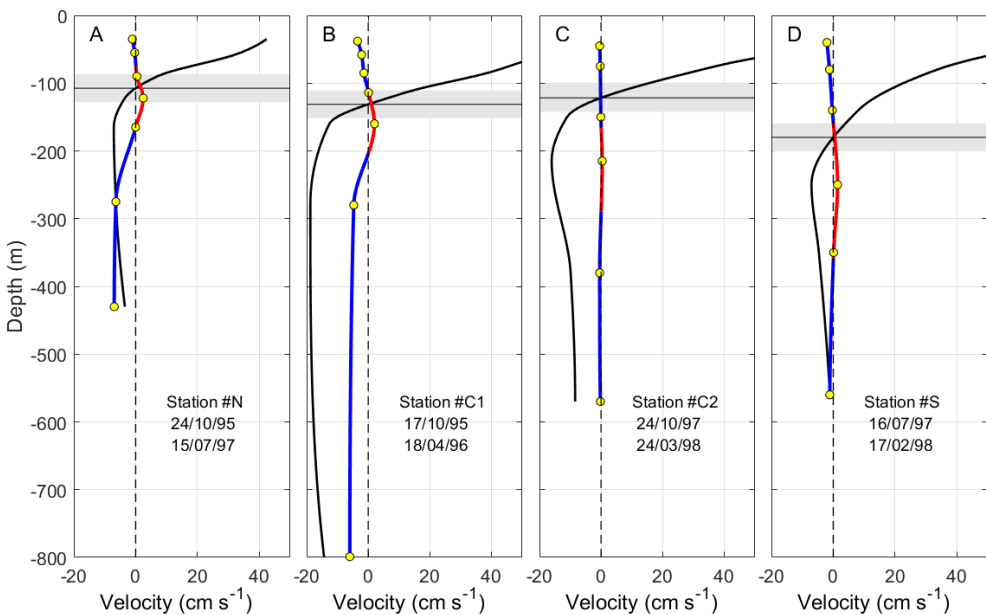


Figure 5.5. Time-average cross-strait (blue and red line) and along-strait (black line) velocity as a function of depth in the stations of the eastern section. Panel A corresponds to site N, panels B and C are for site C in two different periods, and panel D is for site S (see Figure 5.1 and Annex 5A for details). Horizontal black line is the depth of null time-average along-strait velocity, that is, the interface that separates inflow and outflow (notice the greater depth towards the south, in



agreement with the sketch of Figure 5.4A). Shaded rectangle indicates  $\pm$ std (standard deviation) of the subinertial fluctuations of this interface estimated in station CsS2 (see text for details). In all panels, solid lines are interpolated profiles from observations, whose depths are indicated by yellow circles. The depth range of positive (northwards) cross-strait velocity is marked in red. The  $\pm 1$  std interval of this velocity is indicated by light-blue thin lines.

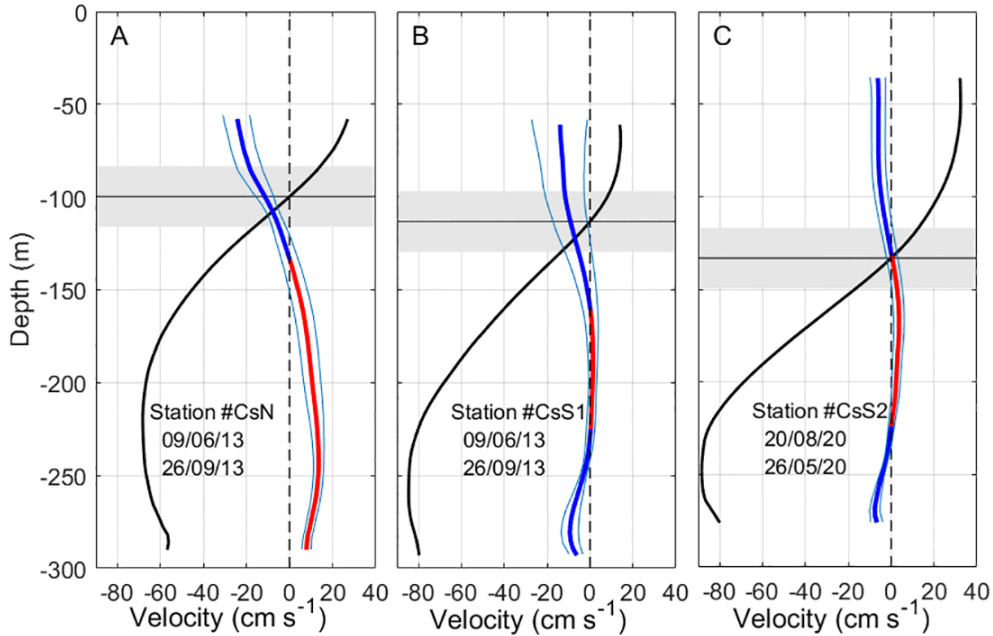


Figure 5.6. Same as Figure 5.5 for Camarinal sill section. Panel A is for site CsN and panels B and C are for site CsS in two different periods (see Figure 5.1 for locations). The profiles are directly computed from ADCP observations (no interpolation required) and circles indicating instrument depths do not apply.

The surface of instantaneous null velocity, which is the intuitive interface separating inflow and outflow, exhibits large tidally-driven oscillations. Even more, it often disappears because the entire water column moves in one direction during parts of the tidal cycle (Bryden et al., 1994; García-Lafuente et al., 2000). Only after removing tidal motions (by a low-pass filtering), this surface can be tracked, although it undergoes noticeable oscillations (Figure 5.7B) of meteorological origin (Candela et al., 1989; García Lafuente, Alvarez Fanjul, et al., 2002) that can exceptionally lead to its collapse during short intervals (García Lafuente, Delgado, et al., 2002).

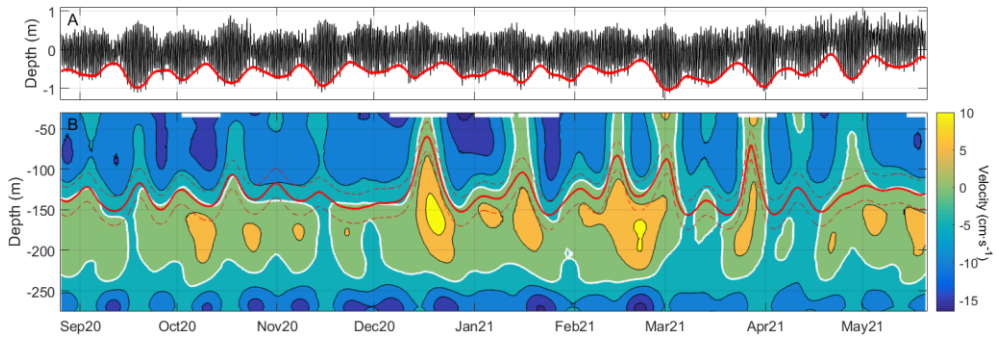


Figure 5.7. A) Pressure oscillations (converted to meters of water column) recorded by the pressure sensor of the ADCP after removing the mean pressure. The spring-neap tidal cycle is easily recognizable and has been made clearer by the smoothed low-water envelope represented by the thick red line. B) Contours (every  $5 \text{ cm}\cdot\text{s}^{-1}$ ) of the subinertial cross-strait velocity. Reddish colors indicate positive (northwards) velocity whereas bluish tones are for negative, the white line being the contour of cross-strait null velocity. Solid red line indicates the depth of along-strait null velocity (interface) flanked by two dashed red lines at  $\pm 1$  std of the mean interface depth. All time series correspond to station CsS2 in Camarinal sill.

A mean local interface has been defined as the time-averaged depth of the surface of null velocity obtained from the vertical profiles of velocity at each station. The horizontal black lines in Figure 5.5 and Figure 5.6 show the interface depth along with a confidence interval, which shows up as a shaded rectangle. This interval has been taken as the standard deviation of the subinertial fluctuations of the interface observed at station CsS2 (cf. Figure 5.7). The reason for choosing station CsS2 is the high spatial resolution provided by ADCP observations, necessary for the accurate determination of the null-velocity depth, and the length of the series, the longest of the ADCP stations (see Table 5.2 in Annex 5A).

## 5.5 Assessment of the possible cross-strait transport

### 5.5.1 Observation-based cross-strait mean secondary circulation

The successful algae spreading between both shores depends on the cross-strait current, as the floating spores or seaweed fragments eventually torn from the substrate behave as passive nearly neutrally-buoyant particles (see

next Section). However, the success is mediated by the along-strait current, which can displace those particles beyond the open boundaries of the SoG before they are transported from one shore to the other. A favorable coupling between both velocity components is thus necessary.

All the profiles in Figure 5.5 and Figure 5.6 show a mid-depth layer of positive cross-strait velocity flanked by negative layers on the surface and at depth, except for CsN site (Figure 5.6A), where the deeper part is lacking. Accordingly, south-to-north connection would be feasible within the intermediate layer (red line in profiles), whereas north-to-south transport could take place within either the surface or the deep layer (in the eastern SoG, in this case). Figure 5.5 and Figure 5.6 show values of cross-strait velocity of around  $5 \text{ cm}\cdot\text{s}^{-1}$  ( $4 \text{ km}\cdot\text{day}^{-1}$ ) or less in the intermediate and deep layers, thus requiring about 4 days at least to cross the SoG at its narrowest section ( $\sim 14 \text{ km}$ ) and longer through other sections. Along-strait mean velocity in the Mediterranean layer changes with depth and geographical location. In its core, the velocity increases from few tens of  $\text{cm}\cdot\text{s}^{-1}$  in the eastern part to nearly  $1 \text{ m}\cdot\text{s}^{-1}$  in the west (Figure 5.5 and Figure 5.6). Even assuming a moderate spatial mean value of  $40 \text{ cm}\cdot\text{s}^{-1}$ , the along-strait displacement undertaken in 4 days is close to 150 km, well above the dimensions of the SoG. The same or even more unfavorable considerations apply to the surface layer. Therefore, only by avoiding the core of greater velocities and remaining close to the interface could the algae have chances to cross the SoG.

According to Figure 5.5 and Figure 5.6, the last condition discards connectivity within the deeper layer and reduces the chances to the upper and intermediate layers. South-to-north (north-to-south) transport could be achieved in the depth range where the red (blue) profile in Figure 5.5 and Figure 5.6 overlaps the shaded grey rectangle. The depth range of positive cross-strait velocity overlaps this rectangle more clearly in the eastern part (red lines in Figure 5.5), suggesting that this section of the SoG gathers better conditions for successful south-to-north connection within the intermediate layer. The contrary would happen in Camarinal sill (Figure 5.6) where north-to-south transport in the upper layer is favored.

## 5.6 Time variability of the cross-strait secondary circulation

The previous description based on time-average values of the velocity must be revised when subinertial variability (from days to few tens of days) is considered. Figure 5.7B shows contours of the cross-strait velocity after filtering the series with a low-pass filter of 3-day cutoff period that removes tides. The depth of the interface of null along-strait velocity together with the  $\pm 1$  std interval (red lines) have been superposed to the contours. Figure 5.7A has been included to disclose the fortnightly spring-neap tidal cycle that modulates the semidiurnal tides.

The intermediate layer of positive cross-strait velocity displayed in Figure 5.6C is easily recognizable in Figure 5.7B, despite its thickness fluctuations. Periods of enhanced velocity alternate with other periods of reduced or, even, reversed (negative) velocity. The point of interest is the existence of sustained periods of enlarged velocity nearby the interface depth that provides good chances for south-to-north transport. According to Figure 5.7, they seem to occur preferably in winter (December 2020 to February 2021). Similar velocity and thickness fluctuations are seen in the surface layer, affecting in this case the north-to-south connectivity. Therefore, subinertial variability offers windows of enhanced cross-strait velocity lasting long enough to allow for successful connection between both shores, a result that applies for both directions.

Velocity fluctuations in Figure 5.7B may have different origins. A correlation study for investigating relationships between the velocity field and external drivers has been done. Absolute velocity values have been used to avoid the unintuitive detail that higher values of negative velocities mean lower intensities and vice-versa. Figure 5.8A to D show the results for along-strait velocity. Since exchanged flows are computed from this component and the response of those flows to external agents is well established (Candela et al., 1989; García Lafuente, Alvarez Fanjul, et al., 2002), these panels are used here as quality tools. They are expected to show confirmation of this response, which in turn will provide support to the conclusions drawn from

Figure 5.8E to 7 for the much less studied cross-strait velocity, the one of interest in this work.

### 5.6.1 Meteorologically-induced fluctuations

The along-strait velocity is negatively correlated with the atmospheric pressure over the western Mediterranean above the interface and positively below it (Figure 5.8A). High pressure will reduce the inflow and increase the outflow, giving rise to a barotropic fluctuation of the net flow towards the Atlantic. Westerlies (positive zonal winds) increase the velocity in the upper layer, easterlies (negative zonal winds) diminish it (Figure 5.8B). Lower layer velocities show positive correlation too, suggesting that wind-stress induces baroclinic fluctuations of the exchange. These results have already been reported (Candela et al., 1989; García Lafuente, Delgado, et al., 2002; García Lafuente, Alvarez Fanjul, et al., 2002; Peliz et al., 2009; Boutov et al., 2014) and provide indirect support to those inferred from the correlation analysis for cross-strait velocities, which are discussed next.

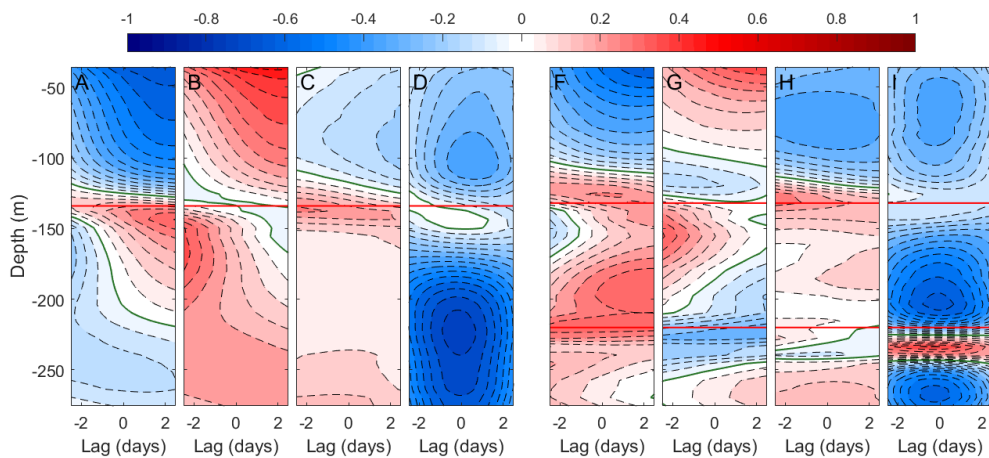


Figure 5.8. Left panels: contours of lagged correlation as a function of depth between the modulus of along-strait velocity with A) the atmospheric pressure in Palma de Mallorca (see red dot in Figure 5.1), taken as representative of the Western Mediterranean basin, B) the local zonal component of wind, C) the meridional component of wind and D) the strength of the spring-neap tidal cycle as determined by the envelope displayed in Figure 5.7A. Contour lines are every 0.05 units of correlation with the zero contour shown in green. Horizontal red line indicates the

depth of zero-crossing of the along-strait velocity (see Figure 5.6C). Right panels: same as left panels but for the cross-strait velocity. Red lines indicate the depths of cross-strait zero velocity. In all cases, positive lags correspond to “forcing” (i.e., atmospheric pressure, wind, strength of the tide) leading the “response” (i.e., the velocity components).

Focusing on the upper and intermediate layers that extend over the depth range occupied by the interface (Figure 5.5 and Figure 5.6), Figure 5.8F shows negative and positive correlations, respectively, with the modulus of the cross-strait velocity. Therefore, high atmospheric pressure will diminish the southward current in the upper layer and increase the northward one in the intermediate layer. It shares characteristics of its counterpart Figure 5.8A in the sense that the response is a barotropic fluctuation that shifts the secondary cross-strait circulation towards a situation of decreased surface current. The opposite would happen under low pressures. Zonal winds (Figure 5.8G) produce positive correlation in the top of the upper layer and in the intermediate layer. Westerlies would increase the velocity in these segments of the water column and enhance the secondary cross-strait circulation. The opposite effect would happen with easterlies. The effect of meridional winds (Figure 5.8H) recalls the one of atmospheric pressure (Figure 5.8F). Northward (positive) wind reduces the mean southward cross-strait velocity in the upper layer and increases the northward one in the intermediate layer. The opposite would happen with southward winds. Both results are expectable.

### 5.6.2 The fortnightly tidal cycle

One of the clearer features in Figure 5.7B is the fortnightly fluctuations of the cross-strait velocity, which reveals their tidal origin. Figure 5.8I, in fact, shows extended negative correlation with the strength of the tide in the upper and intermediate layers, meaning that the secondary cross-strait circulation is diminished during spring tides and enhanced during neap tides. A similar conclusion is drawn from the negative correlation between the strength of the tide and the modulus of the along-strait velocity in practically the entire water column displayed in Figure 5.8D. The correlation is particularly high

in the lower Mediterranean layer, which implies weaker subinertial, tidal-free currents in spring tide and stronger in neap tide. This somewhat unintuitive result has been discussed in (García-Lafuente et al., 2000; Vargas et al., 2006) and is ascribed to enhanced mixing during spring tides which diminishes the horizontal density gradient that drives the flow. Figure 5.8D is encouraging in the sense that depicts a contrasted result that supports the findings for the cross-strait velocity component.

The joint consideration of the outcome of the correlation analysis allows to stress favorable opportunity windows and unfavorable scenarios for cross-strait connections. Regarding meteorological forcing, northward flow within the intermediate layer would increase under high pressure over the western Mediterranean basin and local winds from the southwest. If, moreover, these particular conditions are met during neap tides, the resulting scenario would gather the best conditions for south-to-north connectivity. The opposite would happen under low pressure and local northeasterly in spring tides, which would diminish the chances. As for the upper layer, the southwards flow that favors north-to south connection would increase under low atmospheric pressure and local northwesterly along with neap tides. Chances would decrease with low pressure and southeasterly in spring tides.

## 5.7 Other requirements for a successful connection

Let us consider one of the shores of the SoG with algae settlements while the other is still free of them. What conditions must be met to achieve a successful colonization of the algae-free shore without human intervention? First of all is the existence of the cross-strait system of flows described in the previous sections. The current to take advantage of depends on which shore holds the initial settlement: should it be the north one, the right current is that at the surface layer, but if the initially colonized is the south shore, the proper current lays in the intermediate layer. In addition to this secondary circulation, the successful colonization requires other set of circumstances that include physiological traits and endurance of algae.

The weak cross-strait flow is able to transport products from a shore to the other only if they are available. For south-to-north transport, for instance, algal fragments must reach the interface, situated 100-150 m below the sea surface in the south, be carried to the north at these depths and, once there, be moved upwards into the illuminated layer to settle and thrive. The journey will take days to weeks and be done in dark conditions. The colonization success will thus depend on whether or not the algae arrive in good conditions for reproduction after that period of weak light or no-light conditions.

### 5.7.1 Reaching the right depth for crossing and returning to illuminated layers

Macroalgal strains are attached to rocky illuminated bottom and other type of substrates in the subtidal nearshore zone of the SoG to a maximum observed depth of 40 m (García-Gómez et al., 2020). There are also evidences that they are drifting freely well below this depth (Figure 5.2). They must be torn out from the substrate to provide free spores, propagules or seaweed fragments for transportation. Density of algae and vertical velocity of the flow come into play at this stage. *Rugulopteryx okamurae* is very slightly denser than seawater. Simple experiments performed in calm sea conditions in which thalli were dropped near the surface and allowed to fall freely, yielded sedimentation velocities in the range of 1 to 4 cm·s<sup>-1</sup>, depending on the size and shape of the thalli and on whether they form larger aggregates. Similar experiments carried out under more controlled conditions in the laboratory gave a little broader sedimentation velocity range (from 1 to 6.5 cm·s<sup>-1</sup>) and confirmed its dependence on the shape and size of the specimens. Variations of seawater density within realistic intervals will hardly change that velocity. The small density difference makes the algae be easily re-suspended by wind-induced or current-induced turbulence, carried to the surface and eventually beached on the shores, often in astonishing amounts (García-Gómez et al., 2020; Aamri et al., 2018; García-Gómez et al., 2018; Altamirano Jeschke et al., 2017), see Figure 5.2B.



Flow-topography interaction in the SoG forms internal hydraulic jumps with high levels of turbulence nearby Camarinal sill (Wesson & Gregg, 1994). They decay as short-period, large-amplitude internal waves (Farmer et al., 1988) with associated vertical velocities of tens of  $\text{cm}\cdot\text{s}^{-1}$  (Sánchez-Garrido et al., 2011), greater than the measured sedimentation velocity. Figure 5.9A shows a short time series of vertical velocity near the interface at stations CsN and CsS1 and illustrates the fact. It changes sign and exhibits semidiurnal fluctuations that disclose their tidal origin. Absolute values exceed the sedimentation velocity and can therefore displace algal fragments up or down vertically. Profiles in Figure 5.8B and Figure 5.8C suggest that this result applies to the whole water column. However, nearby the interface, downward advection is more likely to occur in the south and upward advection in the north, as it can also be deduced from Figure 5.9A.

The combination of the very small negative buoyancy of algal fragments and the structure and strength of vertical velocities in the SoG makes it feasible for the algae to reach the suitable depth to be advected across the SoG. They would do it in one direction or the other, depending on the depth range in which they stay (cf., Figure 5.4). Once on the other side, vertical currents could bring them into the illuminated surface layers and allow them to begin colonizing new environments.

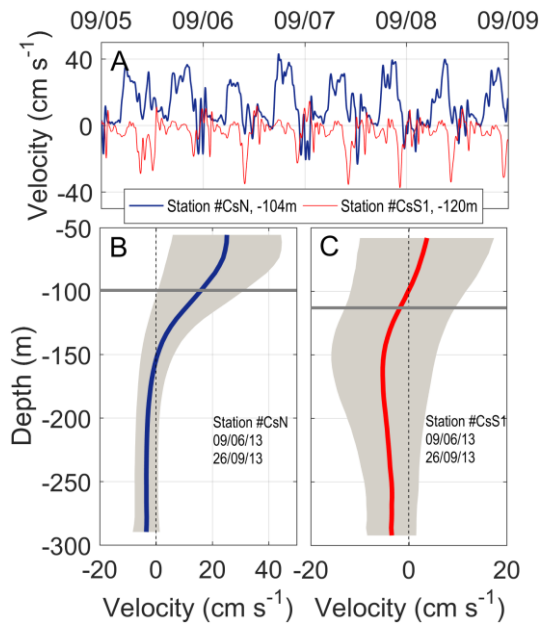


Figure 5.9. A) Vertical velocity recorded at stations CsN and CsS1 at depths of 104m and 120m, respectively, close to the time-averaged interface depth. Dates on the top axis correspond to September 2013. Velocities were recorded every two minutes and have been smoothed by a 5min cut-off period filter. B) Vertical profile of the time-averaged vertical velocity at station CsN (blue line). Shaded area stretches over  $\pm 1$ std and the horizontal grey line indicates the (mean) interface depth. C) Same as B) but for station CsS1.

### 5.7.2 Keeping the right conditions for spreading

The colonization will depend on the health status the algae arrive with after a relatively long journey made in low light or, even, no light conditions. To gain insight into this issue, *Rugulopteryx okamurae* specimens collected in Tarifa (see Figure 5.1 for location) were placed in darkness inside a culture chamber of nutrient-rich seawater at 17°C. After 13 days, they showed a considerable health decay, measured as its photosynthetic capacity. However, these specimens were able to recover partially when they were re-exposed to light after the dark period. Even though the initial condition was not fully achieved, they were able to reactivate their metabolism again, thus offering chances for colonizing the new region of arrival. This outcome agrees with other studies. Photosynthetic measurement using *in vivo* chlorophyll

fluorescence in algae collected in nets during fish activities between 50-100m depth in the same area gave satisfactory value of electron transport rate as indicator of photosynthetic activity (Figuerola et al., 2020). Also, Rosas-Guerrero et al. (2018) observed that adult thalli of the species had survival rates between 80-100% after being cultivated in dark conditions for three weeks, depending on the temperature during cultivation, and that these thalli even increased their biomass during this period.

This outcome is not new in the algae realm. Microscopic stages of macroalgae can withstand long periods of darkness and subsequently develop when conditions improve (Leukart & Lüning, 1994; Santelices et al., 2002; Carney & Edwards, 2006). *Aureococcus anophagefferens* (Pelagophyceae), a heterokont alga responsible for the harmful brown tides, was able to survive for at least 30 days in the dark according to (Popels & Hutchins, 2002). Otherwise, arctic macroalgae (Laminarians and some Rhodophytes) and different polar phytoplankton can survive during the polar night with up to six-month darkness, when they are unable to photosynthesize. They do it by evolving specific strategies during darkness, like maintaining low metabolic state to decrease the consumption of storage compounds and energy. When light returns after the dark period, they re-initiate the growth (Lacour et al., 2019; Li et al., 2020; Gordillo et al., 2022). The mechanisms involved in survival during darkness are not yet well known for these species, nor for *Rugulopteryx okamurae*. Further studies are required on this. However, the point of interest here is that there are real possibilities of survival during the time interval needed for transportation from one shore to the other.

## 5.8 Summary and final remarks

Simultaneous appearance of *Rugulopteryx okamurae* in both shores of the SoG few years ago seems highly improbable. A much more likely situation is that the algae settled in one shore, from which it invaded the opposite one. Favorable environmental conditions propitiated its subsequent explosive spreading. Algae capability to colonize any type of hard substrates (García-Gómez et al., 2018) opens the possibility of accidental crossing attached to ship hulls, fishing nets or other human-mediated mechanisms, but the

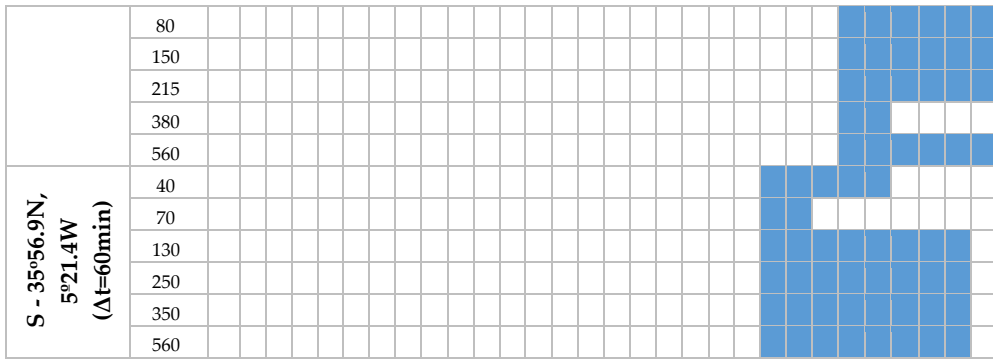
possibility still remains that it could have managed to cross the SoG taking advantage of hydrodynamic processes without human intervention.

The possibility has been assessed in this study using current meter observations collected in the area, which show layers of no null velocity in the cross-strait direction. Chances for cross-strait transport reduce to the depth range around the interface of null along-strait velocity, located at around 100-150 m depth. Within this range, layers of weak cross-strait currents heading south and north have been identified above and below the interface, respectively. They could be used by nearly-neutral buoyant seaweed fragments for being transported from one shore to the other. Outside of this depth range, possibilities drop null, as particles will be advected beyond the lateral open boundaries of the SoG by the strong inflow and outflow.

The successful connection, however, relies on a chain of circumstantial links. Algae should be ripped out from the seafloor by natural (wind-induced or current-induced turbulence) or human (bottom-trawling nets) agents in the surface illuminated layer at the colonized shore. Their propagules or spores should be displaced offshore in the horizontal and to the depth range of the interface in the vertical. Then they should be transported across the deepest part of the SoG until reaching the opposite continental slope, be raised to the surface and displaced to the shore and, finally, settle and thrive in the new environment. The process will take weeks, much of the time the algae being in extreme low or even no-light conditions. This study argues that each and every of these contingencies, considered one by one, are surmountable. For a single experiment, however, the concatenation of the full sequence of events leading to a successful connection is extremely improbable. Obviously, it is only the massive amount of available specimens for transport that can provide a number of successful connections. Even if this number of connections is reduced, it would be enough to colonize the new ecosystem taking into account the huge adaptability of the algae.

The feasibility of this possibility could be tested with the help of very high resolution fully 3D numerical models coupled to high resolution advection





### 5.9.2 Camarinal sill section

Two sites at the Camarinal sill cross-section (CsN, CsS in Figure 5.1) were sampled between June and September of 2013 with Acoustic Current meter Profilers at high sampling rate in order to investigate high-frequency hydrodynamic phenomena occurring in the SoG. Location CsS was revisited in years 2020-2021. Positions, periods of deployment, sampling intervals and depth range are indicated in Table 5.2.

Table 5.2. Information on the acquisition of the current meter data at Camarinal sill section of the SoG used in this study. The two deployments at site “CsS” were several years apart and have been considered as separated stations (“CsS1” and “CsS2”, the former simultaneous with “CsN”).

Station Name	LAT	LON	Bin-max depth	Bin thickness	N° of bins	Start time dd/mm/yyyy	End time dd/mm/yyyy	Sampling (min)
CsN	35°56.9N	5°46.2W	290m	6m	40	09/06/2013	26/09/2013	4
CsS1	35°54.6N	5°44.7W	292m	6m	40	09/06/2013	26/09/2013	4
CsS2	35°54.6N	5°44.7W	276m	6m	42	20/08/2020	26/05/2021	30



# 6 Modeling spread of an alien alga under different temporal scenarios in the Strait of Gibraltar and adjacent basins<sup>4</sup>

## 6.1 Abstract

The expansion of the invasive macroalga *Rugulopteryx okamurae* across the Alboran Sea and northeastern Atlantic since its introduction through the Strait of Gibraltar has been rapid, but the mechanisms by which this successful colonization has occurred have not been fully understood. By using two nested high-resolution hydrodynamic models coupled to a Lagrangian particle tracking algorithm, we tested whether the trajectories of the invasive alga as vectors of biological pollution can be explained by numerical passive dispersal. Virtual tracers, representing free spores, thalli fragments, or detached mats of *Rugulopteryx okamurae* were periodically released in the Strait of Gibraltar during the year 2021. Dispersal simulations indicate that the algal spores first spread eastward before spreading westward, with transport by the Atlantic Jet leaving the Strait of Gibraltar being the most influential process. Tidal strength, followed by winds, is a dominant agent, with spring tides and easterly winds generally promoting higher particle accumulation inside the Alboran basin. The terminal settling velocity of particles is a critical condition, as revealed by a model sensitivity test. The potential utility of numerical tools in elucidating the dispersal dynamics of introduced and expanding species, identifying high-risk areas, and formulating management strategies for these species is discussed.

---

<sup>4</sup>The contents presented in this chapter are the preliminary results of an article that is currently being developed and prepared for submission to the journal Marine Pollution Bulletin in the following months of 2024.



## 6.2 Introduction

Marine invasive alien species cause biological pollution and pose a significant threat to the marine environment, potentially leading, in some cases, to a reduction in biodiversity and ecological functionality (Solís-Díaz et al., 2022). Recent concerns regarding bioinvasions (i.e. the successful establishment and spread of alien species) have focused on exotic macroalgae (Mannino et al., 2021; Tsirintanis et al., 2022; van der Loos et al., 2023), whose proliferation affects native community structures and diversity through competitive resource interactions, including light and nutrients (Strong & Dring, 2011). The Mediterranean Sea has become a hotspot for such algal invasions, with several species introduced via diverse pathways, including ballast water discharge, mariculture, and fishing activities (Z. Wang et al., 2022; Fortič et al., 2023). However, the management and control of the introduced species are impeded by the limited understanding of their origins and dispersal mechanisms in the invaded regions.

Among these, *Rugulopteryx okamuræ* (Dictyotales, Phaeophyta), an alien macroalga, has been identified as a particularly concerning and hard-to-manage invader in the Mediterranean (EU, 2022). Native to the northwestern Pacific Ocean, the brown alga was first detected in the Mediterranean in 2002 in the coastal lagoon of Thau (southwestern France) (Verlaque et al., 2009). In 2016, a subsequent arrival occurred in the Strait of Gibraltar (SoG) off the coast of Ceuta (Altamirano-Jeschke et al., 2016). Shortly after, thousands of tons of decomposing *R. okamuræ* biomass were found along the coasts on both sides of the SoG (Altamirano-Jeschke et al., 2016; Ocaña Vicente et al., 2016) and fishing fleets reported an alarming decline in catches due to the extreme clogging of the alga in their nets (refer to Figure 1 from Báez et al., 2023). In the SoG and surrounding areas, the seaweed has rapidly colonized diverse marine habitats, ranging from shallow to deeper waters (0-40 m depth; García-Gómez et al., 2021), displacing organisms inhabiting soft and rocky seafloors in illuminated and shaded areas (García-Gómez et al., 2018; Estévez et al., 2022), and causing significant alterations to the local biota (Sempere-Valverde et al., 2021; Ferreira-Anta et al., 2023).

Its extraordinarily high connectivity potential, i.e. the effective linkage between the releasing sources and the receiving regions, is facilitated by its dispersal through floating drifting thalli at practically any depth in the water column (Mateo-Ramírez et al., 2023), prolific vegetative production (Altamirano-Jeschke et al., 2016), survival under adverse environmental conditions, such as low or no light (García-Lafuente et al., 2023; Mateo-Ramírez et al., 2023), and wide thermal variations (Rosas-Guerrero et al., 2021). To date, this has resulted in the continued expansion of *R. okamurae* to a large part of the Atlantic and Mediterranean coastal areas (Figure 6.1b,c,d), including the southern and eastern Iberian Peninsula (García-Gómez et al., 2020; Mateo-Ramírez et al., 2023; Rueda et al., 2023; Terradas-Fernández et al., 2023), northern Africa (Aamri et al., 2018), southeastern France (Ruitton et al., 2021), southern Italy (Bellissimo et al., 2023), southwestern Portugal (Liulea et al., 2023), and the Macaronesia Islands (Faria et al., 2022), where it is causing severe environmental, health, and economic impacts (De la Lama-Calvente et al., 2024).

The impacts and adaptability of *R. okamurae* in the Mediterranean environment have been the subject of extensive research recently (García-Gómez et al., 2018, 2020, 2021; Sempere-Valverde et al., 2021; Mercado et al., 2022; Florido et al., 2023). However, critical aspects such as the processes driving their distribution and the origins of their invasive success still remain to be understood. Muñoz et al. (2019) employed an environmental favorability model to predict the alga's expansion within the Mediterranean, highlighting the Alboran Sea coastlines as particularly conducive environments. Subsequent observations in the northern Alboran partially validated this prediction (Mateo-Ramírez et al., 2023; Rueda et al., 2023), although a detailed distribution and density of the settled populations in the basin remain largely undefined. In a more recent observational study, García-Lafuente et al. (2021) explored the origin of the algal invasion and raised the hypothesis that hydrodynamic processes, in addition to human-mediated vectors (e.g. ballast water and hull fouling from shipping), were partially responsible for its nearly simultaneous appearance on both sides of the SoG. While the well-known two-way exchange in the Strait makes a direct link

unlikely, the authors suggest that cross-strait currents at certain depths could be responsible for either the northward or southward algal spread.

Both arguments are candidate processes to be addressed by Lagrangian particle tracking simulations. When coupled with high-resolution numerical models capable of accurately representing circulation features, Lagrangian algorithms are valuable tools for examining the physical processes that affect the dispersal of virtual particles in the marine environment. Dispersing agents in these approaches commonly represent passive target organisms or elements, such as plankton, algae, or debris, whose active mobility is null or negligible when compared to the effect of drift by ocean currents. In particular, numerical results provide significant advantages in invasive species management by identifying potential source locations and paths of marine non-indigenous species, assessing the risk of invasions, and designing early warning systems (Crivellaro et al., 2022). The aim of our study is therefore to employ a Lagrangian tool with virtual tracers representing free spores, thalli fragments, or detached mats of *Rugulopteryx okamurae*, to test whether the trajectories of the invasive alga as vectors of biological pollution can be explained by numerical passive dispersal. The work focuses on the SoG, the location where the macroalga concentrated before its aggressive colonization, and its adjoining basins, the Alboran Sea and the Gulf of Cadiz, which have been significantly affected by the algal invasion so far. An existing numerical model of this region has been refined, particularly in the Strait, to enhance its already high performance in simulating the complex hydrodynamics of this area that could contribute to explain and manage the algal spreading.

The structure of the work is as follows: Section 6.3 provides an overview of relevant circulation features of the regions of study, including a brief literature review of the occurrences of *Rugulopteryx okamurae* in the Mediterranean Sea and northeastern Atlantic since its first detection in the SoG. Section 6.4 describes the hydrodynamic model used to represent the main circulation features, including two subsections on the model domain, initialization, and validation. After assessing its performance, the model results are used to force a Lagrangian particle tracking algorithm, whose

simulation details are described in Section 6.5. Section 6.6 presents the results of this work in terms of particle accumulation in shorelines, with subsections examining the accumulation ratios in particular months, the dependence of the terminal settling velocity on the numerical results, and the implications of the model results for species management. Finally, Section 6.7 contains the concluding remarks.

### 6.3 Relevant hydrodynamic features of the study area

The SoG is the only passage connecting the Atlantic Ocean to the Mediterranean Sea, a semi-enclosed basin where evaporation exceeds precipitation and river runoff (Bethoux, 1979). To compensate for the resulting net buoyancy loss, a two-way exchange occurs therein: lighter Atlantic waters ( $S < 36.5$ ), mainly North Atlantic Central Water (NACW), enter the Mediterranean invading the Alboran Sea at the surface (Echevarría et al., 2002), while saltier Mediterranean waters ( $S > 38.2$ ), mainly Levantine Intermediate Water (LIW) and Western Mediterranean Deep Water (WMDW), flow towards the Atlantic Ocean underneath (Naranjo et al., 2015). On average, the volume transport is slightly less than 1 Sv in both directions ( $1 \text{ Sv} = 10^6 \text{ m}^3/\text{s}$ ).

The mean exchanged flux is subject to variability on different time scales, ranging from tidal to subinertial, seasonal and interannual, modifying its velocity and direction (García Lafuente, Alvarez Fanjul, et al., 2002; García-Lafuente et al., 2000, 2007, 2009). The interaction between tides and topography produces one of the world's most unique internal tides, capable of vertically displacing the interface depth by over 100 meters and inducing substantial temperature and salinity fluctuations at tidal frequencies (Sánchez-Garrido et al., 2011). Also, barotropic flow variability, driven by atmospheric pressure differences between the Atlantic Ocean and Mediterranean Sea, can significantly alter the baroclinic exchange on timescales ranging from a few days to a few weeks (García Lafuente, Alvarez Fanjul, et al., 2002).

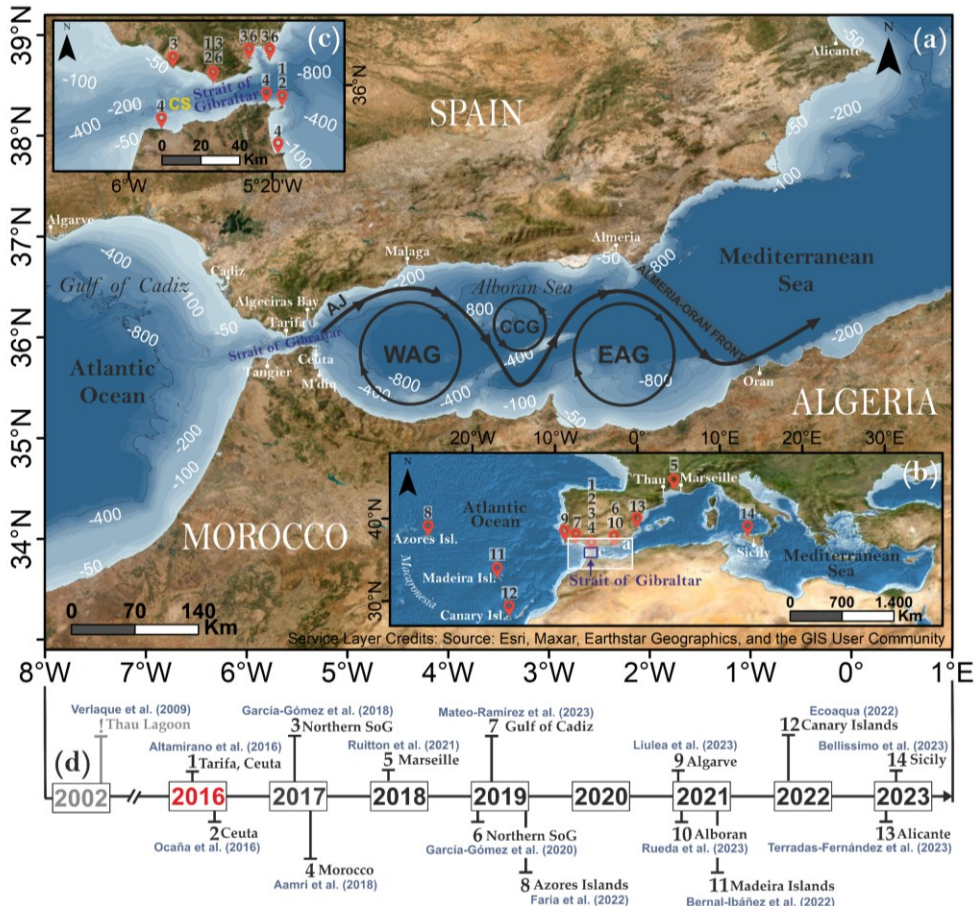


Figure 6.1. (a) Map of the study area showing bathymetric features and outlining its prevailing surface circulation: the Atlantic Jet (AJ), the Western and Eastern Alboran Gyres (WAG, EAG, respectively), and the Central Cyclonic Gyre (CCG). (b) Map of the northeastern Atlantic Ocean and the Mediterranean Sea, highlighting the location of the Alboran Sea (white square) and the SoG (purple square), and spotting records of *Rugulopteryx okamurae* through a sequential number code, where 1 is the first reported detection in the SoG in 2016 and 14 is, to our knowledge, the last reported record to date. (c) Zoomed-in-view of map (b) in the SoG, with a label that indicates the position of the main sill of the Camarinal (CS). (d) Timeline plot of the 14 records of *Rugulopteryx okamurae* spotted in maps (b,c) from the existing scientific literature.

The upper-layer of Atlantic water enters the Alboran Sea through the formation of a swift Atlantic Jet (AJ), which extends over the surface from 0 to 200 m (Figure 6.1a), and features velocities of  $\sim 1$  m/s (Sánchez-Garrido & Nadal, 2022). In its way eastward, it follows a wavy path around the Western

and the Eastern Alboran Gyres (WAG and EAG, respectively; see Figure 6.1a), two mesoscale anticyclonic and oligotrophic gyres typically present in the basin, the EAG being less common, especially in winter (Renault et al., 2012). Between the WAG and the EAG lies a third mesoscale cyclonic gyre of smaller size, referred as the Central Cyclonic Gyre (CCG), which promotes upwelling conditions that enhance primary production in the area (Sánchez-Garrido & Nadal, 2022). The eastern boundary of the Alboran circulation system is marked by the Almería-Oran front, which flanks the eastern side of the EAG (Tintoré et al., 1988; Sanchez-Vidal et al., 2004).

Winds in the Alboran Sea are mainly zonal. Easterly and westerly winds blow with nearly equal magnitude and are equally likely to occur, with slight seasonal variations. The strongest winds in both directions typically occur in winter, while the mildest winds occur in summer, when easterlies are slightly more frequent than westerlies. The overall zonal orientation of the Alboran Sea coastline makes it suitable for wind-driven coastal upwelling to occur on either the northern or southern coast of the basin (Sánchez-Garrido & Nadal, 2022).

## 6.4 Hydrodynamic model

### 6.4.1 Model description and initialization

The result of two-nested numerical models, whose code is based on the MIT General Circulation Model (MITgcm hereafter, Marshall, Adcroft, et al., 1997; Marshall, Hill, et al., 1997) have been applied in this study. MITgcm has been previously used to accurately represent the circulation features of this particular region (Sánchez-Garrido et al., 2011, 2013), among other works), and was further employed by Sammartino et al. (2017) in a successful three-level nesting implementation in the Bay of Algeciras (eastern margin of the SoG, see Figure 6.1a). A detailed description of the equations and technical details of the model can be found in the cited works.

The two nested models are formulated on an orthogonal curvilinear Arakawa C-grid with vertical discretization on Z-levels (Figure 6.2). The first



nesting layer, referred to as the regional model hereinafter, matches the domain with the previous version of the same model (e.g. Sammartino et al., 2017), albeit at a higher horizontal ( $\sim 200$  instead of  $\sim 600$  m within the Strait) and vertical (72 instead of 46 Z-levels) resolution. The second layer, referred to as local model, is focused on the SoG and is nested at a 1:5 downscaling ratio relative to the first domain (see insets of Figure 6.2), resulting in a minimum grid spacing of  $\sim 45$  m, the highest resolution available for modeling the SoG to date. The bottom topography in both domains is derived from four bathymetric sources, namely, the multilayer bathymetric product from the EMODnet Digital Terrain Model (EMODnet Bathymetry Consortium, 2018), the ecocartography campaign developed by the Spanish Ministry of Agriculture, Fisheries and Food between 2000 and 2012 for the Gulf of Cadiz (Gaide et al., 2018), the high-resolution topobathymetric map of the southeastern Spanish continental shelf produced by the Spanish Oceanographic Institute and the General Secretariat of Maritime Fisheries (Acosta Yepes et al., 2006), and the high-resolution coastline of the OpenStreetMap project (OpenStreetMap contributors, 2015).

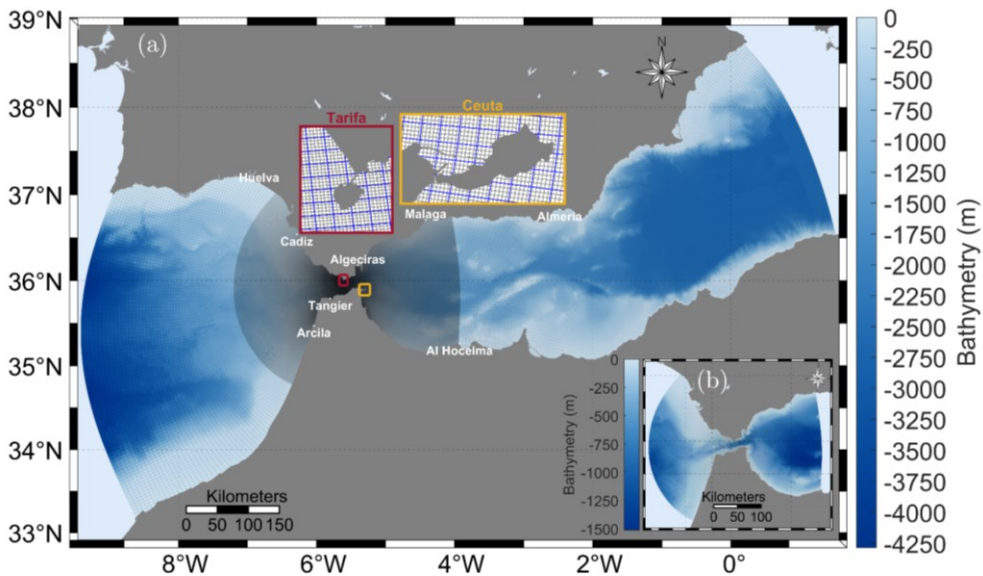


Figure 6.2. Computational grid and bottom topography of the two nested domains, where the regional model (a), of larger extent and less horizontal resolution, embeds the local model (a, b), of less spatial extent and higher horizontal resolution. In the

insets, a zoomed-in view of the outer (blue lines) and inner (grey lines) grids in Tarifa (maroon box) and Ceuta (yellow box) are displayed.

The regional model simulation run from late 2020 to the end of 2021, and it is fed with imposed initial and boundary conditions. The approach is based on a one-way nesting scheme, whereby the model variables at the open boundaries are relaxed within a sponge layer by interpolating the outputs from larger-scale models (Spall & Robinson, 1989). At the two lateral open boundaries, the Mediterranean Sea Physics Analysis and Forecast System (CMEMS MED-Currents, EAS6 system; Clementi et al., 2021) provides the hourly baroclinic (density-varying) fields of temperature, salinity, and zonal (u) and meridional (v) components of velocity. The operational storm surge NIVMAR model (Álvarez-Fanjul et al., 2001) provides meteorologically-driven barotropic velocities to account for the remote effect of the atmospheric forcing over the Mediterranean basin. The MOG2D-G High Resolution barotropic model (Carrère & Lyard, 2003), developed by Legos/CNRS, contributes the tidal harmonics necessary for the calculation of the barotropic tidal velocity forcing, namely,  $M_2$ ,  $S_2$ ,  $N_2$ ,  $K_2$ ,  $K_1$ ,  $O_1$ ,  $Q_1$  and  $P_1$ . The atmospheric forcing at the sea surface, including wind stress, humidity, air temperature, and shortwave and longwave radiation, is computed using data from the ECMWF ERA5 atmospheric reanalysis (Hersbach et al., 2023). Conversely, the inner domain simulation is run from March 1 to March 15, 2021, due to the achieved high-resolution and the computational effort required for a longer simulation. The baroclinic fields of the initial and boundary conditions are provided by the lower resolution model results, while the atmospheric forcing from the ECMWF ERA5 atmospheric reanalysis is interpolated to the grid's surface resolution.

#### 6.4.2 Model validation

Previous studies have satisfactorily validated the regional model at tidal and subinertial timescales using diverse observational data sources, including a set of mooring lines deployed in the Algeciras Bay during the SAMPA project (Sammartino, Sánchez-Garrido, et al., 2014; Sánchez-Garrido et al., 2014), and a network of Lagrangian drifting buoys released in the SoG



as part of the MEDESS-4MS project (Sotillo et al., 2016). Therefore, revalidation of the regional model output used in this study is not necessary, and only a brief description of the local model performance is provided here. It has been evaluated by directly comparing its current velocity outputs with measured velocities from an Acoustic Doppler Current Profiler (ADCP) deployed at the main sill of Camarinal (CS,  $\sim 290$  m depth; refer to Figure 6.1c) in years 2020-2021. The dataset was already used by García-Lafuente et al. (2023) to assess the cross-strait transport of *R. okamurae*, and their work should be consulted for details on the experimental setup. Figure 6.3 presents the result of the time-series comparison.

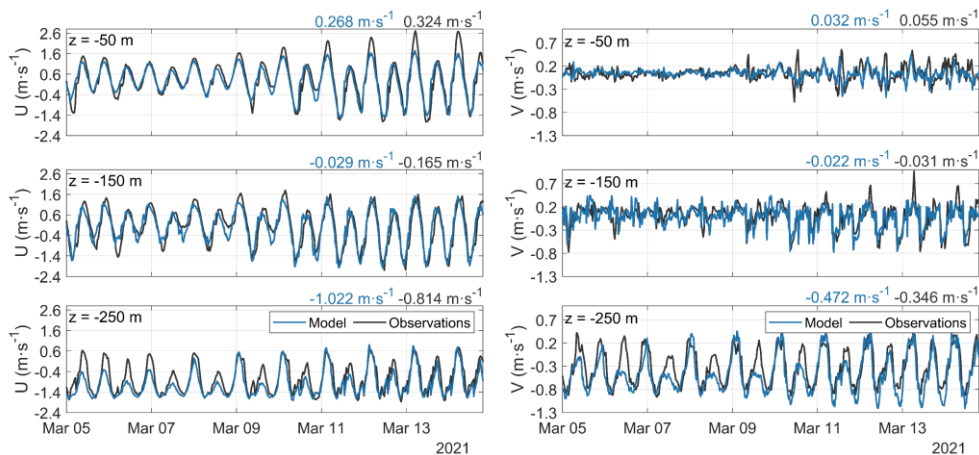


Figure 6.3. Observed (black line) and modeled (blue line) time series of zonal ( $U$ ) and meridional ( $V$ ) velocity obtained in the Camarinal Sill (CS) at the representative depths of the Atlantic inflow (50 m), the interface between inflow and outflow (150 m), and the Mediterranean outflow (250 m). Mean values of each time series are shown at the top of each panel in the corresponding color code.

The comparison shows a satisfactory agreement between the model and observations for the three analyzed horizontal layers, although some minor discrepancies must be noted. These mainly concern the differences in the mean value of the time series, which are particularly noticeable in the case of the prevailing zonal component at a depth of 250 m, where the mean modelled velocity exceeds the observed value by  $0.2 \text{ m}\cdot\text{s}^{-1}$ . The discrepancy can be partially attributed to the fine features of the bottom topography, which are not yet accurately represented by the model. Even so, the model

hindcast matches well with the amplitude and periodicity of the fluctuations, both at the fortnightly period of the spring-neap tidal cycle and also at the diurnal frequency (diurnal inequality), resulting in correlations of 0.9 and a RMSE below  $30 \text{ cm}\cdot\text{s}^{-1}$  for the zonal component. The meridional component exhibits a more irregular pattern which yields poorer correlation and RMSE values, but still agreeably, at above 0.7 and below  $0.2 \text{ m}\cdot\text{s}^{-1}$ , respectively. The results are satisfactory enough to justify the use of the model as a tool for particle advection experiments.

## 6.5 Lagrangian setup

The particle advection experiments were carried out using OpenDrift (version 1.10.6, Dagestad et al., 2018), an open-source framework designed to simulate the trajectories and fate of objects or substances drifting in the ocean. Particles in this application represented healthy fragments or spores of *Rugulopteryx okamurae*. The algorithm was coupled with the nested MITgcm models which provided the three-dimensional fields of zonal (u), meridional (v), and vertical (w) components of velocity for the year 2021 and March 2021 for the regional and local model, respectively. Supplementary Figure S6.1 displays the monthly averaged surface velocity data provided by the regional model for the simulated months (January to February 2021).

Dispersal simulations were conducted within the first 40 meters of the water column, which is the depth where the macroalga has been most frequently observed (García-Gómez et al., 2018, 2020). To calculate particle trajectories, a fourth order Runge-Kutta integration scheme was utilized, which bilinearly interpolated the simulated eastward (u), northward (v), and upward (w) components of current velocity. Wind drift, expressed as a percentage of the wind speed, is a critical parameter in predicting particle transport. Studies using the OpenDrift model suggest that a 10% wind drift factor yields the most accurate results when comparing predicted trajectories with observations and, therefore, this value was incorporated into the experiments.

Considering the detections of *Rugulopteryx okamuræ* spotted in Figure 6.1 and the uncertainty in the precise timing and location of their discharge, the initial experiment assumed a random distribution of 6,000 particles in the SoG from 5.95°W to 5.25°W and from 35.8°N to 36.2°N (Figure 6.4a), released hourly for a 12-hour tidal cycle every six tidal cycles (approximately every 3 days) during the year 2021. Particles were then tracked over a 30-day period, as there is no consensus on the time algae spend freely drifting healthily. The possible combinations added up to 108 different release scenarios, four of which are shown in Figure 6.4b,c where the zonal and meridional components of the winds and sea level at Tarifa, a representative location of the central SoG, are shown for a fraction of the simulated period.

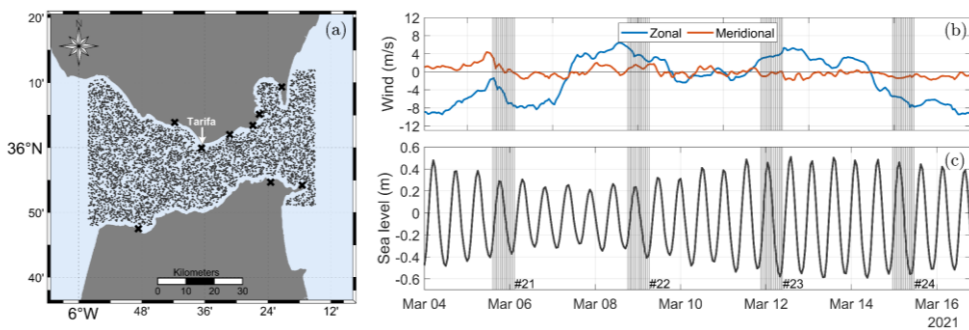


Figure 6.4. (a) Initial positions of particle release in the SoG, with crosses marking the locations where *Rugulopteryx okamuræ* has been detected (Figure 6.1). (b) Zonal (blue) and meridional (orange) wind components extracted from the ECMWF ERA5 reanalysis model at Tarifa in a fraction of the month of March 2021. (c) Simulated sea level extracted at the node closest to the Tarifa tide gauge in the same fraction of the month of March. The particle release times are indicated by grey vertical lines, with each group of lines representing a single scenario.

In addition to the spatio-temporal conditions established in the simulations, a sensitivity analysis was conducted on particle buoyancy, as it is anticipated that this factor will influence the distribution of algae. The terminal settling velocity, which is the steady-state vertical velocity due to positive or negative buoyant individual behavior, is typically neglected in particle advection studies, especially in areas where vertical advection by currents is much lower than horizontal advection, such as the area under

study, or when simulating positively buoyant elements, as certain macroplastic debris (Lebreton et al., 2019), angiosperm fruits (Pastor et al., 2023), or fish eggs (Nadal et al., 2022). Recent studies on *R. okamurae* sinking have found, nonetheless, non-zero sedimentation velocities (García-Lafuente et al., 2023), ranging from 1 to 4 cm·s<sup>-1</sup> in experimental conditions and from 1 to 6 cm·s<sup>-1</sup> in controlled scenarios, for which it is worth testing their influence on model results.

Shorelines are among the areas most affected by the invasion, and it is therefore essential to accurately assess the extent of algal accumulation (Altamirano-Jeschke et al., 2022; García-Gómez et al., 2018, 2020, 2021; Muñoz et al., 2019). To estimate these beaching rates along the coastal zone, the shoreline was divided into 630 segments ( $n$ ), each  $\sim 1000$  m in length and  $\sim 100$  m in width. For each period simulated, the accumulation per segment ( $A_n$ ) and the total accumulation for all segments ( $A_T = \sum_1^n A_n$ ) were obtained. The accumulation ratios for each region were then calculated by dividing the amount of settled particles in each segment by the total accumulation in all segments as  $\frac{A_n}{A_T} \times 100$ .

To illustrate the spatial distribution of *Rugulopteryx okamurae* across the studied coastlines and, thereby, differentiate between low and high accumulation zones, the percentiles P20, P40, P60 and P80 were calculated with respect to the maximum accumulation of all segments. These percentiles were then used to determine the accumulation thresholds for identifying minimal (zero values), low (below the 20th percentile), medium-low (between the 20th and 40th percentiles), medium (between the 40th and 60th percentiles), medium-high (between the 60th and 80th percentiles), and high (above the 80th percentile) levels of risk.

## 6.6 Results and discussion

The spatial distribution of algal accumulation averaged over all simulations for the year 2021 and discretized by the percentile thresholds is shown in Figure 6.5.

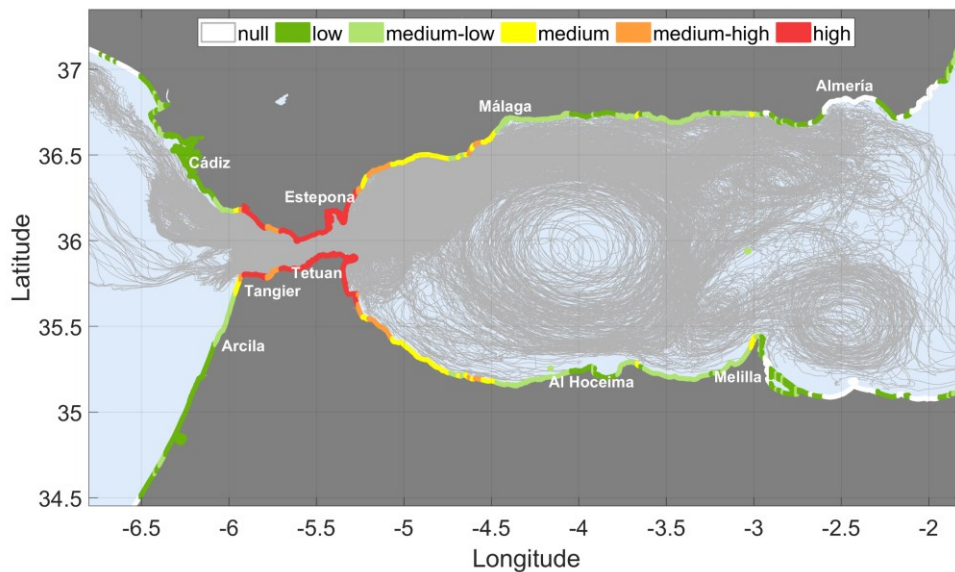


Figure 6.5. Accumulation ratios ( $A_n/A_T$ ) at the end of the tracking period (30 days) averaged over all the 108 simulations described in section 6.5. The classification “null” corresponds to zero accumulation values; “low” corresponds to accumulation values below P20; “medium-low”, between P20 and P40; “medium”, between P40 and P60; “medium-high”, between P60 and P80; and “high”, above P80. A set of particle trajectories extracted from one of the 108 simulations is shown as an example.

The primary spatial pattern that is evident in Figure 6.5 is the role of the eastward-flowing AJ, which is responsible for the almost direct propagation of algal particles from the SoG towards the Alboran Sea, with a markedly reduced transport of particles towards the Atlantic side. As expected, the number of accumulated particles increases in areas most exposed to high dynamic environmental conditions. In particular, the accumulation is highest in the Strait, with an annual mean accumulation of no less than P60, which means that algal particles are registered in these coastlines for at least 60% of the tracked time, a finding that justifies, in the medium to long term, the reported large accumulation of algal biomass in both shores of the SoG (Aamri et al., 2018; García-Gómez et al., 2018; Ocaña Vicente et al., 2016).

Yet inside the Alboran Sea, the map illustrates two clearly defined accumulation zones, identified by the segments with medium (yellow, P40-P60) and medium-high (orange, P60-P80) to high (red, >P80) levels of risk

(Figure 6.5). The first accumulation hotspot is identified in the northwestern Alboran Sea, off the coast of Estepona, whereas the second is in the southwestern Alboran Sea, off Tetuan. The accumulation pattern in the northern zone is again consistent with the AJ flowing into the Alboran Sea, which advects a significant fraction of particles released from the SoG northeastward. Conversely, the accumulation in the southern zone, which stands out from the path of this stream, is attributed to the existence of a small cyclonic eddy between the African coast and the WAG, faintly visible in the background trajectories displayed in Figure 6.5. The central inner region of the Alboran Sea displays an average accumulation value below P40, indicating a low, though not negligible, level of risk in these areas. Conversely, more sheltered areas such as the Gulf of Almería in the north and eastwards Melilla in the south, exhibit the lowest particle accumulation percentages (<P20).

The resulting distribution shown in Figure 6.5 provides insight into the influence of general hydrodynamics on accumulation patterns in the mid- to long-term. The results are consistent with those reported in observational studies (refer to Figure 6.1d), which confirms the predictive capability of the model in preliminarily forecasting the dispersal of the species. It is, however, worth identifying the specific conditions that may lead to lower or higher accumulation on the coasts, as these results may provide valuable information for the early detection and management of the alien algae under these conditions. This can be estimated by directly comparing the total accumulated amounts of virtual algae over time for each release, along with the times at which these accumulations occur on average, with the time series of wind and sea level, as potential causes of accumulation variability. These have been divided into the northern (Iberian Peninsula) and southern (African) coasts, which have shown preliminary indications of high concentrations of particles and variability over time.

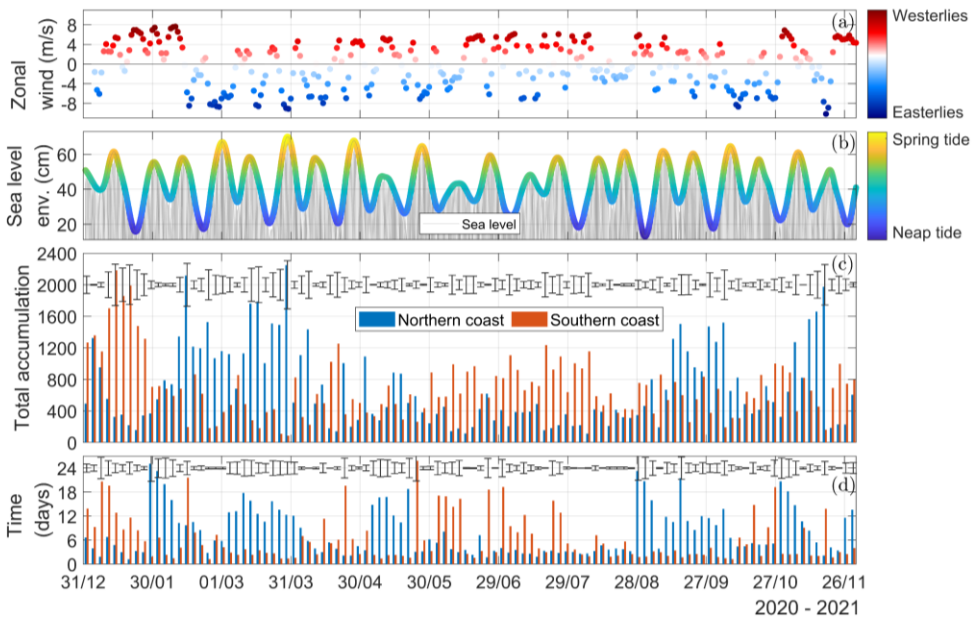


Figure 6.6. (a) Zonal component of the wind ( $\text{m}\cdot\text{s}^{-1}$ ) extracted from the ERA5 dataset at Tarifa. (b) Upper envelope of the sea level amplitude extracted from the regional model at the closest node to the Tarifa tide gauge. (c) Total accumulations along with their corresponding standard deviations for the year 2021, for the northern (blue) and southern (orange) coasts. (d) Same as (c) for the times at which accumulations occur on average for the northern (blue) and southern (orange) coasts.

Spring tides in the SoG typically entail increased surface velocities, which might intuitively lead to diminished particle retention in coastal areas. However, Figure 6.6c illustrates that spring tides (yellowish line in Figure 6.6b) actually result in higher particle accumulation on both the northern and southern coast compared to neap tides (bluish line in Figure 6.6b) throughout the year 2021. Specifically, the accounted accumulation is  $\sim 8\%$  and  $\sim 20\%$  higher in spring than in neap tides for the north and south coasts, respectively. This notable difference can be attributed to the fact that spring tides not only generate stronger currents and inject more energy into the Alboran Sea, but also induce greater variability, which leads to increased particle scattering and consequently increased beaching rates throughout the basin. The difference between tidal conditions is particularly noticeable during the first and last bimester of 2021, when spring tides imply almost 40% more beaching than neap tides. This is likely due to the increase in the

amplitude of the spring tidal excursion associated with the increased atmospheric variability during the winter, which is expected to result in a more dispersed pattern across the basin during this period.

The effect of wind on particle accumulation is subtler, but still worth considering. The role of the local coastline orientation appears to be a critical parameter. On the northern coast, strong episodes of easterly winds contribute to a significant increase in accumulation in 2021. This is particularly noticeable in the period from mid-February to mid-April, where the clear dominance of easterlies (on average  $5 \text{ m}\cdot\text{s}^{-1}$  and up to  $\sim 9 \text{ m}\cdot\text{s}^{-1}$ ) over westerlies (on average  $2 \text{ m}\cdot\text{s}^{-1}$  and up to  $\sim 5 \text{ m}\cdot\text{s}^{-1}$ ) contributes to a mean particle deposition that is 40% higher on the north coast than on the south coast. On the south coast, however, it is the westerlies that generally cause relatively higher deposition than the easterlies, with only the easterlies in May causing a slight increase in particle stranding. This is particularly noticeable in the period from mid-June to mid-August, when the prolonged dominance of westerlies (on average  $4 \text{ m}\cdot\text{s}^{-1}$  and up to  $\sim 8 \text{ m}\cdot\text{s}^{-1}$ ) over easterlies (on average  $2 \text{ m}\cdot\text{s}^{-1}$  and up to  $\sim 7 \text{ m}\cdot\text{s}^{-1}$ ) causes 25% more accumulation in the south than in the north. This can be partially related to the fluctuations in the AJ as a function of wind direction (García Lafuente, Alvarez Fanjul, et al., 2002). In this regard, easterly winds have been demonstrated to diminish the inflow and divert the primary stream towards the north, while westerly winds strengthen the inflow and deflect the flow towards the south (García Lafuente & Delgado, 2004; Sarhan et al., 2000). Consequently, it can be assumed that during easterly (westerly) winds, the AJ leads to higher dispersion and a slight increase in particle accumulation over the northern (southern) coasts.

The main factor accounting for the variability in the times of accumulation Figure 6.6 is the geographic location of the coastlines (north vs. south coast). In the northern coastline, the arrival of particles is faster during spring tides than during neap tides. This phenomenon is attributed to the stronger AJ during spring tides, which is responsible for the direct transport of particles to the northern coasts. It is even further helped by easterly winds, which, as already mentioned, deflect the AJ to the north, thus favoring the fast



accumulation of particles in the north. The influence of the mainstream is less discernible on the southern coast, where the main advection mechanism is wind. In this instance, it is the westerly wind that typically drives an AJ deflection to the south, which is the mechanism that presumably causes the fastest times of accumulation under these conditions. Conversely, accumulation on the southern coast is delayed under easterly wind conditions, which favor higher accumulation to the north.

The scenario-averaged values reflect the prevailing role of the main dynamic structures of the SoG-Alboran Sea system on the accumulation patterns, although the large uncertainties associated with these values reveal high variability attributed to the spatial variability of the receiving regions. These issues are addressed next for a particular case study.

#### 6.6.1 March 2021 as a case of study

In addition to the already commented tidal and wind variability inferred from the Figure 6.6, this section addresses an illustrative case to differentiate the impact that diverse environmental conditions have on accumulation ratios at different coastal locations. In particular, it examines the simulated month of March as an example, when the combination of the two prevailing wind components (westerly and easterly) and the fortnightly tidal cycle (spring and neap tide) occur for a fraction of the month (Figure 6.4b,c). Figure 6.7 depicts the outcome of algal accumulation under these four conditions: spring-easterly (a), spring-westerly (b), neap-easterly (c), and neap-westerly (d).

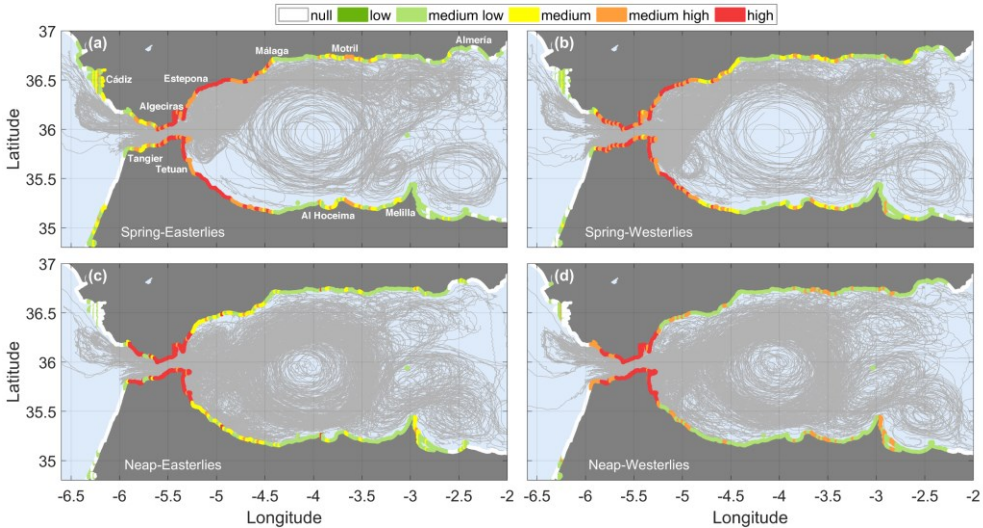


Figure 6.7. Accumulation ratios in the SoG and the Alboran Sea coastlines at the middle of the tracking period (15 days) for the four scenarios illustrated in Figure 6.4: a) an easterly wind during spring tide on March 14, 2021 [#24 in Figure 6.4c], b) a westerly wind during spring tide on March 11, 2021 [#23 in Figure 6.4c], c) an easterly wind during neap tide on March 5, 2021 [#21 in Figure 6.4c], d) a westerly wind during neap tide on March 8, 2021 [#22 in Figure 6.4c]. Particle trajectories are displayed for each scenario. Some relevant locations are displayed in map (a).

The advection of particles is significantly greater during spring (Figure 6.7a,b) than during neap tide (Figure 6.7c,d) due to the higher energy injected into the basing during the former tidal condition. This increased transport is not only apparent in the Alboran Sea, but also within the SoG itself, which reveals greater dispersion and thus lower accumulation of particles during the spring tide (P60-P80 on average) compared to the neap tide (>P80). It is also evident on the Atlantic side, which shows an average low to medium accumulation during spring tide, but low or zero accumulation during neap tide. Upon entering the Alboran Sea, the enhanced advection during spring tides (see trajectories in Figure 6.7a, b), leads to higher scattering throughout the basin, which causes slightly higher accumulation rates along the northern coastlines, as it was preliminarily indicated by Figure 6.6c.

Specifically, accumulation rates are highest (>P80) along the coast of Estepona during easterly winds, extending up with medium-high (P60-P80) values to the bay Malaga. These rates then decrease (P20-P40) towards

Almería, with a notable peak (P60-P80) in Motril. The pattern of accumulation in the northern region is mirrored in the southern region, with high concentrations in Tetuan, followed by a decrease towards Oran, and a peak in Al Hoceima.

During neap tides (Figure 6.7c, d), trajectories reveal a prevalence of gyre circulation, which results in more stable pattern over the entire Alboran Sea. This process is slower and generally results in lower coastal accumulation rates along the coasts. However, certain areas exhibit higher accumulations, which are worthy of note. Coastal regions in proximity to the SoG, such as Estepona and Tetuan, exhibit the most pronounced accumulations, although the values remain below the P40-P60 range observed during spring tides. The least conducive scenario for particle accumulation across both the northern and southern Alboran coasts is provided by the neap-westerly one

Wind plays a secondary role in particle accumulation, and its influence is almost indiscernible from the maps (Figure 6.7). A comprehensive analysis of wind intensity for a given wind direction cannot be accurately achieved using our set of realistic scenarios, due to the concomitant influence of other factors that can mask the potential effects of wind variability, such as tidal strength and tidal phase.

### 6.6.2 Sinking velocity dependence

The impact of the terminal settling velocity of *Rugulopteryx okamurae* on their distribution throughout the basin was further assessed by conducting additional simulations in which a constant sedimentation velocity of 1, 2, and 3  $\text{cm}\cdot\text{s}^{-1}$  was applied to the released particles<sup>5</sup>. Although the sedimentation velocities are relatively small, the particles sink at the very beginning of the experiments, with this sinking being generally greater as the imposed

---

<sup>5</sup> It is important to clarify that these velocities are lower than those obtained in laboratory experiments (García-Lafuente et al., 2023) and should not be considered a realistic representation of the *Rugulopteryx okamurae* sedimentation behavior, but rather an approximation of the possible evolution of particles in the vertical dimension.

sedimentation velocity increases. As a result, some of the particles, especially those released in shallow areas, remain in the same place where they were released because they are stuck to the seafloor. This is particularly evident in the case of  $3 \text{ cm}\cdot\text{s}^{-1}$ , where nearly 20% of the total particles sink to the bottom within a few instants after release, while in the  $1 \text{ cm}\cdot\text{s}^{-1}$  and  $2 \text{ cm}\cdot\text{s}^{-1}$  scenarios, only the 8% and 15% of total particles sink, respectively.

The key point to note is that nearly 7% of the total released particles were able to sink, and if vertical flow velocity or bathymetry permitted, rise to the upper layers. An illustrative example of this is shown by the trajectories in Figure 6.8, released under the three settling velocity scenarios.

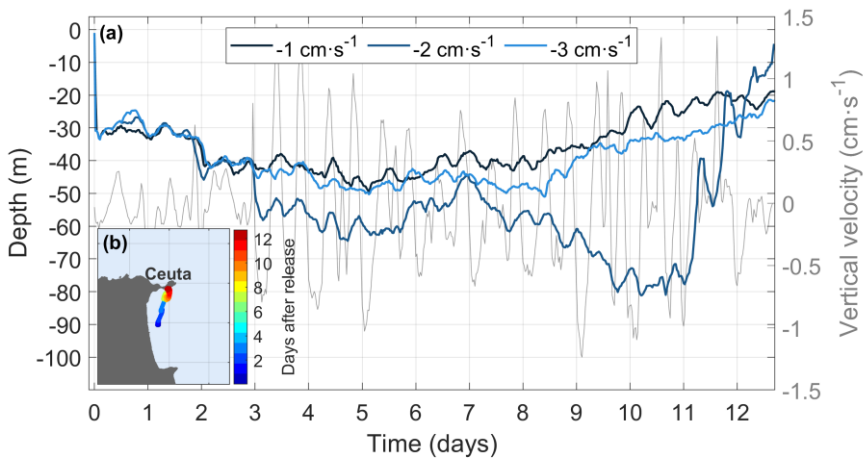


Figure 6.8. (a) Depth time-series of a particle released at surface with a sedimentation velocity of 1 (dark blue), 2 (blue) and 3 (light blue)  $\text{cm}\cdot\text{s}^{-1}$ , superimposed on the vertical velocities encountered by the  $2 \text{ cm}\cdot\text{s}^{-1}$  particle during the first 15 days after the release. (b) Particle trajectory from the  $2 \text{ cm}\cdot\text{s}^{-1}$  sedimentation velocity simulation. The trajectories followed by the  $1 \text{ cm}\cdot\text{s}^{-1}$  and  $3 \text{ cm}\cdot\text{s}^{-1}$  particles diverge only slightly from the  $2 \text{ cm}\cdot\text{s}^{-1}$  trajectories, and are not shown for clarity.

Figure 6.8 demonstrates that the initial settling velocity of the particles exerts a significant influence on their trajectories and ultimate fate within the short to mid-term. This is apparent in the similar dispersion patterns of particles with initial velocities of  $1 \text{ cm}\cdot\text{s}^{-1}$  and  $3 \text{ cm}\cdot\text{s}^{-1}$ , but different from those with an initial velocity of  $2 \text{ cm}\cdot\text{s}^{-1}$ . For instance, particles with  $1 \text{ cm}\cdot\text{s}^{-1}$  and  $3 \text{ cm}\cdot\text{s}^{-1}$  show an initial sinking, after which the particles gradually rise to the

surface with little vertical fluctuations, whereas the trajectory of particles with an initial velocity of  $2 \text{ cm}\cdot\text{s}^{-1}$  shows significant vertical displacements before finally rising to the surface and settling. In both instances, the upwelling is facilitated by the proximity of the trajectories to the continental shelf off the coast of Ceuta, although it is also enhanced by the notable vertical fluctuations of the current in this location. In the case of  $2 \text{ cm}\cdot\text{s}^{-1}$ , the algae would be transported to the area in question after spending several days in low-light or no-light conditions. The success of colonization in the settled environment would thus depend on whether the algae arrive in good reproductive condition after this period.

### 6.6.3 Implications of the results for invasion management

The results have demonstrated the usefulness of numerical models in elucidating the spread of a non-native and range-expanding species in response to changing environmental conditions. In particular, the model has facilitated the identification of high-risk areas, which, when combined with information about biological traits, may incentivate targeted monitoring, early detection, and management strategies for such species under certain favorable conditions.

For instance, the confluence of spring tides and easterly winds results in elevated and accelerated rates of accumulation along the northern Alboran coast, according to the present study (Figure 6.7a, b). It is particularly true in the vicinity of the SoG, and the expectable beaching risk should be considered for early action in the affected coastal regions. It is interesting to note that the scenario depicted in Figure 6.8c is consistent with the massive beaching that took place in the Algeciras Bay shores on that date reported by a local newspaper ([https://www.europasur.es/algeciras/alga-invasora-cubre-nuevo-Getares-Algeciras\\_3\\_1554174568.html](https://www.europasur.es/algeciras/alga-invasora-cubre-nuevo-Getares-Algeciras_3_1554174568.html) accessed 01 June 2024). As a matter of fact, easterlies have been repeatedly reported by the newspapers as a wind associated with important beaching events, an association that is corroborated by the model results, providing reliability to this study. The most favorable scenario for no coastal beaching, on the other hand, is neap tides occurring simultaneously with westerly winds, which have shown the

lesser extent of accumulation on the coasts (Figure 6.7c,d). However, this situation leaves a good proportion of algal particles freely drifting in the Alboran area, which can have consequences in the fishing sector.

## 6.7 Final remarks

Since its initial detection on the coast of the SoG in 2015, the exotic brown alga *Rugulopteryx okamuræ* has spread explosively over a large part of the Atlantic and Mediterranean coasts, producing severe impacts on previously established benthic communities, and causing massive accumulations along the shorelines, affecting fisheries and tourism. The impact and adaptability of the algae in the Mediterranean environment has recently been the subject of extensive research, but crucial aspects of the invasion, including its distribution and the underlying causes of its success, still remain unknown. To gain insight into the spreading and establishment of the species, two nested high-resolution and three-dimensional hydrodynamic models coupled with a Lagrangian particle tracking algorithm have been used, with virtual tracers representing free spores, thalli fragments or detached mats of *Rugulopteryx okamuræ*.

The work has focused on the SoG and its adjacent basins, the Gulf of Cadiz and the Alboran Sea, which have been significantly affected by the algal invasion. The hindcast of the passive spreading of the algae in 2021 indicated a mainly eastward direction, with transport by the AJ entering the Alboran Sea being the most influential physical mechanism. Tides near the SoG are an influential process. The variability due to tidal forcing is particularly noticeable in terms of fortnightly modulation and gives rise to two different outputs: Spring tides tend to favor accumulation by direct advection promoted by the increased energy of the currents. On the contrary, neap tides favor a higher dispersal pattern over the whole Alboran Sea, with consequently slower and generally lower coastal accumulation rates along the coasts. Wind plays a minor role in particle accumulation, although its influence is still not negligible. The role of the local coastline orientation seems to be a critical parameter: on the north coast, easterly winds contribute

to a slight increase in particles, whereas on the south coast, it is the westerly winds that generally cause a relatively higher accumulation compared to the easterly winds. This has been related to the variability of the Atlantic inflow and its own jet as a function of wind direction.

The interpretation and implications of the results presented in this study are valuable for different stakeholders, as it provides insights into the invasion pathways, high risk areas, and managing guidance. Further research is required to ascertain the role of other important biological traits not included in this study, which may help decision-makers to establish effective management strategies. Overall, improving our knowledge on the interaction of this species with its physical environment is a key issue in the efforts towards preventing and managing the invasion, preserving the integrity of ecosystems and minimizing the ecological and economic impacts. This would not only benefit the control of *Rugulopteryx okamurae*, but also serve as a valuable framework for managing the introduction of future invasive species through the Strait of Gibraltar, ultimately minimizing the ecological damage that these introduced species may cause.

## 6.8 Supplementary material

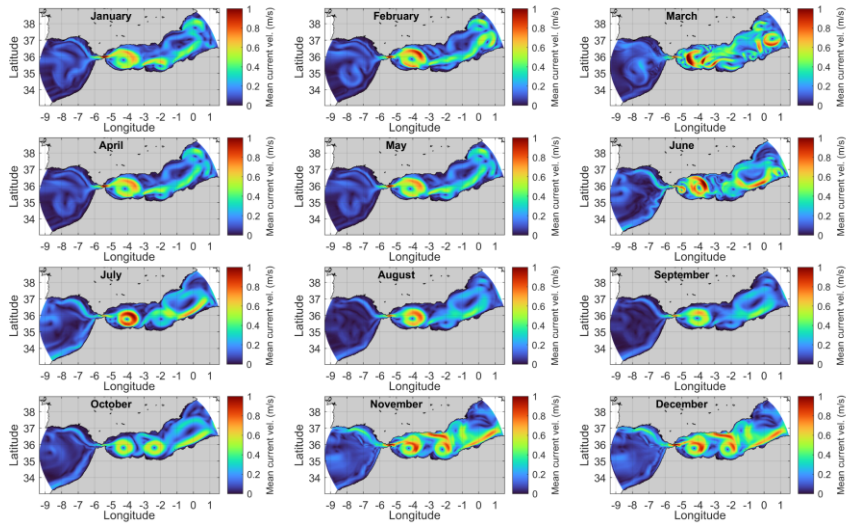


Figure S6.1. Monthly averages of surface velocity data for the year 2021.





# 7 Integrated discussion and conclusion

## 7.1 Thesis synthesis: patterns of connectivity

Two themes have recurrently emerged throughout this thesis. First, oceanographic features play a significant role in shaping population connectivity and dispersal, especially in highly dynamic environments influenced by tidal and wind-driven currents, such as the regions under study. Second, Lagrangian particle tracking has proven to be a valuable and effective technique among the available methods for investigating these complex dynamics. This research has specifically evaluated connectivity and dispersal patterns for populations or population groups in the Alboran and Adriatic Seas. A notable focus has been put on coastal fish populations, including the blackspot seabream population in the Alboran Sea (Chapter 3) and an analysis of key egg and larval fish groups in the Adriatic (Chapter 4). This has been mainly motivated by two main factors: the vulnerability of these species to overfishing, and their crucial role in maintaining the ecological balance of coastal ecosystems. Another major topic addressed in this thesis is the identification of alien species transfer, highlighted by the recent and concerning case of *Rugulopteryx okamurae* in the Strait of Gibraltar (Chapters 5 and 6). Analyzing the findings presented thus far allows for the identification of general connectivity patterns for each region. A summary of these patterns follows.

### 7.1.1 Alboran Sea

Figure 7.1 depicts some general connectivity patterns of the Strait of Gibraltar and Alboran Sea system interpreted in Chapter 3. From a hydrodynamic perspective, the mean circulation patterns favor the zonal (west-to-east) connectivity: the northern coast of the Strait is well-connected to the northern margin of the Alboran Sea, as a result of the direct connection

between the AJ and the northern edge of the WAG, whereas the southern coast of the Strait, diverging from the mainstream, is connected to the southern margin of the Alboran basin.

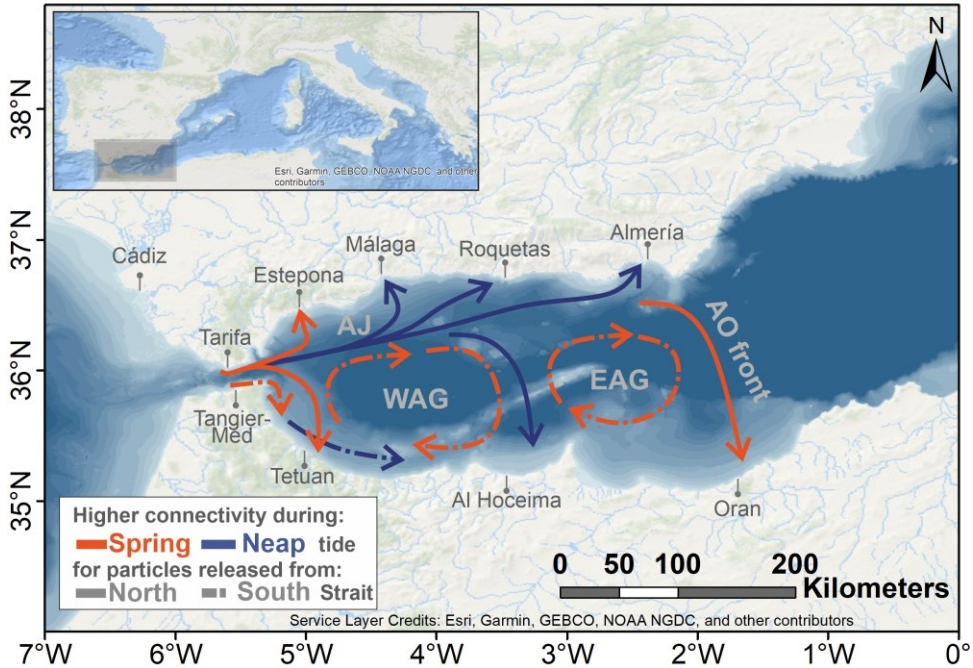


Figure 7.1. Sketch of the main connectivity patterns of particles released from the northern (solid line) and southern (dashed line) Strait under conditions of spring (orange) and neap (blue) tide, based on the information described in Chapter 3.

Dispersal patterns are contingent upon tidal conditions, the tidal strength being more influential than tidal phase. Spreading of particles released from the northern Strait is typically enhanced by spring tides, which facilitate that particles reach nearer coastal areas directly (Figure 7.1, solid lines). This pattern is demonstrated in the case of the study of the Tarifa box and the Estepona and Malaga landings on the north coast in Chapter 3 (see Figure 3.8) and, interestingly, is further confirmed by the patterns of algal accumulation observed in Chapter 6 (Figure 6.7a,b), which shows the highest accumulation in Estepona during the spring tide. The remaining northern coast of Alboran is more efficiently connected under neap tides, which facilitate a steadier and slower dispersal pattern, and result in a greater

distance reached by particles, as displayed in Figure 3.6a,b and Figure 6.7c,d in Chapters 3 and 6, respectively.

Upon reaching its eastern edge, the WAG bifurcates into two main paths. Most part flows eastwards, feeding the rest of the structures of the basin (the EAG and the Almeria-Oran front), whereas another part flows southwards closing the gyre and veering westwards. Eastward connectivity is enhanced under spring tides, while southward is mostly fostered by neap tides. During spring tides, the greater spread of the AJ at its exit facilitates the formation of a southern coastal gyre, which directly feeds the southern coast and gives rise to a much faster and more efficient connection of the northern Strait to the African coast. Conversely, during neap tides, the prevailing direction of particle movement along the southern coast is westward. In both scenarios, the time required for particles to be received from the northern Strait and distributed throughout the southern Alboran region is considerable, as particles arrive after completing at least one WAG turn around.

Conversely, the primary mechanism affecting particles released from the southern margin of the Strait (Figure 7.1, dashed lines) is the incorporation into a coastal gyre that forms at the far southern exit of the Strait, off Tetuan. Then, almost independently of the tidal modulation, the particles are quickly swept southward to flow along the African coast with a more eastward connectivity. When the coastal gyre is wide and strong, as is the case during spring tides, there is a greater likelihood that a significant fraction will break off and flow northeastwards as part of the WAG pathway. This allows particles initially destined for the African coast to be dispersed along the northern coast, favoring delayed south-north connectivity. This is observed in Figure 3.7 and is further supported by the slightly increased accumulation ratios observed on the northern coast during spring tides in Figure 6.7a,b, compared to the lower accumulation observed in this area during the neap tide.

Although the scheme is generally applicable to most situations, it is important to note that depth and subinertial variability, particularly of meteorological nature, can significantly impact the outcome. For instance, in

a hypothetical scenario where the release occurs at a greater depth in the Strait of Gibraltar, below the interface between the upper Atlantic and the lower Mediterranean layers, the mean circulation would favor east-to-west connectivity, as revealed by the sensitivity analysis (Figure 3.10). In this context, another point of interest is the existence of sustained periods of enlarged cross-strait velocity near the interface between Atlantic and Mediterranean waters, that provides opportunities for connectivity not only in the along-strait direction, but also in a cross-strait (north-to-south/south-to-north) scenario.

This possibility, though remote, was considered in Chapter 5 for *Rugulopteryx okamurae* in an attempt to determine the potential origin pathways of the alien algae in the strait and the probable reason for this spread from the initially settled shore to the algae-free shore on the opposite side. The mechanisms responsible for the spread of algae are likely to be multiple and varied. The most plausible of these is linked to human-mediated vectors, with algae attached to ship hulls or fishing nets representing a significant risk. An alternative hypothesis, however, is that the algae managed to cross the SoG taking advantage of hydrodynamic processes without human intervention. Meteorologically induced fluctuations are key processes in that possibility. Northward flow within the intermediate layer would increase under high pressure over the western Mediterranean basin and local winds from the southwest. If these specific conditions occur during neap tides, optimal conditions for south-to-north connectivity would be generated. The north-to-south connection is less achievable, as it would be conversely favored in either the upper or deeper layer, where the strong zonal currents would impede the meridional connection. These patterns are consistent again with the connectivity patterns observed for the blackspot seabream (Chapter 3) and the alien alga (Chapter 6) which, being released in the upper layer of that exchange, exhibit a significant eastward advection of particles, with only a few particles (i.e. those released below the interface in Chapter 3 or those that hypothetically reached that depth by their own means in Chapter 5) being displaced in the westward direction. In both applications, it cannot be excluded that particles may be transported from one shore to

another across the interface, which interestingly could potentially give rise to patterns of connectivity that are at first glance unexpected in both cases.

### 7.1.2 Adriatic Sea

As in the previous region, some general connectivity patterns can be extracted from the analysis of population dynamics in the Adriatic Sea discussed in Chapter 4. These are displayed in Figure 7.2.

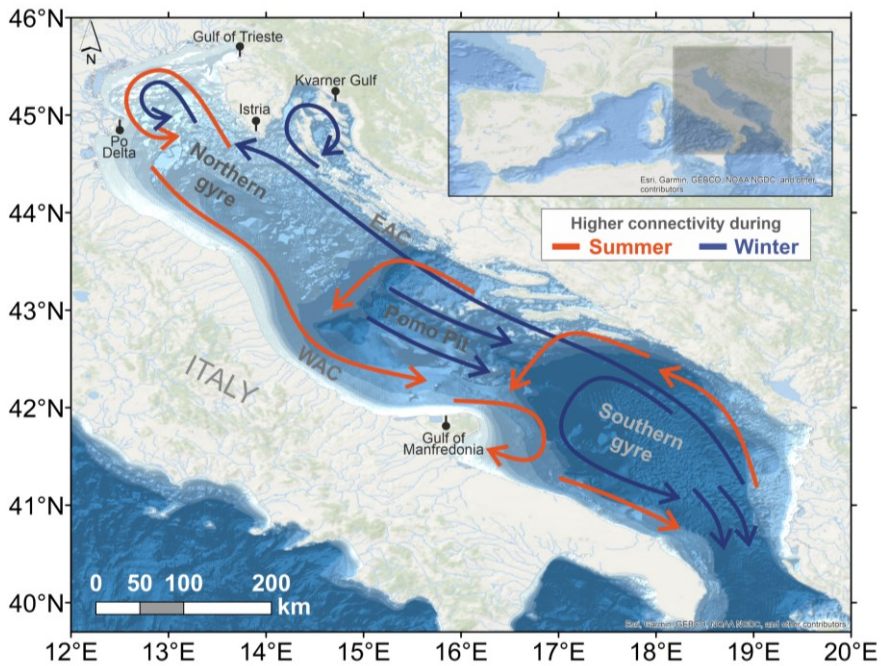


Figure 7.2. Sketch of the main connectivity patterns of particles released throughout the Adriatic Sea during summer (orange) and winter (blue), based on the information described in Chapter 4.

Particles released throughout the Adriatic Sea shown a preferential advection of particles along the coastlines, with the EAC being the primary mechanism for this advection process along the Balkan Peninsula during the winter season, and the WAC being the main advection process responsible for transporting particles along the Italian shelf during the summer. Seasonality is also reflected in the retentive characteristics of the diverse

regions studied within the Adriatic basin. During winter, the prevailing currents over the Adriatic Sea and the more variable atmospheric forcing inject more energy in the basin, leading to a significantly wider dispersal of particles that increases the export of particles to the Ionian Sea. The scattered connections in winter contrast with the much more unidirectional connectivity pathways in summer, which favors generally slower and steadier dispersal patterns in this period and promotes a higher number of retentive areas, curiously resembling the pattern observed in the case of neap against spring tides in the previous region discussion.

Areas distributed along the Italian shelf are identified as essential nursery grounds, particularly when the region's productivity is influenced by wind-induced upwelling and river discharges, creating favorable environmental conditions for larvae. During the summer, when the velocity is reduced, retention is promoted, coinciding with the spawning period of anchovy, Mediterranean horse mackerel, and hake. The observed variability during winter provides advantageous opportunities for marine species with longer pelagic larval durations and spawning periods concentrated in winter, such as sardines and common soles. Specifically, most retentive areas arise in the Kvarner Gulf in winter, which, despite the extremely complex rocky coastline, shows the highest connectivity receptions. Similarly, the Gulf of Manfredonia during summer also shows consistent connectivity with the main path of the prevailing WAC during this period. From a more evolutionary point of view, these dispersal timescales could be associated with typical residence times of coastal waters in order to balance auto-recruitment and larval export/import

## 7.2 Applicability of results and obstacles on current connectivity applications

To date, connectivity studies have addressed a variety of demands emerging from multiple fields, including fisheries (Botsford et al., 2009; Fogarty & Botsford, 2007; Fuller et al., 2017), ecosystem management (Hidalgo et al., 2017), marine pollution (Fifani et al., 2021; Martínez et al., 2024) and climate change (Abernathey et al., 2022; Jönsson & Watson, 2016).

In the context of population connectivity studies aiming to provide insights into the dynamics of such systems, such as those provided in this memory, this need in turn has increased the relevance and applicability of research to marine resource management, ultimately leading to a more comprehensive understanding of all taxa and of controlling processes that influence ecosystem functioning (Pineda et al., 2007).

In particular, the relevance of population connectivity in the design and management of marine protected areas has recently gained increasing attention in the field of marine conservation (Bastari et al., 2016; Batista et al., 2011; Rossi et al., 2014). In fisheries, for instance, estimates of dispersal and connectivity are crucial for understanding the dynamics of target fish populations and for the eventual proper conservation of potentially harvested stocks. The incorporation of such information in this sector is anticipated to be accomplished through the definition of restricted fishing areas, in which both dispersal and retention patterns can provide data regarding the optimal dimensions, distances, and closure periods. In this regard, marine protected areas within a network are more likely to support the persistence and recovery of harvested populations from external disturbances, whereas isolated areas (i.e., not connected by dispersal) are more susceptible to local extinctions due to the lack of natural replenishment (Deudero et al., 2017; Gaines et al., 2010).

In both regions studied, hydrodynamics plays a key role in shaping the dispersal patterns of propagules, with the fortnightly tidal cycle (spring vs. neap tides) in the Alboran Sea and seasonal shifts (winter vs. summer) in the Adriatic Sea acting as dominant forces. While some retention areas are present, the results indicate a high number of spawner migrations, underscoring the role of these basins as a network of interconnected populations. Interestingly, this finding aligns with genetic connectivity studies, which report a homogeneous distribution of genetic components across the two basins for several fish species (Di Franco et al., 2012; Angiulli et al., 2016), including the blackspot seabream (Ferrari et al., 2023).



A network of effective and self-sustaining marine protected areas in both regions could therefore provide enormous benefits for both conservation and fisheries production (Deudero et al., 2017; Di Franco et al., 2012). However, the evaluation of the ecological and economic implications of such regions is still in its early stages and, in practice, information on connectivity has thus far rarely been considered nor incorporated into their design and development (Berkström et al., 2022). Indeed, most marine conservation laws and regulations globally do not explicitly recognize connectivity as a fundamental component of ecosystem management (Estradivari et al., 2022; Lausche et al., 2013). There is therefore a prior urgent need to raise awareness of the importance of marine connectivity, both within and outside protected areas, in order to improve the ecological services they provide (Rossi et al., 2014).

Despite the boundaries that are still in place, there is a growing consensus that the results of ocean connectivity research will increasingly be incorporated into these fields (Andrello et al., 2013; Batista et al., 2011; Crochelet et al., 2016; Demmer et al., 2022). To achieve this, future research should concentrate on improving the integration of functional connectivity at both small and large spatial and temporal scales (Hidalgo et al., 2017). One of the most important challenges will then be to identify the anthropogenic impacts on natural connectivity pathways, as the significant and accelerating pressures of human activities on the marine environment, including habitat alteration, fishing pressure, coastal population growth, introduction of invasive species, climate change, and water quality degradation, are expected to have (and are already having) enormous impacts (Hidalgo et al., 2017). Climate change, in particular, is anticipated to have important consequences on the dispersal and connectivity of marine populations (Gerber et al., 2014), with increasing temperature expectedly affecting community structure through changes in spawning phenology, prey-predator distributions, and larval transport, behavior and mortality (Andrello et al., 2013; Lett et al., 2010; O'Connor et al., 2007).

However, even for models operating under present-day conditions, there is still a significant gap between the ability to simulate larval dispersal and

the ability to measure actual connectivity (Lett et al., 2010). A challenge for the future will be to compare real (observed) and virtual (modeled) drifters to validate the physical transport predicted by biophysical models (G. P. Jones et al., 2009; Levin, 2006). In addition, there are several other limitations that can be pursued within the field of physical oceanography, some of which are described below.

### 7.3 Modelling limitations and future paths

The difficulties associated with direct measurement of larval dispersal in the marine environment have led to a significant increase in the use of alternative methods to quantify larval transport, of which biophysical models have emerged as a relatively affordable and highly effective approach for studying and predicting dispersal patterns at different temporal and spatial scales (Monroy et al., 2017). However, despite their undeniable usefulness in elucidating such dynamics, some of which have been explored in this thesis, models are still limited tools in their ability to provide a fully realistic representation of the complete natural process (Calò et al., 2013).

The predictive performance of biophysical models in simulating larval transport is contingent upon the accuracy and veracity of the input parameters, whether pertaining to hydrodynamic or biological data. In the first case, refinement of models have progressively increased the spatial scale at which they can be applied, thus offering a more complete view of small-scale larval dynamics (Alcaraz & Estrada, 2022; Fuchs et al., 2015, 2017; G. P. Jones et al., 2009). However, parameterization and resolution are limited by the fact that the fine-scale nearshore circulation is still largely unknown, and these models can only be as accurate as the parameters estimated in the field (Metaxas & Saunders, 2009). In the second, knowledge of key biological traits such as spawning areas, larval duration, behavior or mortality rates is still poor (Simons et al., 2013). In our research, this has been no exception, and the limited knowledge of the biology of the species studied has led to uncertain configurations with little or no information, and unavoidable simplifications.

A relevant aspect to note in this regard is the assumption that the larvae are passive (non-swimming) particles during the pelagic larval duration. In a few cases, models have incorporated somewhat more complex biological parameters, such as the swimming speed of larvae, with not entirely consistent, but certainly not null, effects on connectivity patterns (Savina et al., 2010). Other studies suggest that even for actively mobile life stages, dynamics play a key role in regulating the spatial distribution of environmental variables and planktonic food (D'Ortenzio & Ribera d'Alcalà, 2009), thus controlling the location, timing and success of spawning, dispersal and settlement (P. Mariani et al., 2010; Monroy et al., 2017). In practice, the behavior of most species remains largely uncertain, and the ability to actively swim can vary widely among larval stages, with swimming capacities generally expected to increase at more advanced developmental stages. However, the short periods during which the highest connectivity rates occur in the Alboran Sea (less than 20 days in most cases, see Figure 3.6b and Figure 3.7b), due to fast travel times, and in certain areas of the Adriatic Sea (less than 30 days in the majority of the basin during summer, see Figure 4.9), owing to favorable retention conditions, may lead to consider the simplification of movements as a reasonable assumption.

Another simplification in our approach on propagules dispersion studies (Chapters 3, 4) has been to disregard vertical displacement. Most particle advection studies similarly overlook the vertical behaviors of buoyant individuals, particularly in regions like our study area, where horizontal advection dominates over vertical currents. This assumption is further supported by considerable uncertainties around the vertical displacement mechanisms of propagules, which include diel migration cycles, food availability patterns, buoyancy fluctuations due to changing egg lipid content, thermocline variability, and small-scale eddy turbulence, all factors beyond the resolution of our model. Consequently, accurately estimating vertical motion remains a remarkable challenge, and in some cases, even the direction of movement (upward or downward) is indeterminate. Given these complexities, focusing solely on horizontal transport processes provides a more reliable approach for this analysis.

Despite these assumptions, knowledge of the impact of different parameter settings on connectivity estimates and their variability is unclear, and most progress in this regard should be made by re-running Lagrangian analyses with updated biological information, which is still under investigation for the two main species (or group of species) assessed in this thesis. In the case of the blackspot seabream (Chapter 3), this includes key information on egg buoyancy, larval drifting duration, number of spawners, and vertical behavior, among others (Gil Herrera, 2010). This is also the case for the alien alga (Chapters 5, 6), whose specific parameters, such as thermal tolerance, particle size, or sedimentation rates under different environmental conditions, is still undetermined (Mateo-Ramírez et al., 2023). In both cases, the knowledge and inclusion of these parameters is crucial for obtaining results that can be applied effectively for the conservation, in the first case, or for the control, in the second case, of such populations. In this respect, it is also important to note that the adjustment of specific biological and hydrological parameters implicitly entails that these results are only valid for the species and region of interest, and that similar studies should be carried out on a larger number of species with different life history characteristics (life stages, reproductive strategies, etc.) in order to gain further insight into other population dynamics in specific regions.

Ultimately, further research is needed to gain a deeper and more comprehensive understanding of the mechanisms of connectivity. When information on specific parameter values for the species of interest is available, end-to-end ecosystem approaches can be valuable tools. The end-to-end models typically combine a regional circulation, a lower trophic level nutrient-phytoplankton-zooplankton network, and a multispecies individual-based model for the fish species of interest (Sánchez-Garrido et al., 2020). The basic principle of the individual model is that a population or system consists of discrete individuals that have a set of characteristics and can be distinguished from other individuals by life history traits such as fecundity, life span, offspring size, reproductive strategy, biotic interactions, and abundance of its predators, among many others (Deangelis & Mooij, 2005; Megrey, 2001; Mims & Olden, 2012; Sánchez-Garrido et al., 2020). By

filling the aforementioned gaps in biological information, these models can therefore be used to capture individual variation in greater detail than previous modeling approaches and to simulate the biophysical interactions between individuals and their environment. In the near future, the additional knowledge gained from our efforts to understand the functioning and dynamics of those populations will help to develop new perspectives on marine ecological awareness and to implement appropriate adaptive management strategies.

## 7.4 Concluding remarks

The principal findings and conclusions that can be derived from the chapters of this dissertation are as follows:

### *Chapter 1: General Introduction*

- Oceanographic features exert a significant influence on the extent of separation between individuals within and between local populations. An understanding of these dynamics is essential for the study of marine ecosystems, the management of fishery resources, the regulation of invasive species, and the design of marine protected areas.
- Recent efforts have been made to gain a deeper understanding of population dynamics. Several methodologies exist for this purpose, of which hydrodynamical models coupled with Lagrangian particle tracking algorithms are relatively affordable and extremely powerful tools for studying and predicting dispersal patterns at different temporal and spatial scales.
- In the nearshore environment, where several physical processes act at different spatio-temporal scales, connectivity is of particular importance. Two examples of this complexity are provided by:
  - The Strait of Gibraltar and the Alboran Sea.
  - The Strait of Otranto and the Adriatic Sea.

*Chapter 2: Methodology*

- Numerical models are effective tools for reproducing complex geophysical processes occurring in a given domain. A variety of applications have been developed to represent such oceanic flows, and the use of an existing model is considered a reasonable choice over the development of a new one.
- Lagrangian algorithms involve the analysis of sets of virtual particles representing fluid parcels, tracers, or passively drifting individuals. Their primary goal is to estimate the probability distribution of spatial dispersal, providing valuable information about the origins and trajectories of dispersing individuals within populations.
- A key quantitative measure of connectivity is the so-called connectivity matrix, where each cell represents the number of particles released from a given source and collected in a given destination at a given time. Alternative definitions can be adopted by quantifying the maximum percentage of particles in each target region over a given time, or by tracking the temporal changes in source-sink dynamics.

*Chapter 3: Hydrodynamic connectivity and dispersal patterns of a transboundary species (*Pagellus bogaraveo*) in the Strait of Gibraltar and adjacent basins*

- The dynamics of the Strait of Gibraltar play a key role in regulating the dispersal and connectivity patterns of early life stages of blackspot seabream in the Alboran Sea.
- The main differences in connectivity patterns are caused by the geographic location of the spawning areas (north vs. south). The northern strait is mostly connected to the northern basin of Alboran, while the southern Strait is mostly connected to the southern basin of Alboran.
- Tides are an influential phenomenon. The variability is particularly noticeable in terms of fortnightly modulation. Spring tides tend to favor connectivity by direct advection promoted by the increased

energy of the currents. In neap tides, connectivity is achieved by the mean circulation of the Alboran.

- The different depths of spawning create distinct patterns of connectivity. At the surface, particles are more actively scattered by the energetic current, while in deeper layers the circulation weakens, allowing particles to move less chaotically and travel farther.

*Chapter 4: Spatio-temporal connectivity and dispersal seasonal patterns in the Adriatic Sea using a retention clock approach*

- Understanding how species interact with the physical processes occurring in the Adriatic Sea is essential for managing vulnerable populations and identifying areas that require effective conservation efforts for the generic marine organisms inhabiting the region.
- The temporal component of connectivity is highlighted using a previously developed retention clock matrix over different larval durations.
- Seasonality is a critical factor in dispersal, with greater variability and reduced efficiency in winter compared to summer.

*Chapter 5: Could secondary flows have made possible the cross-strait transport and explosive invasion of Rugulopteryx okamurae algae in the Strait of Gibraltar?*

- The simultaneous occurrence of *Rugulopteryx okamurae* on both shores of the SoG is highly unlikely. A more plausible scenario is that the algae first colonized one shore and then spread to the opposite shore. A hydrodynamically-based spreading is assessed, even if highly improbable. This possibility is examined using current meter observations, which show layers with no zero velocity in the cross-strait direction.
- The depth range for cross-strait transport is 100-150 m, where the interface of zero velocity along the Strait is located. Layers of weak southward and northward currents are identified above and below the interface, respectively.
- High pressure over the western Mediterranean and local southwesterly winds associated with neap tides provide the best

conditions for south-to-north connectivity. Conversely, low pressure and local northeasterly spring tides reduce the chances for such transport.

*Chapter 6: Modeling spread of an alien alga under different temporal scenarios in the Strait of Gibraltar and adjacent basins*

- The impact and adaptability of *Rugulopteryx okamurae* in the Mediterranean environment has recently been the subject of extensive research, but crucial aspects of the invasion, including its distribution and the underlying causes of its success, remain unknown.
- The prediction of the passive dispersal of the algae in 2021 indicated a predominantly eastward spread, with transport by the Atlantic jet leaving the Strait being the most influential process.
- Tides depict two different mechanisms: spring tides tend to favor accumulation by direct advection favored by the increased energy of the currents, while neap tides favor a higher dispersion with consequently slower and generally lower accumulation rates along the coasts.





## Resumen en español

Es una realidad evidente que los océanos se encuentran en perpetuo movimiento. Los sistemas costeros, en particular, son entornos altamente dinámicos y sensibles, afectados por diversos procesos a diferentes escalas espaciotemporales que interactúan de forma no lineal. Tal entorno ofrece múltiples vías que, en mayor o menor medida, condicionan el transporte, distribución, conexión o separación de individuos o conjuntos de individuos de un determinado ecosistema. Comprender los procesos que controlan tales movimientos es un desafío crucial en la predicción de la distribución biogeográfica de las especies y la viabilidad de las medidas de conservación en una determinada región, pues estas interacciones biofísicas regulan y determinan ulteriormente la dinámica poblacional.

Dispersión y conectividad son dos términos que emergen al abordar las interacciones entre los individuos y su entorno. El primer término describe el mecanismo empleado para dispersar individuos, mayoritariamente en los primeros estadios vitales del ciclo biológico (esporas, huevos, larvas para especies bentónicas o pelágicas, y también juveniles para las pelágicas) y tiene como objetivo maximizar la distribución de las especies en el área de distribución geográfica. La dispersión de los propágulos está condicionada por la dinámica ambiental, en la que la turbulencia, la advección y la difusión actuando a diferentes escalas determinan las conexiones o la separación de diferentes conjuntos de individuos. Tales patrones de conexión o aislamiento, que determinan el propio desarrollo y abundancia de ciertas especies en determinadas zonas, se resumen bajo el concepto de conectividad. La conectividad es, de hecho, el resultado de la interacción del ciclo biológico de una especie con las condiciones dinámicas del medio marino. En términos más generales, la conectividad puede resumirse como el grado en el que el intercambio de individuos, tratados como partículas pasivas, se produce entre distintas áreas. Por lo tanto, la conectividad puede estimarse no sólo para analizar las interacciones entre individuos dentro de una población, sino también para estimar los flujos de momento y calor en el océano, y los

intercambios de otras partículas inertes en suspensión, incluidos los sedimentos, microplásticos y otras partículas contaminantes.

Debido a su amplia definición y a su creciente relevancia, el término "conectividad" se ha introducido y aplicado en multitud de campos. De esta forma, existen varias interpretaciones, cuyas principales diferencias radican en la escala de aplicabilidad del estudio. En términos ecológicos, la conectividad se refiere al grado en que poblaciones separadas espacialmente están vinculadas por la dispersión de individuos que forman parte de una metapoblación, definida como un conjunto de poblaciones de la misma especie distribuidas por zonas habitables. La conectividad sedimentaria se refiere al grado en que un sistema controla la transferencia de sedimentos entre diferentes formas del terreno o unidades del paisaje. La conectividad genética se define como el grado en que el flujo de genes influye en los procesos evolutivos de una población. Tales definiciones representan sólo una muestra de la multitud de aplicaciones, siendo aquellas que vinculan la influencia de los procesos de conectividad en la función ecológica y los servicios ecosistémicos las más relevantes, un uso que suele denominarse conectividad funcional.

Dependiendo de la magnitud de los fenómenos ambientales implicados y de otros parámetros biológicos, como el tamaño y la edad de los propágulos, se pueden identificar diversas diferencias espaciales en el intercambio de individuos. Estas van desde niveles muy bajos de conectividad entre poblaciones, en las que la estructura y el tamaño de la población se mantienen únicamente a través de la retención larvaria y posterior auto-reclutamiento, hasta altos niveles de conectividad que se producen a través de una elevada dispersión de larvas entre metapoblaciones. Por lo tanto, conocer en detalle tanto la magnitud como las escalas espaciotemporales en las que ocurren dichas conexiones, es esencial para comprender la estructura de las poblaciones marinas y sus interrelaciones.

Las escalas espaciotemporales de conectividad están mediadas por el éxito en el intercambio entre individuos. Esto es particularmente relevante en las primeras etapas de la vida, cuando las esporas, los huevos y las larvas en

desarrollo pueden tratarse, al menos en gran parte, como elementos pasivos. En determinadas especies de peces con fases larvarias pelágicas, la hidrodinámica es fundamental para conectar las poblaciones, condicionando la distribución del plancton a través de procesos de mesoescala y submesoescala que dispersan o retienen partículas vivas e inertes, procesos fundamentales para la supervivencia en las primeras fases de la vida. Ejemplos de estos organismos incluyen la mayoría de las especies pelágicas, algunas de las cuales transitan todo su ciclo de vida (holoplancton), o sólo sus etapas larvarias (meroplancton e ictioplancton) como plancton, aunque también incluyen muchas especies bentónicas, que normalmente se caracterizan por una fase sedentaria precedida por una etapa planctónica, durante la cual se produce la dispersión. Como tal, las distancias de dispersión, y por lo tanto la conectividad, se determinan por el tiempo que los individuos pasan en las etapas de vida planctónicas.

Las escalas temporales y espaciales en las que varía la conectividad durante la fase pelágica aumentan en relación con la fase de desove, cuyo momento y ubicación están a su vez determinados por múltiples factores externos, incluyendo la hidrodinámica del sistema y el comportamiento larvario. Algunas condiciones hidrodinámicas pueden aumentar las distancias de dispersión de las larvas (por ejemplo, las corrientes superficiales gobernadas por el viento y las corrientes de marea), mientras que otras pueden reducirlas (por ejemplo, la turbulencia). Por lo tanto, es razonable esperar variabilidad en los patrones de conectividad no solamente entre especies, sino también entre regiones y periodos de tiempo determinados. En este sentido, las poblaciones marinas que residen en regiones protegidas son menos susceptibles a una fuerte advección, lo que implica una dispersión relativamente limitada, que a su vez podría conducir a una mayor retención local y supervivencia de juveniles, y a una mayor conectividad de la población en de dicha región. Por el contrario, en los entornos expuestos y altamente dinámicos, donde confluyen las mareas, las corrientes impulsadas por el viento y la turbulencia a pequeña escala, la dispersión puede dar lugar a una menor retención de individuos, lo que se traduce en una menor conectividad de la población.

El estudio de la conectividad es, por tanto, esencial para una comprensión integral de la dinámica poblacional de dichas especies, además de una efectiva gestión de recursos pesqueros, control de especies invasoras y diseño de áreas marinas protegidas, entre otros. De hecho, a medida que ha surgido la conciencia de que la conectividad es un componente clave para comprender y gestionar determinadas poblaciones marinas, se ha invertido un esfuerzo considerable en el desarrollo y la aplicación de diversos métodos para obtener información sobre la dinámica de las poblaciones. En el entorno cercano a la costa, los enfoques más utilizados son los análisis moleculares, de otolitos y numéricos, todos con el objetivo común de elucidar los patrones de dispersión. En este sentido, las herramientas de modelación son un buen ejemplo, ya que proporcionan un análisis integral del origen y las trayectorias de individuos. Un método común para aplicar estos resultados numéricos es el análisis Lagrangiano, que implica estudiar conjuntos de partículas virtuales que representan parcelas fluidas, trazadores o individuos que se desplazan pasivamente, para identificar sus rutas, escalas temporales asociadas y transportes entre distintas regiones oceánicas.

Sin embargo, aun habiéndose desarrollado múltiples herramientas para su estimación, los conocimientos sobre la conectividad de especies marinas concretas y regiones geográficas específicas siguen siendo escasos. Esto es ciertamente observable en el Mar Mediterráneo, a pesar de ser considerado un “laboratorio” para tales estudios debido a sus patrones oceanográficos bien estudiados. Sin embargo, la importancia del entorno mediterráneo como punto caliente de biodiversidad y las amenazas humanas acumulativas a las que se enfrentan continuamente las poblaciones marinas, hacen que la investigación de la conectividad sea una tarea urgente.

Ciertas regiones del Mediterráneo proporcionan ejemplos específicos de este hecho. Entre ellos, destaca el mar de Alborán y el mar Adriático, donde los avances en conectividad y dispersión, junto con la orientación sobre cómo integrar esta información en las acciones de gestión, requieren una atención urgente. Sin embargo, las dificultades encontradas para cuantificar la conectividad costera, ya sea mediante métodos observacionales o numéricos, han dado lugar a una falta de comprensión de los vínculos entre la

hidrodinámica de esas regiones mediterráneas y las características biológicas de las especies presentes allí.

Con el objetivo de contribuir a una mejor comprensión de estas dinámicas, esta tesis doctoral tiene como objetivo estimar los patrones potenciales de conectividad y dispersión de ciertos grupos poblacionales importantes a diferentes escalas regionales en el Mar Mediterráneo. Se centra en las dos regiones relevantes mencionadas: a) el mar de Alborán, una cuenca de transición entre el mar Mediterráneo y el océano Atlántico fuertemente influenciada por el flujo de agua atlántica a través del el Estrecho de Gibraltar, y b) el mar Adriático, un cuerpo de agua semicerrado caracterizado por una topografía peculiar y una gran cantidad de fuentes de agua dulce. En particular, se han empleado algoritmos Lagrangianos acoplados a modelos numéricos con el fin de determinar las trayectorias y conectividad de partículas virtuales que emulan larvas u otros organismos entre distintas subáreas por la advección de las corrientes. Dichas herramientas numéricas se describen en detalle en el Capítulo 2. En concreto, se han evaluado los patrones de dispersión y conectividad de tres especies (o grupos de especies) diferenciadas, cuyos resultados se detallan en los Capítulos 3, 4, 5 y 6 de la presente tesis. A continuación, se ofrece un resumen desglosado de cada uno de ellos:

### *Capítulo 3*

El voraz (*Pagellus bogaraveo*) es una especie altamente apreciada tanto por su valor económico como gastronómico, que tiene un importante caladero en el Estrecho de Gibraltar. Por esta misma razón, es una de las especies más sobreexplotadas de la zona, lo que ha provocado que las capturas estén descendiendo significativamente a lo largo de los años. Dentro del ámbito científico, existe un consenso que considera que, para optimizar las pesquerías, simultáneamente a dejar de sobre explotar el recurso, es necesario hacer estudios de dinámica poblacional y conectividad. Con el objetivo de conocer mejor la dinámica poblacional de la especie y sus mecanismos de dispersión en el Mar de Alborán, se ha estudiado su conectividad hidrodinámica y patrones de dispersión a partir de un modelo numérico

utilizando los estadios de vida temprana (huevos y larvas) como partículas virtuales Lagrangianas.

Para determinar los patrones espaciotemporales de dispersión, se definieron tres zonas de suelta de partículas en el Estrecho de Gibraltar, zona preferencial de desove del voraz, cinco profundidades de liberación desde la superficie hasta los 81 metros, y ocho combinaciones de marea en función de la fase mareal y de la modulación quincenal (marea viva-marea muerta). Para cada uno de estos escenarios mareales iniciales se realizaron simulaciones de 60 días, que es la duración pelágica del voraz, en distintas fechas para estudiar la variabilidad subinercial asociada al forzamiento meteorológico, todo ello en el periodo comprendido entre diciembre de 2004 y abril de 2005. En conjunto se realizaron 480 simulaciones, de cuyo análisis se ha deducido que el transporte hacia el este por el chorro Atlántico que sale del Estrecho de Gibraltar es el proceso más influyente. En cuanto a las fluctuaciones temporales, la modulación quincenal es el factor predominante para la dispersión horizontal, siendo el escenario de marea muerta el que produce una dispersión más baja y velocidad más uniforme de los huevos y larvas. La profundidad del desove en el Estrecho de Gibraltar es una condición crítica, como lo revelan las pruebas de sensibilidad del modelo.

#### *Capítulo 4*

Las características hidrodinámicas desempeñan un papel clave en los patrones de dispersión y conectividad de las poblaciones de peces, especialmente en zonas altamente energéticas determinadas por las corrientes, el caudal de los ríos y las fluctuaciones inducidas meteorológicamente. Comprender cómo interactúan las especies con estos procesos físicos es esencial para gestionar las poblaciones vulnerables e identificar las zonas que requieren esfuerzos de conservación eficaces. Este Capítulo examina la hidrodinámica que regula la conectividad en el mar Adriático, una cuenca poco profunda y semicerrada ampliamente reconocida como una de las zonas más importantes del mar Mediterráneo para su protección.

Un modelo hidrodinámico de alta resolución acoplado a un módulo de seguimiento Lagrangiano sirve de herramienta numérica. Las partículas Lagrangianas, que representan huevos y larvas con características biológicas típicas de los organismos marinos genéricos que habitan la región, se liberan por toda la cuenca en diferentes momentos durante un año de prueba para identificar las vías más probables de dispersión. El componente temporal de la conectividad se estima utilizando una matriz de retención, previamente desarrollada, a lo largo de diferentes duraciones larvarias.

Las áreas distribuidas a lo largo de la plataforma italiana se identifican como zonas de retención esenciales, especialmente cuando la productividad de la región se ve influenciada por la surgencia inducida por el viento y las descargas fluviales, creando condiciones ambientales favorables para las larvas. Durante el verano, cuando la velocidad se reduce, se promueve la retención, coincidiendo con el período de desove de la anchoa, y la merluza. La variabilidad observada durante el invierno se atribuye a las fluctuaciones ambientales, específicamente a la presencia de vientos fuertes que afectan significativamente el desplazamiento de las partículas. Este fenómeno brinda oportunidades favorables para las especies marinas con duraciones pelágicas larvarias más largas y períodos de desove concentrados en invierno, como la sardina y el lenguado. Muchas partículas llegan después de someterse a una recirculación, proceso que requiere más tiempo y se traduce en duraciones de llegada extendidas.

### *Capítulo 5*

Actualmente, el Estrecho de Gibraltar está experimentando una invasión sin precedentes del alga exótica *Rugulopteryx okamurae*, originaria del Pacífico Norte. Según la escasa literatura disponible, el alga se asentó primero en la costa sur, probablemente debido a los intercambios comerciales con puertos franceses donde fue introducida accidentalmente junto con ostras japonesas importadas para la maricultura. Sin embargo, no hay certeza de que el alga colonizara primero la costa sur del Estrecho y, desde allí, se extendiera hacia el norte. Podría haber sucedido al revés. Sea como fuere, se extendió por todo el Estrecho y áreas circundantes con una rapidez sorprendente. La



intervención humana (algas adheridas a los cascos de los barcos o redes de pesca, por ejemplo) pueden estar detrás de la propagación desde la costa inicialmente colonizada hasta la costa opuesta libre de algas. Pero también podría haber sucedido mediante procesos hidrodinámicos sin intervención humana directa. Esta posibilidad se evalúa en este Capítulo revisando perfiles históricos de corrientes recogidos en el Estrecho de Gibraltar en busca de flujos secundarios a través del Estrecho.

El transporte de las esporas del alga entre ambas costas del Estrecho, consideradas como partículas pasivas advectadas por las corrientes, implica cruzar las intensas corrientes zonales ligadas al intercambio bicapa entre el Atlántico y el Mediterráneo, que desplazarían las esporas más allá de las dimensiones espaciales del Estrecho antes de que éstas alcanzaran la costa opuesta. Sí existe, sin embargo, una posibilidad para este transporte transversal si éste puede realizarse en la profundidad de la interfaz entre ambos flujos, ubicada a 100-150 m, donde la corriente se anula. Si existen corrientes secundarias transversales a esta profundidad, aunque sean débiles, las posibilidades de cruzar con éxito el Estrecho no serían nulas. La hipótesis se evalúa empleando observaciones históricas de velocidad en la zona. En todas las estaciones, los perfiles medios de velocidad presentan una componente no-nula de la componente transversal que sugieren la posibilidad de cruzar el Estrecho meridionalmente. Los perfiles muestran una estructura común, caracterizada por una capa de profundidad media de velocidad transversal positiva, flanqueada por una parte negativa, tanto en superficie como en profundidad. De esta forma, la conexión de la costa sur a la norte sería posible en la capa intermedia, mientras que el transporte de norte a sur tendría lugar en las capas superficiales y profundas de la columna de agua. Los valores de velocidad transversal son de unos  $5 \text{ cm}\cdot\text{s}^{-1}$  por lo que las algas requerirían unos 4 días al menos para atravesar el Estrecho por su parte más estrecha ( $\sim 14 \text{ km}$ ). Incluso para un valor medio moderado de  $40 \text{ cm}\cdot\text{s}^{-1}$  para la velocidad longitudinal, en 4 días las partículas serían desplazadas zonalmente unos 150 km, mucho más que las dimensiones del Estrecho, por lo que no alcanzarían la orilla opuesta. Sólo evitando las capas

de mayor velocidad y permaneciendo cerca de la interfaz, las algas podrían tener posibilidades de cruzar el Estrecho meridionalmente.

Aun considerando estas condiciones, el éxito del transporte transversal depende de una cadena de eventos circunstanciales. Las algas deben ser arrancadas y resuspendidas del fondo (por redes de arrastre u otros agentes) en la zona iluminada donde se establece. Sus propágulos o esporas deben ser desplazados mar adentro en la horizontal y hasta la profundidad de la interfaz en la vertical. Luego, deberían ser transportados a través del Estrecho hasta alcanzar el talud continental opuesto, llevados a la superficie y desplazados hacia la costa y, finalmente, asentarse y prosperar en el nuevo entorno. Este proceso lleva de días a semanas, gran parte de cuyo tiempo el alga estaría en condiciones de oscuridad. La factibilidad de esta posibilidad sólo puede comprobarse con la ayuda de esquemas de advección acoplados a modelos numéricos tridimensionales de alta resolución.

### *Capítulo 6*

Desde su detección inicial en la costa del Estrecho de Gibraltar en 2015, el alga parda exótica *Rugulopteryx okamurae* se ha extendido de forma explosiva por gran parte de las costas Atlántica y Mediterránea, produciendo graves impactos en comunidades bentónicas previamente establecidas y provocando acumulaciones masivas a lo largo de las costas, afectando a la pesca y al turismo. Su extraordinariamente elevado potencial de conectividad (es decir, la conexión efectiva entre las fuentes de liberación del alga y las costas de recepción), se ve facilitada por su dispersión a través de talos flotantes a la deriva a prácticamente cualquier profundidad en la columna de agua, la propagación por esporas y la supervivencia en condiciones ambientales adversas, como la escasa o nula luminosidad y las amplias variaciones térmicas. El impacto y la adaptabilidad del alga en el entorno mediterráneo han sido objeto recientemente de numerosas investigaciones, pero aspectos cruciales de la invasión, como su distribución y las causas subyacentes de su éxito, aún se desconocen.

Para comprender mejor la propagación y el asentamiento de la especie, se han empleado dos modelos hidrodinámicos anidados de alta resolución

acoplados a un algoritmo Lagrangiano de seguimiento de partículas, con trazadores virtuales que representaban esporas libres, fragmentos de talos de *Rugulopteryx okamurae*. El trabajo se centra en el Estrecho de Gibraltar y sus cuencas adyacentes, el Golfo de Cádiz y el Mar de Alborán, que hasta el momento se han visto significativamente afectadas por la invasión de dicha alga. Las simulaciones de la dispersión de larvas a partir de una introducción en el Estrecho indican que los propágulos de algas se propagaron primero hacia el este antes de extenderse hacia el oeste, siendo el transporte por el chorro atlántico que sale del Estrecho de Gibraltar el proceso más influyente. El ciclo de marea, seguido de los vientos, es un agente dominante, siendo las mareas vivas y los vientos de levante los que generalmente promueven una mayor acumulación de partículas dentro de la cuenca de Alborán. La velocidad de sedimentación terminal de las partículas es una condición crítica, tal como revela una prueba de sensibilidad del modelo.

## Bibliography

- Aamri, F. E., Idhalla, M., & Tamsouri, M. N. (2018). Occurrence of the invasive brown seaweed *Rugulopteryx okamurae* (E.Y.Dawson) I.K.Hwang, W.J.Lee & H.S.Kim (Dictyotales, Phaeophyta) in Morocco (Mediterranean Sea). *Mediterranean Fisheries and Aquaculture Research*, 1(2), 92–96.
- Abaunza, P., Gordo, L., Karlou-Riga, C., Murta, A., Zimmermann, C., Hammer, C., Lucio, P., Iversen, S. A., Molloy, J., & Gallo, E. (2003). *Growth and reproduction of horse mackerel, Trachurus trachurus (carangidae)*.
- Abernathy, R., Bladwell, C., Froyland, G., & Sakellariou, K. (2022). Deep Lagrangian Connectivity in the Global Ocean Inferred from Argo Floats. *Journal of Physical Oceanography*, 52(5), 951–963. <https://doi.org/10.1175/JPO-D-21-0156.1>
- Acosta Yepes, Juan, Rivera Martínez, Jesús, & Hidalgo Bravo, Jesús. (2006). *Submarine Topobathymetric Relief Map of the Alboran Sea and the Strait of Gibraltar—How is the seabed and its geology in the Alboran Sea*.
- Albérola, C., Rousseau, S., Millot, C., Astraldi, M., Font, J., García-Lafuente, J., Gasparini, G. P., Send, U., & Vangriesheim, A. (1995). *Tidal currents in the western Mediterranean Sea*. <https://digital.csic.es/handle/10261/194257>
- Alcaraz, M., & Estrada, M. (2022). *Turbulence and plankton dynamics in a warmer ocean*. Consejo Superior de Investigaciones Científicas (España). <https://digital.csic.es/handle/10261/255537>
- Altamirano Jeschke, M., Rosa Álamos, J. C. de la, Martínez Gil, F. J., & Muñoz Gallego, A. R. (2017). Prolifera en el Estrecho un alga nunca citada en nuestro litoral: De origen asiático, “*Rugulopteryx okamurae*” ocupa ya una gran extensión. *Quercus*, 374, 32–33.
- Altamirano-Jeschke, M., De la Rosa Álamos, J., & Martínez Medina, F. J. (2016). *Arribazones de la especie exótica Rugulopteryx okamurae (E.Y. Dawson) en el Estrecho de Gibraltar*. Sesión Científica de la Sociedad Española de Ficología, Madrid, Spain. <https://riuma.uma.es/xmlui/handle/10630/12433>
- Altamirano-Jeschke, M., Rosa, J. de la, Carmona-Fernández, R., Kawai, H., Hanyuda, T., Gómez, A., Rull, J., Zanolla-Balbuena, M. F., Rosas-Guerrero, J., Blasco, C., & Muñoz-Gallego, A. R. (2022). *Arguments to consider Rugulopteryx okamurae (Dictyotales, Ochrophyta) the potential first seaweed species to be included in the lists of invasive species of European*

- Union concern*. 22nd International Conference on Aquatic Invasive Species, Oostende, Belgium.  
<https://riuma.uma.es/xmlui/handle/10630/23989>
- Álvarez Fanjul, E., Pérez Gómez, B., & Rodríguez Sánchez Arévalo, I. (2001). Nivmar: A storm surge forecasting system for Spanish waters. *Scientia Marina*, 65(S1), 145–154. <https://doi.org/10.3989/scimar.2001.65s1145>
- Alvarez, P., Fives, J., Motos, L., & Santos, M. (2004). Distribution and abundance of European hake *Merluccius merluccius* (L.), eggs and larvae in the North East Atlantic waters in 1995 and 1998 in relation to hydrographic conditions. *Journal of Plankton Research*, 26(7), 811–826. <https://doi.org/10.1093/plankt/fbh074>
- Amoroso, P. P., Aguilar, F. J., Parente, C., & Aguilar, M. A. (2023). Statistical Assessment of Some Interpolation Methods for Building Grid Format Digital Bathymetric Models. *Remote Sensing*, 15(8), Article 8. <https://doi.org/10.3390/rs15082072>
- Andrello, M., Mouillot, D., Beuvier, J., Albouy, C., Thuiller, W., & Manel, S. (2013). Low Connectivity between Mediterranean Marine Protected Areas: A Biophysical Modeling Approach for the Dusky Grouper *Epinephelus marginatus*. *PLoS ONE*, 8(7). <https://doi.org/10.1371/journal.pone.0068564>
- Angiulli, E., Sola, L., Ardizzone, G., Fassatoui, C., & Rossi, A. R. (2016). Phylogeography of the common pandora *Pagellus erythrinus* in the central Mediterranean Sea: Sympatric mitochondrial lineages and genetic homogeneity. *Marine Biology Research*, 12(1), 4–15. <https://doi.org/10.1080/17451000.2015.1069355>
- Antell, G. T., Kiessling, W., Aberhan, M., & Saupe, E. E. (2020). Marine Biodiversity and Geographic Distributions Are Independent on Large Scales. *Current Biology*, 30(1), 115–121.e5. <https://doi.org/10.1016/j.cub.2019.10.065>
- Arneri, E., & Morales-Nin, B. (2000). Aspects of the early life history of European hake from the central Adriatic. *Journal of Fish Biology*, 56(6), 1368–1380. <https://doi.org/10.1111/j.1095-8649.2000.tb02149.x>
- Ashton, G., Zabin, C., Davidson, I., & Ruiz, G. (2022). Recreational boats routinely transfer organisms and promote marine bioinvasions. *Biological Invasions*, 24, 1–14. <https://doi.org/10.1007/s10530-021-02699-x>
- Assis, J., Zupan, M., Nicastro, K. R., Zardi, G. I., McQuaid, C. D., & Serrão, E. A. (2015). Oceanographic Conditions Limit the Spread of a Marine

- Invader along Southern African Shores. *PLoS ONE*, 10(6), e0128124. <https://doi.org/10.1371/journal.pone.0128124>
- Ayata, S. D., Lazure, P., & Thiébaud, É. (2010). How does the connectivity between populations mediate range limits of marine invertebrates? A case study of larval dispersal between the Bay of Biscay and the English Channel (North-East Atlantic). *Progress in Oceanography*, 57(1–4), 18–36. <https://doi.org/10.1016/j.pocean.2010.09.022>
- Báez, J. C., Camiñas, J. A., Aguilera, R., Castro-Gutiérrez, J., & Real, R. (2023). When non-target wildlife species and alien species both affect negatively to an artisanal fishery: The case of trammel net in the Alboran Sea. *Reviews in Fish Biology and Fisheries*, 33(3), 785–799. <https://doi.org/10.1007/s11160-023-09759-6>
- Báez, J. C., Macías, D., & De Castro, M. (2014). Assessing the response of exploited marine populations in a context of rapid climate change: The case of blackspot seabream from the Strait of Gibraltar. In *Animal Biodiversity and Conservation* (Vol. 37).
- Bajo, M., Ferrarin, C., Dinu, I., Umgiesser, G., & Stanica, A. (2014). The water circulation near the Danube Delta and the Romanian coast modelled with finite elements. *Continental Shelf Research*, 34, 62–74. <https://doi.org/10.1016/j.csr.2014.02.006>
- Barton, E. D. (2001). Canary And Portugal Currents. In *Encyclopedia of Ocean Sciences* (pp. 380–389). Academic Press. <https://doi.org/10.1006/rwos.2001.0360>
- Baschek, B., Send, U., García Lafuente, J., & Candela, J. (2001). Transport estimates in the Strait of Gibraltar with a tidal inverse model. *Journal of Geophysical Research: Oceans*, 106(C12), 31033–31044. <https://doi.org/10.1029/2000JC000458>
- Basilone, G., Ferreri, R., Aronica, S., Mazzola, S., Bonanno, A., Gargano, A., Pulizzi, M., Fontana, I., Giacalone, G., Calandrino, P., Genovese, S., & Barra, M. (2021). Reproduction and Sexual Maturity of European Sardine (*Sardina pilchardus*) in the Central Mediterranean Sea. *Frontiers in Marine Science*, 8. <https://doi.org/10.3389/fmars.2021.715846>
- Basilone, G., Guisande, C., Patti, B., Mazzola, S., Cuttitta, A., Bonanno, A., Vergara, A. r., & Maneiro, I. (2006). Effect of habitat conditions on reproduction of the European anchovy (*Engraulis encrasicolus*) in the Strait of Sicily. *Fisheries Oceanography*, 15(4), 271–280. <https://doi.org/10.1111/j.1365-2419.2005.00391.x>

- Bastari, A., Micheli, F., Ferretti, F., Pusceddu, A., & Cerrano, C. (2016). Large marine protected areas (LMPAs) in the Mediterranean Sea: The opportunity of the Adriatic Sea. *Marine Policy*, *68*, 165–177. <https://doi.org/10.1016/j.marpol.2016.03.010>
- Batista, M. I., Baeta, F., Costa, M. J., & Cabral, H. N. (2011). MPA as management tools for small-scale fisheries: The case study of Arrábida Marine Protected Area (Portugal). *Ocean & Coastal Management*, *54*(2), 137–147. <https://doi.org/10.1016/j.ocecoaman.2010.10.032>
- Beca-Carretero, P., Winters, G., Teichberg, M., Procaccini, G., Schneekloth, F., Zambrano, R. H., Chiquillo, K., & Reuter, H. (2024). Climate change and the presence of invasive species will threaten the persistence of the Mediterranean seagrass community. *Science of The Total Environment*, *910*, 168675. <https://doi.org/10.1016/j.scitotenv.2023.168675>
- Bellafiore, D., & Umgiesser, G. (2010). Hydrodynamic coastal processes in the North Adriatic investigated with a 3D finite element model. *Ocean Dynamics*, *60*(2), 255–273. <https://doi.org/10.1007/s10236-009-0254-x>
- Bellissimo, G., Altamirano Jeschke, M., Muñoz, A.-R., De la Rosa, J., Hung, T. H., Rizzuto, G., Vizzini, S., & Tomasello, A. (2023). The invasive brown seaweed *Rugulopteryx okamurae* (Dictyotales, Ochrophyta) continues to expand: First record in Italy. *BioInvasions Records*, *13*(2), 385–401. <https://doi.org/10.1101/2023.09.23.559131>
- Berkström, C., Wennerström, L., & Bergström, U. (2022). Ecological connectivity of the marine protected area network in the Baltic Sea, Kattegat and Skagerrak: Current knowledge and management needs. *Ambio*, *51*(6), 1485–1503. <https://doi.org/10.1007/s13280-021-01684-x>
- Bethoux, J. P. (1979). Budgets of the mediterranean sea—Their dependance on the local climate and on the characteristics of the atlantic waters. *Oceanologica Acta*, *2*(2), 157–163.
- Bethoux, J. P., Gentili, B., Morin, P., Nicolas, E., Pierre, C., & Ruiz-Pino, D. (1999). The Mediterranean Sea: A miniature ocean for climatic and environmental studies and a key for the climatic functioning of the North Atlantic. *Progress in Oceanography*, *44*(1), 131–146. [https://doi.org/10.1016/S0079-6611\(99\)00023-3](https://doi.org/10.1016/S0079-6611(99)00023-3)
- Beudin, A., Ganju, N. K., Defne, Z., & Aretxabaleta, A. L. (2017). Physical response of a back-barrier estuary to a post-tropical cyclone. *Journal of Geophysical Research: Oceans*, *122*(7), 5888–5904. <https://doi.org/10.1002/2016JC012344>

- Biagi, F., Gambaccini, S., & Zazzetta, M. (1998). Settlement and recruitment in fishes: The role of coastal areas. *Italian Journal of Zoology*, 65(sup1), 269–274. <https://doi.org/10.1080/11250009809386831>
- Bignami, F., Sciarra, R., Carniel, S., & Santoleri, R. (2007). Variability of Adriatic Sea coastal turbid waters from SeaWiFS imagery. *Journal of Geophysical Research*, 112, C03S10. <https://doi.org/10.1029/2006JC003518>
- Bomers, A., Schielen, R. M. J., & Hulscher, S. J. M. H. (2019). The influence of grid shape and grid size on hydraulic river modelling performance. *Environmental Fluid Mechanics*, 19(5), 1273–1294. <https://doi.org/10.1007/s10652-019-09670-4>
- Bonnin, L., Lett, C., Dagorn, L., Filmlalter, J. D., Forget, F., Verley, P., & Capello, M. (2021). Can drifting objects drive the movements of a vulnerable pelagic shark? *Aquatic Conservation: Marine and Freshwater Ecosystems*, 31(1), 74–82. <https://doi.org/10.1002/aqc.3420>
- Boog, C., Pietrzak, J., Dijkstra, H., Brüggemann, N., Westen, R., James, R., Bouma, T., Riva, R., Slobbe, D., Klees, R., Zijlema, M., & Katsman, C. (2019). The impact of upwelling on the intensification of anticyclonic ocean eddies in the Caribbean Sea. *Ocean Science*, 15, 1419–1437. <https://doi.org/10.5194/os-15-1419-2019>
- Book, J. W., Signell, R. P., & Perkins, H. (2007). Measurements of storm and nonstorm circulation in the northern Adriatic: October 2002 Through April 2003. *Journal of Geophysical Research: Oceans*, 112(C11). <https://doi.org/10.1029/2006JC003556>
- Boon, J. D. (2004). *Secrets of the Tide: Tide and Tidal Current Analysis and Predictions, Storm Surges and Sea Level Trends*. Horwood Publishing.
- Botsford, L., Brumbaugh, D., Grimes, C., Kellner, J., Largier, J., O'Farrell, M., Ralston, S., Soulanille, E., & Wespestad, V. (2009). Connectivity, sustainability, and yield: Bridging the gap between conventional fisheries management and marine protected areas. *Reviews in Fish Biology and Fisheries*, 19, 69–95. <https://doi.org/10.1007/s11160-008-9092-z>
- Boutov, D., Peliz, Á., Miranda, P. M. A., Soares, P. M. M., Cardoso, R. M., Prieto, L., Ruiz, J., & García-Lafuente, J. (2014). Inter-annual variability and long term predictability of exchanges through the Strait of Gibraltar. *Global and Planetary Change*, 114, 23–37. <https://doi.org/10.1016/j.gloplacha.2013.12.009>
- Bracken, L., Turnbull, L., Wainwright, J., & Bogaart, P. (2015). Sediment connectivity: A framework for understanding sediment transfer at



- multiple scales. *Earth Surface Processes and Landforms*, 40. <https://doi.org/10.1002/esp.3635>
- Bradford, R., Griffin, D., & Bruce, B. (2015). Estimating the duration of the pelagic phyllosoma phase of the southern rock lobster, *Jasus edwardsii* (Hutton). *Marine and Freshwater Research*, 66, 213–219. <https://doi.org/10.1071/MF14065>
- Bray, L., Kassis, D., & Hall-Spencer, J. M. (2017). Assessing larval connectivity for marine spatial planning in the Adriatic. *Marine Environmental Research*, 125, 73–81. <https://doi.org/10.1016/j.marenvres.2017.01.006>
- Brown, C. J., Harborne, A. R., Paris, C. B., & Mumby, P. J. (2016). Uniting paradigms of connectivity in marine ecology. *Ecology*, 97(9), 2447–2457.
- Brünnich, M. T. (1768). *Ichthyologia Massiliensis, sistens piscium descriptiones eorumque apud incolas nomina. Accedunt Spolia Maris Adriatici. Hafniae et Lipsiae. I-xvi + 1-110. [In 2 parts; first as i-xvi + 1-84; 2nd as Spolia e Mari Adriatica reportata: 85-110.]*
- Bryden, H. L., Candela, J., & Kinder, T. H. (1994). Exchange through the Strait of Gibraltar. *Progress in Oceanography*, 33, 201–248. [https://doi.org/10.1016/0079-6611\(94\)90028-0](https://doi.org/10.1016/0079-6611(94)90028-0)
- Burgos, C., Gil, J., & Olmo, L. (2013). The Spanish blackspot seabream (*Pagellus bogaraveo*) fishery in the Strait of Gibraltar: Spatial distribution and fishing effort derived from a small-scale GPRS/GSM based fisheries vessel monitoring system. *Aquatic Living Resources*, 26, 399–407. <https://doi.org/10.1051/alr/2013068>
- Calò, A., Félix-Hackradt, F. C., Garcia, J., Hackradt, C. W., Rocklin, D., Treviño Otón, J., & Charton, J. A. G. (2013). A review of methods to assess connectivity and dispersal between fish populations in the Mediterranean Sea. *Advances in Oceanography and Limnology*, 4(2), 150–175. <https://doi.org/10.1080/19475721.2013.840680>
- Calò, A., Lett, C., Mourre, B., Pérez-Ruzafa, Á., & García-Charton, J. A. (2018). Use of Lagrangian simulations to hindcast the geographical position of propagule release zones in a Mediterranean coastal fish. *Marine Environmental Research*, 134, 16–27. <https://doi.org/10.1016/j.marenvres.2017.12.011>
- Campana, S. (1999). Chemistry and composition of fish otoliths: Pathways, mechanisms and applications. *Marine Ecology-Progress Series - MAR ECOL-PROGR SER*, 188, 263–297. <https://doi.org/10.3354/meps188263>
- Candela, J., Winant, C. D., & Bryden, H. L. (1989). Meteorologically forced subinertial flows through the Strait of Gibraltar. *Journal of Geophysical*

- Research: Oceans*, 94(C9), 12667–12679.  
<https://doi.org/10.1029/JC094iC09p12667>
- Candelma, M., Marisaldi, L., Daniela, B., Radaelli, G., Gioacchini, G., Santojanni, A., Colella, S., & Carnevali, O. (2021). Aspects of Reproductive Biology of the European Hake (*Merluccius merluccius*) in the Northern and Central Adriatic Sea (GSA 17-Central Mediterranean Sea). *Journal of Marine Science and Engineering*, 9, 389. <https://doi.org/10.3390/jmse9040389>
- Carbonara, P., Intini, S., Modugno, E., Maradonna, F., Spedicato, M. T., Lembo, G., Zupa, W., & Carnevali, O. (2015). Reproductive biology characteristics of red mullet (*Mullus barbatus* L., 1758) in Southern Adriatic Sea and management implications. *Aquat. Living Resour.*, 28, 21–31. <https://doi.org/10.1051/alr/2015005>
- Carney, L., & Edwards, M. (2006). Cryptic Processes in the Sea: A Review of Delayed Development in the Microscopic Life Stages of Marine Macroalgae. *ALGAE*, 21. <https://doi.org/10.4490/ALGAE.2006.21.2.161>
- Carrère, L., & Lyard, F. (2003). Modeling the barotropic response of the global ocean to atmospheric wind and pressure forcing—Comparisons with observations. *Geophysical Research Letters*, 30(6). <https://doi.org/10.1029/2002GL016473>
- Carrere, L., Lyard, F., Cancet, M., Guillot, A., & Roblou, L. (2013). *FES 2012: A New Global Tidal Model Taking Advantage of Nearly 20 Years of Altimetry*. 710, 13. 20 Years of Progress in Radar Altimetry.
- Cavraro, F., Anelli Monti, M., Matić-Skoko, S., Caccin, A., & Pranovi, F. (2023). Vulnerability of the Small-Scale Fishery to Climate Changes in the Northern-Central Adriatic Sea (Mediterranean Sea). *Fishes*, 8(1), Article 1. <https://doi.org/10.3390/fishes8010009>
- Chassignet, E. P., Hurlburt, H. E., Metzger, E. J., Smedstad, O. M., Cummings, J. A., Halliwell, G. R., Bleck, R., Baraille, R., Wallcraft, A. J., Lozano, C., Tolman, H. L., Srinivasan, A., Hankin, S., Cornillon, P., Weisberg, R., Barth, A., He, R., Werner, F., & Wilkin, J. (2009). US GODAE: Global Ocean Prediction with the HYbrid Coordinate Ocean Model (HYCOM). *Oceanography*, 22(2), 64–75.
- Ciannelli, L., Bailey, K., & Olsen, E. M. (2015). Evolutionary and ecological constraints of fish spawning habitats. *ICES Journal of Marine Science*, 72(2), 285–296. <https://doi.org/10.1093/icesjms/fsu145>
- Civitaresse, G., Gačić, M., Vetrano, A., Boldrin, A., Bregant, D., Rabitti, S., & Souvermezoglou, E. (1998). Biogeochemical fluxes through the Strait

- of Otranto (Eastern Mediterranean). *Continental Shelf Research*, 18(7), 773–789. [https://doi.org/10.1016/S0278-4343\(98\)00016-8](https://doi.org/10.1016/S0278-4343(98)00016-8)
- Clementi, E., Aydogdu, A., Goglio, A. C., Pistoia, J., Escudier, R., Drudi, M., Grandi, A., Mariani, A., Lyubartsev, V., Lecci, R., Creti, S., Coppini, G., Masina, S., & Pinardi, N. (2021). *Mediterranean Sea Physical Analysis and Forecast (CMEMS MED-Currents, EAS6 system) (Version 1) [Data set]*. [Dataset]. Copernicus Monitoring Environment Marine Service (CMEMS).  
[https://doi.org/10.25423/CMCC/MEDSEA\\_ANALYSISFORECAST\\_P HY\\_006\\_013\\_EAS6](https://doi.org/10.25423/CMCC/MEDSEA_ANALYSISFORECAST_P HY_006_013_EAS6)
- Coll, M., Santojanni, A., Palomera, I., & Arneri, E. (2010). Ecosystem assessment of the North-Central Adriatic Sea: Towards a multivariate reference framework. *Marine Ecology Progress Series*, 417, 193–210. <https://doi.org/10.3354/meps08800>
- Commission Implementing Regulation (EU) 2016/1141 of 13 July 2016 Adopting a List of Invasive Alien Species of Union Concern Pursuant to Regulation (EU) No 1143/2014 of the European Parliament and of the Council (2022).  
[http://data.europa.eu/eli/reg\\_impl/2016/1141/2022-08-02/eng](http://data.europa.eu/eli/reg_impl/2016/1141/2022-08-02/eng)
- CopeMed II. (2017). *Report of the CopeMed II Workshop on methodologies for the identification of stock units in the Alboran Sea* (CopeMed II Technical Documents Technical Documents N°46; (GCP/INT/028/SPA - GCP/INT/270/EC), p. 58). Food and Agriculture Organization of the United Nations (FAO).
- CopeMed II. (2019). *Report of the Mid-Term Workshop on TRANSBORAN project, “Transboundary population structure of sardine, European hake and blackspot seabream in the Alboran Sea and adjacent waters: A multidisciplinary approach”* (CopeMed II Technical Documents Technical Documents N°52; (GCP/INT/028/SPA - GCP/INT/270/EC), p. 33). Food and Agriculture Organization of the United Nations (FAO).
- Costa, A. M. (2013). Somatic Condition, Growth and Reproduction of Hake, *Merluccius merluccius* L., in the Portuguese Coast. *Open Journal of Marine Science*, 13, 12–30. <https://doi.org/10.4236/ojms.2013.31002>
- Costello, M. J., & Chaudhary, C. (2017). Marine Biodiversity, Biogeography, Deep-Sea Gradients, and Conservation. *Current Biology*, 27(11), R511–R527. <https://doi.org/10.1016/j.cub.2017.04.060>
- Cowen, R. K., Gawarkiewicz, G., Pineda, J., Thorrold, S. R., & Werner, F. E. (2007). Population connectivity in marine systems: An overview.

- Oceanography*, 20(SPL.ISS. 3), 14–21.  
<https://doi.org/10.5670/oceanog.2007.26>
- Cowen, R. K., Lwiza, K. M., Sponaugle, S., Paris, C. B., & Olson, D. B. (2000). Connectivity of marine populations: Open or closed? *Science (New York, N.Y.)*, 287(5454), 857–859.  
<https://doi.org/10.1126/science.287.5454.857>
- Cowen, R. K., Paris, C. B., & Srinivasan, A. (2006). Scaling of connectivity in marine populations. *Science (New York, N.Y.)*, 311(5760), 522–527.  
<https://doi.org/10.1126/science.1122039>
- Cowen, R. K., & Sponaugle, S. (2009). Larval dispersal and marine population connectivity. *Annual Review of Marine Science*, 1, 443–466.  
<https://doi.org/10.1146/annurev.marine.010908.163757>
- Cozzi, S., & Giani, M. (2011). River water and nutrient discharges in the Northern Adriatic Sea: Current importance and long term changes. *Continental Shelf Research*, 31(18), 1881–1893.  
<https://doi.org/10.1016/j.csr.2011.08.010>
- Criado-Aldeanueva, F., Soto-Navarro, F. J., & García-Lafuente, J. (2012). Seasonal and interannual variability of surface heat and freshwater fluxes in the Mediterranean Sea: Budgets and exchange through the Strait of Gibraltar. *International Journal of Climatology*, 32(2), 286–302.  
<https://doi.org/10.1002/joc.2268>
- Crivellaro, M. S., Candido, D. V., Silveira, T. C. L., Fonseca, A. C., & Segal, B. (2022). A tool for a race against time: Dispersal simulations to support ongoing monitoring program of the invasive coral *Tubastraea coccinea*. *Marine Pollution Bulletin*, 185(Pt B), 114354.  
<https://doi.org/10.1016/j.marpolbul.2022.114354>
- Crochelet, E., Roberts, J., Lagabrielle, E., Obura, D., Petit, M., & Chabanet, P. (2016). A model-based assessment of reef larvae dispersal in the Western Indian Ocean reveals regional connectivity patterns—Potential implications for conservation policies. *Regional Studies in Marine Science*, 7. <https://doi.org/10.1016/j.rsma.2016.06.007>
- Cushman-Roisin, B., & Beckers, J.-M. (2006). *Introduction to Geophysical Fluid Dynamics: Physical and Numerical Aspects*. Academic Press.
- Cushman-Roisin, B., Gacic, M., Poulain, P.-M., & Artegiani, A. (2001). *Physical Oceanography of the Adriatic Sea: Past, Present and Future*. <https://doi.org/10.1007/978-94-015-9819-4>
- Da Ros, Z., Fanelli, E., Cassatella, S., Biagiotti, I., Canduci, G., Menicucci, S., De Felice, A., Malavolti, S., & Leonori, I. (2023). Resource Partitioning among “Ancillary” Pelagic Fishes (*Scomber* spp., *Trachurus* spp.) in the

- Adriatic Sea. *Biology*, 12(2), Article 2.  
<https://doi.org/10.3390/biology12020272>
- Dagestad, K.-F., Röhrs, J., Breivik, Ø., & Ådlandsvik, B. (2018). OpenDrift v1.0: A generic framework for trajectory modelling. *Geoscientific Model Development*, 11(4), 1405–1420. <https://doi.org/10.5194/gmd-11-1405-2018>
- D'Agostini, A., Gherardi, D. F. M., & Pezzi, L. P. (2015). Connectivity of Marine Protected Areas and Its Relation with Total Kinetic Energy. *PLOS ONE*, 10(10), e0139601. <https://doi.org/10.1371/journal.pone.0139601>
- D'Aloia, C. C., Bogdanowicz, S. M., Francis, R. K., Majoris, J. E., Harrison, R. G., & Buston, P. M. (2015). Patterns, causes, and consequences of marine larval dispersal. *Proceedings of the National Academy of Sciences*, 112(45), 13940–13945. <https://doi.org/10.1073/pnas.1513754112>
- Darnaude, A., Arnaud-Haond, S., Hunter, E., Gaggiotti, O., Sturrock, A., Beger, M., Volckaert, F., Pérez-Ruzafa, A., López-López, L., Tanner, S. E., Turan, C., Doğdu, S. A., Katsanevakis, S., & Costantini, F. (2022). Unifying approaches to Functional Marine Connectivity for improved marine resource management: The European SEA-UNICORN COST Action. *Research Ideas and Outcomes*, 8, e80223. <https://doi.org/10.3897/rio.8.e80223>
- Daskalaki, E., Koufalis, E., Dimarchopoulou, D., & Tsikliras, A. C. (2022). Scientific progress made towards bridging the knowledge gap in the biology of Mediterranean marine fishes. *PLoS One*, 17(11), e0277383. <https://doi.org/10.1371/journal.pone.0277383>
- Daud, N. R., Akhir, M. F., & Muslim, A. M. (2019). Dynamic of ENSO towards upwelling and thermal front zone in the east coast of Peninsular Malaysia. *Acta Oceanologica Sinica*, 38(1), 48–60. <https://doi.org/10.1007/s13131-019-1369-7>
- De la Lama-Calvente, D., Mancilla-Leytón, J. M., Borja, R., & Fernández-Rodríguez, M. J. (2024). Use of anaerobic digestate as biofertilizer: Another step forward in the valorisation of the invasive brown macroalgae *Rugulopteryx okamurae*. *Scientia Horticulturae*, 325, 112638. <https://doi.org/10.1016/j.scienta.2023.112638>
- De Pascalis, F., Pérez-Ruzafa, A., Gilabert, J., Marcos, C., & Umgiesser, G. (2012). Climate change response of the Mar Menor coastal lagoon (Spain) using a hydrodynamic finite element model. *Estuarine, Coastal and Shelf Science*, 114, 118–129. <https://doi.org/10.1016/j.ecss.2011.12.002>

- Deangelis, D., & Mooij, W. (2005). Individual-Based Modeling of Ecological and Evolutionary Processes 1. *Annu. Rev. Ecol. Evol. Syst.*, *36*, 147–168. <https://doi.org/10.1146/annurev.ecolsys.36.102003.152644>
- Defne, Z., Ganju, N. K., & Aretxabaleta, A. (2016). Estimating time-dependent connectivity in marine systems. *Geophysical Research Letters*, *43*(3), 1193–1201. <https://doi.org/10.1002/2015GL066888>
- Demmer, J., Neill, S. P., Andres, O., Malham, S. K., Jones, T., & Robins, P. (2022). Larval dispersal from an energetic tidal channel and implications for blue mussel (*Mytilus edulis*) shellfisheries. *Aquaculture International*, *30*(6), 2969–2995. <https://doi.org/10.1007/s10499-022-00948-x>
- Desbrosses, P. (1932). La dorade commune (*Pagellus centrodontus* Delaroché) et sa pêche. *Revue Du Travail de L'Office Des Pêches Maritime*, *5*(18), 167–222.
- Deudero, S., Arnaud-Haond, S., Di Franco, A., Fromentin, J.-M., Gucu, A. C., Hilário, A., Mariani, P., Panigada, S., Pascual, M., Rossi, V., Soldo, A., Villamor, A., Zalota, A., & Briand, F. (2017). Marine connectivity: Migration and larval dispersal - An overview. *CIESM Workshop Monographs*, *48*, 5–18.
- Di Franco, A., Coppini, G., Pujolar, J. M., Leo, G. A. D., Gatto, M., Lyubartsev, V., Melià, P., Zane, L., & Guidetti, P. (2012). Assessing Dispersal Patterns of Fish Propagules from an Effective Mediterranean Marine Protected Area. *PLOS ONE*, *7*(12), e52108. <https://doi.org/10.1371/journal.pone.0052108>
- Dickey, T. (2001). The Role of New Technology in Advancing Ocean Biogeochemical Research. *Oceanography*, *14*(4), 108–120. <https://doi.org/10.5670/oceanog.2001.11>
- Dominique, P. (2011). INDICATORS – Constructing and validating indicators of the effectiveness of marine protected areas. In *Marine Protected Areas: A Multidisciplinary Approach* (pp. 247–266). <https://doi.org/10.1017/CBO9781139049382.014>
- Döös, K., Kjellsson, J., & Jönsson, B. (2013). TRACMASS—A Lagrangian Trajectory Model. In T. Soomere & E. Quak (Eds.), *Preventive Methods for Coastal Protection: Towards the Use of Ocean Dynamics for Pollution Control* (pp. 225–249). Springer International Publishing. [https://doi.org/10.1007/978-3-319-00440-2\\_7](https://doi.org/10.1007/978-3-319-00440-2_7)
- Dorostkar, A., Boegman, L., Schweitzer, S., & Pollard, A. (2022). Three-dimensional numerical simulation of basin-scale internal waves in a

- long narrow lake. *Environmental Fluid Mechanics*, 23. <https://doi.org/10.1007/s10652-022-09868-z>
- D'Ortenzio, F., & Ribera d'Alcalà, M. (2009). On the trophic regimes of the Mediterranean Sea: A satellite analysis. *Biogeosciences*, 6(2), 139–148. <https://doi.org/10.5194/bg-6-139-2009>
- Dubois, M., Rossi, V., Ser-Giacomi, E., Arnaud-Haond, S., López, C., & Hernández-García, E. (2016). Linking basin-scale connectivity, oceanography and population dynamics for the conservation and management of marine ecosystems. *Global Ecology and Biogeography*, 25(5), 503–515. <https://doi.org/10.1111/geb.12431>
- Echevarría, F., García Lafuente, J., Bruno, M., Gorsky, G., Goutx, M., González, N., García, C. M., Gómez, F., Vargas, J. M., Picheral, M., Striby, L., Varela, M., Alonso, J. J., Reul, A., Cózar, A., Prieto, L., Sarhan, T., Plaza, F., & Jiménez-Gómez, F. (2002). Physical–biological coupling in the Strait of Gibraltar. *Deep Sea Research Part II: Topical Studies in Oceanography*, 49(19), 4115–4130. [https://doi.org/10.1016/S0967-0645\(02\)00145-5](https://doi.org/10.1016/S0967-0645(02)00145-5)
- Edson, J., Jampana, V., Weller, R., Bigorre, S., Plueddemann, A., Fairall, C., Miller, S., Mahrt, L., Vickers, D., & Hersbach, H. (2013). On the Exchange of Momentum over the Open Ocean. *Journal of Physical Oceanography*, 43, 1589–1610. <https://doi.org/10.1175/JPO-D-12-0173.1>
- EMODnet Bathymetry Consortium. (2018). *European Marine Observation and Data Network (EMODnet)* [Map]. Energy, Climate change, Environment. European Commission. 10.12770/18ff0d48-b203-4a65-94a9-5fd8b0ec35f6
- Esposito, G., Donnet, S., Berta, M., Shcherbina, A. Y., Freilich, M., Centurioni, L., D'Asaro, E. A., Farrar, J. T., Johnston, T. M. S., Mahadevan, A., Özgökmen, T., Pascual, A., Poulain, P., Ruiz, S., Tarry, D. R., & Griffa, A. (2023). Inertial Oscillations and Frontal Processes in an Alboran Sea Jet: Effects on Divergence and Vertical Transport. *Journal of Geophysical Research: Oceans*, 128(3), e2022JC019004. <https://doi.org/10.1029/2022JC019004>
- Estévez, R., Palacios, M., Cervera, J., & González-Duarte, M. (2022). Expansion of the invasive alga *Rugulopteryx okamurae* (Dictyotaceae, Ochrophyta) in the Mediterranean Sea: First evidence as epiphyte of the cold-water coral *Dendrophyllia ramea* (Cnidaria: Scleractinia). *BioInvasions Records*, 11(4), 925–936. <https://doi.org/10.3391/bir.2022.11.4.11>

- Estradivari, Agung, Muh. F., Adhuri, D. S., Ferse, S. C. A., Sualia, I., Andradi-Brown, D. A., Campbell, S. J., Iqbal, M., Jonas, H. D., Lazuardi, M. E., Nanlohy, H., Pakiding, F., Pusparini, N. K. S., Ramadhana, H. C., Ruchimat, T., Santiadji, I. W. V., Timisela, N. R., Veverka, L., & Ahmadia, G. N. (2022). Marine conservation beyond MPAs: Towards the recognition of other effective area-based conservation measures (OECMs) in Indonesia. *Marine Policy*, 137, 104939. <https://doi.org/10.1016/j.marpol.2021.104939>
- Faillottaz, R., Paris, C. B., & Irisson, J. O. (2018). Larval fish swimming behavior alters dispersal patterns from marine protected areas in the North-Western Mediterranean Sea. *Frontiers in Marine Science*, 5(MAR). <https://doi.org/10.3389/fmars.2018.00097>
- Fanelli, E., Da Ros, Z., Menicucci, S., Malavolti, S., Biagiotti, I., Canduci, G., De Felice, A., & Leonori, I. (2023). The pelagic food web of the Western Adriatic Sea: A focus on the role of small pelagics. *Scientific Reports*, 13(1), 14554. <https://doi.org/10.1038/s41598-023-40665-w>
- Fanelli, E., Principato, E., Monfardini, E., Da Ros, Z., Scarcella, G., Santojanni, A., & Colella, S. (2022). Seasonal Trophic Ecology and Diet Shift in the Common Sole *Solea solea* in the Central Adriatic Sea. *Animals*, 12(23), Article 23. <https://doi.org/10.3390/ani12233369>
- Fanjul, E. Á., Gómez, B. P., & Arévalo, I. R. S. (2001). Nivmar: A storm surge forecasting system for Spanish waters. *Scientia Marina*, 65(S1), Article S1. <https://doi.org/10.3989/scimar.2001.65s1145>
- Faria, J., Prestes, A. C. L., Moreu, I., Cacabelos, E., & Martins, G. M. (2022). Dramatic changes in the structure of shallow-water marine benthic communities following the invasion by *Rugulopteryx okamurae* (Dictyotales, Ochrophyta) in Azores (NE Atlantic). *Marine Pollution Bulletin*, 175, 113358. <https://doi.org/10.1016/j.marpolbul.2022.113358>
- Farmer, D. M., Armi, L., Armi, L., & Farmer, D. M. (1988). The flow of Atlantic water through the Strait of Gibraltar. *Progress in Oceanography*, 21(1), 1–103. [https://doi.org/10.1016/0079-6611\(88\)90055-9](https://doi.org/10.1016/0079-6611(88)90055-9)
- Federico, I., Pinardi, N., Coppini, G., Oddo, P., Lecci, R., & Mossa, M. (2017). Coastal ocean forecasting with an unstructured grid model in the southern Adriatic and northern Ionian seas. *Natural Hazards and Earth System Sciences*, 17(1), 45–59. <https://doi.org/10.5194/nhess-17-45-2017>
- Féral, J.-P. (2002). How useful are the genetic markers in attempts to understand and manage marine biodiversity? *Journal of Experimental Marine Biology and Ecology*, 268(2), 121–145. [https://doi.org/10.1016/S0022-0981\(01\)00382-3](https://doi.org/10.1016/S0022-0981(01)00382-3)



- Ferrari, A., Spiga, M., Rodriguez, M. D., Fiorentino, F., Gil-Herrera, J., Hernandez, P., Hidalgo, M., Johnstone, C., Khemiri, S., Mokhtar-Jamaï, K., Nadal, I., Pérez, M., Sammartino, S., Vasconcellos, M., & Cariani, A. (2023). Matching an Old Marine Paradigm: Limitless Connectivity in a Deep-Water Fish over a Large Distance. *Animals*, 13(17), Article 17. <https://doi.org/10.3390/ani13172691>
- Ferrarin, C., Cucco, A., Umgiesser, G., Bellafore, D., & Amos, C. L. (2010). Modelling fluxes of water and sediment between Venice Lagoon and the sea. *Continental Shelf Research*, 30(8), 904–914. <https://doi.org/10.1016/j.csr.2009.08.014>
- Ferrarin, C., Davolio, S., Bellafore, D., Ghezzi, M., Maicu, F., Mc Kiver, W., Drofa, O., Umgiesser, G., Bajo, M., De Pascalis, F., Malguzzi, P., Zaggia, L., Lorenzetti, G., & Manfè, G. (2019). Cross-scale operational oceanography in the Adriatic Sea. *Journal of Operational Oceanography*, 12(2), 86–103. <https://doi.org/10.1080/1755876X.2019.1576275>
- Ferrarin, C., Maicu, F., & Umgiesser, G. (2017). The effect of lagoons on Adriatic Sea tidal dynamics. *Ocean Modelling*, 119, 57–71. <https://doi.org/10.1016/j.ocemod.2017.09.009>
- Ferrarin, C., Umgiesser, G., Cucco, A., Hsu, T.-W., Roland, A., & Amos, C. L. (2008). Development and validation of a finite element morphological model for shallow water basins. *Coastal Engineering*, 55(9), 716–731. <https://doi.org/10.1016/j.coastaleng.2008.02.016>
- Ferrarin, C., Umgiesser, G., Roland, A., Bajo, M., De Pascalis, F., Ghezzi, M., & Scroccaro, I. (2016). Sediment dynamics and budget in a microtidal lagoon—A numerical investigation. *Marine Geology*, 381, 163–174. <https://doi.org/10.1016/j.margeo.2016.09.006>
- Ferraro, G., & Failler, P. (2022). Bringing nature into decision-making and policy design: Experiences from overseas Europe. *Policy Design and Practice*, 5(2), 226–244. <https://doi.org/10.1080/25741292.2021.1885797>
- Ferreira-Anta, T., Flórez-Fernández, N., Torres, M. D., Mazón, J., & Dominguez, H. (2023). Microwave-Assisted Hydrothermal Processing of *Rugulopteryx okamurae*. *Marine Drugs*, 21(6), 319. <https://doi.org/10.3390/md21060319>
- Fifani, G., Baudena, A., Fakhri, M., Baaklini, G., Faugère, Y., Morrow, R., Mortier, L., & d'Ovidio, F. (2021). Drifting Speed of Lagrangian Fronts and Oil Spill Dispersal at the Ocean Surface. *Remote Sensing*, 13(22), Article 22. <https://doi.org/10.3390/rs13224499>
- Figuerola, F. L., Vega, J., Valderrama, M., Korbee, N., Mercado, J., Bañares España, E., & Flores-Moya, A. (2020). Invasión de la especie exótica

- Rugulopteryx okamurae* en Andalucía I: Estudios preliminares de la actividad fotosintética. *Algas*, 56, 35–46.
- Fiksen, Ø., Jørgensen, C., Kristiansen, T., Vikebø, F., & Huse, G. (2007). Linking behavioural ecology and oceanography: Larval behaviour determines growth, mortality and dispersal. *Marine Ecology Progress Series*, 347, 195–205. <https://doi.org/10.3354/meps06978>
- Flexas, M. M., Gomis, D., Ruiz, S., Pascual, A., & León, P. (2006). In situ and satellite observations of the eastward migration of the Western Alboran Sea Gyre. *Progress in Oceanography*, 70(2–4), 486–509. <https://doi.org/10.1016/j.pocean.2006.03.017>
- Florido, M., Megina, C., & García, J. (2023). Coexistiendo con una invasora en el estrecho de Gibraltar: La integración de *Rugulopteryx okamurae* en la fauna y flora residente. *Almoraima. Revista de Estudios Campogibraltareños*, 58.
- Fogarty, M., & Botsford, L. (2007). Population Connectivity and Spatial Management of Marine Fisheries. *Oceanography*, 20(3), 112–123. <https://doi.org/10.5670/oceanog.2007.34>
- Fortič, A., Alshikh Rasheed, R., Almagid, Z., Badreddine, A., Báez, J., Belmonte-Gallegos, Á., Bettoso, N., Borme, D., Camisa, F., Caracciolo, D., Çinar, M., Crocetta, F., Ćetković, I., Doğan, A., Galiya, M., huertos, alvaro, Grech, D., Guallart, J., Gündeğer, G., & Virgili, R. (2023). New records of introduced species in the Mediterranean Sea (April 2023). *Mediterranean Marine Science*, 24, 182–202. <https://doi.org/10.12681/mms.34016>
- Fox-Kemper, B., & Menemenlis, D. (2008). Can Large Eddy Simulation Techniques Improve Mesoscale Rich Ocean Models? In *Ocean Modeling in an Eddying Regime* (pp. 319–337). American Geophysical Union (AGU). <https://doi.org/10.1029/177GM19>
- Fredj, E., Carlson, D. F., Amitai, Y., Gozolchiani, A., & Gildor, H. (2016). The particle tracking and analysis toolbox (PaTATO) for Matlab. *Limnology and Oceanography: Methods*, 14(9), 586–599. <https://doi.org/10.1002/lom3.10114>
- Fuchs, H. L., Gerbi, G. P., Hunter, E. J., Christman, A. J., & Diez, F. J. (2015). Hydrodynamic sensing and behavior by oyster larvae in turbulence and waves. *Journal of Experimental Biology*, 218(9), 1419–1432. <https://doi.org/10.1242/jeb.118562>
- Fuchs, H. L., Specht, J. A., Adams, D. K., & Christman, A. J. (2017). Turbulence induces metabolically costly behaviors and inhibits food capture in

- oyster larvae, causing net energy loss. *Journal of Experimental Biology*, 220(19), 3419–3431. <https://doi.org/10.1242/jeb.161125>
- Fuller, E., Samhoury, J., Stoll, J., Levin, S., & Watson, J. (2017). Characterizing fisheries connectivity in marine social– ecological systems. *ICES Journal of Marine Science*, 74. <https://doi.org/10.1093/icesjms/fsx128>
- Fumagalli, M. (2013). Assessing the effect of sequencing depth and sample size in population genetics inferences. *PloS One*, 8(11), e79667. <https://doi.org/10.1371/journal.pone.0079667>
- Gaide, S., Bender, M., & Wintersteller, P. (2018). Gridded EM122 multibeam-echosounder bathymetry of cruise MSM36—Gulf of Cadiz [Dataset]. In *MARUM - Center for Marine Environmental Sciences, University Bremen*. PANGAEA. <https://doi.org/10.1594/PANGAEA.893200>
- Gaines, S., Gaylord, B., Gerber, L., Hastings, A., & Kinlan, B. (2007). Connecting Places: The Ecological Consequences of Dispersal in the Sea. *Oceanography*, 20(3), 90–99. <https://doi.org/10.5670/oceanog.2007.32>
- Gaines, S., White, C., Carr, M., & Palumbi, S. (2010). Designing Marine Reserve Networks for Both Conservation and Fisheries Management. *Proceedings of the National Academy of Sciences of the United States of America*, 107, 18286–18293. <https://doi.org/10.1073/pnas.0906473107>
- Galland, J.-C., Goutal, N., & Hervouet, J.-M. (1991). TELEMAC: A new numerical model for solving shallow water equations. *Advances in Water Resources*, 14(3), 138–148. [https://doi.org/10.1016/0309-1708\(91\)90006-A](https://doi.org/10.1016/0309-1708(91)90006-A)
- Gamoyo, M., Obura, D., & Reason, C. J. C. (2019). Estimating Connectivity Through Larval Dispersal in the Western Indian Ocean. *Journal of Geophysical Research: Biogeosciences*, 124(8), 2446–2459. <https://doi.org/10.1029/2019JG005128>
- García Lafuente, J., Alvarez Fanjul, E., Vargas, J., & Ratsimandresy, A. (2002). Subinertial variability in the flow through the Strait of Gibraltar. *Journal of Geophysical Research*, 107. <https://doi.org/10.1029/2001JC001104>
- García Lafuente, J., Bruque Pozas, E., Sánchez Garrido, J. C., Sannino, G., & Sammartino, S. (2013). The interface mixing layer and the tidal dynamics at the eastern part of the Strait of Gibraltar. *Journal of Marine Systems*, 117, 31–42. <https://doi.org/10.1016/j.jmarsys.2013.02.014>
- García Lafuente, J., Cano, N., Vargas, M., Rubín, J. P., & Hernández-Guerra, A. (1998). Evolution of the Alboran Sea hydrographic structures

- during July 1993. *Deep Sea Research Part I: Oceanographic Research Papers*, 45(1), 39–65. [https://doi.org/10.1016/S0967-0637\(97\)00216-1](https://doi.org/10.1016/S0967-0637(97)00216-1)
- García Lafuente, J., & Delgado, J. (2004). The Meandering Path of a Drifter around the Western Alboran Gyre. *Journal of Physical Oceanography*, 34(3), 685–692. <https://doi.org/10.1175/3516.1>
- García Lafuente, J., Delgado, J., & Criado, F. (2002). Inflow interruption by meteorological forcing in the Strait of Gibraltar. *Geophysical Research Letters*, 29(19), 20-1-20–24. <https://doi.org/10.1029/2002GL015446>
- García Lafuente, J., Sammartino, S., Sánchez Garrido, J. C., & Naranjo, C. (2019). On the role of the Bay of Algeciras in the exchange across the Strait of Gibraltar. *Regional Studies in Marine Science*, 29, 100620. <https://doi.org/10.1016/j.rsma.2019.100620>
- García-Gómez, J. C., Florido, M., Olaya-Ponzzone, L., Rey Díaz de Rada, J., Donázar-Aramendía, I., Chacón, M., Quintero, J. J., Magariño, S., & Megina, C. (2021). Monitoring Extreme Impacts of *Rugulopteryx okamurae* (Dictyotales, Ochrophyta) in El Estrecho Natural Park (Biosphere Reserve). Showing Radical Changes in the Underwater Seascape. *Frontiers in Ecology and Evolution*, 9. <https://doi.org/10.3389/fevo.2021.639161>
- García-Gómez, J. C., Sempere-Valverde, J., González, A. R., Martínez-Chacón, M., Olaya-Ponzzone, L., Sánchez-Moyano, E., Ostalé-Valriberas, E., & Megina, C. (2020). From exotic to invasive in record time: The extreme impact of *Rugulopteryx okamurae* (Dictyotales, Ochrophyta) in the Strait of Gibraltar. *Science of The Total Environment*, 704, 135408. <https://doi.org/10.1016/j.scitotenv.2019.135408>
- García-Gómez, J. C., Sempere-Valverde, J., Ostalé-Valriberas, E., Martínez, M., González, A. R., Espinosa, F., Sánchez-Moyano, E., Megina, C., & Parada, A. (2018). RUGULOPTERYX OKAMURAE (E.Y. DAWSON) I.K. HWANG, W. J. LEE & H.S. KIM (DICTYOTALES, OCHROPHYTA), ALGA EXÓTICA “EXPLOSIVA” EN EL ESTRECHO DE GIBRALTAR. OBSERVACIONES PRELIMINARES DE SU DISTRIBUCIÓN E IMPACTO. *Almoraima. Revista de Estudios Campogibraltareños*.
- García-Lafuente, J., Delgado, J., Sánchez Román, A., Soto, J., Carracedo, L., & Díaz del Río, G. (2009). Interannual variability of the Mediterranean outflow observed in Espartel sill, western Strait of Gibraltar. *Journal of Geophysical Research: Oceans*, 114(C10). <https://doi.org/10.1029/2009JC005496>

- García-Lafuente, J., Nadal, I., Sammartino, S., Korbee, N., & Figueroa, F. L. (2023). Could secondary flows have made possible the cross-strait transport and explosive invasion of *Rugulopteryx okamuræ* algae in the Strait of Gibraltar? *PLOS ONE*, *18*(5), e0285470. <https://doi.org/10.1371/journal.pone.0285470>
- García-Lafuente, J., Naranjo, C., Sammartino, S., Sánchez-Garrido, J. C., & Delgado, J. (2017). The Mediterranean outflow in the Strait of Gibraltar and its connection with upstream conditions in the Alborán Sea. *Ocean Science*, *13*(2), 195–207. <https://doi.org/10.5194/os-13-195-2017>
- García-Lafuente, J., Sammartino, S., Huertas, I. E., Flecha, S., Sánchez-Leal, R. F., Naranjo, C., Nadal, I., & Bellanco, M. J. (2021). Hotter and Weaker Mediterranean Outflow as a Response to Basin-Wide Alterations. *Frontiers in Marine Science*, *8*. <https://doi.org/10.3389/fmars.2021.613444>
- García-Lafuente, J., Sammartino, S., Sánchez-Garrido, J. C., & Naranjo, C. (2018). Asymmetric Baroclinic Response to Tidal Forcing Along the Main Sill of the Strait of Gibraltar Inferred from Mooring Observations. In M. G. Velarde, R. Yu. Tarakanov, & A. V. Marchenko (Eds.), *The Ocean in Motion: Circulation, Waves, Polar Oceanography* (pp. 193–210). Springer International Publishing. [https://doi.org/10.1007/978-3-319-71934-4\\_14](https://doi.org/10.1007/978-3-319-71934-4_14)
- García-Lafuente, J., Sánchez Román, A., Díaz del Río, G., Sannino, G., & Sánchez Garrido, J. C. (2007). Recent observations of seasonal variability of the Mediterranean outflow in the Strait of Gibraltar. *Journal of Geophysical Research: Oceans*, *112*(C10). <https://doi.org/10.1029/2006JC003992>
- García-Lafuente, J., Sanchez-Garrido, J. C., Garcia, A., Hidalgo, M., Sammartino, S., & Laiz, R. (2021). Biophysical Processes Determining the Connectivity of the Alboran Sea Fish Populations. In J. C. Báez, J.-T. Vázquez, J. A. Camiñas, & M. Malouli Idrissi (Eds.), *Alboran Sea – Ecosystems and Marine Resources* (pp. 459–487). Springer International Publishing. [https://doi.org/10.1007/978-3-030-65516-7\\_12](https://doi.org/10.1007/978-3-030-65516-7_12)
- García-Lafuente, J., Vargas, J. M., Plaza, F., Sarhan, T., Candela, J., & Bascheck, B. (2000). Tide at the eastern section of the Strait of Gibraltar. *Journal of Geophysical Research: Oceans*, *105*(C6), 14197–14213. <https://doi.org/10.1029/2000JC900007>

- Garrett, C. (2004). Frictional processes in straits. *Deep Sea Research Part II: Topical Studies in Oceanography*, 51(4), 393–410. <https://doi.org/10.1016/j.dsr2.2003.10.005>
- Garrett, C., Maccready, P., & Rhines, P. (1993). Boundary Mixing and Arrested Ekman Layers: Rotating Stratified Flow Near a Sloping Boundary. *Annu. Rev. Fluid Mech.*, 25, 291–323. <https://doi.org/10.1146/annurev.fl.25.010193.001451>
- Gerber, L. R., Mancha-Cisneros, M. D. M., O'Connor, M. I., & Selig, E. R. (2014). Climate change impacts on connectivity in the ocean: Implications for conservation. *Ecosphere*, 5(3), art33. <https://doi.org/10.1890/ES13-00336.1>
- GFCM. (2009). *Resolution GFCM/33/2009/2 on the establishment of geographical subareas in the GFCM area of application, amending Resolution GFCM/31/2007/2.*
- GFCM. (2021a). *Recommendation GFCM/44/2021/2 on the establishment of a fisheries restricted area in the Jabuka/Pomo Pit in the Adriatic Sea (geographical subarea 17), amending Recommendation GFCM/41/2017/3.*
- GFCM. (2021b). *Report of the Working Group on Stock Assessment of Demersal species (WGSAD). General Fisheries Commission for the Mediterranean. Online, 18–30 January 2021.*
- Ghezzi, M., De Pascalis, F., Umgiesser, G., Zemlys, P., Sigovini, M., Marcos, C., & Pérez-Ruzafa, A. (2015). Connectivity in Three European Coastal Lagoons. *Estuaries and Coasts*, 38(5), 1764–1781. <https://doi.org/10.1007/s12237-014-9908-0>
- Ghezzi, M., Pellizzato, M., De Pascalis, F., Silvestri, S., & Umgiesser, G. (2018). Natural resources and climate change: A study of the potential impact on Manila clam in the Venice lagoon. *Science of the Total Environment*, 645, 419–430. <https://doi.org/10.1016/j.scitotenv.2018.07.060>
- Ghezzi, M., Sarretta, A., Sigovini, M., Guerzoni, S., Tagliapietra, D., & Umgiesser, G. (2011). Modeling the inter-annual variability of salinity in the lagoon of Venice in relation to the water framework directive typologies. *Ocean & Coastal Management*, 54(9), 706–719. <https://doi.org/10.1016/j.ocecoaman.2011.06.007>
- Gil Herrera, J. (2006). *Biología y pesca del voraz [Pagellus bogaraveo (Brünnich, 1768)] en el Estrecho de Gibraltar [PhD thesis].* Universidad de Cádiz. Cadiz, Spain.
- Gil Herrera, J. (2010). *SPANISH INFORMATION ABOUT THE RED SEABREAM (PAGELLUS BOGARAVEO) FISHERY IN THE STRAIT*

- OF GIBRALTAR REGION CopeMed II Occasional Paper N° 2 (GCP/INT/028/SPA-GCP/INT/006/EC). [www.faocopemed.org](http://www.faocopemed.org)
- Gil, J., Silva, L., & Sobrino, I. (2001). Results of two tagging survey of red seabream *Pagellus bogaraveo*, (Brunnich, 1768) in the Spanish south Mediterranean region. *Thalassas: An International Journal of Marine Sciences*, 17(2), 43–46.
- Gil-Herrera, J., Gutiérrez-Estrada, J. C., Benchoucha, S., Pérez-Gil, J. L., Sanz-Fernández, V., el Arraf, S., Burgos, C., Malouli Idrissi, M., & Farias, C. (2021). The Blackspot Seabream Fishery in the Strait of Gibraltar: Lessons and Future Perspectives of Shared Marine Resource. In J. C. Báez, J.-T. Vázquez, J. A. Camiñas, & M. Malouli Idrissi (Eds.), *Alboran Sea—Ecosystems and Marine Resources* (pp. 629–657). Springer International Publishing. [https://doi.org/10.1007/978-3-030-65516-7\\_19](https://doi.org/10.1007/978-3-030-65516-7_19)
- Gill, A. E. (1982). *Atmosphere-Ocean Dynamics*. Academic Press.
- Goethel, D. R., & Berger, A. M. (2017). Accounting for spatial complexities in the calculation of biological reference points: Effects of misdiagnosing population structure for stock status indicators. *Canadian Journal of Fisheries and Aquatic Sciences*, 74(11), 1878–1894. <https://doi.org/10.1139/cjfas-2016-0290>
- Goodwin, J. D., Munroe, D. M., Defne, Z., Ganju, N. K., & Vasslides, J. (2019). Estimating Connectivity of Hard Clam (*Mercenaria mercenaria*) and Eastern Oyster (*Crassostrea virginica*) Larvae in Barnegat Bay. *Journal of Marine Science and Engineering*, 7(6), Article 6. <https://doi.org/10.3390/jmse7060167>
- Gordillo, F. J. L., Carmona, R., & Jiménez, C. (2022). A Warmer Arctic Compromises Winter Survival of Habitat-Forming Seaweeds. *Frontiers in Marine Science*, 8. <https://doi.org/10.3389/fmars.2021.750209>
- Graham, J., Watson, J., García-García, L., Bradley, K., Bradley, R., Brown, M., Ciotti, B., Goodwin, D., Nash, R., Roche, W., Wogerbauer, C., & Hyder, K. (2023). Pelagic connectivity of European sea bass between spawning and nursery grounds. *Frontiers in Marine Science*. <https://doi.org/10.3389/fmars.2022.1046585>
- Grati, F., Aladžuz, A., Azzurro, E., Bolognini, L., Carbonara, P., Çobani, M., Domenichetti, F., Dragičević, B., Dulčić, J., Durović, M., Ikica, Z., Joksimović, A., Kolutari, J., Marčeta, B., Matić-Skoko, S., Vrdoljak, D., Lembo, G., Santojanni, A., Spedicato, M. T., ... Milone, N. (2018). Seasonal dynamics of small-scale fisheries in the Adriatic Sea.

- Mediterranean Marine Science*, 19(1), 21–35.  
<https://doi.org/10.12681/mms.2153>
- Greenberg, D., Dupont, F., Lyard, F., Lynch, D., & Werner, F. (2007). Resolution issues in numerical models of oceanic and coastal circulation. *Continental Shelf Research*, 27, 1317–1343.  
<https://doi.org/10.1016/j.csr.2007.01.023>
- Griffies, S. M., & Adcroft, A. J. (2008). Formulating the equations of ocean models. In M. W. Hecht & H. Hasumi (Eds.), *Geophysical Monograph Series* (Vol. 177, pp. 281–317). American Geophysical Union.  
<https://doi.org/10.1029/177GM18>
- Guidetti, P., & Claudet, J. (2010). Comanagement practices enhance fisheries in marine protected areas. *Conservation Biology: The Journal of the Society for Conservation Biology*, 24(1), 312–318.  
<https://doi.org/10.1111/j.1523-1739.2009.01358.x>
- Hansen, F., Pastor-Rollan, A., Christensen, A., & Stuer-Lauridsen, F. (2024). Using biophysical modelling and marine connectivity to assess the risk of natural dispersal of non-indigenous species to comply with the Ballast Water Management Convention. *Biological Invasions*, 1–22.  
<https://doi.org/10.1007/s10530-024-03327-0>
- Hariri, S., Meier, H. E. M., & Väli, G. (2024). Investigating the influence of sub-mesoscale current structures on Baltic Sea connectivity through a Lagrangian analysis. *Frontiers in Marine Science*, 11.  
<https://doi.org/10.3389/fmars.2024.1340291>
- Hauser, L., & Ward, R. (1998). Population identification in pelagic fish: The limits of molecular markers. In *Advances in Molecular Ecology* (pp. 191–224).
- Hedgecock, D., Barber, P., & Edmands, S. (2007). Genetic Approaches to Measuring Connectivity. *Oceanography (Washington D.C.)*, 20, 70–79.  
<https://doi.org/10.5670/oceanog.2007.30>
- Hersbach, H., Bell, B., Berrisford, P., Biavati, G., Horányi, A., Muñoz Sabater, J., Nicolas, J., Peubey, C., Radu, R., Rozum, I., Schepers, D., Simmons, A., Soci, C., Dee, D., Thépaut, J-N. (2023). ERA5 hourly data on single levels from 1940 to present. Copernicus Climate Change Service (C3S) Climate Data Store (CDS) [Dataset].  
<https://doi.org/10.24381/cds.adbb2d47>
- Hidalgo, M., Kaplan, D. M., Kerr, L. A., Watson, J. R., Paris, C. B., & Browman, H. I. (2017). Advancing the link between ocean connectivity, ecological function and management challenges. *Ices Journal Of*



- Marine Science*, 74(6), 1702–1707.  
<https://doi.org/10.1093/icesjms/fsx112>
- Hidalgo, M., Ligas, A., Bellido, J. M., Bitetto, I., Carbonara, P., Carlucci, R., Guijarro, B., Jadaud, A., Lembo, G., Manfredi, C., Esteban, A., Garofalo, G., Ikica, Z., García, C., de Sola, L. G., Kavadas, S., Maina, I., Sion, L., Vittori, S., & Vrgoc, N. (2019). Size-dependent survival of european hake juveniles in the Mediterranean sea. *Scientia Marina*, 83(S1), 207–221. <https://doi.org/10.3989/scimar.04857.16A>
- Hidalgo, M., Rossi, V., Monroy, P., Ser-Giacomi, E., Hernández-García, E., Guijarro, B., Massutí, E., Alemany, F., Jadaud, A., Perez, J. L., & Reglero, P. (2019). Accounting for ocean connectivity and hydroclimate in fish recruitment fluctuations within transboundary metapopulations. *Ecological Applications*, 29(5). <https://doi.org/10.1002/eap.1913>
- Hsu, P.-C., Ho, C.-Y., Lee, H.-J., Lu, C.-Y., & Ho, C.-R. (2020). Temporal Variation and Spatial Structure of The Kuroshio-Induced Submesoscale Island Vortices Observed from GCOM-C and Himawari-8 Data. *Remote Sensing*, 12, 883. <https://doi.org/10.3390/rs12050883>
- Huang, Z. G. (1994). *Marine Species and Their Distributions in China's Seas*. China Ocean Press.
- Hwang, I.-K., Lee, W., Kim, H.-S., & Clerck, O. (2009). Taxonomic Reappraisal of *Dilophus okamuræ* (Dictyotales, Phaeophyta) from The Western Pacific Ocean. *Phycologia*, 48, 1–12. <https://doi.org/10.2216/07-68.1>
- Hyun, B., Shin, K., Jang, M.-C., Jang, P.-G., Lee, W.-J., Park, C., & Choi, K.-H. (2015). Potential invasions of phytoplankton in ship ballast water at South Korean ports. *Marine and Freshwater Research*, 67. <https://doi.org/10.1071/MF15170>
- Iacono, R., Napolitano, E., Palma, M., & Sannino, G. (2021). The Tyrrhenian Sea Circulation: A Review of Recent Work. *Sustainability*, 13(11), Article 11. <https://doi.org/10.3390/su13116371>
- Ibáñez-Tejero, L., Ladah, L. B., Sánchez-Velasco, L., Barton, E. D., & Jiménez-Rosenberg, S. P. A. (2019). Vertical distribution and abundance of copepod nauplii and ichthyoplankton in northern Baja California during strong internal tidal forcing. *Journal of Plankton Research*, 41(2), 177–187. <https://doi.org/10.1093/plankt/fbz007>
- Jalón-Rojas, I., Wang, X. H., & Fredj, E. (2019). A 3D numerical model to Track Marine Plastic Debris (TrackMPD): Sensitivity of microplastic trajectories and fates to particle dynamical properties and physical

- processes. *Marine Pollution Bulletin*, 141, 256–272. <https://doi.org/10.1016/j.marpolbul.2019.02.052>
- Jardas, I., Šantić, M., & Pallaoro, A. (2004). Diet composition and feeding intensity of horse mackerel, *Trachurus trachurus* (Osteichthyes: Carangidae) in the eastern Adriatic. *Marine Biology*, 144(6), 1051–1056. <https://doi.org/10.1007/s00227-003-1281-7>
- Jensen, M., Nisancioglu, K., & Spall, M. (2018). Large Changes in Sea Ice Triggered by Small Changes in Atlantic Water Temperature. *Journal of Climate*, 31. <https://doi.org/10.1175/JCLI-D-17-0802.1>
- Johnson, G. C., & Ohlsen, D. R. (1994). Frictionally Modified Rotating Hydraulic Channel Exchange and Ocean Outflows. *Journal of Physical Oceanography*, 24(1), 66–78. [https://doi.org/10.1175/1520-0485\(1994\)024<0066:FMRHCE>2.0.CO;2](https://doi.org/10.1175/1520-0485(1994)024<0066:FMRHCE>2.0.CO;2)
- Jones, B. (2014). Nemo: A parallelized Lagrangian particle-tracking model. *Computer Science, Environmental Science*.
- Jones, G. P., Almany, G. R., Russ, G. R., Sale, P. F., Steneck, R. S., Van Oppen, M. J. H., & Willis, B. L. (2009). Larval retention and connectivity among populations of corals and reef fishes: History, advances and challenges. *Coral Reefs*, 28(2), 307–325. <https://doi.org/10.1007/s00338-009-0469-9>
- Jönsson, B. F., & Watson, J. R. (2016). The timescales of global surface-ocean connectivity. *Nature Communications*, 7, 11239. <https://doi.org/10.1038/ncomms11239>
- Jungclauss, J. H., Fischer, N., Haak, H., Lohmann, K., Marotzke, J., Matei, D., Mikolajewicz, U., Notz, D., & von Storch, J. S. (2013). Characteristics of the ocean simulations in the Max Planck Institute Ocean Model (MPIOM) the ocean component of the MPI-Earth system model. *Journal of Advances in Modeling Earth Systems*, 5(2), 422–446. <https://doi.org/10.1002/jame.20023>
- Juza, M., Renault, L., Ruiz, S., & Tintoré, J. (2013). Origin and pathways of Winter Intermediate Water in the Northwestern Mediterranean Sea using observations and numerical simulation. *Journal of Geophysical Research: Oceans*, 118(12), 6621–6633. <https://doi.org/10.1002/2013JC009231>
- Kadoya, T. (2009). Assessing functional connectivity using empirical data. *Population Ecology*, 51(1), 5–15. <https://doi.org/10.1007/s10144-008-0120-6>
- Kasapidis, P., & Magoulas, A. (2008). Development and application of microsatellite markers to address the population structure of the

- horse mackerel *Trachurus trachurus*. *Fisheries Research*, 89(2), 132–135. <https://doi.org/10.1016/j.fishres.2007.09.015>
- Katsanevakis, S., Poursanidis, D., Hoffmann, R., Rizgalla, J., Rothman, S. B.-S., Levitt-Barmats, Y., & Espinosa Torre, F. (2020). *Unpublished Mediterranean records of marine alien and cryptogenic species*. <https://doi.org/10.3391/bir.2020.9.2.01>
- Kendrick, G. A., Orth, R. J., Statton, J., Hovey, R., Ruiz Montoya, L., Lowe, R. J., Krauss, S. L., & Sinclair, E. A. (2017). Demographic and genetic connectivity: The role and consequences of reproduction, dispersal and recruitment in seagrasses. *Biological Reviews*, 92(2), 921–938. <https://doi.org/10.1111/brv.12261>
- Khoufi, W., Ferreri, R., Jaziri, H., El Fehri, S., Gargano, A., Mangano, S., Ben Meriem, S., Romdhane, M. S., Bonanno, A., Aronica, S., Genovese, S., Mazzola, S., & Basilone, G. (2014). Reproductive traits and seasonal variability of *Merluccius merluccius* from the Tunisian coast. *Journal of the Marine Biological Association of the United Kingdom*, 94, 1545–1556. <https://doi.org/10.1017/S0025315414000356>
- Kinder, T. H., & Bryden, H. L. (1990). Aspiration of Deep Waters through Straits. In L. J. Pratt (Ed.), *The Physical Oceanography of Sea Straits* (pp. 295–319). Springer Netherlands. [https://doi.org/10.1007/978-94-009-0677-8\\_14](https://doi.org/10.1007/978-94-009-0677-8_14)
- Kowalik, Z., & Murty, T. S. (1993). *Numerical Modeling Of Ocean Dynamics*. World Scientific.
- Krueck, N. C., Treml, E. A., Innes, D. J., & Ovenden, J. R. (2020). Ocean currents and the population genetic signature of fish migrations. *Ecology*, 101(3), e02967. <https://doi.org/10.1002/ecy.2967>
- Krug, H. M. (1994). *Biologia e avaliação do stock Açoreano de goraz, Pagellus bogaraveo*. [PhD thesis]. Universidade dos Açores. Azores, Portugal.
- Kundu, P. K., Cohen, I. M., & Dowling, D. R. (Eds.). (2012). Chapter 4—Conservation Laws. In *Fluid Mechanics (Fifth Edition)* (pp. 95–169). Academic Press. <https://doi.org/10.1016/B978-0-12-382100-3.10004-6>
- Kuzmić, M., Janeković, I., Book, J. W., Martin, P. J., & Doyle, J. D. (2006). Modeling the northern Adriatic double-gyre response to intense bora wind: A revisit. *Journal of Geophysical Research: Oceans*, 111(C3). <https://doi.org/10.1029/2005JC003377>
- Kwon, K., Choi, B.-J., Kim, K. Y., Kim, K., Kwon, K., Choi, B.-J., Kim, K. Y., & Kim, K. (2019). Tracing the trajectory of pelagic *Sargassum* using satellite monitoring and Lagrangian transport simulations in the East

- China Sea and Yellow Sea. *Algae*, 34(4), 315–326.  
<https://doi.org/10.4490/algae.2019.34.12.11>
- LaCasce, J. H. (2008). Statistics from Lagrangian observations. *Progress in Oceanography*, 77(1), 1–29. <https://doi.org/10.1016/j.pocean.2008.02.002>
- Lacour, T., Morin, P.-I., Sciandra, T., Donaher, N., Campbell, D. A., Ferland, J., & Babin, M. (2019). Decoupling light harvesting, electron transport and carbon fixation during prolonged darkness supports rapid recovery upon re-illumination in the Arctic diatom *Chaetoceros neogracilis*. *Polar Biology*, 42(10), 1787–1799.  
<https://doi.org/10.1007/s00300-019-02507-2>
- Lalire, M., & Gaspar, P. (2019). Modeling the active dispersal of juvenile leatherback turtles in the North Atlantic Ocean. *Movement Ecology*, 7(1), 7. <https://doi.org/10.1186/s40462-019-0149-5>
- Lange, M., & Van Sebille, E. (2017). *Parcels v0.9: Prototyping a Lagrangian Ocean Analysis framework for the petascale age*. *Oceanography*.  
<https://doi.org/10.5194/gmd-2017-167>
- Lanoix, F. (1974). *Projet Alboran, Etude hydrologique et dynamique de la Mer d'Alboran, Tech. Lep.* (66; p. 39).
- Largier, J. (2003). Considerations in estimating larval dispersal distances from oceanographic data. *Ecological Applications - ECOL APPL*, 13, 71–89.  
[https://doi.org/10.1890/1051-0761\(2003\)013\[0071:CIELDD\]2.0.CO;2](https://doi.org/10.1890/1051-0761(2003)013[0071:CIELDD]2.0.CO;2)
- Lausche, B., Farrier, D., Verschuuren, J., Viña, A., Trouwborst, A., Born, C.-H., & Aug, L. (2013). *The Legal Aspects of Connectivity Conservation: A Concept Paper* (Vol. 1). IUCN.
- Le Corre, N., Guichard, F., & Johnson, L. (2012). *Connectivity as a Management Tool for Coastal Ecosystems in Changing Oceans*.  
<https://doi.org/10.5772/27704>
- Lebreton, L., Egger, M., & Slat, B. (2019). A global mass budget for positively buoyant macroplastic debris in the ocean. *Scientific Reports*, 9(1), 12922. <https://doi.org/10.1038/s41598-019-49413-5>
- Lee, S., Kim, J. K., Zheng, X., Ho, Q., Gibson, G. A., & Xing, E. P. (2014). On Model Parallelization and Scheduling Strategies for Distributed Machine Learning. *Advances in Neural Information Processing Systems*, 27.
- Legrand, T., Chenuil, A., Ser-Giacomi, E., Arnaud-Haond, S., Bierne, N., & Rossi, V. (2022). Spatial coalescent connectivity through multi-generation dispersal modelling predicts gene flow across marine phyla. *Nature Communications*, 13(1), Article 1.  
<https://doi.org/10.1038/s41467-022-33499-z>

- Legrand, T., Di Franco, A., Ser-Giacomi, E., Caló, A., & Rossi, V. (2019). A multidisciplinary analytical framework to delineate spawning areas and quantify larval dispersal in coastal fish. *Marine Environmental Research*, 151, 104761. <https://doi.org/10.1016/j.marenvres.2019.104761>
- Leon, L. F., Antenucci, J. P., Rao, Y. R., & McCrimmon, C. (2012). Summary performance of the Estuary and Lake Computer Model (ELCOM): Application in the Laurentian and other Great Lakes. *Water Quality Research Journal*, 47(3–4), 252–267. <https://doi.org/10.2166/wqrjc.2012.022>
- Lester, S. E., Ruttenberg, B. I., Gaines, S. D., & Kinlan, B. P. (2007). The relationship between dispersal ability and geographic range size. *Ecology Letters*, 10(8), 745–758. <https://doi.org/10.1111/j.1461-0248.2007.01070.x>
- Lett, C., Ayata, S.-D., Huret, M., & Irisson, J.-O. (2010). Biophysical modelling to investigate the effects of climate change on marine population dispersal and connectivity. *Progress in Oceanography*, 87(1), 106–113. <https://doi.org/10.1016/j.pocean.2010.09.005>
- Lett, C., Verley, P., Mullon, C., Parada, C., Brochier, T., Penven, P., & Blanke, B. (2008). A Lagrangian tool for modelling ichthyoplankton dynamics. *Environmental Modelling & Software*, 23(9), 1210–1214. <https://doi.org/10.1016/j.envsoft.2008.02.005>
- Leukart, P., & Lüning, K. (1994). Minimum spectral light requirements and maximum light levels for long-term germling growth of several red algae from different water depths and a green alga. *European Journal of Phycology*, 29, 103–112. <https://doi.org/10.1080/09670269400650551>
- Levin, L. (2006). Recent progress in understanding larval dispersal: New directions and digressions. *Integrative and Comparative Biology*, 46, 282–297. <https://doi.org/10.1093/icb/icj024>
- Li, H., Scheschonk, L., Heinrich, S., Valentin, K., Harms, L., Glöckner, G., Corre, E., & Bischof, K. (2020). Transcriptomic Responses to Darkness and the Survival Strategy of the Kelp *Saccharina latissima* in the Early Polar Night. *Frontiers in Marine Science*, 7. <https://doi.org/10.3389/fmars.2020.592033>
- Ličer, M., Estival, S., Reyes-Suarez, C., Deponte, D., & Fettich, A. (2020). Lagrangian modelling of a person lost at sea during the Adriatic scirocco storm of 29 October 2018. *Natural Hazards and Earth System Sciences*, 20(8), 2335–2349. <https://doi.org/10.5194/nhess-20-2335-2020>
- Lipcius, R. N., Eggleston, D. B., Fodrie, F. J., van der Meer, J., Rose, K. A., Vasconcelos, R. P., & van de Wolfshaar, K. E. (2019). Modeling

- Quantitative Value of Habitats for Marine and Estuarine Populations. *Frontiers in Marine Science*, 6. <https://doi.org/10.3389/fmars.2019.00280>
- Lipizer, M., Partescano, E., Rabitti, A., Giorgetti, A., & Crise, A. (2014). Qualified temperature, salinity and dissolved oxygen climatologies in a changing Adriatic Sea. *Ocean Science*, 10(5), 771–797. <https://doi.org/10.5194/os-10-771-2014>
- Liulea, S., Serrão, E. A., & Santos, R. (2023). *Spread and Impact of the Invasive Brown Algae Rugulopteryx okamurae On The Algarve Coast, Southern Portugal (Ne Atlantic)* (SSRN Scholarly Paper 4446622). <https://doi.org/10.2139/ssrn.4446622>
- López-Márquez, V., Templado, J., Buckley, D., Marino, I., Boscari, E., Micu, D., Zane, L., & Machordom, A. (2019). Connectivity Among Populations of the Top Shell *Gibbula divaricata* in the Adriatic Sea. *Frontiers in Genetics*, 10, 177. <https://doi.org/10.3389/fgene.2019.00177>
- López-Parages, J., Rodríguez-Fonseca, B., & Terray, L. (2015). A mechanism for the multidecadal modulation of ENSO teleconnection with Europe. *Climate Dynamics*, 45(3), 867–880. <https://doi.org/10.1007/s00382-014-2319-x>
- Lorance, P. (2011). History and dynamics of the overexploitation of the blackspot sea bream (*Pagellus bogaraveo*) in the Bay of Biscay. *ICES Journal of Marine Science*, 68(2), 290–301. <https://doi.org/10.1093/icesjms/fsq072>
- Loseille, A. (2017). Chapter 10—Unstructured Mesh Generation and Adaptation. In R. Abgrall & C.-W. Shu (Eds.), *Handbook of Numerical Analysis* (Vol. 18, pp. 263–302). Elsevier. <https://doi.org/10.1016/bs.hna.2016.10.004>
- Maicu, F., De Pascalis, F., Ferrarin, C., & Umgiesser, G. (2018). Hydrodynamics of the Po River-Delta-Sea System. *Journal of Geophysical Research: Oceans*, 123(9), 6349–6372. <https://doi.org/10.1029/2017JC013601>
- Malanotte-Rizzoli, P., Robinson, A. R., Roether, W., Manca, B., Bergamasco, A., Brenner, S., Civitarese, G., Georgopoulos, D., Haley, P. J., Kioroglou, S., Kontoyannis, H., Kress, N., Latif, M. A., Leslie, W. G., Ozsoy, E., d'Alcala, M. R., Salihoglu, I., Sansone, E., & Theocharis, A. (1996). Experiment in eastern Mediterranean probes origin of deep water masses. *Eos, Transactions American Geophysical Union*, 77(32), 305–311. <https://doi.org/10.1029/96EO00212>
- Mannino, A. M., Borfecchia, F., & Micheli, C. (2021). Tracking Marine Alien Macroalgae in the Mediterranean Sea: The Contribution of Citizen

- Science and Remote Sensing. *Journal of Marine Science and Engineering*, 9(3), Article 3. <https://doi.org/10.3390/jmse9030288>
- Marandel, F., Lorance, P., Andrello, M., Charrier, G., Le Cam, S., Lehuta, S., & Trenkel, V. M. (2018). Insights from genetic and demographic connectivity for the management of rays and skates. *Canadian Journal of Fisheries and Aquatic Sciences*, 75(8), 1291–1302. <https://doi.org/10.1139/cjfas-2017-0291>
- Marcos, C., Díaz, D., Fietz, K., Forcada, A., Ford, A., García-Charton, J. A., Goñi, R., Lenfant, P., Mallol, S., Mouillot, D., Pérez-Marcos, M., Puebla, O., Manel, S., & Pérez-Ruzafa, A. (2021). Reviewing the Ecosystem Services, Societal Goods, and Benefits of Marine Protected Areas. *Frontiers in Marine Science*, 8. <https://doi.org/10.3389/fmars.2021.613819>
- Margalef López, R. (1997). Turbulence and marine life. *Scientia Marina*, 61(Extra 1), 109–123.
- Mariani, P., Mackenzie, B., Iudicone, D., & Bozec, A. (2010). Modelling retention and dispersion mechanisms of bluefin tuna eggs and larvae in the northwest Mediterranean Sea. *Progress in Oceanography*, 86, 45–58. <https://doi.org/10.1016/j.pocean.2010.04.027>
- Mariani, S., Casaioli, M., Coraci, E., & Malguzzi, P. (2015). A new high-resolution BOLAM-MOLOCH suite for the SIMM forecasting system: Assessment over two HyMeX intense observation periods. *Natural Hazards and Earth System Science*, 15, 1–24. <https://doi.org/10.5194/nhess-15-1-2015>
- Mariano, A. J., Kourafalou, V. H., Srinivasan, A., Kang, H., Halliwell, G. R., Ryan, E. H., & Roffer, M. (2011). On the modeling of the 2010 Gulf of Mexico Oil Spill. *Dynamics of Atmospheres and Oceans*, 52(1), 322–340. <https://doi.org/10.1016/j.dynatmoce.2011.06.001>
- Marshall, J., Adcroft, A., Hill, C., Perelman, L., & Heisey, C. (1997). A finite-volume, incompressible Navier Stokes model for studies of the ocean on parallel computers. *Journal of Geophysical Research: Oceans*, 102(C3), 5753–5766. <https://doi.org/10.1029/96JC02775>
- Marshall, J., Hill, C., Perelman, L., & Adcroft, A. (1997). Hydrostatic, quasi-hydrostatic, and nonhydrostatic ocean modeling. *Journal of Geophysical Research: Oceans*, 102(C3), 5733–5752. <https://doi.org/10.1029/96JC02776>
- Martin, P. J., Book, J. W., Burrage, D. M., Rowley, C. D., & Tudor, M. (2009). Comparison of model-simulated and observed currents in the central

- Adriatic during DART. *Journal of Geophysical Research: Oceans*, 114(C2).  
<https://doi.org/10.1029/2008JC004842>
- Martínez, A., Abascal, A. J., García, A., Aragón, G., & Medina, R. (2024). Lagrangian modelling of oil concentrations at sea: A sensitivity analysis to the grid resolution and number of Lagrangian elements. *Marine Pollution Bulletin*, 198, 115787.  
<https://doi.org/10.1016/j.marpolbul.2023.115787>
- Mason, E., Ruiz, S., Bourdalle-Badie, R., Reffray, G., Garcia-Sotillo, M., & Pascual, A. (2019). Copernicus (CMEMS) operational model intercomparison in the western Mediterranean Sea: Insights from an eddy tracker. *Ocean Science Discussions*, 1–32.  
<https://doi.org/10.5194/os-2018-169>
- Mateo-Ramírez, Á., Iñiguez, C., Fernández-Salas, L. M., Sánchez-Leal, R. F., Farias, C., Bellanco, M. J., Gil, J., & Rueda, J. L. (2023). Healthy thalli of the invasive seaweed *Rugulopteryx okamurae* (Phaeophyceae) being massively dragged into deep-sea bottoms by the Mediterranean Outflow Water. *Phycologia*, 62(2), 99–108.  
<https://doi.org/10.1080/00318884.2023.2177057>
- Mayorga-Adame, C., Polton, J., Fox, A., & Henry, L. (2022). Spatiotemporal scales of larval dispersal and connectivity among oil and gas structures in the North Sea. *Marine Ecology Progress Series*, 685, 49–67.  
<https://doi.org/10.3354/meps13970>
- McKiver, W. J., Sannino, G., Braga, F., & Bellafigliore, D. (2016). Investigation of model capability in capturing vertical hydrodynamic coastal processes: A case study in the north Adriatic Sea. *Ocean Science*, 12(1), 51–69. <https://doi.org/10.5194/os-12-51-2016>
- McWilliams, J. C. (2006). *Fundamentals of Geophysical Fluid Dynamics*. Cambridge University Press.
- Medvedev, I. P., Vilibić, I., & Rabinovich, A. B. (2020). Tidal Resonance in the Adriatic Sea: Observational Evidence. *Journal of Geophysical Research: Oceans*, 125(8), e2020JC016168. <https://doi.org/10.1029/2020JC016168>
- Meer, M., Berumen, M., Hobbs, J.-P., & Herwerden, L. (2015). Population connectivity and the effectiveness of marine protected areas to protect vulnerable, exploited and endemic coral reef fishes at an endemic hotspot. *The Raffles Bulletin of Zoology*, 34. <https://doi.org/10.1007/s00338-014-1242-2>
- Megrey, B. (2001). Effect of turbulence on feeding of larval fishes: A sensitivity analysis using an individual-based model. *ICES Journal of*



- Marine Science*, 58(5), 1015–1029.  
<https://doi.org/10.1006/jmsc.2001.1104>
- Mercado, J. M., Gómez-Jakobsen, F., Korbee, N., Aviles, A., Bonomi-Barufi, J., Muñoz, M., Reul, A., & Figueroa, F. L. (2022). Analyzing environmental factors that favor the growth of the invasive brown macroalga *Rugulopteryx okamuræ* (Ochrophyta): The probable role of the nutrient excess. *Marine Pollution Bulletin*, 174, 113315. <https://doi.org/10.1016/j.marpolbul.2021.113315>
- Metaxas, A., & Saunders, M. (2009). Quantifying the “bio-” components in biophysical models of larval transport in marine benthic invertebrates: Advances and pitfalls. *The Biological Bulletin*, 216(3), 257–272. <https://doi.org/10.1086/BBLv216n3p257>
- Micheli, F., Halpern, B., Walbridge, S., Ciriaco, S., Ferretti, F., Frascchetti, S., Lewison, R., Nykjaer, L., & Rosenberg, A. (2013). Cumulative Human Impacts on Mediterranean and Black Sea Marine Ecosystems: Assessing Current Pressures and Opportunities. *PloS One*, 8, e79889. <https://doi.org/10.1371/journal.pone.0079889>
- Miller, J. A., & Shanks, A. (2004). Evidence for limited larval dispersal in black rockfish (*Sebastes melanops*): Implications for population structure and marine-reserve design. *Canadian Journal of Fisheries and Aquatic Sciences*, 61, 1723–1735. <https://doi.org/10.1139/f04-111>
- Millot, C. (2013). Levantine Intermediate Water characteristics: An astounding general misunderstanding! *Scientia Marina*, 77(2), Article 2. <https://doi.org/10.3989/scimar.03518.13A>
- Mims, M. C., & Olden, J. D. (2012). Life history theory predicts fish assemblage response to hydrologic regimes. *Ecology*, 93(1), 35–45. <https://doi.org/10.1890/11-0370.1>
- Mogé, M., Russcher, M. J., Emerson, A., & Genseberger, M. (2019). *Scalable Delft3D Flexible Mesh for Efficient Modelling of Shallow Water and Transport Processes*.
- Molinaroli, E., Peschiutta, M., & Rizzetto, F. (2023). Long-Term Evolution of an Urban Barrier Island: The Case of Venice Lido (Northern Adriatic Sea, Italy). *Water (Switzerland)*, 15(10). <https://doi.org/10.3390/w15101927>
- Monismith, S. G., & Fong, D. A. (2004). A note on the potential transport of scalars and organisms by surface waves. *Limnology and Oceanography*, 49(4), 1214–1217. <https://doi.org/10.4319/lo.2004.49.4.1214>
- Monroy, P., Rossi, V., Ser-Giacomi, E., López, C., & Hernández-García, E. (2017). Sensitivity and robustness of larval connectivity diagnostics

- obtained from Lagrangian Flow Networks. *ICES Journal of Marine Science*, 74(6), 1763–1779. <https://doi.org/10.1093/icesjms/fsw235>
- Morales-Nin, B., & Moranta, J. (2004). Recruitment and post-settlement growth of juvenile *Merluccius merluccius* on the western Mediterranean shelf. *Scientia Marina*, 68(3), Article 3. <https://doi.org/10.3989/scimar.2004.68n3399>
- Morat, F., Letourneur, Y., Dierking, J., Pécheyran, C., Bareille, G., Blamart, D., & Harmelin-Vivien, M. (2014). The Great Melting Pot. Common Sole Population Connectivity Assessed by Otolith and Water Fingerprints. *PLoS ONE*, 9(1), e86585. <https://doi.org/10.1371/journal.pone.0086585>
- Morello, E. B., & Arneri, E. (2009). Anchovy and Sardine in the Adriatic Sea — An Ecological Review. In *Oceanography and Marine Biology*. CRC Press.
- Motos, L. (1996). Reproductive biology and fecundity of the Bay of Biscay Anchovy population (*Engraulis encrasicolus* L.). *Scientia Marina*, 60.
- Muller, H., Blanke, B., Dumas, F., Lekien, F., & Mariette, V. (2009). Estimating the Lagrangian residual circulation in the Iroise Sea. *Journal of Marine Systems*, 78, S17–S36. <https://doi.org/10.1016/j.jmarsys.2009.01.008>
- Muñoz, A.R., Martín-Taboada, A., De la Rosa, J., Carmona, R., Zanolla, M., & Altamirano, M. (2019). La modelación de la distribución de especies como herramienta en la gestión de invasiones biológicas en el medio marino: El caso de *Rugulopteryx okamurae* (Dictyotaceae, Ochrophyta) en el Mediterráneo. In *Número Especial Boletín de la Sociedad Española de Ficología Diciembre 2019: Gestión de Especies Invasoras Marinas: Construyendo una Propuesta para Andalucía*.
- Muñoz, M., Reul, A., Plaza, F., Gómez-Moreno, M.-L., Vargas-Yañez, M., Rodríguez, V., & Rodríguez, J. (2015). Implication of regionalization and connectivity analysis for marine spatial planning and coastal management in the Gulf of Cadiz and Alboran Sea. *Ocean & Coastal Management*, 118, 60–74. <https://doi.org/10.1016/j.ocecoaman.2015.04.011>
- Muntoni, M. (2015). *A multidisciplinary approach for puzzling over fish connectivity in the Mediterranean Sea: The role of early life history stages of red mullet (Mullus barbatus)* [PhD thesis]. Università degli Studi di Cagliari. Cagliari, Italy.
- Murua, H., & Motos, L. (2006). Reproductive strategy and spawning activity of the European hake *Merluccius merluccius* (L.) in the Bay of Biscay. *Journal of Fish Biology*, 69(5), 1288–1303. <https://doi.org/10.1111/j.1095-8649.2006.01169.x>

- Nadal, I., Sammartino, S., García-Lafuente, J., Sánchez Garrido, J. C., Gil-Herrera, J., Hidalgo, M., & Hernández, P. (2022). Hydrodynamic connectivity and dispersal patterns of a transboundary species (*Pagellus bogaraveo*) in the Strait of Gibraltar and adjacent basins. *Fisheries Oceanography*, 31(4), 384–401. <https://doi.org/10.1111/fog.12583>
- Najafi, S., Dragovich, D., Heckmann, T., & Sadeghi, S. H. (2021). Sediment connectivity concepts and approaches. *CATENA*, 196, 104880. <https://doi.org/10.1016/j.catena.2020.104880>
- Naranjo, C., Sammartino, S., García-Lafuente, J., Bellanco, M. J., & Taupier-Letage, I. (2015). Mediterranean waters along and across the Strait of Gibraltar, characterization and zonal modification. *Deep Sea Research Part I: Oceanographic Research Papers*, 105, 41–52. <https://doi.org/10.1016/j.dsr.2015.08.003>
- Nathan, R., & Muller-Landau, H. C. (2000). *Spatial Patterns of Seed Dispersal, Their Determinants and Consequences for Recruitment*. <http://repository.si.edu/xmlui/handle/10088/18540>
- Navarro, G., Gutiérrez, F. J., Díez-Minguito, M., Losada, M. A., & Ruiz, J. (2011). Temporal and spatial variability in the Guadalquivir estuary: A challenge for real-time telemetry. *Ocean Dynamics*, 61(6), 753–765. <https://doi.org/10.1007/s10236-011-0379-6>
- Navarro-Barranco, C., Muñoz-Gómez, B., Saiz, D., Ros, M., Guerra-García, J. M., Altamirano, M., Ostalé-Valriberas, E., & Moreira, J. (2019). Can invasive habitat-forming species play the same role as native ones? The case of the exotic marine macroalga *Rugulopteryx okamurae* in the Strait of Gibraltar. *Biological Invasions*, 21(11), 3319–3334. <https://doi.org/10.1007/s10530-019-02049-y>
- Nicolle, A., Dumas, F., Foveau, A., Foucher, E., & Thiébaud, E. (2013). Modelling larval dispersal of the king scallop (*Pecten maximus*) in the English Channel: Examples from the bay of Saint-Brieuc and the bay of Seine. *Ocean Dynamics*, 63(6), 661–678. <https://doi.org/10.1007/s10236-013-0617-1>
- Nicolle, A., Moitié, R., Ogor, J., Dumas, F., Foveau, A., Foucher, E., & Thiébaud, E. (2017). Modelling larval dispersal of *Pecten maximus* in the English Channel: A tool for the spatial management of the stocks. *ICES Journal of Marine Science*, 74(6), 1812–1825. <https://doi.org/10.1093/icesjms/fsw207>
- Nilsson, H., & Page, M. (2005). OpenFOAM simulation of the flow in the Hölleforsen draft tube model. *Turbine-99 III*, 8, 6.

- Nolasco, R., Gomes, I., Peteiro, L., Albuquerque, R., Luna, T., Dubert, J., Swearer, S. E., & Queiroga, H. (2018). Independent estimates of marine population connectivity are more concordant when accounting for uncertainties in larval origins. *Scientific Reports*, 8(1), 2641. <https://doi.org/10.1038/s41598-018-19833-w>
- Novi, L., Bracco, A., & Falasca, F. (2021). Uncovering marine connectivity through sea surface temperature. *Scientific Reports*, 11(1), 8839. <https://doi.org/10.1038/s41598-021-87711-z>
- Ocampo-Torres, F. J. (2001). On the homogeneity of the wave field in coastal areas as determined from ERS-2 and RADARSAT synthetic aperture radar images of the ocean surface. *Scientia Marina*, 65(S1), Article S1. <https://doi.org/10.3989/scimar.2001.65s1215>
- Ocaña Vicente, O., Afonso-Carrillo, J., & Ballesteros, E. (2016). *Massive proliferation of a dictyotalean species (Phaeophyceae, Ochrophyta) through the Strait of Gibraltar (Research note)*. *Rev Acad Canaria Cienc.* 28, 165–170.
- O'Connor, M. I., Bruno, J. F., Gaines, S. D., Halpern, B. S., Lester, S. E., Kinlan, B. P., & Weiss, J. M. (2007). Temperature control of larval dispersal and the implications for marine ecology, evolution, and conservation. *Proceedings of the National Academy of Sciences*, 104(4), 1266–1271. <https://doi.org/10.1073/pnas.0603422104>
- Oguz, T., Macias, D., Garcia-Lafuente, J., Pascual, A., & Tintore, J. (2014). Fueling Plankton Production by a Meandering Frontal Jet: A Case Study for the Alboran Sea (Western Mediterranean). *PLOS ONE*, 9(11), e111482. <https://doi.org/10.1371/journal.pone.0111482>
- Oke, P. R., Proctor, R., Rosebrock, U., Brinkman, R., Cahill, M. L., Coghlan, I., Divakaran, P., Freeman, J., Pattiaratchi, C., Roughan, M., Sandery, P. A., Schaeffer, A., & Wijeratne, S. (2016). The Marine Virtual Laboratory (version 2.1): Enabling efficient ocean model configuration. *Geoscientific Model Development*, 9(9), 3297–3307. <https://doi.org/10.5194/gmd-9-3297-2016>
- Olivier, R. (1928). Poissons de chalut. La dorade (*Pagellus centrodontus*) (Resume pratique de nos connaissances sur ce poisson). *Rev. Trav. De l'Off. Peches Marit.*, Tome I, fasc. IV. *Revue Des Travaux de l'Institut Des Pêches Maritimes*, 1(4), 5–32.
- OpenStreetMap contributors. (2015). *Map data copyrighted OpenStreetMap contributors and available from <https://www.openstreetmap.org>* [Map].
- Orlić, M., Gačić, M., & Laviolette, P. (1992). The currents and circulation of the Adriatic Sea. *Oceanologica Acta*.

- <https://www.semanticscholar.org/paper/The-currents-and-circulation-of-the-Adriatic-Sea-Orli%C4%87-Ga%C4%8Di%C4%87/0d5b7c22b203a499911d877c6c4dc03ca6058ba9>
- Orlić, M., Kuzmić, M., & Pasarić, Z. (1994). Response of the Adriatic Sea to the bora and sirocco forcing. *Continental Shelf Research*, 14(1), 91–116. [https://doi.org/10.1016/0278-4343\(94\)90007-8](https://doi.org/10.1016/0278-4343(94)90007-8)
- Ormerod, S., I., D., Hatton-Ellis, T., Cable, J., Chadwick, E., S., G., Jones, T., Larsen, S., F.L., M., W.O.C., S., Thomas, R., & I.P., V. (2011). Landscape Connectivity of Freshwater Ecosystems: Strategic Review and Recommendations. *Report to the Countryside Council for Wales*.
- Palacios-Abrantes, J., Reygondeau, G., Wabnitz, C. C. C., & Cheung, W. W. L. (2020). The transboundary nature of the world's exploited marine species. *Scientific Reports*, 10(1), 17668. <https://doi.org/10.1038/s41598-020-74644-2>
- Palumbi, S. R. (2003). Population Genetics, Demographic Connectivity, and the Design of Marine Reserves. *Ecological Applications*, 13(sp1), 146–158. [https://doi.org/10.1890/1051-0761\(2003\)013\[0146:PGDCAT\]2.0.CO;2](https://doi.org/10.1890/1051-0761(2003)013[0146:PGDCAT]2.0.CO;2)
- Paoletti, S., Bekaert, K., Barbut, L., Lacroix, G., Volckaert, F. A. M., & Hostens, K. (2021). Validating a biophysical dispersal model with the early life-history traits of common sole (*Solea solea* L.). *PloS One*, 16(9), e0257709. <https://doi.org/10.1371/journal.pone.0257709>
- Parrilla, G., & Kinder, T. (1987). *The Physical Oceanography of the Alboran Sea* (Vol. 40). Oceanography Group, Division of Applied Sciences.
- Pasarić, Z., Belu, D., & Klai, Z. B. (2007). Orographic influences on the Adriatic sirocco wind. *Annales Geophysicae*, 25(6), 1263–1267. <https://doi.org/10.5194/angeo-25-1263-2007>
- Pasarić, Z., Belušić, D., & Chiggiato, J. (2009). Orographic effects on meteorological fields over the Adriatic from different models. *Journal of Marine Systems*, 78, S90–S100. <https://doi.org/10.1016/j.jmarsys.2009.01.019>
- Pascual, M., & Macpherson, E. (2016). *Population genetic connectivity among marine species; a matter of dispersal, selection and drift* (CIESM Monograph 48, 172 pages, Publisher: CIESM Publisher, Monaco, Editors: F. Briand, pp. 59–64).
- Pastor, A., Catalán, I. A., Terrados, J., Moure, B., & Ospina-Alvarez, A. (2023). Connectivity-based approach to guide conservation and restoration of seagrass *Posidonia oceanica* in the NW Mediterranean. *Biological Conservation*, 285, 110248. <https://doi.org/10.1016/j.biocon.2023.110248>

- Patti, B., Torri, M., & Cuttitta, A. (2020). General surface circulation controls the interannual fluctuations of anchovy stock biomass in the Central Mediterranean Sea. *Scientific Reports*, 10(1), 1554. <https://doi.org/10.1038/s41598-020-58028-0>
- Pawlowicz, R., Pawlowicz, R., Beardsley, R. C., Beardsley, R., Lentz, S., & Lentz, S. (2002). Classical tidal harmonic analysis including error estimates in MATLAB using T\_TIDE. *Computers & Geosciences*, 28(8), 929–937.
- Peleteiro-Alonso, J. B., Olmedo-Herrero, M., Gómez-Ceruelo, M. C., & Álvarez-Blázquez, B. (1997). *Study of reproduction in captivity of blackspot sea bream (Pagellus bogaraveo B.). Embryonic development and consumption of viteline sac.* ICES 85th Statutory Meeting, Baltimore, USA. <http://hdl.handle.net/10261/315570>
- Peliz, Á., Teles-Machado, A., Marchesiello, P., Dubert, J., & García Lafuente, J. (2009). Filament generation off the Strait of Gibraltar in response to Gap winds. *Dynamics of Atmospheres and Oceans*, 46(1), 36–45. <https://doi.org/10.1016/j.dynatmoce.2008.08.002>
- Pineda, J. (1991). Predictable upwelling and the shoreward transport of planktonic larvae by internal tidal bores. *Science (New York, N.Y.)*, 253(5019). <https://doi.org/10.1126/science.253.5019.548>
- Pineda, J., Hare, J., & Sponaugle, S. (2007). Larval Transport and Dispersal in the Coastal Ocean and Consequences for Population Connectivity. *Oceanography*, 20(3), 22–39. <https://doi.org/10.5670/oceanog.2007.27>
- Pineda, J., & López, M. (2002). Effects of El Niño on Nearshore Stratification and Larval Settlement. *Investigaciones Marinas*, 30(1), 126–127. <https://doi.org/10.4067/S0717-71782002030100036>
- Pineda, J., Reynolds, N., & Lentz, S. J. (2018). Reduced barnacle larval abundance and settlement in response to large-scale oceanic disturbances: Temporal patterns, nearshore thermal stratification, and potential mechanisms. *Limnology and Oceanography*, 63(6), 2618–2629. <https://doi.org/10.1002/lno.10964>
- Pinho, M., Diogo, H., Carvalho, J., & Pereira, J. G. (2014). Harvesting juveniles of blackspot sea bream (*Pagellus bogaraveo*) in the Azores (Northeast Atlantic): Biological implications, management, and life cycle considerations. *ICES Journal of Marine Science*, 71(9), 2448–2456. <https://doi.org/10.1093/icesjms/fsu089>
- Pinsky, M. L., Reygondeau, G., Caddell, R., Palacios-Abrantes, J., Spijkers, J., & Cheung, W. W. L. (2018). Preparing ocean governance for species

- on the move. *Science (New York, N.Y.)*, 360(6394), 1189–1191.  
<https://doi.org/10.1126/science.aat2360>
- Planes, S., Jones, G. P., & Thorrold, S. R. (2009). Larval dispersal connects fish populations in a network of marine protected areas. *Proceedings of the National Academy of Sciences*, 106(14), 5693–5697.  
<https://doi.org/10.1073/pnas.0808007106>
- Podda, C., & Porporato, E. M. D. (2023). Marine spatial planning for connectivity and conservation through ecological corridors between marine protected areas and other effective area-based conservation measures. *Frontiers in Marine Science*, 10.  
<https://doi.org/10.3389/fmars.2023.1271397>
- Popels, L., & Hutchins, D. (2002). Factors affecting dark survival of the brown tide alga *Aureococcus anophagefferens* (Pelagophyceae). *Journal of Phycology*, 38, 738–744. <https://doi.org/10.1046/j.1529-8817.2002.01115.x>
- Popova, E., Vousden, D., Sauer, W. H. H., Mohammed, E. Y., Allain, V., Downey-Breedt, N., Fletcher, R., Gjerde, K. M., Halpin, P. N., Kelly, S., Obura, D., Pecl, G., Roberts, M., Raitsos, D. E., Rogers, A., Samoily, M., Sumaila, U. R., Tracey, S., & Yool, A. (2019). Ecological connectivity between the areas beyond national jurisdiction and coastal waters: Safeguarding interests of coastal communities in developing countries. *Marine Policy*, 104, 90–102.  
<https://doi.org/10.1016/j.marpol.2019.02.050>
- Poulain, P.-M. (2001). Adriatic Sea surface circulation as derived from drifter data between 1990 and 1999. *Journal of Marine Systems*, 29, 3–32.  
[https://doi.org/10.1016/S0924-7963\(01\)00007-0](https://doi.org/10.1016/S0924-7963(01)00007-0)
- Pratt, L. L. J., & Whitehead, J. A. (2007). *Rotating Hydraulics: Nonlinear Topographic Effects in the Ocean and Atmosphere*. Springer Science & Business Media.
- Punt, A. E. (2019). Spatial stock assessment methods: A viewpoint on current issues and assumptions. *Fisheries Research*, 213, 132–143.  
<https://doi.org/10.1016/j.fishres.2019.01.014>
- Rahman, R. O. A. (2019). Introductory Chapter: Development of Assessment Models to Support Pollution Preventive and Control Decisions. In *Kinetic Modeling for Environmental Systems*. IntechOpen.  
<https://doi.org/10.5772/intechopen.83822>
- Reed, D., Kinlan, B., Raimondi, P., Washburn, L., Gaylord, B., & Drake, P. (2006). A Metapopulation Perspective on the Patch Dynamics of Giant

- Kelp in Southern California. *Marine Metapopulations*, 353–386. <https://doi.org/10.1016/B978-012088781-1/50013-3>
- Renault, L., Oguz, T., Pascual, A., Vizoso, G., & Tintore, J. (2012). Surface circulation in the Alborán Sea (western Mediterranean) inferred from remotely sensed data. *Journal of Geophysical Research: Oceans*, 117(C8). <https://doi.org/10.1029/2011JC007659>
- Revelante, N., & Gilmartin, M. (1992). The lateral advection of particulate organic matter from the Po delta region during summer stratification, and its implications for the northern Adriatic. *Estuarine, Coastal and Shelf Science*, 35(2), 191–212. [https://doi.org/10.1016/S0272-7714\(05\)80113-1](https://doi.org/10.1016/S0272-7714(05)80113-1)
- Riha, S. (2017). *Grid generation for numerical ocean models*.
- Rodríguez-Díaz, L., & Gómez-Gesteira, M. (2017). Can lagrangian models reproduce the migration time of European eel obtained from otolith analysis? *Journal of Sea Research*, 130, 17–23. <https://doi.org/10.1016/j.seares.2017.06.010>
- Rodríguez, J. M., Barton, E. D., Eve, L., & Hernández-León, S. (2001). Mesozooplankton and ichthyoplankton distribution around Gran Canaria, an oceanic island in the NE Atlantic. *Deep Sea Research Part I: Oceanographic Research Papers*, 48(10), 2161–2183. [https://doi.org/10.1016/S0967-0637\(01\)00013-9](https://doi.org/10.1016/S0967-0637(01)00013-9)
- Roelvink, J., & Banning, G. V. (1995). Design and development of DELFT3D and application to coastal morphodynamics. *Oceanographic Literature Review*.
- Rosas-Guerrero, J., Carmona-Fernández, R., & Altamirano-Jeschke, M. (2021). *Efecto de la temperatura y la irradiancia sobre el crecimiento, la propagación vegetativa y la actividad fotosintética del alga invasora Rugulopteryx okamurae (Dictyotales, Ochrophyta)*. III JIs del Mar, Granada, Spain. <https://riuma.uma.es/xmlui/handle/10630/22870>
- Rosas-Guerrero, J., Meco, Y. E., & Altamirano, M. (2018). Could *Rugulopteryx okamurae* (Dictyotales, Ochrophyta) have been introduced by ballast waters. *Algas*, 54(52).
- Rossi, V., Ser-Giacomi, E., López, C., & Hernández-García, E. (2014). Hydrodynamic provinces and oceanic connectivity from a transport network help designing marine reserves. *Geophysical Research Letters*, 41(8), 2883–2891. <https://doi.org/10.1002/2014GL059540>
- Rueda, J. L., Mena-Torres, A., Gallardo-Núñez, M., González-García, E., Martín-Arjona, A., Valenzuela, J., García-Ruiz, C., González-Aguilar, M., Mateo-Ramírez, Á., García, M., Sayago-Gil, M., & Vázquez, J. T.



- (2023). Spatial Distribution and Potential Impact of Drifted Thalli of the Invasive Alga *Rugulopteryx okamurae* in Circalittoral and Bathyal Habitats of the Northern Strait of Gibraltar and the Alboran Sea. *Diversity*, 15(12), Article 12. <https://doi.org/10.3390/d15121206>
- Rühs, S. (2018). *Lagrangian connectivity of the upper limb of the overturning circulation studied with high-resolution ocean models* [PhD thesis]. Universität Kiel. Kiel, Germany.
- Ruitton, S., Blanfuné, A., Boudouresque, C.-F., Guillemain, D., Michotey, V., Roblet, S., Thibault, D., Thibaut, T., & Verlaque, M. (2021). Rapid Spread of the Invasive Brown Alga *Rugulopteryx okamurae* in a National Park in Provence (France, Mediterranean Sea). *Water*, 13(16), 2306. <https://doi.org/10.3390/w13162306>
- Russo, A., & Artegiani, A. (1996). *Adriatic Sea hydrography* (Vol. 60, Issue 2, pp. 33–43). Scientia Marina.
- Ruti, P. M., Somot, S., Giorgi, F., Dubois, C., Flaounas, E., Obermann, A., Dell'Aquila, A., Pisacane, G., Harzallah, A., Lombardi, E., Ahrens, B., Akhtar, N., Alias, A., Arsouze, T., Aznar, R., Bastin, S., Bartholy, J., Béranger, K., Beuvier, J., ... Vervatis, V. (2016). Med-CORDEX Initiative for Mediterranean Climate Studies. *Bulletin of the American Meteorological Society*, 97(7), 1187–1208. <https://doi.org/10.1175/BAMS-D-14-00176.1>
- Ružić, I., Dugonjić Jovančević, S., Benac, Č., & Krvavica, N. (2019). Assessment of the Coastal Vulnerability Index in an Area of Complex Geological Conditions on the Krk Island, Northeast Adriatic Sea. *Geosciences*, 9(5), Article 5. <https://doi.org/10.3390/geosciences9050219>
- Safin, A., Bouffard, D., Ozdemir, F., Ramón, C. L., Runnalls, J., Georgatos, F., Minaudo, C., & Šukys, J. (2021). *A Bayesian data assimilation framework for lake 3D hydrodynamic models with a physics-preserving particle filtering method using SPUX-MITgcm v1*. <https://doi.org/10.5194/gmd-2021-305>
- Sale, P. F., & Kritzer, J. P. (2003). Determining the extent and spatial scale of population connectivity: Decapods and coral reef fishes compared. *Fisheries Research*, 65(1), 153–172. <https://doi.org/10.1016/j.fishres.2003.09.013>
- Sammartino, S., García Lafuente, J., Naranjo, C., Sánchez Garrido, J. C., Sánchez Leal, R., & Sánchez Román, A. (2015). Ten years of marine current measurements in Espartel Sill, Strait of Gibraltar. *Journal of Geophysical Research: Oceans*, 120(9), 6309–6328. <https://doi.org/10.1002/2014JC010674>

- Sammartino, S., García Lafuente, J., Sánchez Garrido, J. C., De los Santos, F. J., Álvarez Fanjul, E., Naranjo, C., Bruno, M., & Calero, C. (2014). A numerical model analysis of the tidal flows in the Bay of Algeciras, Strait of Gibraltar. *Continental Shelf Research*, *72*, 34–46. <https://doi.org/10.1016/j.csr.2013.11.002>
- Sammartino, S., Sanchez, J., Naranjo, C., García Lafuente, J., Rodríguez-Rubio, P., & Sotillo, M. (2017). Water renewal in semi-enclosed basins: A high resolution Lagrangian approach with application to the Bay of Algeciras, Strait of Gibraltar: Water renewal in semi-enclosed basins. *Limnology and Oceanography: Methods*, *16*. <https://doi.org/10.1002/lom3.10231>
- Sammartino, S., Sánchez-Garrido, J. C., Delgado, J., Naranjo, C., Aldeanueva, F., & García Lafuente, J. (2014). Experimental and numerical characterization of harbor oscillations in the port of Málaga, Spain. *Ocean Engineering*, *88*, 110–119. <https://doi.org/10.1016/j.oceaneng.2014.06.011>
- Sánchez, F. (1983). *Biology and fishery of the red sea-bream (Pagellus bogaraveo B.) in VI, VII and VIII Subareas of ICES. ICES C.M. 1983/G:38.*
- Sánchez-Garrido, J. C., Fiechter, J., Rose, K., Werner, F., & Curchitser, E. (2020). Dynamics of anchovy and sardine populations in the Canary Current off NW Africa: Responses to environmental and climate forcing in a climate-to-fish ecosystem model. *Fisheries Oceanography*, *30*. <https://doi.org/10.1111/fog.12516>
- Sánchez-Garrido, J. C., García Lafuente, J., Álvarez Fanjul, E., Sotillo, M. G., & de los Santos, F. J. (2013). What does cause the collapse of the western alboran gyre? Results of an operational ocean model. *Progress in Oceanography*, *116*, 142–153. <https://doi.org/10.1016/j.pocean.2013.07.002>
- Sánchez-Garrido, J. C., García Lafuente, J., Sammartino, S., Naranjo, C., de los Santos, F. J., & Álvarez Fanjul, E. (2014). Meteorologically-driven circulation and flushing times of the Bay of Algeciras, Strait of Gibraltar. *Marine Pollution Bulletin*, *80*(1), 97–106. <https://doi.org/10.1016/j.marpolbul.2014.01.036>
- Sánchez-Garrido, J. C., & Nadal, I. (2022). The Alboran Sea circulation and its biological response: A review. *Frontiers in Marine Science*, *9*. <https://doi.org/10.3389/fmars.2022.933390>
- Sánchez-Garrido, J. C., Naranjo, C., Macías, D., García-Lafuente, J., & Oguz, T. (2015). Modeling the impact of tidal flows on the biological

- productivity of the Alboran Sea. *Journal of Geophysical Research: Oceans*, 120(11), 7329–7345. <https://doi.org/10.1002/2015JC010885>
- Sánchez-Garrido, J. C., Sannino, G., Liberti, L., García Lafuente, J., & Pratt, L. (2011). Numerical modeling of three-dimensional stratified tidal flow over Camarinal Sill, Strait of Gibraltar. *Journal of Geophysical Research: Oceans*, 116(C12). <https://doi.org/10.1029/2011JC007093>
- Sánchez-Garrido, J. C., & Vlasenko, V. (2009). Long-term evolution of strongly nonlinear internal solitary waves in a rotating channel. *Nonlinear Processes in Geophysics*, 16(5), 587–598. <https://doi.org/10.5194/npg-16-587-2009>
- Sanchez-Vidal, A., Calafat, A., Canals, M., & Fabres, J. (2004). Particle fluxes in the Almeria-Oran Front: Control by coastal upwelling and sea surface circulation. *Journal of Marine Systems*, 52(1), 89–106. <https://doi.org/10.1016/j.jmarsys.2004.01.010>
- Sannino, G., Carillo, A., Iacono, R., Ernesto, N., Palma, M., Pisacane, G., & Struglia, M. (2022). Modelling present and future climate in the Mediterranean Sea: A focus on sea-level change. *Climate Dynamics*, 59. <https://doi.org/10.1007/s00382-021-06132-w>
- Sannino, G., Herrmann, M., Carillo, A., Rupolo, V., Ruggiero, V., Artale, V., & Heimbach, P. (2009). An eddy-permitting model of the Mediterranean Sea with a two-way grid refinement at the Strait of Gibraltar. *Ocean Modelling*, 30(1), 56–72. <https://doi.org/10.1016/j.ocemod.2009.06.002>
- Santelices, B., Aedo, D., & Hoffmann, A. (2002). Banks of microscopic forms and survival to darkness of propagules and microscopic stages of macroalgae. *Revista Chilena de Historia Natural*, 75(3), 547–555. <https://doi.org/10.4067/S0716-078X2002000300006>
- Sarhan, T., García Lafuente, J., Vargas, M., Vargas, J. M., & Plaza, F. (2000). Upwelling mechanisms in the northwestern Alboran Sea. *Journal of Marine Systems*, 23, 317–331.
- Savina, M., Lacroix, G., & Ruddick, K. (2010). Modelling the transport of common sole larvae in the southern North Sea: Influence of hydrodynamics and larval vertical movements. *Journal of Marine Systems*, 81(1), 86–98. <https://doi.org/10.1016/j.jmarsys.2009.12.008>
- Schemmel, E., Bohaboy, E. C., Kinney, M. J., & O'Malley, J. M. (2022). An assessment of sampling approaches for estimating growth from fishery-dependent biological samples. *ICES Journal of Marine Science*, 79(5), 1497–1514. <https://doi.org/10.1093/icesjms/fsac075>
- Schilling, H. T., Kalogirou, S., Michail, C., & Kleitou, P. (2023). Testing passive dispersal as the key mechanism for lionfish invasion in the

- Mediterranean Sea using Lagrangian particle tracking. *Biological Invasions*. <https://doi.org/10.1007/s10530-023-03187-0>
- Schneider, D. (1991). The role of fluid dynamics in the ecology of marine birds. *Oceanography and Marine Biology Annual Review*, 29, 487-521.
- Schröder, A., & Schanz, D. (2023). 3D Lagrangian Particle Tracking in Fluid Mechanics. *Annual Review of Fluid Mechanics*, 55(1), 511-540. <https://doi.org/10.1146/annurev-fluid-031822-041721>
- Schunter, C., Carreras-Carbonell, J., Macpherson, E., Tintoré, J., Vidal-Vijande, E., Pascual, A., Guidetti, P., & Pascual, M. (2011). Matching genetics with oceanography: Directional gene flow in a Mediterranean fish species. *Molecular Ecology*, 20(24), 5167-5181. <https://doi.org/10.1111/j.1365-294X.2011.05355.x>
- Schunter, C., Pascual, M., Raventos, N., Garriga, J., Garza, J. C., Bartumeus, F., & Macpherson, E. (2019). A novel integrative approach elucidates fine-scale dispersal patchiness in marine populations. *Scientific Reports*, 9(1), 10796. <https://doi.org/10.1038/s41598-019-47200-w>
- Sciascia, R., Berta, M., Carlson, D. F., Griffa, A., Panfili, M., La Mesa, M., Corgnati, L., Mantovani, C., Domenella, E., Fredj, E., Magaldi, M. G., D'Adamo, R., Pazienza, G., Zambianchi, E., & Poulain, P.-M. (2018). Linking sardine recruitment in coastal areas to ocean currents using surface drifters and HF radar: A case study in the Gulf of Manfredonia, Adriatic Sea. *Ocean Science*, 14(6), 1461-1482. <https://doi.org/10.5194/os-14-1461-2018>
- Sempere-Valverde, J., Ostalé-Valriberas, E., Maestre, M., González Aranda, R., Bazairi, H., & Espinosa, F. (2021). Impacts of the non-indigenous seaweed *Rugulopteryx okamurae* on a Mediterranean coralligenous community (Strait of Gibraltar): The role of long-term monitoring. *Ecological Indicators*, 121, 107135. <https://doi.org/10.1016/j.ecolind.2020.107135>
- Sentchev, A., & Korotenko, K. (2003). *Effect of tides and frontal scale processes on larval transport in the eastern English Channel: Observations and numerical modelling*.
- Ser-Giacomi, E., Martinez-Garcia, R., Dutkiewicz, S., & Follows, M. J. (2023). A Lagrangian model for drifting ecosystems reveals heterogeneity-driven enhancement of marine plankton blooms. *Nature Communications*, 14(1), 6092. <https://doi.org/10.1038/s41467-023-41469-2>
- Shanks, A. (2009). Pelagic Larval Duration and Dispersal Distance Revisited. *The Biological Bulletin*, 216, 373-385. <https://doi.org/10.2307/25548167>

- Shchepetkin, A. F., & McWilliams, J. C. (2005). The regional oceanic modeling system (ROMS): A split-explicit, free-surface, topography-following-coordinate oceanic model. *Ocean Modelling*, 9(4), 347–404. <https://doi.org/10.1016/j.ocemod.2004.08.002>
- Siegel, D. A., Kinlan, B. P., Gaylord, B., & Gaines, S. D. (2003). Lagrangian descriptions of marine larval dispersion. *Marine Ecology Progress Series*, 260, 83–96. <https://doi.org/10.3354/meps260083>
- Siegel, D. A., Mitarai, S., Costello, C. J., Gaines, S. D., Kendall, B. E., Warner, R. R., & Winters, K. B. (2008). The stochastic nature of larval connectivity among nearshore marine populations. *Proceedings of the National Academy of Sciences*, 105(26), 8974–8979. <https://doi.org/10.1073/pnas.0802544105>
- Simons, R. D., Siegel, D. A., & Brown, K. S. (2013). Model sensitivity and robustness in the estimation of larval transport: A study of particle tracking parameters. *Journal of Marine Systems*, 119–120, 19–29. <https://doi.org/10.1016/j.jmarsys.2013.03.004>
- Simpson, S., Piercy, J., King, J., & Codling, E. (2013). Modelling larval dispersal and behaviour of coral reef fishes. *Ecological Complexity*, 16, 68–76. <https://doi.org/10.1016/j.ecocom.2013.08.001>
- Sirviente, S., Bolado-Penagos, M., Gomiz-Pascual, J. J., Romero-Cózar, J., Vázquez, A., & Bruno, M. (2023). Dynamics of Atmospheric-Driven Surface Currents on The Gulf of Cadiz Continental Shelf and its link with The Strait of Gibraltar and The Western Alboran Sea. *Progress in Oceanography*, 219, 103175. <https://doi.org/10.1016/j.pocean.2023.103175>
- Solís-Díaz, M., Navarro-Barranco, C., Mateu-Vicens, G., & Espinosa, F. (2022). Distribution patterns of epibiotic macrobenthic foraminifera associated to coralligenous habitats of the strait of Gibraltar. *Regional Studies in Marine Science*, 49, 102096. <https://doi.org/10.1016/j.rsma.2021.102096>
- Somarakis, S., Palomera, I., García, A., Quintanilla, L., Koutsikopoulos, C., Uriarte, A., & Motos, L. (2004). Daily Egg Production of anchovy in European waters. *Ices Journal of Marine Science - ICES J MAR SCI*, 61, 944–958. <https://doi.org/10.1016/j.icesjms.2004.07.018>
- Sotillo, M. G., Amo-Baladrón, A., Padorno, E., Garcia-Ladona, E., Orfila, A., Rodríguez-Rubio, P., Conti, D., Madrid, J. A. J., de los Santos, F. J., & Fanjul, E. A. (2016). How is the surface Atlantic water inflow through the Gibraltar Strait forecasted? A lagrangian validation of operational oceanographic services in the Alboran Sea and the Western

- Mediterranean. *Deep Sea Research Part II: Topical Studies in Oceanography*, 133, 100–117. <https://doi.org/10.1016/j.dsr2.2016.05.020>
- Sotillo, M. G., Cailleau, S., Lorente, P., Levier, B., Aznar, R., Reffray, G., Amo-Baladrón, A., Chanut, J., Benkiran, M., & Alvarez-Fanjul, E. (2015). The MyOcean IBI Ocean Forecast and Reanalysis Systems: Operational products and roadmap to the future Copernicus Service. *Journal of Operational Oceanography*, 8(1), 63–79. <https://doi.org/10.1080/1755876X.2015.1014663>
- Sotillo, M. G., Fanjul, E. A., Castanedo, S., Abascal, A. J., Menendez, J., Emelianov, M., Olivella, R., García-Ladona, E., Ruiz-Villarreal, M., Conde, J., Gómez, M., Conde, P., Gutierrez, A. D., & Medina, R. (2008). Towards an operational system for oil-spill forecast over Spanish waters: Initial developments and implementation test. *Marine Pollution Bulletin*, 56(4), 686–703. <https://doi.org/10.1016/j.marpolbul.2007.12.021>
- Soto Navarro, J. (2012). *Exchange through the Strait of Gibraltar in relation to the climatic forcing over the Mediterranean Sea* [PhD thesis]. Universidad de Málaga. Málaga, Spain.
- Soto-Navarro, J., Jordá, G., Deudero, S., Alomar, C., Amores, Á., & Compa, M. (2020). 3D hotspots of marine litter in the Mediterranean: A modeling study. *Marine Pollution Bulletin*, 155, 111159. <https://doi.org/10.1016/j.marpolbul.2020.111159>
- Spall, M., & Robinson, A. (1989). A new open ocean, hybrid coordinate primitive equation model. *Mathematics and Computers in Simulation*, 31, 241–269. [https://doi.org/10.1016/0378-4754\(89\)90162-6](https://doi.org/10.1016/0378-4754(89)90162-6)
- Specchiulli, A., Bignami, F., Marini, M., Fabbrocini, A., Scirocco, T., Campanelli, A., Penna, P., Santucci, A., & D'Adamo, R. (2016). The role of forcing agents on biogeochemical variability along the southwestern Adriatic coast: The Gulf of Manfredonia case study. *Estuarine, Coastal and Shelf Science*, 183, 136–149. <https://doi.org/10.1016/j.ecss.2016.10.033>
- Spiga, M. (2020). *A multidisciplinary approach to assess population structure of Pagellus bogaraveo for a correct delineation of stock units in the Alboran Sea*. [MSc Thesis]. Università di Bologna. Bologna, Italy.
- Stewart, R. H. (2009). *Introduction to Physical Oceanography*. University Press of Florida.
- Strong, J., & Dring, M. (2011). Macroalgal competition and invasive success: Testing competition in mixed canopies of *Sargassum muticum* and

- Saccharina latissima*. *Botanica Marina*, 54, 223–229.  
<https://doi.org/10.1515/bot.2011.034>
- Sun, R., Subramanian, A., Miller, A., Mazloff, M., Hoteit, I., & Cornuelle, B. (2019). SKRIPS v1.0: A regional coupled ocean–atmosphere modeling framework (MITgcm–WRF) using ESMF/NUOPC, description and preliminary results for the Red Sea. *Geoscientific Model Development*, 12, 4221–4244. <https://doi.org/10.5194/gmd-12-4221-2019>
- Sundby, S., & Kristiansen, T. (2015). The Principles of Buoyancy in Marine Fish Eggs and Their Vertical Distributions across the World Oceans. *PLOS ONE*, 10(10), e0138821.  
<https://doi.org/10.1371/journal.pone.0138821>
- Sundelöf, A., & Jonsson, P. R. (2012). Larval dispersal and vertical migration behaviour – a simulation study for short dispersal times. *Marine Ecology*, 33(2), 183–193. <https://doi.org/10.1111/j.1439-0485.2011.00485.x>
- Tamsitt, V., Abernathy, R. P., Mazloff, M. R., Wang, J., & Talley, L. D. (2018). Transformation of Deep Water Masses Along Lagrangian Upwelling Pathways in the Southern Ocean. *Journal of Geophysical Research: Oceans*, 123(3), 1994–2017. <https://doi.org/10.1002/2017JC013409>
- Taylor, G. I. (1922). Diffusion by Continuous Movements. *Proceedings of the London Mathematical Society*, s2-20(1), 196–212.  
<https://doi.org/10.1112/plms/s2-20.1.196>
- Taylor, P. D., Fahrig, L., Henein, K., & Merriam, G. (1993). Connectivity Is a Vital Element of Landscape Structure. *Oikos*, 68(3), 571–573.  
<https://doi.org/10.2307/3544927>
- Teles-Machado, A., Peliz, Á., Dubert, J., & Sánchez, R. F. (2007). On the onset of the Gulf of Cadiz Coastal Countercurrent. *GEOPHYSICAL RESEARCH LETTERS*, 34. <https://doi.org/10.1029/2007GL030091>
- Terradas-Fernández, M., Pena-Martín, C., Valverde-Urrea, M., Gran, A., Blanco-Murillo, F., Leyva, L., Abellán-Gallardo, E., Beresaluze, E., Izquierdo, A., del Pilar-Ruso, Y., Aguilar, J., & Fernández-Torquemada, Y. (2023). An outbreak of the invasive macroalgae *Rugulopteryx okamurae* in Alicante Bay and its colonization on dead *Posidonia oceanica* matte. *Aquatic Botany*, 189, 103706.  
<https://doi.org/10.1016/j.aquabot.2023.103706>
- Tintoré, J., La Violette, P., Bladé, I., & Cruzado, A. (1988). A Study of an Intense Density Front in the Eastern Alboran Sea: The Almeria-Oran Front. *Journal of Physical Oceanography*, 18, 17.  
[https://doi.org/10.1175/1520-0485\(1988\)018<1384:ASOAIID>2.0.CO;2](https://doi.org/10.1175/1520-0485(1988)018<1384:ASOAIID>2.0.CO;2)

- Tonani, M., Nadia, P., S, D., Pujol, I., & Fratianni, C. (2008). A high-resolution free-surface model of the Mediterranean Sea. *Ocean Science (OS)*, 4. <https://doi.org/10.5194/osd-4-213-2007>
- Torrado, H., Mourre, B., Raventos, N., Carreras, C., Tintoré, J., Pascual, M., & Macpherson, E. (2021). Impact of individual early life traits in larval dispersal: A multispecies approach using backtracking models. *Progress in Oceanography*, 192, 102518. <https://doi.org/10.1016/j.pocean.2021.102518>
- Trautman, N., & Walter, R. K. (2021). Seasonal variability of upwelling and downwelling surface current patterns in a small coastal embayment. *Continental Shelf Research*, 226, 104490. <https://doi.org/10.1016/j.csr.2021.104490>
- Treml, E. A., Roberts, J. J., Chao, Y., Halpin, P. N., Possingham, H. P., & Riginos, C. (2012). Reproductive output and duration of the pelagic larval stage determine seascape-wide connectivity of marine populations. *Integrative and Comparative Biology*, 52(4), 525–537. <https://doi.org/10.1093/icb/ics101>
- Tsikliras, A., Antonopoulou, E., & Stergiou, K. (2010). Spawning period of Mediterranean marine fishes. *Reviews in Fish Biology and Fisheries*, 20, 499–538. <https://doi.org/10.1007/s11160-010-9158-6>
- Tsirintanis, K., Azzurro, E., Crocetta, F., Dimiza, M., Froglija, C., Gerovasileiou, V., Langeneck, J., Mancinelli, G., Rosso, A., Stern, N., Triantaphyllou, M., Tsiamis, K., Turon, X., Verlaque, M., Zenetos, A., & Katsanevakis, S. (2022). Bioinvasion impacts on biodiversity, ecosystem services, and human health in the Mediterranean Sea. *Aquatic Invasions*, 17(3), 308–352. <https://doi.org/10.3391/ai.2022.17.3.01>
- Umgiesser, G., Canu, D., Cucco, A., & Solidoro, C. (2004). A finite element model for the Venice Lagoon. Development, set up, calibration and validation. *Journal of Marine Systems*, 51, 123–145. <https://doi.org/10.1016/j.jmarsys.2004.05.009>
- Umgiesser, G., Ferrarin, C., Bajo, M., Bellafiore, D., Cucco, A., De Pascalis, F., Ghezzi, M., McKiver, W., & Arpaia, L. (2022). Hydrodynamic modelling in marginal and coastal seas—The case of the Adriatic Sea as a permanent laboratory for numerical approach. *Ocean Modelling*, 179, 102123. <https://doi.org/10.1016/j.ocemod.2022.102123>
- Umgiesser, G., Ferrarin, C., Cucco, A., De Pascalis, F., Bellafiore, D., Ghezzi, M., & Bajo, M. (2014). Comparative hydrodynamics of 10 Mediterranean lagoons by means of numerical modeling. *Journal of*



- Geophysical Research: Oceans*, 119(4), 2212–2226.  
<https://doi.org/10.1002/2013JC009512>
- UNEP/MAP-RAC/SPA. (2015). *Adriatic Sea: Description of the Ecology and Identification of the Areas that May Deserve to be Protected*; Cerrano, C., Ed.; UNEP/MAP-RAC/SPA: Tunis, Tunisia, 2015; p. 92. (Eds. Cerrano C., Cebrian D., Requena S. (Tunis: RAC/SPA), 92. doi: 10.13140/RG.2.2.14080.79368).
- Ungaro, N., Rizzi, E., & Marano, G. (1993). Note sulla biologia e pesca di *Merluccius merluccius* (L.) nell'Adriatico pugliese. *Biol Mar Suppl al Notiziario SIBM*, 1, 329–334.
- Van Beveren, E. (2012). *Patterns of recruitment and early life history traits of Trachurus trachurus in a nearshore temperate reef* [MSc thesis]. Universidade do Algarve. Faro, Portugal.
- van der Loos, L. M., Bafort, Q., Bosch, S., Ballesteros, E., Bárbara, I., Berecibar, E., Blanfuné, A., Bogaert, K., Bouckenoghe, S., Boudouresque, C.-F., Brodie, J., Cecere, E., Díaz-Tapia, P., Engelen, A. H., Gunnarson, K., Shabaka, S. H., Hoffman, R., Husa, V., Israel, Á., ... De Clerck, O. (2023). Non-indigenous seaweeds in the Northeast Atlantic Ocean, the Mediterranean Sea and Macaronesia: A critical synthesis of diversity, spatial and temporal patterns. *European Journal of Phycology*, 0(0), 1–30. <https://doi.org/10.1080/09670262.2023.2256828>
- van Sebille, E., Aliani, S., Law, K. L., Maximenko, N., Alsina, J. M., Bagaev, A., Bergmann, M., Chapron, B., Chubarenko, I., Cózar, A., Delandmeter, P., Egger, M., Fox-Kemper, B., Garaba, S. P., Goddijn-Murphy, L., Hardesty, B. D., Hoffman, M. J., Isobe, A., Jongedijk, C. E., ... Wichmann, D. (2020). The physical oceanography of the transport of floating marine debris. *Environmental Research Letters*, 15(2), 023003. <https://doi.org/10.1088/1748-9326/ab6d7d>
- van Sebille, E., Griffies, S. M., Abernathey, R., Adams, T. P., Berloff, P., Biastoch, A., Blanke, B., Chassignet, E. P., Cheng, Y., Cotter, C. J., Deleersnijder, E., Döös, K., Drake, H. F., Drijfhout, S., Gary, S. F., Heemink, A. W., Kjellsson, J., Koszalka, I. M., Lange, M., ... Zika, J. D. (2018). Lagrangian ocean analysis: Fundamentals and practices. *Ocean Modelling*, 121, 49–75. <https://doi.org/10.1016/j.ocemod.2017.11.008>
- Vargas, J. M., García-Lafuente, J., Candela, J., & Sánchez, A. J. (2006). Fortnightly and monthly variability of the exchange through the Strait of Gibraltar. *Progress in Oceanography*, 70(2), 466–485. <https://doi.org/10.1016/j.pocean.2006.07.001>

- Vargas-Yáñez, M., Plaza, F., García-Lafuente, J., Sarhan, T., Vargas, J. M., & Vélez-Belchi, P. (2002). About the seasonal variability of the Alboran Sea circulation. *Journal of Marine Systems*, 35(3–4), 229–248. [https://doi.org/10.1016/S0924-7963\(02\)00128-8](https://doi.org/10.1016/S0924-7963(02)00128-8)
- Ventosa-Molina, J., Chiva, J., Lehmkuhl, O., Muela, J., Pérez-Segarra, C. D., & Oliva, A. (2017). Numerical analysis of conservative unstructured discretisations for low Mach flows. *International Journal for Numerical Methods in Fluids*, 84(6), 309–334. <https://doi.org/10.1002/flid.4350>
- Verlaque, M., Steen, F., & Clerck, O. (2009). *Rugulopteryx* Dictyotales, Phaeophyceae), a genus recently introduced to the Mediterranean. *Phycologia*, 48, 536–542. <https://doi.org/10.2216/08-103.1>
- Viette, M. (1997). Reproductive biology of scad, *Trachurus mediterraneus* (Teleostei, Carangidae), from the Gulf of Trieste. *ICES Journal of Marine Science*, 54(2), 267–272. <https://doi.org/10.1006/jmsc.1996.0185>
- Vilibić, I., Matijević, S., Šepić, J., & Kušpilić, G. (2012). Changes in the Adriatic oceanographic properties induced by the Eastern Mediterranean Transient. *Biogeosciences*, 9(6), 2085–2097. <https://doi.org/10.5194/bg-9-2085-2012>
- Virtanen, E. A., Moilanen, A., & Viitasalo, M. (2020). Marine connectivity in spatial conservation planning: Analogues from the terrestrial realm. *Landscape Ecology*, 35(5), 1021–1034. <https://doi.org/10.1007/s10980-020-00997-8>
- Viúdez, Á. (1997). An Explanation for the Curvature of the Atlantic Jet past the Strait of Gibraltar. *Journal of Physical Oceanography*, 27(8), 1804–1810. [https://doi.org/10.1175/1520-0485\(1997\)027<1804:AEFTCO>2.0.CO;2](https://doi.org/10.1175/1520-0485(1997)027<1804:AEFTCO>2.0.CO;2)
- Vrgoč, N., Arneri, E., Jukić-Peladić, S., Krstulović-Šifner, S., Mannini, P., Marčeta, B., Osmani, K., & Piccinetti, C. U. (2004). *N.(2004): Review of current knowledge on shared demersal stocks of the Adriatic Sea. FAO-MiPAF Scientific Cooperation to Support Responsible Fisheries in the Adriatic Sea. GCP/RER/010/ITA/TD-12. AdriaMed Technical Documents, 12.*
- Walsh, S. (2020). *Simulating Wintertime Lake Dynamics Using the MITgcm Ice Model* [MSc Thesis]. University of Waterloo. Waterloo, Canada.
- Wang, Y., Raitos, D. E., Krokos, G., Gittings, J. A., Zhan, P., & Hoteit, I. (2019). Physical connectivity simulations reveal dynamic linkages between coral reefs in the southern Red Sea and the Indian Ocean. *Scientific Reports*, 9(1), 16598. <https://doi.org/10.1038/s41598-019-53126-0>

- Wang, Z., Saebi, M., Grey, E. K., Corbett, J. J., Chen, D., Yang, D., & Wan, Z. (2022). Ballast water-mediated species spread risk dynamics and policy implications to reduce the invasion risk to the Mediterranean Sea. *Marine Pollution Bulletin*, 174, 113285. <https://doi.org/10.1016/j.marpolbul.2021.113285>
- Wejnerowski, Ł., Aykut, T., Pełechata, A., Rybak, M., Dulic, T., Meriluoto, J., & Dziuba, M. (2022). Plankton hitch-hikers on naturalists' instruments as silent intruders of aquatic ecosystems: Current risks and possible prevention. *NeoBiota*, 73, 193–219. <https://doi.org/10.3897/neobiota.73.82636>
- Werner, F., Cowen, R., & Paris, C. (2007). Coupled Biological and Physical Models: Present Capabilities and Necessary Developments for Future Studies of Population Connectivity. *Oceanography*, 20(3), 54–69. <https://doi.org/10.5670/oceanog.2007.29>
- Wesson, J. C., & Gregg, M. C. (1994). Mixing at Camarinal Sill in the Strait of Gibraltar. *Journal of Geophysical Research: Oceans*, 99(C5), 9847–9878. <https://doi.org/10.1029/94JC00256>
- Williams, J. J., & Esteves, L. S. (2017). *Guidance on Setup, Calibration, and Validation of Hydrodynamic, Wave, and Sediment Models for Shelf Seas and Estuaries*. <https://doi.org/10.1155/2017/5251902>
- Williams, P. D., & Hastings, A. (2013). Stochastic dispersal and population persistence in marine organisms. *The American Naturalist*, 182(2), 271–282. <https://doi.org/10.1086/671059>
- Wor, C., McAllister, M. K., Martell, S. J. D., Taylor, N. G., & Walters, C. J. (2018). A lagrangian approach to model movement of migratory species. *Canadian Journal of Fisheries and Aquatic Sciences*, 75(8), 1203–1214. <https://doi.org/10.1139/cjfas-2017-0093>
- Wu, L., Chen, C., Guo, P., Shi, M., Qi, J., & Ge, J. (2011). A FVCOM-based unstructured grid wave, current, sediment transport model, I. Model description and validation. *Journal of Ocean University of China*, 10(1), 1–8. <https://doi.org/10.1007/s11802-011-1788-3>
- Xue, Q., Liang, S., Sun, Z., Xu, Y., & Tian, Z. (2023). Near-surface characteristics of velocity profile and momentum transport after wave-breaking in deep water. *Ocean Engineering*, 276, 114223. <https://doi.org/10.1016/j.oceaneng.2023.114223>
- Yuan, S., Zhu, S., Luo, X., & Mu, B. (2024). A deep learning-based bias correction model for Arctic sea ice concentration towards MITgcm. *Ocean Modelling*, 188, 102326. <https://doi.org/10.1016/j.ocemod.2024.102326>

- Zapata, C., Puente, A., García, A., García-Alba, J., & Espinoza, J. (2019). The Use of Hydrodynamic Models in the Determination of the Chart Datum Shape in a Tropical Estuary. *Water*, 11(5), 902. <https://doi.org/10.3390/w11050902>
- Zardoya, R., Castilho, R., Grande, C., Favre-Krey, L., Caetano, S., Marcato, S., Krey, G., & Patarnello, T. (2004). Differential population structuring of two closely related fish species, the mackerel (*Scomber scombrus*) and the chub mackerel (*Scomber japonicus*), in the Mediterranean Sea. *Molecular Ecology*, 13(7), 1785–1798. <https://doi.org/10.1111/j.1365-294X.2004.02198.x>
- Zhang, Y. J., Ye, F., Stanev, E. V., & Grashorn, S. (2016). Seamless cross-scale modeling with SCHISM. *Ocean Modelling*, 102, 64–81. <https://doi.org/10.1016/j.ocemod.2016.05.002>
- Zhao, G., Gao, X., Zhang, C., & Sang, G. (2020). The effects of turbulence on phytoplankton and implications for energy transfer with an integrated water quality-ecosystem model in a shallow lake. *Journal of Environmental Management*, 256, 109954. <https://doi.org/10.1016/j.jenvman.2019.109954>
- Zore, M. (1956). On gradient currents in the Adriatic Sea. *Acta Adriatica*, 8, 1–40.
- Zorica, B., Anđelić, I., & Keč, V. Č. (2019). Sardine (*Sardina pilchardus*) spawning in the light of fat content analysis. *Scientia Marina*, 83(3), Article 3. <https://doi.org/10.3989/scimar.04898.07A>
- Zorica, B., Keč, V. Č., Vrgoč, N., Isajlović, I., Piccinetti, C., Mandić, M., Marčeta, B., & Pešić, A. (2020). A review of reproduction biology and spawning/ nursery grounds of the most important Adriatic commercial fish species in the last two decades. *Acta Adriatica*, 61(1), Article 1. <https://doi.org/10.32582/aa.61.1.7>



## Annex: Publications



Received: 1 October 2021 | Revised: 18 February 2022 | Accepted: 28 March 2022  
DOI: 10.1111/fog.12583

## ORIGINAL ARTICLE



## Hydrodynamic connectivity and dispersal patterns of a transboundary species (*Pagellus bogaraveo*) in the Strait of Gibraltar and adjacent basins

Irene Nadal<sup>1</sup> | Simone Sammartino<sup>2</sup> | Jesús García-Lafuente<sup>1</sup> |  
José C. Sánchez Garrido<sup>1</sup> | Juan Gil-Herrera<sup>3</sup> | Manuel Hidalgo<sup>4</sup> |  
Pilar Hernández<sup>5</sup>

<sup>1</sup>Universidad de Málaga, Instituto de Biotecnología y Desarrollo Azul (BYDA), Physical Oceanography Group, Málaga, Spain

<sup>2</sup>Instituto de Ingeniería Oceánica (IO), Physical Oceanography Group, Universidad de Málaga, Málaga, Spain

<sup>3</sup>Centro Oceanográfico de Cádiz (IEO, CSIC), Cádiz, Spain

<sup>4</sup>Ecosystem Oceanography Group (GRECO), Centro Oceanográfico de Baleares (IEO, CSIC), Palma, Spain

<sup>5</sup>General Fisheries Commission for the Mediterranean, Technical Unit for Western Mediterranean, Food and Agriculture Organization of the United Nations, Málaga, Spain

## Correspondence

Irene Nadal, Universidad de Málaga, Instituto de Biotecnología y Desarrollo Azul (BYDA), Physical Oceanography Group, Málaga, Spain.  
Email: irenenadal@cima.uma.es

## Abstract

The blackspot seabream (*Pagellus bogaraveo*) is a benthopelagic fish species highly appreciated by consumers and an important target of the Spanish and Moroccan fisheries in the transcontinental waters of the Strait of Gibraltar area. It is also one of the most exploited resources of the region, which has led to a situation of overexploitation and a notable drop of catches. To gain insight into the sustainability of this resource and certain patterns of the spatial adaptation of the species, a high-resolution circulation model coupled to a Lagrangian tracking module has been employed to investigate the dispersal pathways of blackspot seabream, using eggs and larvae (early-life-stages, ELS) as purely passive particles advected by currents. Several spawning scenarios consisting of different spatial (depths and sites) and temporal (tidal phase and strength) initial conditions have been analyzed to identify the most likely pathways of ELS dispersion. Eastward transport by the Atlantic Jet exiting the Strait of Gibraltar is the most influencing process in that dispersion. Regarding temporal fluctuations, fortnightly tidal modulation is the prevailing factor to determine the horizontal paths of the ELS, spring tides being the cause of the greatest scattering of propagules. Spawning depth in the Strait of Gibraltar is a critical condition, as revealed by the model sensitivity tests. Potential implications of the results of the study to improve the assessment and management of this species are discussed.

## KEYWORDS

Alboran Sea, blackspot seabream, early-life-stages (ELS), hydrodynamic connectivity, pelagic larval duration (PLD), Strait of Gibraltar, transboundary stock

## 1 | INTRODUCTION

Oceanographic features largely control the dispersal of fish eggs and larvae and thereby the dynamic connectivity of geographically separated fish subpopulations (Cowen & Sponaugle, 2009). Such control is

particularly tight in highly energetic areas influenced by tides, wind-driven currents and small-scale turbulence (Cowen et al., 2006; Sakina-Dorothee et al., 2010). Dynamic connectivity concerns to those interactions between the life cycle of the fish species in question and the physical processes that drive the dispersal of early life

This is an open access article under the terms of the [Creative Commons Attribution](https://creativecommons.org/licenses/by/4.0/) License, which permits use, distribution and reproduction in any medium, provided the original work is properly cited.

© 2022 The Authors. *Fisheries Oceanography* published by John Wiley & Sons Ltd.

stage individuals (ELS, hereinafter) at different spatial and temporal scales. Understanding the processes and scales controlling ELS dispersal and how connectivity influences the dynamics of the affected populations is a major challenge of special interest for vulnerable species (Cowen et al., 2006; Pineda et al., 2007), particularly relevant for species inhabiting across jurisdictional waters of different countries (Hidalgo et al., 2019; Palacios-Abantes et al., 2020; Pinsky et al., 2018). Resolving the mechanisms controlling ELS dispersal entails the understanding of the relevant physical processes and how the species mediate the physical outcome (García-Lafuente, Sánchez-Garrido, et al., 2021). Currently, studies of dispersal dynamics and larval connectivity are being used to provide an approach to improve fisheries management and assessment (Fogarty & Botsford, 2007; Hidalgo et al., 2019). Focusing on fisheries health in the Strait of Gibraltar (SoG hereinafter, see Figure 1) the blackspot seabream [*Pagellus bogaraveo* (Brünnich, 1768)] is one of the most affected stocks (Gil, 2006, 2010). It is targeted by local fishermen from Spain and Morocco using a special longline gear, known as voracera.

Landings from this shared fishery exhibit a clear decreasing trend since 2009, which shows up a vulnerability that is raising serious concerns at local and international levels in a socioeconomic context (Báez et al., 2014). In 1998, the Spanish Government introduced technical measures to manage this fishery, and few years later, the Andalusian Regional Government developed a specific fishing plan that included a biological rest period and the limitation of the number of hooks per voracera (Burgos et al., 2013). Transitional measures for the management of blackspot seabream in the Alboran Sea (AS, hereinafter) were primarily set out by the General Fisheries Commission for the Mediterranean (GFCM) in 2017 (Recommendation GFCM/41/2017/2). Later on, the Recommendation GFCM/43/2019/2 establishes an adaptive multiannual management plan for its sustainable exploitation in the AS. Last GFCM stock assessment indicated that the SoG and population (geographical sub-areas, hereafter GSAs, 1 and 3; see Figure 1) is overexploited and in overexploited status and, consequently, a reduction of fishing mortality towards sustainability levels was recommended (GFCM, 2021). Even so, the sustainability of blackspot seabream fisheries requires more efforts (Gil-Herrera et al., 2021).

The optimization of the fishery stock and the curbing of the over-exploitation of the resource require further studies of population dynamics and hydrodynamic and demographic connectivity, especially during larval stages. They should address the consequences of the connectivity on the production of the stocks and other characteristics at interannual time-scales. Trying to fill these gaps, the Regional Cooperation Project for Fisheries in Western Mediterranean (CopeMed) and the GFCM of the Food and Agriculture Organization (FAO) developed the EU-funded project "Transboundary population structure of Sardine, European hake and blackspot seabream in the Alboran Sea and adjacent waters: a multidisciplinary approach" (TRANSBORAN; CopeMed, 2017, 2019), which focused on the management of the fishery stocks of these species in the AS and adjacent waters. One of the main objectives of the project was to understand and identify the mechanisms of larval dispersal in the area, which is

crucial to determine the populations structure and to optimize the fisheries functioning (Pineda et al., 2007; Virtanen et al., 2020).

From a hydrodynamic point of view, ELS dispersal is usually investigated by means of tracking algorithms fed by hydrodynamic numerical models (e.g., Dubois et al., 2014; Rossi et al., 2014). Some studies suggest that ELS information concerning larval behavior, egg buoyancy or diel vertical cycles is critical (Fiksen et al., 2007; Sundelöf & Jonsson, 2012), whereas others show that active swimming during ELS is negligible when compared with the effect of the drifting by the ocean currents (Hidalgo et al., 2019). This biological aspect has not been elucidated yet for the blackspot seabream. Nevertheless, the high dynamics of the area strongly supports the second hypothesis. Consequently, the present study considers the ELS as passive tracers advected by the currents and investigates their dispersion and connectivity patterns using a high-resolution ( $\approx 1$  km) circulation model of the SoG, the spawning area of the species (Gil, 2006, 2010), and the AS. Different scenarios have been considered in order to assess the sensitivity of the resulting patterns against the initial conditions. The scenarios include diverse spawning grounds and depths in the SoG as well as distinct hydrodynamic initial conditions associated to the tidal phase and strength (spring-neap tidal cycle) of the currents at the moment of the spawning.

The paper is organized as follows: next subsections present the main traits of the biology of the blackspot seabream and of the hydrodynamic features of the area of study. Section 2 describes the numerical model and the Lagrangian approach and provides details about the experimental procedure. Section 3 reviews and discusses the results of the numerical experiments. It has been organized into seven subsections addressing different aspects of the dependency of the specific spatial and temporal initial conditions on the ELS dispersal paths and the potential implications for fishery management of the species. Section 4 includes a summary of the results and conclusions of this work.

## 1.1 | Life cycle of blackspot seabream

As other Sparidae species, the blackspot seabream is a sequential protandric hermaphrodite, starting as males and then changing into females at 30–35 cm length and around 4 to 6 years age (Alicaraz et al., 1987; Gil, 2006; Krug, 1994). It grows relatively slow to a maximum size of 70 cm, weight of 4 kg and about 15 years age (Gil, 2006; Krug, 1994; Sánchez, 1983). Juveniles inhabit inshore areas while adults have deeper distribution (Desbrosses, 1932). Olivier (1928) and Desbrosses (1932) report species vertical movements during the night and in certain seasons, related to daylight and spawning. However, this has not been already demonstrated for the case of the SoG population. Fish populations are potentially able to adapt to the mean horizontal transport and dispersion pattern of its ELS by influencing the vertical position of their planktonic offspring either by its spawning behavior (fish selection of spawning area and depth) or by producing eggs of certain specific gravity (Sundby & Kristiansen, 2015). The ontogeny of the species ELS is only available from aquaculture

experiments estimating a pelagic larval duration (PLD) from 40 to 60 days (Peleteiro et al., 1997).

The AS might be considered as a hatchery and nursery area of the species (Gil et al., 2001). Juveniles are mostly caught close to the shore by recreational angling fishery, following similar patterns seen in other places like the Bay of Biscay (Lorance, 2011), the Azores Islands (Pirho et al., 2014), and the Mediterranean Sea (Biagi et al., 1998). Adults, targeted by the Spain and Morocco voracera fishing fleets, spawn during the first quarter of the year in the SoG (Gil, 2006, 2010). Interconnected cycles of recruitment in both sides of the nearby coastal areas of the SoG followed by juveniles returning to the grounds where the fishery takes place were suggested by Gil et al. (2001).

## 1.2 | Relevant hydrodynamic features of the area

The SoG connects the North Atlantic Ocean and the Mediterranean Sea and is one of the most energetic spots in the world ocean. The net freshwater deficit of the Mediterranean basin drives an archetypical baroclinic exchange that involves very large currents. Lighter Atlantic water flows into the Mediterranean basin invading the AS in the form of a swift Atlantic Jet (AJ hereinafter), while denser Mediterranean water flows underneath toward the Atlantic Ocean (García-Lafuente et al., 2013). On average, each of these flows are slightly less than 1 Sv ( $1\text{ Sv} = 10^6 \text{ m}^3 \text{ s}^{-1}$ ; García-Lafuente, Sammartino, et al., 2021; Sammartino et al., 2015), but they can quadruple the values during certain moments of the tidal cycle due to the strength of the tidal currents (García-Lafuente et al., 2000). Actually, the tide-topography interaction in the area gives rise to one of the most noticeable internal tides in the world ocean (Sánchez-Garrido et al., 2011), which displaces vertically the interface between Atlantic and Mediterranean waters by more than 100 m periodically. Also

forced barotropic flow through the SoG driven by the changing atmospheric pressure field over the Mediterranean basin modifies the baroclinic exchange by significant fractions of their average values at few-days' timescale (García-Lafuente et al., 2002).

The general circulation of the AS is determined by the mentioned AJ (see the pioneer paper by Lanoix, 1974, or the extensive review by Parrilla and Kinder, 1987, for details). The AJ sets up two anticyclonic structures: the Western and the Eastern Alboran Gyre (WAG and EAG, respectively; see sketch of Figure 1), which exhibit seasonal and shorter time-scale variability. In winter, the WAG tends to be replaced by a coastal jet attached to the African coast (Flexas et al., 2006; Vargas-Yáñez et al., 2002). Surface variability is reduced during summer, when the atmospheric forcing is less variable (Sánchez-Garrido et al., 2013). Smaller scale processes such as tidally driven relative vorticity imported from the SoG, westerly winds and occasional AJ drifts, propitiate the formation of cyclonic eddies along the northern side of the jet in the western Alboran basin (Sánchez-Garrido et al., 2013; Sañan et al., 2000) and also in the southern coast (Mason et al., 2019). These eddies induce upward pumping of deep waters, entailing high productivity areas favorable for mesopelagic species development (Sánchez Garrido et al., 2015).

## 2 | NUMERICAL DATA AND METHODS

### 2.1 | The hydrodynamic model

The numerical model used to simulate the hydrodynamics of the studied area is based on the MITgcm code (Marshall, Adcroft, et al., 1997; Marshall, Hill, et al., 1997), which has been already used in previous studies of this particular region (Sammartino et al., 2014; Sánchez-Garrido et al., 2011, 2013). The general configuration of the model, its advection scheme, and other technical details are provided in these

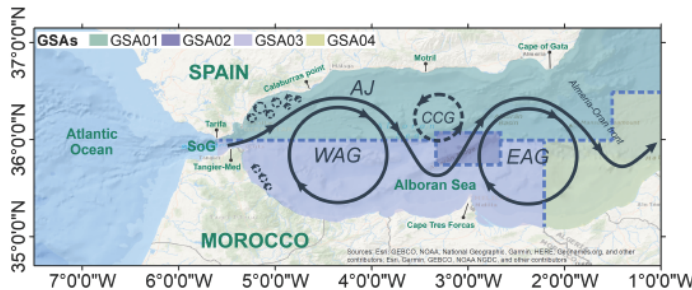


FIGURE 1 Map of the Alboran Sea showing the Strait of Gibraltar (SoG) and sketching its general surface circulation: the Atlantic Jet (AJ) and the western and eastern Alboran Gyres (WAG and EAG, respectively). CCG stands for Central Cyclonic Gyre, a weaker structure that normally develops whenever the WAG and EAG are fully developed (adapted from Sánchez-Garrido et al., 2013). Smaller cyclonic eddies, represented by dashed lines, are often found rightwards and leftwards of the AJ main path. Some relevant locations are displayed and the GSAs (1–4), defined by the GFCM (2021) are patched



works. It has been implemented on a curvilinear grid that covers the Gulf of Cadiz (from 9.4°W) and the AS to its eastern limit (around 1.6°E). The horizontal resolution and vertical discretization are uneven, being maximal in the SoG area and near the surface in the vertical (see Figure S1). At the two open lateral boundaries, the model is forced with baroclinic horizontal velocities, temperature, and salinity fields imported from CMEMS-IBI model (Sotillo et al., 2015). Tides are also prescribed in these open boundaries using the harmonic constants of the eight most important tidal constituents (the main semi-diurnal:  $M_2$ ,  $S_2$ ,  $N_2$ ,  $K_2$ , and diurnal:  $K_1$ ,  $O_1$ ,  $Q_1$ ,  $P_1$ ). The meteorologically driven barotropic flow prescribed at the SoG by the NIVMAR storm surge model (Álvarez Farjuel et al., 2001) is distributed throughout these boundaries to incorporate the meteorological forcing into the model. At surface, the model is forced with atmospheric conditions provided by the MED-Cortex model (Ruti et al., 2016). The model has been run from November 2004 to April 2005 in order to cover the most active spawning months of the blackspot seabream (Gil, 2004, 2010), and the 3D velocity field has been stored every 30 min.

In the vicinity of the SoG, but yet inside the AS, the highest variability of the velocity field is associated with the tidal dynamics of the Strait (García-Lafuente et al., 2000). Figure 2 shows the surface velocity and the kinetic energy per unit of mass (computed as  $K_E = \frac{1}{2} (U^2 + V^2)$ ,  $U$  and  $V$  the zonal and meridional surface velocity components, respectively) over two different periods. The panel on the left corresponds to neap tide and illustrates a surface pattern with diminished velocities. Right panel is for spring tide and presents the characteristic average circulation that uses to prevail the AJ flowing into the AS, the WAG and EAG, a small CCG in between, and the Almería-Oran (AO) front in the eastern limit of the AS. Both panels show similar circulation patterns, although velocity field is noticeably larger during spring than in neap tides. In fact, spring tides not only generate stronger currents and inject more energy, but also induce higher variability and, expectedly, rates of dispersion all over the

basin. Even though the simulated period does not cover a seasonal cycle, some hints of seasonal variability are reflected in the monthly averaged velocity at the surface and the sea surface height (SSH) during the simulation months (Figure S2).

## 2.2 | Releasing boxes and landing areas selection

To investigate the dispersion of blackspot seabream ELS in the area, a set of numerical experiments have been run and their outputs subsequently analyzed. All of them make use of what has been named "releasing boxes" and "landing areas" in this study. Releasing boxes embrace the most probable spawning areas of blackspot seabream. Three boxes have been established, two along the north and south shores of the SoG, labeled Tarifa and Tangier-Med, respectively (see inset in Figure 3), and a third one in between occupying the center-west area of the SoG (Tangier box). The three boxes not only cover what is currently thought to be the main spawning grounds of the species (Gil et al., 2001) but also address the geographical differentiation of the spawning area, which will have consequences on the spreading of the ELSs of blackspot seabream.

These spawning products are then transported by the currents and their fate is interpreted in terms of concentration within landing areas, which are understood as potential coastal nursery grounds. In a broad sense, a strip few kilometer wide along the coasts of the whole region should be considered as such. However, the remarkable spatial variability of the hydrodynamics of the region recommends the splitting of the strip into more reduced landing areas. The presence of notable topographic features such as Cape Tres Forcas, or Calaburras Point or Cape Gata (see Figure 1) also favors this division. On the other hand, the zonal orientation of the AS suggests a mirror-like correspondence of landing areas in the north and south shores. According to these premises, a total of ten areas have been defined,

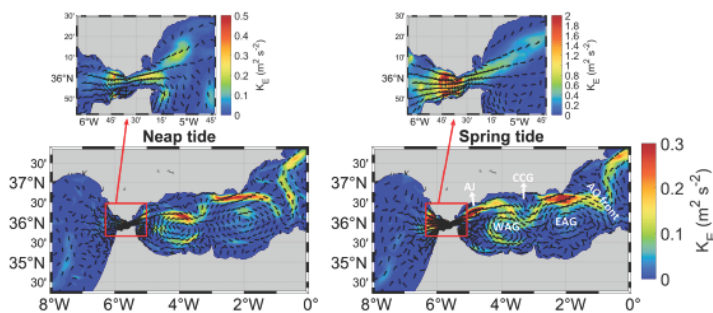


FIGURE 2 Surface current direction and kinetic energy per unit of mass ( $\text{m}^2\text{s}^{-2}$ ) in the AS (lower panels) during neap (left side) and spring tide (right side). The main surface structures sketched in Figure 1 have been tagged in the lower right panel using the same acronyms

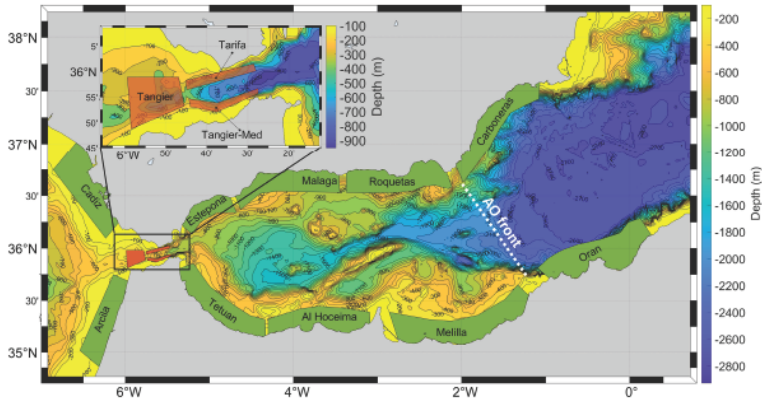


FIGURE 3 Map of the study area showing the releasing boxes of Tarifa, Tangier and Tangier-Med (brown polygons in the inset) and the landing areas of Cadiz, Estepona, Malaga, Roquetas, Carboneras, Oran, Melilla, Al Hoceima, Tetuan, and Arcila (green polygons). Adapted from CopeMed (2019)

five in each shore (Figure 3). Two of them are in the Gulf of Cadiz (Cadiz and Arcila) to check eventual westward transport of ELS, and other two in the opposite end of the region to the east of the AO front, out of the AS (Carboneras and Oran). The remaining six are located in the AS, two in the vicinity of the SoG (Estepona, Tetuan), which leaves them exposed to high-energy dynamics, two (Malaga, Al Hoceima) in the western Alboran basin under the influence of the WAG and the last two (Roquetas, Melilla) in the eastern basin under the influence of the EAG. All the landing areas are attached to the shore and subjected to different oceanographic regimes.

### 2.3 | Lagrangian particle tracking algorithm and experiments setup

A Lagrangian particle tracking algorithm (LaCasce, 2008; Nicolle et al., 2013, 2017) has been used to study the transport and dispersion of blackspot seabream ELS. A detailed description of the procedure can be consulted in Sammartino et al. (2018). In this Lagrangian approach, eggs and larvae are virtual passive tracers during the PLD phase. Larvae swimming capability, although barely known, appears to be insufficient to overcome the strong currents of this region and has not been considered. Therefore, ELSs are just advected by the model horizontal velocity. The horizontal trajectories have been computed by integrating the bilinearly interpolated horizontal velocity field at every grid point of the domain using a Runge-Kutta fourth-order scheme (Rossi et al., 2014). Vertical larvae migration is a sensitive information that is not yet demonstrated for the studied species, so it has been neglected for simplicity (Rodríguez et al., 2001).

In order to investigate the influence of the depth on the dispersion patterns, five different vertical spawning layers have been selected: surface (from 0 to 3 m), 12 m (from 10 to 14 m), 25 m (from 23 to 28 m), 52 m (from 48 to 56 m), and 81 m (from 76 to 87 m). To account for the effects of the time variability associated with tides, releasing times have been selected with the aim of covering a wide variety of tidal conditions that combine semidiurnal phase during four fortnightly cycles. This approach allows for replicating four times every tidal condition. Figure 4 gives information on the tidal conditions at the moment of the release for all the experiments. Lagrangian particle tracking simulations have then been run starting from every releasing time during a period of 60 days, which is the maximum PLD estimated for the blackspot seabream (Peleteiro et al., 1997).

### 2.4 | Pool of experiments and connectivity computation

The combination of spatial and temporal conditions gives a total of 160 numerical runs per releasing box (4 tidal phase  $\times$  2 tidal strength  $\times$  4 replicas  $\times$  5 depths), or a grand total of 480 experiments for the three boxes. The following table (Table 1) summarizes the set of numerical batches combination that has been performed with the numerical model.

As the analysis searches for ELS within each of the 10 landing areas in each experiment, a total of 4800 cases have been handled for the main analysis (to which 320 more from the depth-sensitivity study must be added). For each experiment, ~1000 particles have been released, and the position of each particle has been computed every

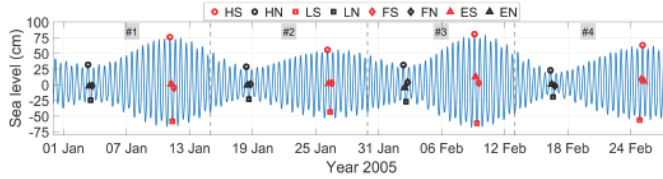


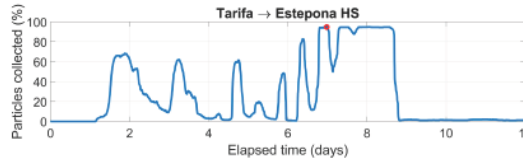
FIGURE 4 Sea level in Tarifa (blue line) during the period used for ELS release. Releasing times are shown by symbols whose meaning is indicated in the legend. It makes use of the following code to specify tidal conditions: first letter refers to tidal phase according to: H, high water; L, low water; F, maximum flood (westward) tidal current; E, maximum ebb (eastward) tidal current. Second letter specifies the fortnightly cycle according to: S, spring; N, neap tides. The gray vertical lines divide the series into four pieces that correspond to each replica

TABLE 1 Summary of the different spatial and temporal conditions configured in each numerical experiment

Releasing area	Spawning depth	Tidal phase	Tidal strength	Releasing times	Total
Tarifa	[1,12,25,52,81]	[High, Low, Ebb, Flood]	[Spring, Neap]	#1, #2, #3, #4	160
	[120,150]	[Flood, Ebb]	[Spring, Neap]	#2, #4	16
Tangier-Med	[1,12,25,52,81]	[High, Low, Ebb, Flood]	[Spring, Neap]	#1, #2, #3, #4	160
	[120,150]	[Flood, Ebb]	[Spring, Neap]	#2, #4	16
Tangier	[1,12,25,52,81]	[High, Low, Ebb, Flood]	[Spring, Neap]	#1, #2, #3, #4	160
Total					512

Note: From left to right: Releasing area refers to the assumed spawning zones of blackspot seabream. Spawning depth represent the depth of the spawning layers; the five depths in the range [1–81]m corresponds to the main analysis (black text), and depths 120 m and 150 m, to the tests carried out in the boxes of Tarifa and Tangier-Med to assess depth sensitivity (gray text; see Section 2.2 for details). Tidal phase refers to tidal conditions within the semidiurnal cycle (see also Figure 4): High and low correspond to high and low water, ebb is the time of maximum eastward tidal current, which happens mid-time from high-to-low water and flood is the time of maximum westward tidal flow (from low to high water). Tidal strength denotes spring and neap tides within the fortnightly cycle. Releasing times refer to the four replicas of every single experiment carried out in different times, as indicated by the numbered boxes in Figure 4. Last column is the total batch of experiments for the main analyses and the sensitivity tests.

FIGURE 5 Time series of the percentage of ELS released in Tarifa box at the surface that were found in Estepona landing area as a function of time, in a high-spring (HS) tide scenario. Red dot indicates the maximum value of 94.85% on day 7



5 min. The huge amount of information needs to be processed and summarized in order to depict a relatively straightforward pattern of the ELS dispersal pathways. From an ecological point of view, dynamic connectivity is usually assessed as the percentage of particles (ELS) collected in a landing area *b* at a time *t* ( $p_b(t)$ ) compared with those released in box *a* ( $p_a$ ) (Cowen et al., 2006; Crochelet et al., 2016; Nicolle et al., 2017; Gamoyo et al., 2019), where *t* corresponds to a certain PLD, or to a fraction of it, which is fixed *a-priori*:

$$C_{a \rightarrow b}(t) = \frac{p_b(t)}{p_a} \cdot 100$$

In these works, the output usually consists of a connectivity squared matrix in which each cell is the probability of exchange of individuals between regions (row and column of the matrix), and the diagonal stands for the self-recruitment, that is, the percentage of ELS released and settled in the same box (Cowen et al., 2006). However, this approach is inappropriate in this study for two reasons. First, releasing boxes are different from landing areas because of the biological habits of the blackspot seabream, which has its only spawning area in the SoG. Hence, a reciprocal connectivity matrix is not feasible. Second, the strong and highly variable dynamics of the region makes the propagules to be swiftly advected away shortly after the release, hampering self-recruitment (Gil, 2006, 2010).

13491819, 2022, 4, Downloaded from https://onlinelibrary.wiley.com/doi/10.1111/fis.12503 by Chon-Chancho, Wiley Online Library on [08/03/2023]. See the Terms and Conditions (https://onlinelibrary.wiley.com/terms-and-conditions) on Wiley Online Library for rules of use; OA articles are governed by the applicable Creative Commons License

Figure 5 illustrates the shortcomings of this standard approach when it is applied to this study. It shows the time evolution during the first 12 days of simulation of the percentage of particles collected in Estepona landing area that were released at the surface in Tarifa releasing box (see Figure 3) under high-spring tidal conditions. The percentage may change from 10% to 90% in few hours (also the reciprocal), which makes meaningless the computation of the connectivity at a given time because of its strong dependence on the selected instant: the resulting value will not be representative.

In order to cope with this limitation, an alternative connectivity definition is adopted as the maximum percentage of particles (MPoP hereinafter) collected in each landing area throughout the total duration of simulation (60 days; see Section 2.3):

$$C_{a \rightarrow b} = \max \left( \frac{P_b(t)}{P_a} \right) \cdot 100.$$

Associated with this maximum percentage is the time at which it is achieved (time of maximum connectivity; ToMC hereinafter). This time is of concern as far as it must be compared with the actual PLD. Notice that contrary to the fixed time interval, the ToMC is not imposed or prescribed *a-priori*, but it is deduced from the analysis.

### 3 | RESULTS AND DISCUSSION

#### 3.1 | MPoP and ToMC averages

Table 2 shows the MPoP released at the three boxes that were found in the different landing areas and the ToMC when this percentage is attained. They are averaged over the whole combination of spatial and temporal releasing conditions and provide global connectivity values that summarize the huge amount of information generated in

the study. Table 2 highlights the fundamental role of the eastward flowing AJ, which is responsible for the direct spread of the ELS released in the SoG toward the AS and the nearly null abundance of particles in the Atlantic landing areas of Cadiz and Arcila.

A high connectivity (i.e., high value of MPoP) for Tarifa releasing box is observed in Malaga, Estepona, and Roquetas landing areas (45%, 38%, and 17%, respectively), followed by Oran (14%). This spatial pattern is to be expected as the AJ acts as the main advection mechanism (see Figure 1). Carboneras landing area, located outside of the AS on the northern shore, stands apart from the path of this stream and, consequently, the MPoP falls well below the previous values. A weak north-to-south connectivity is inferred from the non-null MPoP of 8% computed in Tetuan and Al Hoceima. This spatial distribution is consistent with results of larvae distribution obtained from samples collected during a scientific survey carried out in the area in the late winter 2020: a considerable number of larvae (~8 mm length) of *P. bogaraveo* were collected in the AS, the greatest abundance (from 10 to 14.96 larvae 10 m<sup>-2</sup>) having been found in Estepona and Malaga coasts (TRANSBORAN survey; J.M. Rodríguez, Pers. Comm.).

Similar zonal spread is found in the case of Tangier-Med releasing box, the southern counterpart of Tarifa box. Highest connectivity is reached in Tetuan and Al Hoceima in the south shore (MPoP of 45% and 17%, respectively). Again, a south-to-north connection is suggested by the significant MPoP of 11% and 8% in Malaga and Estepona, respectively, though the associated standard deviation, which is comparable to the mean, sheds uncertainty on the result. Roquetas and Oran areas have values of 5%, compatible with the isolation effect of the eastern rim of the WAG and the own EAG. This effect would also explain the very low values in Mellilla and Carboneras (4% and 2%, respectively). Results for Tangier releasing box are similar to those of Tangier-Med. The reason is the Coriolis force that deflects particles to the south within the limits of the very SoG before the AJ

TABLE 2 Maximum percentage of particles (MPoP column) and time of maximum connectivity (ToMC column) of ELS with their corresponding standard deviations for all landing areas and releasing boxes, averaged for all scenarios of initial conditions

Landing area	Tarifa		Tangier-Med		Tangier		
	MPoP (%)	ToMC (days)	MPoP (%)	ToMC (days)	MPoP (%)	ToMC (days)	
Northern coast	Cadiz	0 ± 0*	1 ± 3	0	-	0 ± 0*	1 ± 4
	Estepona	38 ± 11	4 ± 3	8 ± 8	21 ± 9	10 ± 6	13 ± 6
	Malaga	45 ± 12	7 ± 3	11 ± 8	22 ± 9	15 ± 7	11 ± 6
	Roquetas	17 ± 8	22 ± 8	5 ± 4	32 ± 6	5 ± 4	26 ± 7
	Carboneras	6 ± 4	31 ± 7	2 ± 3	33 ± 6	2 ± 2	35 ± 6
Southern coast	Arcila	0	-	0 ± 0*	1 ± 2	1 ± 2	5 ± 5
	Tetuan	8 ± 5	30 ± 13	45 ± 19	25 ± 9	33 ± 17	25 ± 7
	Al Hoceima	8 ± 5	34 ± 8	17 ± 18	40 ± 9	14 ± 13	41 ± 11
	Mellilla	6 ± 3	41 ± 10	4 ± 3	46 ± 8	3 ± 2	47 ± 9
	Oran	14 ± 4	36 ± 7	5 ± 3	42 ± 6	6 ± 4	38 ± 8

Note: Landing areas have been grouped according to its geographical location. Asterisks indicate values of MPoP very close to zero (that round to zero), but not strictly null. In such situation, the ToMC is meaningless, and these cases are ignored and not discussed in the text. The two special cases of Tarifa-Arcila and Tangier-Med-Cadiz in which MPoP is strictly null; the ToMC is not defined.



spreads into the AS (Albérola et al., 1995). Therefore, once the ELS enter the AS, their trajectories should not be much different regardless the particles were released in one box or the other.

ToMCs in Table 2 are consistent with the ELS dispersal inferred from the MPoP analysis. Shorter ToMCs are found in the landing areas closer to the releasing boxes. For particles released in Tarifa box, the shortest time is found in Estepona area (4 days). The result applies for Tangier-Med and Tangier boxes and Tetuan landing area in the southern coast (3 and 4 days, respectively). A shorter ToMC is obtained for Tangier box and Arcila area (1 day), but the very low MPoP of 1% in the area makes it not worth discussing. As distances increase, ToMC also does. In the case of Tarifa box and for northern landing areas, the greatest ToMC is found in Carboneras, the easternmost area (31 days). The same applies in the south coast, where the easternmost area (Oran) shows ToMC of 46 and 47 days with Tangier-Med and Tangier boxes, respectively. A curious case that deserves comment is that the northern landing areas have shorter ToMC with these two releasing boxes than the areas in the south (except for Tetuan). The interpretation of this somewhat anti-intuitive result is the advection of ELS by the western rim of the WAG towards the north shore. Once there, the products follow similar trajectories as the particles released in Tarifa box.

These scenario-averaged values reflect the prevailing role of the main dynamic structures of the SoG-AS system on the ELS dispersion and provide foreseeable connectivity patterns. Nonetheless, the large standard deviations (uncertainties) associated to the mean values reveal high variability related to the temporal and spatial variability of the SoG hydrodynamics as well as to the very location of the releasing boxes. These issues are addressed next for Tarifa (Section 3.2.1) and Tangier-Med (Section 3.2.2) boxes. Tarifa box is presented in Figure S3 due to the aforementioned similitude with Tangier-Med, and it is not discussed here.

### 3.2 | Release area dependency

#### 3.2.1 | Tarifa releasing box

Table 2 shows that, as a result of the advection by the AJ, the main connections of ELS released at the surface in Tarifa box take place with the northwestern areas of the AS. However, some differences appear when specific tidal conditions and depths are considered (Figure 6). Figure 6a shows that the highest connectivity in Estepona for surface release is achieved under ebb (E) condition in spring (S) tide (~60%), when the eastward flow in the SoG is boosted by the strong ebb current of spring tides. The same applies for near-surface releases, 12 and 25 m, which give MPoP values of ~63% and ~61%, respectively. In Malaga, MPoP is consistently greater and, somewhat paradoxically, ToMC is smaller in neap than in spring tides (Figure 6b). The behavior is reproduced by the remaining landing areas of the northern coast. As the distance of the landing area increases, however, the ratio of MPoP neap/spring increases until it reaches the highest value in the farthest landing area of Carboneras (Figure 6a).

The effect that initial conditions in Tarifa box has on the dispersal patterns is less defined in the southern landing areas. MPoPs are systematically inferior to their mirror area in the northern shore except for the two easternmost areas, with Oran showing a slightly higher MPoP than Carboneras. Such structure emphasizes the fact that north-to-south connectivity is less achievable than west-to-east connectivity due to the role of hydrodynamic barrier played by the AJ for meridional exchange. ToMCs are consequently greater than in the northern areas, except for Tetuan in spring tides, where they are similar to those found in Estepona in the north (Figure 6b).

The behavior in Tetuan contrasts with the much larger ToMCs in the other southern landing areas, which are rather independent of the tidal variability. Two different mechanisms seem to be at work. Particle scattering promoted by the intensified inflow would be the reason for the reduced ToMC in Tetuan during spring tides (Figure 6b) and for the relatively large MPoP of 23% under FS conditions in particular (Figure 6a). ToMCs in the three other areas, on the contrary, are rather independent of tidal conditions (Figure 6b). The interpretation given to this different response is that Tetuan area is directly reachable by southeastward trajectories scattered from Tarifa releasing box during the spring tide periods of enhanced currents. This process is unfeasible for the three other areas where particles will most likely arrive after completing one WAG turn around at least. It requires a time long enough to smooth out the effects of the SoG tide and the particles end up being transported by a tidal-free large-scale circulation that propitiates ToMC as large as 40 days in Al Hoceima, in sharp contrast with the scarce 6 days of Tetuan in spring tides (Figure 6b).

#### 3.2.2 | Tangier-Med releasing box

The most obvious feature is the high MPoP in the nearest eastward landing area of Tetuan, increased during spring tides to values of ~60% (Figure 7a). The behavior resembles the east-to-west connectivity between Tarifa and Estepona area in the northern shore. Both would have the same cause, which is the zonal advection by the AJ. But the similitude Tarifa-northern areas versus Tangier-Med-southern areas finishes just here. Whereas in the first case MPoPs were clearly higher in all northern areas of the AS, in the case of Tangier-Med releasing box, south areas of Al Hoceima and Melilla have MPoP of the same magnitude, if not less, than in the north areas. In other words, zonal connectivity in the south is not as efficient as in the north, except for Tetuan area.

The explanation provided for this unexpected behavior is that the coastal eddy that usually forms south of the AJ and close to the African shore at the exit of the SoG (Sánchez-Garrido et al., 2013; see Figures 1 and 2) favors high MPoPs in the Tetuan area. This structure propitiates ELS retention. The trapped propagules can be eventually transferred to the western rim of the WAG and advected to the northern coast, making south-to-north connectivity feasible, and hampering west-to-east transport. The rather low values of MPoP in the upper layers of the northern areas indicate that the connection is weak. However, and this is an intriguing question, the connectivity

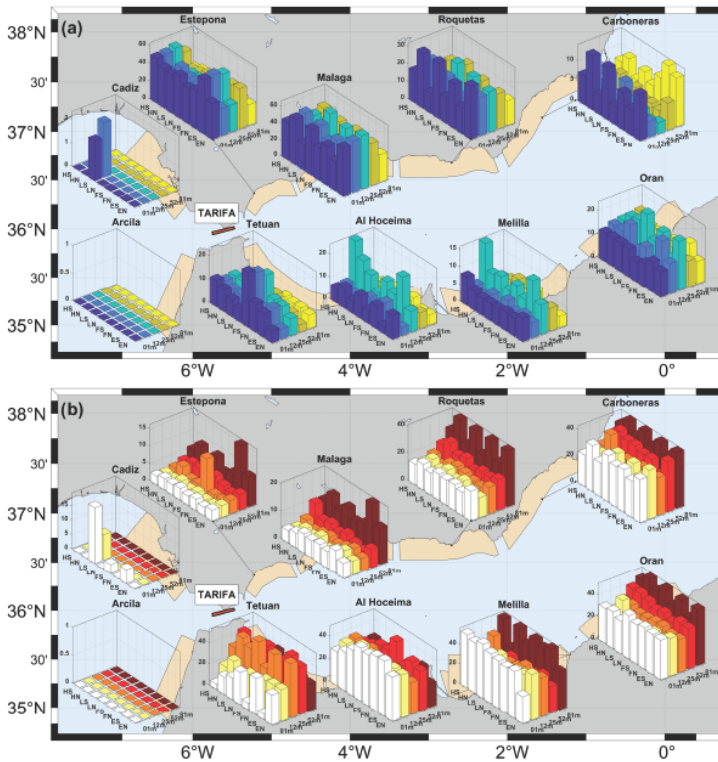


**FIGURE 6** (a) Diagrams of MPOp (%) in each landing area, averaged over the four replicas of the ELS released at Tarifa box (red rectangle) for the 40 combinations of spatial (5 depths, Y-axis) and temporal (8 tidal conditions, X-axis; see acronym code in Figure 4) conditions. (b) Same as panel (a) for ToMC (days). Notice the changing Z-axis scale in the different diagrams of both panels

Increases with depth (Figure 7a, yellow bars), a behavior not shared so clearly by the southern areas. Such increase raises new questions because, intuitively, connectivity should be greater at the surface, where the WAG and EAG hold stronger currents. But high velocities also entail more instabilities and turbulence that increase ELS scattering toward the interior of the Alboran basin. Velocity reduction with depth would diminish the scattering and improve the chances for ELS to arrive to farther landing areas. Consistent with this conceptual model is the fact that MPOps at 81 m depth tend to reach absolute maxima during neap tides in Estepona area (Figure 7a).

ToMC also shows unexpected behavior. The most striking one is the large values in Tetuan area considering its proximity to the

releasing box. ToMCs are even noticeably larger than those obtained for the Tarifa releasing box, particularly during spring tides (compare Figures 6b and 7b). Particles released in Tarifa box reach Tetuan area much faster than those released in Tanger-Med under the same initial conditions. It is particularly true during spring tides. But the number of particles that reaches the area is appreciably less when they come from Tarifa box (Figure 6a,b). Same conclusions apply to the other areas, the northern ones showing less ToMC than the southern ones systematically. This would confirm the aforementioned slightly better connectivity that this releasing box establishes with the north part of the AS.

Regarding the areas in the Gulf of Cadiz, Figures 6 and 7 show very poor connectivity for both releasing boxes that only occurs in

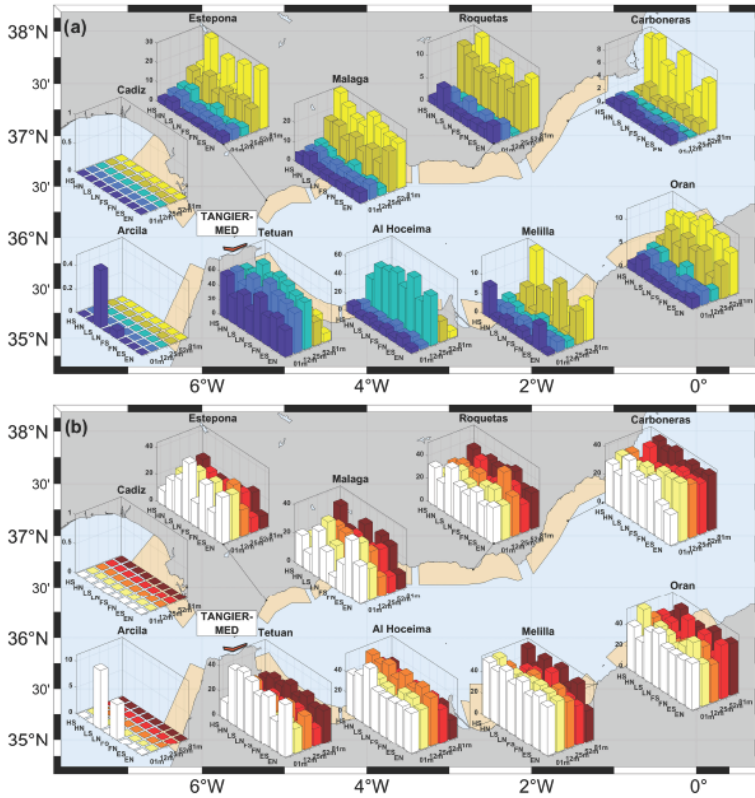


FIGURE 7 Same as Figure 6 for Tangier-Med releasing box, indicated by the red polygon

zonal direction (Tarifa-Cadiz, Tangier-Med-Arcila), not north-to-south (Tarifa-Arcila, Tangier-Med-Cadiz). It is almost uniquely met under LS initial conditions, that is, particles released at low water in spring tides. They are the most favorable conditions, as low water is the moment when barotropic tidal current reverses towards the Atlantic and spring tide enhances its intensity. The low-to-high semicycle that follows maintain relatively favorable conditions for westward transport, which causes the very low, though not null, MPoP found in those areas.

Previous discussion indicates that the dispersal of ELS is highly sensitive to the tidal phase and depth. Tidal phase and, more specifically, tidal strength related to the fortnightly spring-neap cycle is relevant for Tarifa releasing box (Figure 6) while spawning depth causes higher variability in the Tangier-Med case (Figure 7). Both initial

conditions are examined in more detail for selected cases of study in the following sections.

### 3.3 | Tide dependence: A case of study in the northern shore

In addition to the tidal variability that can be inferred from the abundant information in the diagrams of Figures 6 and 7, part of which has been already commented, this section addresses an illustrative case of study to assess the tidal influence. The specific instant of spawning in a given semidiurnal cycle (tidal phase) affects the initial ELS dispersion trajectories at the very beginning of the experiment, as it depends on

13491519, 2022, 4, Downloaded from https://onlinelibrary.wiley.com/doi/10.1111/fisg.12503 by Chon-Chanchoo, Wiley Online Library on [08/03/2023]. See the Terms and Conditions (https://onlinelibrary.wiley.com/terms-and-conditions) on Wiley Online Library for rules of use; OA articles are governed by the applicable Creative Commons License

the direction of the instantaneous velocity at that time. Its importance, however, fades out shortly after because of its short time scale that implies reduced Lagrangian correlation scales (Taylor, 1922), leaving only the effect of the spring-neap intensity. It mostly determines the final evolution of ELS dispersion in the middle-long term, as it is demonstrated in the following case of study that involves Tarifa box and Estepona and Malaga landing areas in the north coast.

Figure 8 shows that the dispersion of ELSs released in Tarifa that induces the AJ in spring tide is greater than in neap tide (see inset) because of stronger tidal currents. When ELSs enter the AS in spring tide, the augmented scattering allows particles to reach the nearer landing areas directly, whereas particles follow the farther-from-shore AJ trajectory in neap tides (inset of Figure 8). As a result, particle concentration in Estepona is much higher in spring tide (Figure 8, solid lines). The deflection to the south of blue lines in the inset also illustrates the already discussed result of enhanced MPoP in Tetuan area in spring tides (Figure 6a). The progressive decrease of connectivity from HS to FS in spring-tide experiments (solid lines in left panel of Figure 8) follows the fact that eastward velocity reaches larger values during ebb tide (from HS to LS, peaking at ES) and a minimum at FS. Notice, however, that these differences are less than the ones observed between spring and neap tides (compare solid and dashed lines in this panel). It confirms the fact that tidal strength is more influential than tidal phase, what is further supported by the fortnightly modulation of ToMC in this area, with systematically shorter times in spring tides (Figure 6b).

The opposite situation is seen in Malaga area (Figure 8, right panel), where particle percentages in neap tides is almost twice than in spring tides. Moreover, as mentioned previously, ToMCs are greater in spring tides (Figure 6b). Inset in Figure 8 helps to explain these facts: during neap tides, a good fraction of trajectories invades directly the landing area (red lines), with reduced dispersion seaward. In spring tide, many particles arrive after having undergone some recirculation, a process that takes longer and results in greater ToMC, as discussed in Section 3.2.1. Also, more particles are scattered seaward, reducing the number of particles that reach the area. This behavior is shared by Roquetas and Carboneras landing areas to the east, confirming the better connectivity efficiency during neap tides (Figure 6).

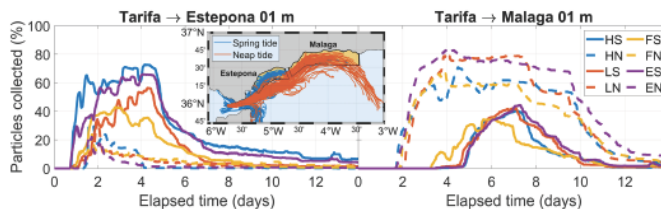
### 3.4 | Depth dependence

Figure 6 and Figure 7 show that, on average, MPoP tends to increase with depth in all landing areas and for all releasing boxes and, simultaneously, ToMC tends to be shorter. On the other hand, the present uncertainty on the actual spawning depth of the blackspot seabream along with the marked baroclinity of the exchange through the SoG raises the question of whether the so far ignored westward connectivity gains prominence for hypothetical deeper layers of spawning. Both questions are addressed next.

#### 3.4.1 | A case study of south-to-north connectivity as function of depth

Figure 7a shows a rather clear increase of MPoP with depth in all landing areas of the north coast for particles released in Tangier-Med box. For Estepona area, this depth dependence is concomitant with the spring-neap fortnightly modulation. Overall, the influence of depth on the connectivity is less marked than that associated to tides and does not exhibit a regular pattern. Nevertheless, the diminution of the AJ intensity with depth allows for establishing a rough analogy between releasing depth and strength of the tide. For a given tidal condition, the patterns associated with releasing at the surface would differ from those at depth in a similar way to how patterns produced during spring tides differ from neap tides for a given depth.

Figure 9 illustrates the connectivity between Tangier-Med box and Estepona landing area under HN initial conditions (release at high water in neap tides). The larger surface current scatters more particles than the diminished current at 81 m depth, resembling the pattern observed in the case of spring against neap tides in the previous discussion. As a result, arrival time of particles released at surface levels ( $z \leq 25$  m) in Tangier-Med box is noticeably shorter (~4 days) than that of particles released at 25 m (ToMC ~7 days) or 81 m (ToMC ~15 days), and the chance of arrival is notoriously reduced (MPoP of 17% for  $z \leq 25$  m, which increases to 32% at 52 m and to 78% at 81 m, see also Figure 7a). As the depth increases, ELSs follow smoothed trajectories with reduced dispersion, which improves not



**FIGURE 8** Time series of percentage of particles released at the surface in Tarifa releasing box collected in Estepona (left panel) and Malaga (right panel) for all tidal combinations discussed in text (see legend). The inset shows trajectories for the whole combination of phases in spring (blue lines) and neap (red lines) tides during the first 6 days after the release



**FIGURE 9** Time series of percentage of particles released in Tangier-Med releasing box under HN conditions and collected in Estepona landing area for the five depths considered (1, 12, 25, 52, and 81 m). Inset map shows trajectories for surface and 81 m depth spawning levels after 30 days of simulation using the same color code as in the main panel

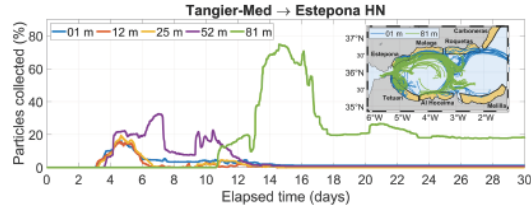
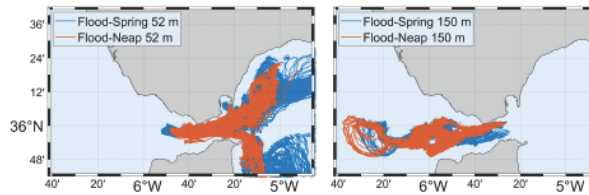


**FIGURE 10** ELS trajectories after 3.5 days of simulation for particles released in Tarifa box at 52 m (left panel) and 150 m (right panel) in case of FS (blue lines) and FN (orange lines) initial conditions



only the chance for more particles to arrive but also for them to arrive further. The behavior, which can be applied to the other areas in the north coast, is similar to that described in neap tides for the connectivity Tarifa-Málaga.

### 3.4.2 | A sensitivity analysis on spawning depth in the SoG

The effect of depth on connectivity patterns, and its interaction with tide in the case of this species, raises the question of whether or not the species has adapted its life cycle to optimize the reproductive success. For instance, blackspot seabream should spawn at greater depths if the survival success relies on chances of reaching further landing areas (see previous section) with suitable nursery conditions. It represents a plausible method of colonization, which maximizes the population survival (Krueck et al., 2020). Selecting the highly dispersive environment of the SoG as spawning grounds almost rejects the hypothesis that this species attempts to maximize self-recruitment as observed in other species (e.g., European hake; Hidalgo et al., 2019). Since the SoG holds a permanent two-way exchange, depth results are critical to determine the direction of the ELS dispersion. At greater depths than those considered so far in the main study, eggs would be advected toward the Atlantic Ocean by the Mediterranean undercurrent and the connectivity with landing areas of the AS be drastically reduced.

Given the degree of uncertainty about the range of plausible spawning depths, it is worth exploring that possibility with the model. To this aim, a spawning depth of 150 m has been selected in Tarifa and Tangier-Med boxes and initial conditions of ES, EN, FS, and FN have been then applied.

Figure 10 shows the trajectories of particles released at 52 and 150 m under identical initial conditions of maximum westward tidal current at spring (FS) and neap (FN) tides. In the case of 52 m depth, particles make small incursions to the west transported by the flood, west-going tidal current that overcomes the average eastward inflow during short intervals. After this otherwise brief current reversal, particles enter the AS and remain there following trajectories similar to those depicted in the previous section. At the deeper layer of 150 m, however, flood tidal current increases the Mediterranean undercurrent extent at this depth and ELSs will spread westwards, with no particles entering the AS. Therefore, Atlantic (Cadiz and Arcila) landing areas are accessible as far as the direction of propagation is concerned. However, both landing areas are shallower than 100 m, whereas ELS propagates at 150 m. Unless vertical and onshore motions occur, the connectivity with the selected Atlantic landing areas is unfeasible.

The western half of the SoG is a well-known mixing area with large vertical motions driven by the amazing internal tide generated by topographic interaction (García-Lafuente et al., 2000, 2013; Wesson & Gregg, 1994). Such turbulent mixing is a potential mechanism to bring particles to shallower layers, in a similar manner as it does the westerly inducing upwelling and turbulence in the Gulf of Cadiz (Navarro et al., 2011; Sánchez Gamido et al., 2015). All of them can modify the horizontal depth of ELS advection but does not necessarily imply shoreward advection, which should be achieved by other concomitant processes. Recent scientific surveys have detected ELSs of the species in the Atlantic region, but their relative abundances are noticeably lower than those reported in the Alboran basin: 0.46 larvae  $10 \text{ m}^{-2}$  ( $\pm 1.39 \text{ SD}$ ) in the Atlantic region versus 2.03 larvae  $10 \text{ m}^{-2}$  (4.86 SD) in the northwest Alboran areas (maximum abundances of 5 and 15 larvae  $10 \text{ m}^{-2}$ , respectively; J.M. Rodríguez, Pers. Comm.).

These observational and numerical results keep open the feasibility of the Atlantic connectivity, which requires further studies to give an adequate answer. Observational research on the spawning behavior is also needed to elucidate the question of the spawning depth range of the spedes. From a modelling perspective, new experiments are necessary to assess how different larval behavior (vertical migration) and hydrodynamic secondary patterns (vertical velocity ignored in this study) affect the dispersion patterns and survival probabilities of ELS under different scenarios.

### 3.5 | A sensitivity analysis on PLD

From a biological point of view, time of arrival of ELS at a given landing area only makes sense if it is less than the assumed PLD of the species (Shanks, 2009). In order to investigate the dependence of connectivity on PLD, MPoPs between releasing boxes and landing areas have been re-calculated for PLD windows of 15 and 30 days. The new values of MPoP (denoted by  $C_n$ ,  $n = 15, 30$ , in the following discussion), have been compared with those of the original PLD window of 60 days ( $C_{60}$ ) to obtain a metric  $\Delta_n$  defined as the ratio:

$$\Delta_n = \frac{C_n}{C_{60}} \cdot 100$$

in order to assess the differences.

Table 3 summarizes the results of this analysis and confirms the fact that the MPoP is constrained by the available time of arrival, that is, the assumed PLD. In the landing areas nearest to the releasing boxes (i.e., Tangier-Med/Tangier - Tetuan, Tarifa - Estepora) arrival times keep on being short and maximum ratios obtained with different PLDs (15, 30, 60 days) are little altered (high values of  $\Delta_n$ ,  $n = 15, 30$ ). On the contrary, in the furthest landing areas (Carboneras, Melilla, or Oran), large MPoPs are only obtained after completing a long path that requires dilated elapsed times, which makes the result sensitive to the assumed PLD. It results in substantial discrepancies (low ratio values). Extreme cases are provided by Tarifa-Carboneras or Tangier-Med/Tangier-Melilla, which shows ratios of  $\Delta_{15}$  less than 1%.

Landing area		MPoP differences (%)					
		Tarifa		Tangier-Med		Tangier	
		$\Delta_{15}$	$\Delta_{30}$	$\Delta_{15}$	$\Delta_{30}$	$\Delta_{15}$	$\Delta_{30}$
Northern Alboran	Estepona	77.69	92.79	49.65	83.79	50.22	84.40
	Malaga	62.02	94.37	62.49	94.20	63.20	95.60
	Roquetas	27.16	72.97	40.35	80.40	37.96	79.02
	Carboneras	0.92	36.55	2.290	31.31	1.610	26.19
Southern Alboran	Tetuan	89.90	95.92	96.10	98.60	95.56	99.16
	Al Hoceima	68.57	89.70	74.89	88.01	74.14	84.50
	Melilla	2.77	41.34	0.56	28.40	0.41	34.30
	Oran	7.44	55.11	3.59	61.64	1.47	60.07

Note: Cadiz and Ardia have been excluded because of its low representativeness.

The range of variation of the MPoPs recalls the need of improving the knowledge about the blackspot seabream life cycle, particularly PLD.

### 3.6 | Release time dependency (replicas)

To prove the representativeness and reliability of the Lagrangian particle tracking experiments, the uncertainty of each single run has been assessed by means of four replicas of the same combinations of semi-diurnal tide and depth conditions during four fortnightly cycles. Despite the same initial conditions with respect to the releasing time, the overall situation is not exactly the same in the replicas. This is so because the four spring-neap tidal cycles considered comprises the monthly cycle arising from the modulation of the semidiurnal constituents  $M_2$  and  $N_2$ , responsible for the greater similarity of alternate than contiguous spring cycles. In addition, subinertial meteorologically induced fluctuations due to atmospheric pressure and wind variations change from one replica to the other. The unavoidably, yet small, difference of the initial conditions of the replicas lead to concomitant differences in the outputs (not shown for the sake of clarity) and allows for assessing the variability of each experiment by means of the standard deviation of the four replicas. The averaged standard deviation of the whole pool of experiments is ~8%, which is approximately the same value obtained by comparing scenarios of different tidal phases but the same tidal strength. If the metric is used to compare spring and neap tidal scenarios (different tidal strength), the averaged standard deviation is ~30%. Therefore, subinertial variability and lower frequency tidal modulations could account for approximately one quarter of the variability of the fortnightly tidal cycle, which has been shown to be the prevailing factor for connectivity.

### 3.7 | Implications for the species assessment and management

Transboundary fish stock management is based in the cooperation and collaboration among countries to assess shared resources status and regulate harvest according to common measures and controls or

TABLE 3 Differences of MPoP computed using PLD windows of 60 and 30 days ( $\Delta_{30}$  column) and 60 and 15 days ( $\Delta_{15}$  column) for the three releasing boxes and the Alboran Sea landing areas

joint decision-making. However, to build an effective management framework, a solid scientific basis is required. The present study provides this basis to potentially improve the assessment and management of this species harvested by Moroccan and Spanish fleets, while we acknowledge that further work is needed. First, it provides evidence of the differential role of different spawning grounds in the AS, which could be useful in the future if the spatial dynamics is implemented in the stock assessment models and procedures (e.g., Goethel & Berger, 2017; Punt, 2019). While the results of the study point at independent dispersal and connectivity patterns of north and south Strait spawning grounds due to the role of the AJ, they do not imply stock differentiation consistent with recent genetic studies (Spiga, 2020), but different spawning locations, which is an important element to be considered in spatial stock structure approaches. Second, in terms of spatial management and potential spatiotemporal closures already applied to other Mediterranean species (Regulation [EU] 2019/1022 of the European Parliament and of the Council of June 20, 2019, OJEU L172/1 and GFCM Recomm. GFCM/42/2018/5), the study facilitates information of the role of the spawning sites investigated, and also the interaction with depth and tidal regime that could potentially lead to seasonal or, even, short term (i.e., attending to tidal phase) fisheries closure. The information made available here is relevant for the ongoing process for the establishment of a specific joint (Spain and Morocco) management plan for blackspot seabream in the SoG within the framework of GFCM (2021). Notwithstanding, further studies are needed as it is not yet clear whether the spawning strategy of the species attempts to minimize dispersal time, maximize dispersal distance, or even a more complex trade-off between both. The interpretation and implications of the results presented in this study can be certainly different attending to the species strategy. The role of other important larval traits not included in this study requires also further research.

#### 4 | SUMMARY AND FUTURE WORKS

The differences observed in the ELS connectivity patterns are mainly caused by the geographical location of the spawning areas in the SoG (north shore versus south shore). From a hydrodynamic perspective, the mean circulation patterns favor the zonal (west-to-east) connectivity. Particles released in the northern margin of the Strait are mostly registered in the northern areas of the AS, while particles released in the south are collected in the southern shores of the AS. Thus, the eastward transport linked to the AJ entering the Alboran basin appears as the main mechanism of connectivity. On the other hand, meridional connectivity (north-to-south, south-to-north) is hampered by the very AJ that is a potential hydrodynamic barrier (García-Lafuente, Sánchez-Garrido, et al., 2021). Overcoming this obstacle depends on the stability of the mean patterns of circulation of the SoG-AS system and its evolution. Non-geostrophic motions, instabilities associated with the WAG-AJ collapse (García-Lafuente et al., 1998; García-Lafuente, Sánchez-Garrido, et al., 2021; Sánchez-Garrido et al., 2013) or the AJ meandering (García-Lafuente &

Delgado, 2004) or, even, the WAG or EAG themselves can entail occasional meridional ELS transports. For instance, the study shows that ELSs released in Tangier-Med box are more susceptible to latitudinal (south-to-north) migration. Apparently, Tetuan area in the south exhibits characteristics of particle concentration/retention zone related to the existence of a small cyclonic eddy between the African coast and the WAG (Figure 1). Particle transfer from the eddy to the north-flowing western rim of gyre is practicable, after which particles reach the northern areas without impediment. This process impairs west-to-east connectivity in the south coast, which is therefore less efficient than in the north coast (compare Figures 6a and 7a). Another example is provided by the EAG, whose eastern edge can transport particles from the north to the south. This process makes Oran landing area be connected with Tarifa releasing box in the north better than with Tangier-Med in the south, despite being in the same coast (Table 2).

Atlantic, that is, east-to-west, connectivity at surface layers is prevented by the AJ. But it does not have to be so at greater depths where the Mediterranean undercurrent flows. In a hypothetical situation of deeper spawning (150 m), the model shows ELS transport towards the Atlantic Ocean exclusively, which opens the possibility of connection with landing areas in the Gulf of Cadiz (Cadiz, Arcila). However, achieving a successful connectivity with Atlantic landing areas requires additional processes to carry the ELS to shallower levels. Enhanced tidal mixing and turbulence occurring in the western part of the SoG, or wind-inducing upwelling in the Gulf of Cadiz are candidate processes.

Tides in the neighborhood of the SoG are influential. Variability due to tidal forcing is especially noticeable in terms of fortnightly modulation. In the landing areas closer to the spawning boxes (Estepona in the north, Tetuan in the south), connectivity is more efficient in spring tides. In these conditions, north-to-south connectivity is achieved by direct advection of ELSs from the releasing box of Tarifa to Tetuan landing area (Figure 6; see also inset in Figure 8). During neap tide, on the contrary, particles suffer less scattering and increase chances of reaching further landing areas. Overall, tidal conditions depict two different mechanisms: spring tides tend to favor connectivity (increase MPoP) by the direct advection promoted by the increased energy of the flows. It applies to landing areas adjacent to the releasing boxes in both, west-to-east and north-to-south, directions and yields relatively small ToMC. On the contrary, in neap tides connectivity is mainly achieved by the mean circulation of the AS, connecting far away landing areas with releasing boxes after considerably large ToMC (Figures 6 and 7). This pattern is consistent with previous studies on connectivity analysis in the region (Muñoz et al., 2015), who used altimetry-derived geostrophic currents, a product that removes tidal contribution during the data-processing. The circulation emerging from such an approach would be more similar to the pattern of neap tides (less tidal variability) inferred from the numerical outputs.

The depth of spawning also results in different patterns of conductivity. Obviously, the greatest differences arise when comparing patterns associated with spawning at depths immersed in one or

another layer of the baroclinic exchange, as illustrated by the case of 150 m releasing depth already discussed. But there are still differences even if spawning takes place at different depths within the very surface layer (Figures 6a and 7a). The origin of the differences has been ascribed to the diminution of the velocity of the current with depth. At shallow depths, ELSs are scattered more actively by the more energetic current, recalling the effect of the spring tide. At deeper layers, the main circulation weakens and allows ELS to move less chaotically and reach greater distances. The behavior resembles the pattern observed during neap tides, when far away areas are connected to the releasing boxes. Such connection may demand high ToMCs (Table 2, Figures 6b and 7b) which represent a potential constrain for connectivity, since the time must be less than PLD for obvious reasons. The need of improving the knowledge of blackspot seabream ontogeny, particularly the possible range of variation of its PLD, becomes crucial to achieve an optimization of the fishery management. As indicated in Falletta et al. (2018), this factor strongly influences the larval dispersal patterns and connectivity among adult subpopulations whose calculation is fully based in passive drifting larvae.

Larval dispersal studies rely on the dependence of numerous biological and physical key factors, which must be considered to determine broad-scale ecological connectivity. Egg buoyancy, vertical migrations, and the possible influences on the ELS fate of other biogeochemical features (Wor et al., 2017) are sensible information that is not yet well determined for the studied species (Gil, 2006), nor incorporated to the model. The 150 m depth case study addressed in this study illustrates how drastically different the results of connectivity can be. Even in the case that depths were restricted to the upper 100 m, the depth range mainly explored in this study (which results in connectivity patterns involving the AS exclusively), vertical motions in the SoG as well as other processes not considered, such as the egg buoyancy or the diel vertical cycle, can displace ELSs to greater depths. If so, part of the spawning products will go beyond the critical depth for which Atlantic connectivity is feasible. Covering these complexities is crucial to be able to implement fully 3D approaches, and, consequently, attain a more reliable vision of population dynamics of blackspot seabream and ultimately transfer this new knowledge to improve the management of this overexploited species. Further studies are needed as it is not yet clear whether the spawning strategy of the species attempts to minimize dispersal time, maximize dispersal distance, or even a more complex trade-off between both. The interpretation and implications of the results presented in this study can be certainly different attending to the species strategy. The role of other important larval traits not included in this study requires also further research that may help decision-makers to establish biological rest periods that lead to maximize connectivity and sustainability. All in all, improving our knowledge on the interaction of this species with its physical environment is a key issue in the efforts towards rebuilding the fishery target population until its maximum sustainable yield.

#### ACKNOWLEDGMENTS

This work was partially funded by the FAO Project: CopeMed phase II "Coordination to Support Fisheries Management in the Western and

Central Mediterranean" and the General Fisheries Commission of the Mediterranean GFCM, both with the financial support of the Directorate-General for Maritime Affairs and Fisheries of the European Commission (DG-MARE) and the Spanish Ministry of Agriculture, Fishery and Food. Funding for open access charge was provided by Universidad de Málaga/CBUA.

#### CONFLICT OF INTEREST

I hereby certify that there is no actual or potential conflict of interest in relation to this article.

#### AUTHOR CONTRIBUTION

IN, SS and JGL wrote the bulk of the paper. JGH contributed in the paper regarding the biological aspects of the blackspot seabream. MH and PH provided the fisheries arguments supporting the larvae dispersal patterns. IN, SS and JCSG designed and carried out the modeling experiments. All authors participated and contributed in the interpretation, discussion and revision of the manuscript.

#### AUTHOR DISCLAIMER

The views expressed in this publication are those of the author(s) and do not necessarily reflect the views or policies of the Food and Agriculture Organization of the United Nations.

#### DATA AVAILABILITY STATEMENT

The data that support the findings of this study are available from the corresponding author upon reasonable request.

#### ORCID

Irene Nadal  <https://orcid.org/0000-0002-1642-1606>

Simone Sammartino  <https://orcid.org/0000-0001-7052-5468>

Jesús García-Lafuente  <https://orcid.org/0000-0001-7816-576X>

José C. Sánchez Garrido  <https://orcid.org/0000-0003-1524-7391>

Juan Gil-Herrera  <https://orcid.org/0000-0001-8940-5749>

Manuel Hidalgo  <https://orcid.org/0000-0002-3494-9658>

#### REFERENCES

- Albérola, C., Rousseau, S., Millot, C., Astraldi, M., Font, J., García-Lafuente, J., Gasparini, G. P., Send, U., & Vangrishesheim, A. (1995). Tidal currents in the Western Mediterranean Sea. *Oceanologia Acta*, 18(2), 273–284.
- Alcaraz, J. L., Carrasco, J. F., Ullera, E. M., Menéndez, M., Ortea, J. A., & Vizcaino, A. (1987). *Aportación al estudio del besugo en el Principado de Asturias*. Recursos pesqueros de Asturias, 4. Servicio de publicaciones del Principado de Asturias.
- Álvarez Fanjul, E., Pérez Gómez, B., & Sánchez-Arévalo, I. R. (2001). Nivmar: A storm surge forecasting system for Spanish Waters'. 65(51), 145–154. <https://doi.org/10.3989/scimar.2001.65s1145>
- Báez, J. C., Macías, D., de Castro, M., Gómez-Gesteira, M., Gimeno, L., & Real, R. (2014). Assessing the response of exploited marine populations in a context of rapid climate change: The case of blackspot seabream from the Strait of Gibraltar. *Animal Biodiversity and Conservation*, 37(1), 35–47. <https://doi.org/10.32800/abc.2014.37.0035>
- Blagi, F., Gambaccini, S., & Zazzeta, M. (1998). Settlement and recruitment in fishes: The role of coastal areas. *The Italian Journal of Zoology*, 65-(Suppl), 269–274. <https://doi.org/10.1080/11250009809386831>



- Brünnich, M. T. (1768). *Ichthyologia Massiliensis, sistens piscium descriptiones eorumque apud incolos nomina. Accedunt Spolia Maris Adriatici. Hafniae et Lipsiae, i-xvi + 1-110*. In 2 parts: first as i-xvi + 1-84; 2<sup>nd</sup> as Spolia e Mari Adriatica reportata: 85-110, 49.
- Burgos, C., Gil, J., & del Olmo, L. A. (2013). The Spanish blackspot seabream (*Pagellus bogaraveo*) fishery in the Strait of Gibraltar: Spatial distribution and fishing effort derived from a small-scale GPRS/GSM based fisheries vessel monitoring system. *Aquatic Living Resources*, 26(4), 399-407. <https://doi.org/10.1051/alr/2013068>
- CopeMed II. (2017). Report of the CopeMed II Workshop on methodologies for the identification of stock units in the Alboran Sea, Alicante, Spain, 3-6 April 2017. CopeMed II Technical documents N° 46 (GCP/INT/028/SPA - GCP/INT/270/EC), Alicante, 58 pp.
- CopeMed II. (2019). Report of the Mid-Term Workshop on TRANSBORAN project, "Transboundary population structure of sardine, European hake and blackspot seabream in the Alboran Sea and adjacent waters: a multidisciplinary approach" Malaga, Spain, 22-24 July 2019. CopeMed II Technical Documents N° 52 (GCP/INT/028/SPA - GCP/INT/270/EC), Málaga, 33 pp.
- Cowen, R. K., Paris, C. R., & Srinivasan, A. (2006). Scaling of connectivity in marine populations. *Science*, 311(5760), 522-527. <https://doi.org/10.1126/science.1122039>
- Cowen, R. K., & Sponaugle, S. (2009). Larval dispersal and marine population connectivity. *Annual Review of Marine Science*, 1, 443-466. <https://doi.org/10.1146/annurev.marine.010908.163757>
- Crochet, E., Roberts, J., Lagabrielle, E., Obura, D., Petit, M., & Chabane, P. (2016). A model-based assessment of reef larvae dispersal in the Western Indian Ocean reveals regional connectivity patterns—Potential implications for conservation policies. *Regional Studies in Marine Science*, 7, 159-167. <https://doi.org/10.1016/j.rsma.2016.06.007>
- Desbrosses, P. (1932). La dorade commune (*Pagellus centrodontus*) et sa pêche. *Revue du Travail de L'Office Des Pêches Maritimes*, 5, 167-222.
- Dubois, M., Rossi, V., Ser-Giacomi, E., Arnaud-Haond, S., López, C., & Hernández-García, E. (2016). Large-scale connectivity and management of marine ecosystems. *Global Ecology and Biogeography*, 25, 503-515. <https://doi.org/10.1111/geb.12431>
- Faillat, R., Paris, C., & Ifrison, J.-O. (2018). Larval fish swimming behavior alters dispersal patterns from marine protected areas in the North-Western Mediterranean Sea. *Frontiers in Marine Science: Marine Ecosystem Ecology*, 5, 97. <https://doi.org/10.3389/fmars.2018.00097>
- Fiksen, Ø., Jørgensen, C., Kristiansen, T., Vikebø, F., & Huse, G. (2007). Linking behavioural ecology and oceanography: Larval behaviour determines growth, mortality and dispersal. *Marine Ecology: Progress Series*, 347, 195-205. <https://doi.org/10.3354/meps06978>
- Flexas, M. M., Gomis, D., Rutz, S., Pascual, A., & León, P. (2006). In situ and satellite observations of the eastward migration of the Western Alboran Sea Gyre. *Progress in Oceanography*, 70, 486-509. <https://doi.org/10.1016/j.pocean.2006.03.017>
- Fogarty, M., & Botsford, L. (2007). Population connectivity and spatial management of marine fisheries. *Oceanography*, 20(3), 112-123. <https://doi.org/10.5670/oceanog.2007.34>
- Gamoyo, M., Obura, D., & Reason, C. (2019). Estimating connectivity through larval dispersal in the Western Indian Ocean. *Journal of Geophysical Research: Biogeosciences*, 124(8), 2446-2459. <https://doi.org/10.1029/2019JG005128>
- García-Lafuente, J., Alvarez, E., Vargas, J. M., & Ratsimandry, W. (2002). Subinertial variability in the flow through the strait of Gibraltar. *Journal of Geophysical Research*, 107(C10), 32.1-32.9. <https://doi.org/10.1029/2001JC001104>
- García-Lafuente, J., Bruque Pozas, E., Sánchez-Garrido, J. C., Sannino, G., & Sammartino, S. (2013). The interface mixing layer and the tidal dynamics at the eastern part of the Strait of Gibraltar. *Journal of Marine Systems*, 117-118, 31-42. <https://doi.org/10.1016/j.jmarsys.2013.02.014>
- García-Lafuente, J., Cano, N., Vargas, M., Rubin, J. P., & Guerra, A. (1998). Evolution of the Alboran Sea hydrographic structures during July 1993. *Deep-Sea Research*, 45, 39-65. [https://doi.org/10.1016/S0967-0637\(97\)00216-1](https://doi.org/10.1016/S0967-0637(97)00216-1)
- García-Lafuente, J., & Delgado, J. (2004). The meandering path of a drifter around the Western Alboran gyre. *Journal of Physical Oceanography*, 34(3), 685-692. <https://doi.org/10.1175/JPO316.1>
- García-Lafuente, J., Sammartino, S., Huertas, I. E., Flecha, S., Sánchez-Leal, R., Naranjo, C., Nadal, I., & Bellanco, M. J. (2021). Hotter and weaker Mediterranean outflow as a response to basin-wide alterations. *Frontiers in Marine Science*, 8, 613444. <https://doi.org/10.3389/fmars.2021.613444>
- García-Lafuente, J., Sánchez-Garrido, J. C., García, A., Hidalgo, M., Sammartino, S., & Laiz, R. (2021). Biophysical processes determining the connectivity of the Alboran Sea fish populations. In J. C. Báez, J. T. Vázquez, J. A. Caminas, & M. Malouli (Eds.), *Alboran Sea—Ecosystems and marine resources*. Springer Nature Switzerland AG. ISBN 978-3-030-65515-0. [https://doi.org/10.1007/978-3-030-65515-0\\_7\\_12](https://doi.org/10.1007/978-3-030-65515-0_7_12)
- García-Lafuente, J., Vargas, J. M., Plaza, F., Sarhan, T., Candela, J., & Bascheck, B. (2000). Tide at the eastern section of the Strait of Gibraltar. *Journal of Geophysical Research: Oceans*, 105(C6), 14197-14213. <https://doi.org/10.1029/2000JC90007>
- GFCEM. (2021). Report of the Working Group on Stock Assessment of Demersal species (WGSAD). General Fisheries Commission for the Mediterranean. Online, 18-30 January 2021.
- Gil, J. (2006). *Biología y pesca del voraz [Pagellus bogaraveo (Brünnich, 1768)] en el Estrecho de Gibraltar*. Ph.D. Universidad de Cádiz.
- Gil, J. (2010). Spanish information about the red seabream (*Pagellus bogaraveo*) fishery in the Strait of Gibraltar region. A CopeMed II contribution to the SRWG on shared demersal resources. Ad hoc scientific working group between Morocco and Spain on *Pagellus bogaraveo* in the Gibraltar Strait area (Málaga, Spain, 22 July, 2010). GCP/INT/028/SPA-GCP/INT/006/EC. CopeMed II Occasional Paper N° 2: 30 pp.
- Gil, J., Silva, L., & Sobrino, I. (2001). Results of two tagging surveys of red seabream [*Pagellus bogaraveo*, (Brünnich, 1768)] in the Spanish South Mediterranean region. *Thalassas*, 17(2), 43-46.
- Gil-Herrera, J., Gutiérrez-Estrada, J. C., Benchoucha, S., Pérez-Gil, J. L., Sanz-Fernández, V., el Arraf, S., Burgos, C., Malouli Khrissi, M., & Fariás, C. (2021). The Blackspot seabream fishery in the Strait of Gibraltar: Lessons and future perspectives of shared marine resource. In J. C. Báez, J. T. Vázquez, J. A. Caminas, & M. Malouli (Eds.), *Alboran Sea—Ecosystems and marine resources*. Springer Nature Switzerland AG. [https://doi.org/10.1007/978-3-030-65516-7\\_19](https://doi.org/10.1007/978-3-030-65516-7_19)
- Goethel, D. R., & Berger, A. M. (2017). Accounting for spatial complexities in the calculation of biological reference points: Effects of misdiagnosing population structure for stock status indicators. *Canadian Journal of Fisheries and Aquatic Sciences*, 74(11), 1878-1894. <https://doi.org/10.1139/cjfas-2016-0290>
- Hidalgo, M., Rossi, V., Monroy, P., Ser-Giacomi, E., Hernández-García, E., Gujjarro, B., Massutí, E., Alemany, F., Jadaud, A., Pérez, J. L., & Reglero, P. (2019). Accounting for ocean connectivity and hydroclimate in fish recruitment fluctuations within transboundary metapopulations. *Ecological Applications*, 29(5), e01913. <https://doi.org/10.1002/eap.1913>
- Krueck, N., Tremblay, L., Innes, D., & Ovenden, J. (2020). Ocean currents and the population genetic signature of fish migrations. *Ecology (Ecological Society of America)*, 101(3), e02967. <https://doi.org/10.1002/ecy.2967>
- Krug, H. M. (1994). *Biologia e avaliação do stock Açoreano de goraz, Pagellus bogaraveo*. Ph.D. Universidade dos Açores
- LaCasce, J. H. (2008). Statistics from Lagrangian observations. *Progress in Oceanography*, 77, 1-29. <https://doi.org/10.1016/j.pocean.2008.02.002>

- Lanob, F. (1974) *Projet Alboran, Etude hydrologique et dynamique de la Mer d'Alboran*, Tech. lep. 66, 39 pp., NATO, Brussels.
- Lorance, P. (2011) History and dynamics of the overexploitation of the blackspot sea bream (*Pagellus bogaraveo*) in the Bay of Biscay. *ICES Journal of Marine Science*, 68, 290–301. <https://doi.org/10.1093/icesjms/fsq072>
- Marshall, J., Adcroft, A., Hill, C., Perelman, L., & Heisey, C. (1997). A finite-volume, incompressible Navier Stokes model for studies of the ocean on parallel computers. *Journal of Geophysical Research: Oceans*, 102(C3), 5753–5766. <https://doi.org/10.1029/96JC02775>
- Marshall, J., Hill, C., Perelman, L., & Adcroft, A. (1997). Hydrostatic, quasi-hydrostatic and nonhydrostatic ocean modelling. *Journal of Geophysical Research: Oceans*, 102(C3), 5733–5752. <https://doi.org/10.1029/96JC02776>
- Mason, E., Ruiz, S., Bourdalle-Badie, R., García-Sotillo, M., & Pascual, A. (2019). Copernicus (CMEM5) operational model Intercomparison in the western Mediterranean Sea: Insights from an eddy trader. *Ocean Science Discussions*, 15, 1111–1131. <https://doi.org/10.5194/os-2018-169>
- Muñoz, M., Reul, A., Plaza, F., Gómez-Moreno, M. L., Vargas-Yáñez, M., Rodríguez, V., & Rodríguez, J. (2015). Implication of regionalization and connectivity analysis for marine spatial planning and coastal management in the Gulf of Cadiz and Alboran Sea. *Ocean and Coastal Management*, 118, 60–74. <https://doi.org/10.1016/j.ocecoaman.2015.04.011>
- Navarro, G., Gutiérrez, F. J., Díez-Minguito, M., Losada, M. A., & Ruiz, J. (2011). Temporal and spatial variability in the Guadalquivir estuary: A challenge for real-time telemetry. *Ocean Dynamics*, 61, 753–765. <https://doi.org/10.1007/s10236-011-0379-6>
- Nicolle, A., Dumas, F., Foveau, A., Foucher, E., & Thiébaud, E. (2013). Modelling larval dispersal of the king scallop (*Pecten maximus*) in the English Channel: Examples from the bay of Saint-Brieuc and the bay of Seine. *Ocean Dynamics*, 63, 661–678. <https://doi.org/10.1007/s10236-013-0617-1>
- Nicolle, A., Moitzié, R., Ogor, J., Dumas, F., Foveau, A., Foucher, E., & Thiébaud, E. (2017). Modelling larval dispersal of *Pecten maximus* in the English Channel: A tool for the spatial management of the stocks. *ICES Journal of Marine Science*, 74(6), 1812–1825. <https://doi.org/10.1093/icesjms/fsw207>
- Olivier, R. (1928). Poissons de chalut. La dorade (*Pagellus centrodontus*) (Resume pratique de nos connaissances sur ce poisson). *Rev. Trav. de l'Off. Peches Marit.*, Tome I, fasc. IV.
- Palacios-Abbrantes, J., Reygondeau, G., Wabnitz, C. C., & Cheung, W. W. (2020). The transboundary nature of the worlds exploited marine species. *Scientific Reports*, 10(1), 1–12. <https://doi.org/10.1038/s41598-020-74644-2>
- Parrilla, G., & Kinder, T. H. (1987). The physical oceanography of the Alboran Sea. [Rep]. In *Meteorology and Oceanography*, 40 (Vol. 1) (pp. 143–184). *Oceanogr. Group Div. of Applied Sciences*, Harvard Univ.
- Peleteiro, J. B., Olmedo, M., Gómez, C., & Álvarez-Blázquez, B. (1997). Study of reproduction in captivity of black-spot sea bream (*Pagellus bogaraveo*). Embryonic development and consumption of vitelline sac. *ICES C.M.* 1997/HH: 19
- Pineda, J., Hare, J., & Sponaugle, S. (2007). Larval transport and dispersal in the coastal ocean and consequences for population connectivity. *Oceanography Society*, 20(3), 22–39. <https://doi.org/10.5670/oceanog.2007.27>
- Pinho, M. R., Diogo, H., Carvalho, J., & Pereira, J. G. (2014). Harvesting juveniles of red (blackspot) seabream (*Pagellus bogaraveo* B.) in the Azores: Biological implications, management and life cycle considerations. *ICES Journal of Marine Science*, 71(9), 2448–2456. <https://doi.org/10.1093/icesjms/fst089>
- Pinsky, M. L., Reygondeau, G., Caddell, R., Palacios-Abbrantes, J., Spijkers, J., & Cheung, W. W. (2018). Preparing ocean governance for species on the move. *Science*, 360(6394), 1189–1191. <https://doi.org/10.1126/science.aat2360>
- Punt, A. (2019). Spatial stock assessment methods: A viewpoint on current issues and assumptions. *Fisheries Research*, 213, 132–143. <https://doi.org/10.1016/j.fishres.2019.01.014>
- Rodríguez, J. M., Barton, E. D., Eve, L., & Hernandez-Leon, S. (2001). Mesozooplankton and ichthyoplankton distribution around Gran Canaria, an oceanic island in the NE Atlantic. *Deep Sea Research, Part I*, 48(10), 2161–2183. [https://doi.org/10.1016/S0967-0637\(01\)00013-9](https://doi.org/10.1016/S0967-0637(01)00013-9)
- Rossi, V., Ser-Giacomi, E., López, C., & Hernández-García, E. (2014). Hydrodynamic provinces and oceanic connectivity from a transport network help designing marine reserves. *Geophysical Research Letters*, 41(8), 2883–2891. <https://doi.org/10.1002/2014GL059540>
- Ruti, P. M., Somot, S., Giorgi, F., Dubois, C., Flaounas, E., Obermann, A., Dell'Aquila, A., Pisacane, G., Harzallah, A., Lombardi, E., Ahrens, B., Akhtar, N., Alias, A., Arsouze, T., Aznar, R., Bastin, S., Bartholy, J., Béranger, K., Beuvier, J., ... Vervatis, V. (2016). Med-CORDEX Initiative for Mediterranean climate studies. *Bulletin of the American Meteorological Society*, 97(7), 1187–1208. <https://doi.org/10.1175/BAMS-D-14-00176.1>
- Sakina-Dorothea, A., Pascal, L., & Éric T. (2010). How does the connectivity between populations mediate range limits of marine invertebrates? A case study of larval dispersal between the Bay of Biscay and the English Channel (North-East Atlantic). *Progress in Oceanography*, 87(1–4), 18–36. <https://doi.org/10.1016/j.pocan.2010.09.022>
- Sammartino, S., García-Lafuente, J., Naranjo, C., Sánchez-Garrido, J. C., Sánchez-Leal, R., & Sánchez-Román, A. (2015). Ten years of marine current measurements in Espartel Sill, Strait of Gibraltar. *Journal of Geophysical Research: Oceans*, 120, 6309–6328. <https://doi.org/10.1002/2014JC010674>
- Sammartino, S., García-Lafuente, J., Sánchez Garrido, J. C., De los Santos, F. J., Álvarez Fanjul, E., Naranjo, C., Bruno, M., & Calero, C. (2014). Experimental and numerical characterization of harbor oscillations in the port of Málaga, Spain. *Continental Shelf Research*, 72, 34–36. <https://doi.org/10.1016/j.oceaneng.2014.06.011>
- Sammartino, S., Sánchez-Garrido, J. C., Naranjo, C., García-Lafuente, J., Rodríguez-Rubio, P., & Sotillo, M. (2018). Water renewal in semi-enclosed basins: A high resolution Lagrangian approach with application to the Bay of Algeciras, Strait of Gibraltar. *Limnology and Oceanography: Methods*, 16, 106–118. <https://doi.org/10.1002/lom3.10231>
- Sánchez, F. (1983). Biology and fishery of the red sea-bream (*Pagellus bogaraveo* B.) in VI, VII and VIII Subareas of ICES. *ICES C.M.* 1983/G:38.
- Sánchez Garrido, J. C., Naranjo, C., Macías, D., García-Lafuente, J., & Oguz, T. (2015). Modeling the impact of tidal flows on the biological productivity of the Alboran Sea. *Journal of Geophysical Research: Oceans*, 120(11), 7329–7345. <https://doi.org/10.1002/2015JC010885>
- Sánchez-Garrido, J. C., García-Lafuente, J., Álvarez Fanjul, E., García Sotillo, M., & de los Santos, F. J. (2013). What does cause the collapse of the Western Alboran Gyre? Results of an operational ocean model. *Progress in Oceanography*, 116, 142–153. <https://doi.org/10.1016/j.pocan.2013.07.002>
- Sánchez-Garrido, J. C., Sannino, G., Liberti, L., García-Lafuente, J., & Pratt, L. (2011). Numerical modeling of three-dimensional stratified tidal flow over Camarinal Sill, Strait of Gibraltar. *Journal of Geophysical Research*, 116, C12026. <https://doi.org/10.1029/2011JC007093>
- Sarhan, T., García-Lafuente, J., Vargas, M., Vargas, J. M., & Plaza, F. (2000). Upwelling mechanisms in the northwestern Alboran Sea. *Journal of Marine Systems*, 23(4), 317–331. [https://doi.org/10.1016/S0924-7963\(99\)00068-8](https://doi.org/10.1016/S0924-7963(99)00068-8)
- Shanks, A. L. (2009). Pelagic larval duration and dispersal distance revisited. *The Biological Bulletin*, 216(3), 373–385. <https://doi.org/10.1086/BBLv216n3p373>

- Sotillo, M. G., Cailleau, S., Lorente, P., Levier, B., Aznar, R., Reffray, G., Amo-Baladrón, A., Chanut, J., Benkiran, M., & Alvarez-Fanjul, E. (2015). The MyOcean IBI ocean forecast and reanalysis systems: Operational products and roadmap to the future Copernicus service. *Journal of Operational Oceanography*, 8(1), 63–79. <https://doi.org/10.1080/1755876X.2015.1014663>
- Spiga, M. (2020). A multidisciplinary approach to assess population structure of *Pagellus bogaraveo* for a correct delineation of stock units in the Alboran Sea. University of Bologna. MSc Thesis, 74 pp.
- Sundby, S., & Kristiansen, T. (2015). The principles of buoyancy in marine fish eggs and their vertical distributions across the World Oceans. *PLoS ONE*, 10(10), e0138821. <https://doi.org/10.1371/journal.pone.0138821>
- Sundelöf, A., & Jonsson, P. R. (2012). Larval dispersal and vertical migration behaviour—A simulation study for short dispersal times. *Marine Ecology*, 33, 183–193. <https://doi.org/10.1111/j.1439-0485.2011.00485>
- Taylor, G. I. (1922). Diffusion continuous movements. *Proceedings of the London Mathematical Society*, 20, 196–212. <https://doi.org/10.1112/plms/s2-20.1.196>
- Vargas-Yáñez, M., Plaza, F., García-Lafuente, J., Sarhan, T., Vargas, J. M., & Vélez-Belchi, P. (2002). About the seasonal variability of the Alboran Sea circulation. *Journal of Marine Systems*, 35(3–4), 229–248. [https://doi.org/10.1016/S0924-7963\(02\)00128-8](https://doi.org/10.1016/S0924-7963(02)00128-8)
- Virtanen, E. A., Mollanen, A., & Viitasalo, M. (2020). Marine connectivity in spatial conservation planning: Analogues from the terrestrial realm. *Landscape Ecology*, 35(5), 1021–1034. <https://doi.org/10.1007/s10980-020-00997-8>
- Wesson, J. C., & Gregg, M. C. (1994). Mixing at Camarinal Sill in the Strait of Gibraltar. *Journal of Geophysical Research: Oceans*, 99(C5), 9847–9878. <https://doi.org/10.1029/94JC00256>
- Wor, C., McAllister, M., Martell, S., & Taylor, N. (2017). A Lagrangian approach to model movement of migratory species. *Canadian Journal of Fisheries and Aquatic Sciences*, 75(8), 1203–1214. <https://doi.org/10.1139/cjfas-2017-0093>

## SUPPORTING INFORMATION

Additional supporting information may be found in the online version of the article at the publisher's website.

How to cite this article: Nadal, I., Sammartino, S., García-Lafuente, J., Sánchez Garrido, J. C., Gil-Herrera, J., Hidalgo, M., & Hernández, P. (2022). Hydrodynamic connectivity and dispersal patterns of a transboundary species (*Pagellus bogaraveo*) in the Strait of Gibraltar and adjacent basins. *Fisheries Oceanography*, 31(4), 384–401. <https://doi.org/10.1111/fog.12583>



## OPEN ACCESS

EDITED BY  
 Jorge Paramo,  
 University of Magdalena, Colombia

REVIEWED BY  
 Salvatore Aronica,  
 National Research Council (CNR), Italy  
 Adolf Konrad Stips,  
 European Commission, Italy

\*CORRESPONDENCE  
 Irene Nadal  
 ✉ irenenadal@ctima.uma.es

RECEIVED 22 December 2023  
 ACCEPTED 26 February 2024  
 PUBLISHED 02 April 2024

CITATION  
 Nadal I, Picciulin M, Falcieri FM,  
 García-Lafuente J, Sammartino S and  
 Ghezzi M (2024) Spatio-temporal  
 connectivity and dispersal seasonal  
 patterns in the Adriatic Sea using a  
 retention clock approach.  
*Front. Mar. Sci.* 11:1360077.  
 doi: 10.3389/fmars.2024.1360077

COPYRIGHT  
 © 2024 Nadal, Picciulin, Falcieri,  
 García-Lafuente, Sammartino and Ghezzi. This  
 is an open-access article distributed under the  
 terms of the [Creative Commons Attribution  
 License \(CC BY\)](https://creativecommons.org/licenses/by/4.0/). The use, distribution or  
 reproduction in other forums is permitted,  
 provided the original author(s) and the  
 copyright owner(s) are credited and that the  
 original publication in this journal is cited, in  
 accordance with accepted academic  
 practice. No use, distribution or reproduction  
 is permitted which does not comply with  
 these terms.

# Spatio-temporal connectivity and dispersal seasonal patterns in the Adriatic Sea using a retention clock approach

Irene Nadal<sup>1,2\*</sup>, Marta Picciulin<sup>3</sup>, Francesco M. Falcieri<sup>3</sup>,  
 Jesús García-Lafuente<sup>1,2</sup>, Simone Sammartino<sup>1,4</sup>  
 and Michol Ghezzi<sup>3</sup>

<sup>1</sup>Physical Oceanography Group, Department of Applied Physics II, University of Málaga, Málaga, Spain, <sup>2</sup>Instituto de Biotecnología y Desarrollo Azul (IBYDA), University of Málaga, Málaga, Spain, <sup>3</sup>National Research Council (CNR), Institute of Marine Science (ISMAR), Venice, Italy, <sup>4</sup>Instituto de Ingeniería Oceánica (IIO), University of Málaga, Málaga, Spain

Hydrodynamic features play a key role in determining the dispersal and connectivity of fish populations, especially in highly energetic areas determined by currents, river flow, and meteorologically induced fluctuations. Understanding how species interact with these physical processes is essential for managing vulnerable populations and identifying areas that require effective conservation efforts. This study examines the hydrodynamics that regulate connectivity in the Adriatic Sea, a shallow and semi-enclosed basin that is widely recognized as one of the most important areas in the Mediterranean Sea for protection. A high-resolution hydrodynamic model coupled with a lagrangian tracking module serves as the numerical tool. Lagrangian particles, representing eggs and larvae with typical biological characteristics of generic marine organisms inhabiting the region, are released throughout the basin at different times during a test year to identify the most likely pathways of individual dispersal. The temporal component of connectivity is highlighted using a previously developed retention clock matrix over different larval durations. Seasonality is a critical factor in dispersal, with greater variability and reduced efficiency in winter compared to summer. The potential implications of the results for improved assessment and management of high value marine species in the basin are discussed.

## KEYWORDS

Adriatic Sea, numerical modeling, hydrodynamic connectivity, dispersal patterns, Retention Clock Matrix



## 1 Introduction

In marine systems, the persistence and recovery of a population are influenced by the dispersal and transport processes of individuals within it, which are controlled by the hydrodynamic circulation of a given study area (Williams and Hastings, 2013). When complemented by favorable environmental conditions that support the survival of the dispersed organisms, this dynamic process gives rise to the concept of population connectivity, a phenomenon that encompasses the exchange of individuals within and between geographical subregions through the transport of water bodies (Cowen and Sponaugle, 2009; García-Lafuente et al., 2021). For most marine species, exchanges occur through the pelagic dispersal of early life stages, when eggs and developing larvae can be treated, at least to some degree, as plankton (Largier, 2003). However, circulation can still play a key role in the success of organisms at advanced developmental stages, by conditioning their settlement and dispersal in particular locations, or by influencing the reproductive stock, e. g., altering the spawning location and time (Ciannelli et al., 2014). Estimating these transport pathways is a necessary step towards understanding the regional functioning of pelagic ecosystems, as well as for marine ecosystem management, the design of marine protected areas (Lester et al., 2009; D'Agostini et al., 2015) and the optimization of vulnerable fisheries resources (Fogarty and Botsford, 2007; Gaines et al., 2010; Nadal et al., 2022), among others.

A key component to estimate hydrodynamic connectivity, this understood as the potential of a hydrodynamic field to connect different sub-areas through the exchange of its individuals (García-Lafuente et al., 2021), is the spatio-temporal context in which sub-populations are connected (Tremblé et al., 2012). To this aim, hydrodynamic numerical models have become robust tools capable of representing circulation features and, when coupled with appropriate mathematical approaches, effectively analyzing dispersal pathways by simulating the lagrangian transport of virtual particles (Van Sebille et al., 2018). This is particularly relevant for coastal environments, which normally are highly dynamic regions dominated by tides, upwelling or small-scale turbulence processes, harsh to study via observational methodologies (Pineda, 1991). Ideally, a numerical model of a continental shelf should capture these small-scale coastal features on a high-resolution grid (at least, 0.5-1 km horizontally), with accurate near-shore tidal and meteorological forcing implementation and satisfactory calibration and validation.

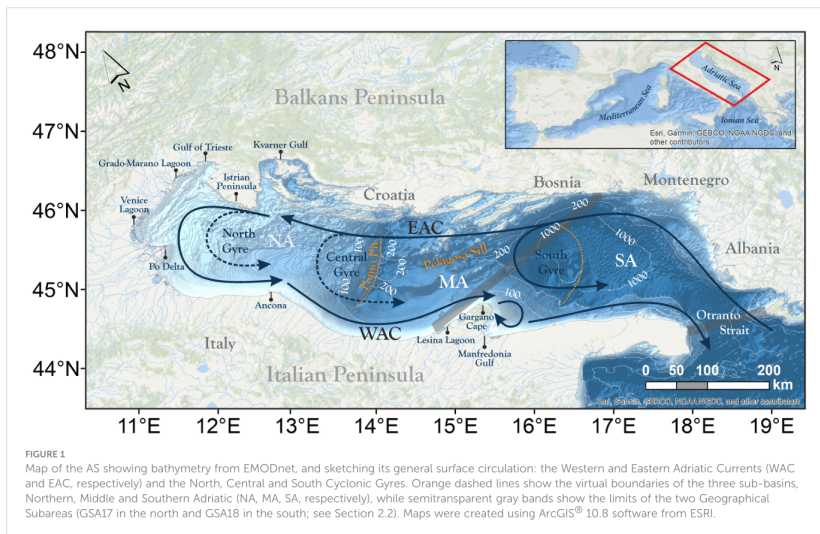
An example of such complex application with a strong linkage to its coastal system is found in the Adriatic Sea (AS hereafter), a marginal water body characterized by a peculiar topography, having a very shallow northern area gradually deepening towards the southeast, and by a large number of freshwater sources (Russo and Artegiani, 1996). This paper explores the role of AS hydrodynamic circulation in governing population connectivity and entails the understanding of key physical processes and temporal-scales controlling the drifting of individuals, including spawning, dispersal and final settlement. The relevance of each species-specific behavior within the hydrodynamic circulation of

the area makes every specific case study challenging. Thus, this study did not aim to replicate the behavior of any specific species, but rather focused on resolving the physical mechanisms controlling dispersal of passive elements, representing propagules of generic abundant species within the specified region. A high-resolution circulation model, already used in previous studies of this particular region, coupled to a lagrangian tracking module, is used as a numerical tool for the estimation of population connectivity and dispersal. A sophisticated concept introduced by Defne et al. (2016), consisting of a “retention clock” that highlights the evolution of source-sink connections through time, is employed to compare simultaneous spatio-temporal analysis of connectivity. The proposed methodological approach is applied on a tested year as a case of study.

The paper is organized as follows: Section 2 presents the hydrodynamic characteristics of the study area and the biodiversity of the region, including a list of ichthyofauna inhabiting the basin to which the results of our research may apply. The model framework used to represent the main circulation features of the AS and the lagrangian approach used to study the transport of virtual tracers, as well as the methods used to estimate connectivity from model results, are described in Section 3. The results of the lagrangian experiments on the tested year are discussed in Section 4, which includes subsections examining the influence of seasonality on virtual particle dispersal pathways and factors related to developmental aspects of abundant fish species in the AS, with a particular focus on pelagic larval duration. Finally, Section 5 contains the concluding remarks of this work.

## 2 Study area

The AS is a semi-enclosed basin in the northernmost Mediterranean (Figure 1). It is narrow and elongated in a NW-SE direction, with a length of ~800 km and a maximum width of ~200 km. It is bounded by an extremely complex rocky coast along the Balkans peninsula and by a sandy and regularly shaped shore along the Italian coastline (Ružić et al., 2019). It is divided into three main sub-basins, explained by the diverse bathymetric profiles (Russo and Artegiani, 1996). The Northern Adriatic (“NA” in Figure 1), extending from the Gulf of Venice and Trieste to the 100 m isobath, is characterized by an extremely shallow mean depth (~30 m) with a very weak bathymetric gradient, and occupies the flooded seaward extension of the Po Delta. The Middle Adriatic (“MA” in Figure 1), still has relatively shallow waters, and constitutes the transition between the northern and southern sub-basins. MA is characterized by two depressions, the Pelagosa Sill and the Pomo (or Jabuka) Pit, with depths of ~170 m and ~270 m, respectively. The southern part (“SA” in Figure 1) extends to the Strait of Otranto, the channel connecting the Adriatic with the Ionian Sea, and is characterized by the depression of the Otranto Basin, with a maximum depth of ~1270 m. The Otranto Channel, which is ~75 km wide and ~800 m deep, acts as an exchange area for water masses, and export of nutrients from the AS (Civitarese et al., 1998; Fanelli et al., 2023).



## 2.1 Relevant hydrologic features

The surface flow dynamics of the AS are characterized, with a certain seasonal variability, by a general cyclonic circulation (Russo and Artegiani, 1996). Levantine intermediate waters and Ionian surface waters flow northward from the Otranto Channel along the Balkans coast within the Eastern Adriatic Current (EAC), and return southward with the Western Adriatic Current (WAC) along the Italian peninsula (Orlić et al., 1992). Coastal currents exhibit seasonal variability, with the WAC generally stronger in summer, and the EAC stronger in winter (Zore, 1956; Poulain, 2001). Prevalently during winter, part of the EAC recirculates, shaping the nearly-permanent Southern Adriatic Gyre in the southern sub-basin (López-Márquez et al., 2019), and less frequently, the Northern and Central Adriatic gyres (Martin et al., 2009) in the upper and middle sub-basins. These eddies partially favor the cross-basin (east-to-west) transport via their northern rims (López-Márquez et al., 2019), and also result in the pumping of highly productive waters that entail rich areas favorable for mesopelagic spawners (Specchiulli et al., 2016).

Tides in the AS are amplified northwesterly (from the Strait of Otranto to the northernmost Adriatic), reaching amplitudes up to 1 m in the Venice shoreline, an exceptionally large value in the Mediterranean basin (Medvedev et al., 2020). The influence of tides and local winds, namely Bora and Sirocco, induce an important variability in the main circulation pattern (Orlić et al., 1994). The dry, cold and strong northeasterly Bora, more frequent in winter storms, provokes a double gyre response in the North Adriatic circulation, consisting of a cyclonic loop drifting northward and an anticyclonic

drifting southward (Kuzmić et al., 2006). Otherwise, the wetter and warmer southeasterly Sirocco, typical from late autumn to early spring, tends to accumulate water near the northernmost coasts (Pasarić et al., 2007; Molinaroli et al., 2023), usually strengthening the EAC (Book et al., 2007) and weakening or even reversing the WAC (Bignami et al., 2007). Summer winds (e.g. the northwesterly Mistral) are weaker and more stable, which favors a slower and steadier circulation during this period (Pasarić et al., 2009).

## 2.2 Ichthyo-biodiversity in the AS

The AS is a recognized biodiversity hotspot in the Mediterranean, driven by the nutrient transport and runoff by rivers and the consequent phytoplankton primary production, and marked by the strong seasonality of the Po River discharges (Cozzi and Gianni, 2011). It is a highly productive fishing ground (Cavraro et al., 2022), grouped into two Geographical Subareas (GSA17 in the north, and GSA18 in the south, as shown in Figure 1) according to the General Fisheries Commission for the Mediterranean (GFCM, 2009). GSA17 has a wide variety of seabed habitats, from shallow and muddy bottoms in the east to steep and rocky bottoms in the west, whereas GSA18 is predominantly deep, steep, and rocky, supporting sensitive marine habitats that are under high fishing pressure (Grati et al., 2018). Despite the differences, both GSAs share important fish stocks (UNEP/MAP-RAC/SPA, 2015), which has led to the proposal of a large transboundary marine protected area (Bastari et al., 2016). Particularly, the AS supports regionally important

fisheries of small pelagic stocks such as sardine (*Sardina pilchardus*) and anchovy (*Engraulis encrasicolus*) (Morello and Arneri, 2009), which are widely distributed throughout the whole AS. Over the last two decades, sardine specimens in the AS have tended to spawn from early autumn until late spring (Zorica et al., 2020). The peak of reproductive activity occurs between November and February, primarily depending on environmental parameters such as temperature (Zorica et al., 2019). In contrast to the AS, the spawning period for *S. pilchardus* appears to end earlier in other Mediterranean areas (Tsikliras et al., 2010; Basilone et al., 2021). The Adriatic anchovy spawns from the end of March (winter) to October (autumn), with its peak spawning season occurring in July (Zorica et al., 2020). According to Somarakis et al. (2004) and Basilone et al. (2006), the species' reproductive peak is in the summer in the central Mediterranean. In the Bay of Biscay, anchovy spawn earlier and for a shorter period, peaking in May and June (Motos, 1996).

As for the bottom trawl fishery, the European hake (*Merluccius merluccius*) is the most important target species in terms of both landed weight and value for the fleets involved (Arneri and Morales, 2000). Unlike the other demersal species, it has two recognized spawning phases in the AS: the first occurring in winter in deeper waters, and then, a second occurring in summer after an adult migration to shallower waters (Ungaro et al., 1993; Vrgoč et al., 2004). Based on a recent study conducted on specimens sampled from the GSA17 (Candelma et al., 2021), the hake reproductive season peaks from April to July. However, spawning females can be found throughout the year, indicating a protracted spawning period (Zorica et al., 2019). It should be noted that the reproductive peak of *M. merluccius* varies in different geographical areas. Along the Tunisian coasts, the main peak is recorded from June to October, with minor peaks in January and April (Khoufi et al., 2014). In the Gulf of Lion, spawning is highlighted in autumn (Morales-Nin and Moranta, 2004). Along the Portuguese coast, spawning peaks are observed in March, May, and August (Costa, 2013). In North Atlantic waters, the spawning peak lasts from January to April (Alvarez et al., 2004; Murua and Motos, 2006).

Medium-sized pelagic fish species such as the Atlantic mackerel (*Scomber scombrus*), horse mackerel (*Trachurus trachurus*) and Mediterranean horse mackerel (*Trachurus mediterraneus*), despite their relatively lower commercial value compared to other pelagic fish species, play also a key trophic role as mesopredators in the basin (Da Ros et al., 2023), with their reproductive activity peaking in winter, late winter and summer, respectively (Jardas et al., 2004; Zardoya et al., 2004). High variability in range and peak spawning season is associated with latitude, with *T. trachurus* spawning season extending up to 8 months, with a peak in spring, in both the Atlantic and the Mediterranean (Abaunza et al., 2003). Other relevant fish stocks targeted by the bottom fleet are the red mullet (*Mullus barbatus*) and the common pandora (*Pagellus erythrinus*), with a spawning peak during summer (Carbonara et al., 2015; Muntoni, 2015; Zorica et al., 2020), as well as flatfish species such as the common sole (*Solea solea*), with a spawning peak in winter (Fanelli et al., 2022).

Some of the authors previously cited in their works indicate that some of the most important spawning and nursery grounds on the

AS for these species are the Gulf of Trieste, Po Delta, Gargano Cape, Manfredonia Gulf, Kvarner Gulf, and the northern and the central Italian coastlines (see locations in Figure 1). Management measures intended to protect marine resources in the AS were additionally set out by the (GFCM, 2021) in the Pomo Pit (Figure 1), an area recognized as a critical habitat for demersal species and identified as an Ecologically or Biologically Significant Area (EBSA) under the 1992 Convention on Biological Diversity.

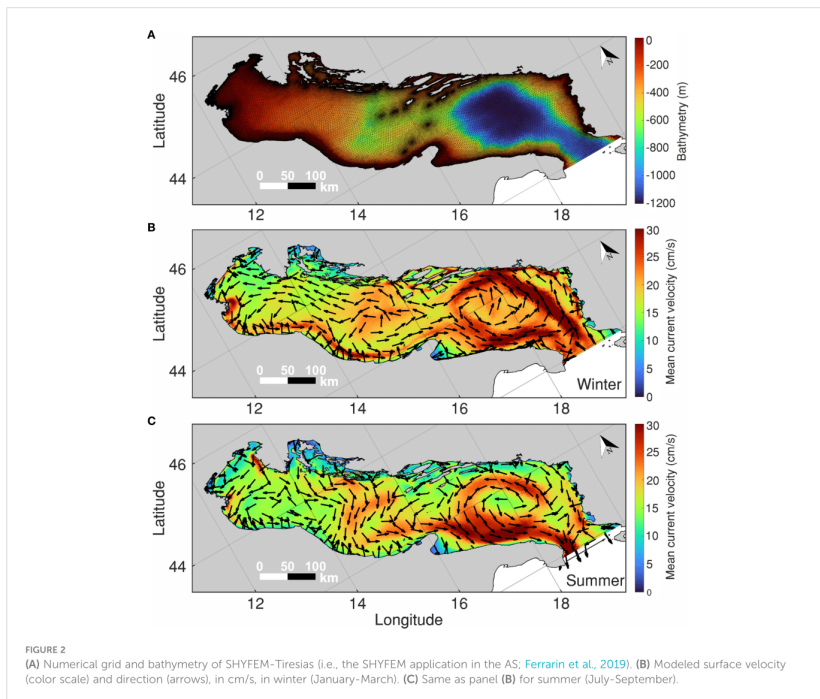
## 3 Experimental procedure

### 3.1 Hydrodynamic model

Modeling the hydrodynamic processes of the Adriatic is challenging due to the large number of spatial scales involved and the extremely intricate coastal morphology (McKiver et al., 2016). Such complex application was carried out with a high-resolution numerical model, whose code is based on the Shallow Water Hydrodynamic Finite Element Model (hereafter SHYFEM; Umgiesser et al., 2004). SHYFEM solves the shallow water equations of motion for complex morphology and wide bathymetric gradients on unstructured grids. The effectiveness of SHYFEM is well-documented in various applications in Europe (Bajo et al., 2014; Umgiesser et al., 2014 among others) and in the Adriatic basin (Bellafiore and Umgiesser, 2010; Ghezzi et al., 2015; Ghezzi et al., 2018; Umgiesser et al., 2022 and citations therein). The version used in this study (SHYFEM-Tiresias, Ferrarin et al., 2019) covers the entire AS, from 12.05° E to 19.92° E and from 39.95° N to 45.80° N, including the small lagoons of Grado-Marano, Lesina and Venice and the Po Delta (Figure 1).

The full numerical grid consists of 96,392 triangular elements with horizontal resolution varying from 5 km in the open-sea to a few dozens of meters along the coastlines (Figure 2A), and 72 vertical Z-layers of uneven discretization (Ferrarin et al., 2019). It includes the contribution of five boundary conditions, namely, the sea level, current velocity, temperature and salinity fluxes at the Strait of Otranto, and the freshwater discharges from 17 tributaries. Temperature and salinity fluxes were provided by the oceanographic fields of Mediterranean Forecast System (Tonani et al., 2008), and the freshwater discharges were obtained from monthly and annual climatological values at the river boundaries (for the location of tributaries, see Ferrarin et al., 2019 and references therein). Atmospheric forcing, i.e., pressure and wind, is given by the ECMWF ERA-5 atmospheric reanalysis (Hersbach et al., 2023).

The model outputs in this study are hourly surface values of zonal (u) and meridional (v) components of drift velocity, sea level, temperature, and salinity for the year 2018. The selected year is as a representative scenario for the general hydrographic conditions of the AS and is accessible in NetCDF through the Institute of Marine Sciences of the National Research Council of Italy (CNR-ISMAR) OpenDAP catalog (<https://tws.ismar.cnr.it/thredds/catalog/emer/ge/catalog.html>). It serves as a case study, examining spawning areas and intra-annual connectivity patterns, rather than assessing inter-annual variability, which is currently being investigated but not shown for simplicity in this first application. Supplementary Figure



S1 displays the monthly averaged surface velocity data from SHYFEM and the ECMWF ERA-5 wind fields for the simulated months (January to December 2018). Winter and summer averaged surface circulation is presented in Figures 2B and C, respectively.

The synoptic fields in Figure 2 reveal similar circulation patterns, with the velocity field exhibiting greater variability in winter than in summer. The winter mean (Figure 2B) shows a more prevalent WAC in the northern sub-basin, and a stronger EAC along the north-flowing eastern rim of the southern gyre. The circulation is weaker in summer (Figure 2C), although the WAC is stronger along the south-flowing rim of the southern gyre in this season. Despite not being the most typical configuration reported in the AS, which is characterized by the presence of the EAC and the WAC and the three reported cyclonic gyres, the slight weakening of the currents during summer is not unusual. The prevailing northwesterly Mistral winds during summer intensify the east-to-west cross-basin transport, leading to stronger southeastward coastal currents and increased export to the northern Ionian Sea. During winter, the effect of both easterly and southeasterly winds disrupts the unidirectional shore transport, resulting in a more dispersed and irregular pattern within the basin.

### 3.2 Particle tracking module

Dispersal and connectivity were assessed by implementing a lagrangian particle tracking algorithm based on the open-source software OpenDrift (version 1.10.6, Dagestad et al., 2018). OpenDrift consists of several particle-based sub-models that can be used to predict the transport and fate of different types of elements. This study applies the main sub-model, OceanDrift, that uses neutral buoyant particles as tracers. Virtual particles represent propagules (i.e., eggs and larvae) with the typical biological traits of generic marine organisms (Table 1). The analysis focuses on basin-scale larval connectivity from an ecosystem perspective, rather than on specific target species.

Horizontal trajectories were simulated by integrating the zonal and meridional velocity field using a 4<sup>th</sup> order Runge-Kutta advection scheme, where particle positions are bilinearly interpolated using the model output data in the hydrodynamic grid. Vertical velocities, mainly associated with wind-driven upwelling/downwelling in certain AS areas, are of small magnitude (less than mm/s to cm/s) compared to horizontal velocities (cm/s to dm/s). Vertical motions are influenced by



other phenomena such as diel cycles, feeding patterns, egg buoyancy or settlement due to changes in fat content, diurnal temperature variations affecting buoyancy, etc. As a result, the vertical velocity is poorly determined, with an uncertainty in its value that could even change its sign, for which it has not been considered in the advection module. Another simplification adopted in our method is that the tracers are fully-passive, meaning that complex larval traits, such as swimming capability, migrations, and natality and mortality rates are not considered in the approach. Under these assumptions, transport of eggs and developing larvae is determined by the PLD (i.e., the time propagules spend drifting with currents), the duration of spawning, and the time-varying horizontal velocity. To prevent particle stranding near the release site, a strategy of relocating particles to the open sea was implemented upon encountering the continental coastline or islands when oceanographic conditions allowed. The coastline was represented using the Global Self-Consistent Hierarchical High-Resolution Geography in its full resolution version (GSHHG\_F, version 2.3.7). A 30-minute time step with non-additional diffusion nor wind field were added to the trajectories, as they were already included in the hydrodynamic simulation run of SHYFEM-Tiresias.

To investigate the spatial connectivity patterns, the AS basin was divided into 40 sub-zones, 21 along the coastlines and 19 distributed by the open sea (Figure 3). These areas were partially selected based on the experience gained from studies on the circulation and ecological characteristics of the region of interest (Coll et al., 2010; Lipizer et al., 2014; UNEP/MAP-RAC/SPA, 2015; Bastari et al., 2016). Each area played, simultaneously, the role of source and destination of particles. Two hundred lagrangian particles as a representative number of propagules are seeded in each box randomly distributed in the surface layer, so each release allocates 8,000 new particles in the AS, and their position is computed every 30 min. To avoid any potential bias that could be introduced in trajectories if particles were only released at a single time of the day, particles are released four times per day for 14 days (56 releases, 448,000 particles in total). All the particle tracks were stored in netCDF format and the post-processing and visualization of the simulations were performed in Matlab (version 2023a).

In addition to the spatio-temporal analysis of the trajectories of eggs and larvae, several factors related to the biology and development of common fish stocks in the AS with influence on the dispersal pathways of particles were tested. Table 1 provides the biological parameters considered in the lagrangian experiments. The first one is the spawning time, understood as the time of particle release. Simulations were run for winter and summer, representing the most active spawning periods of the abundant species inhabiting the region. The second parameter being tested is the pelagic larval duration (PLD), which is the time between when a pelagic propagule leaves the spawning site and when it finally settles. In practice, the duration of egg and larval drift of marine organisms varies from weeks to months, depending on the ontogeny of fish larvae. The value of this parameter *per species* has been inferred from the literature cited in Table 1. Overall, given the uncertainties in determining the transition from passive to active behavior, we considered a wide PLD of 60 days as a good

TABLE 1 Literature review of biological traits for some emblematic species relevant for modeling in relation to the AS oceanographic conditions.

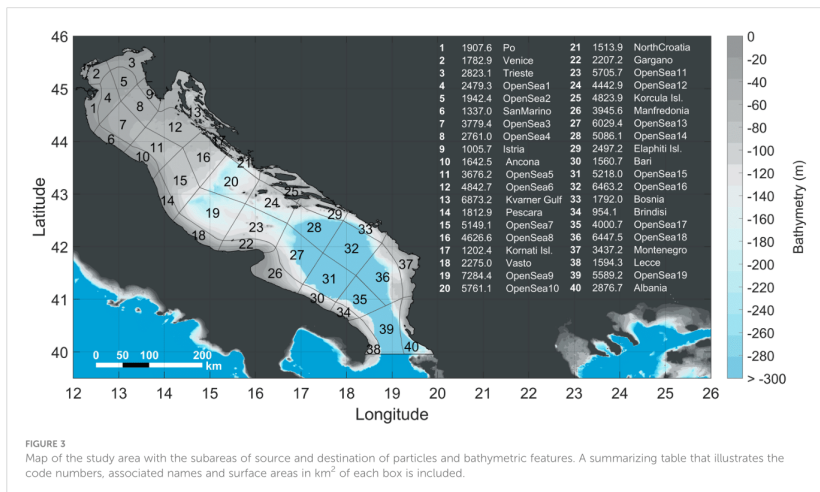
Marine species (habitat) Common name Scientific name	Spawning season	PLD [days]	Bibliography
Sardine (P) <i>Sardina pilchardus</i>	Winter	40-60	Sciaccia et al. (2018) Zorica et al. (2019, 2020)
Anchovy (P) <i>Engraulis encrasicolus</i>	Early summer	30-40	Morello and Arneri (2009) Patti et al. (2020) Zorica et al. (2020)
Atlantic mackerel (P) <i>Scomber scombrus</i>	Winter	n.f.	Zardoya et al. (2004)
Horse mackerel (P) <i>Trachurus trachurus</i>	Late winter	21-30	Jardas et al. (2004) Van Beveren (2012)
Mediterranean horse mackerel (P) <i>Trachurus mediterraneus</i>	Summer	n.f.	Viette et al. (1997)
European hake (D) <i>Merluccius merluccius</i>	Winter, Summer	40	Arneri and Morales (2000) Hidalgo et al. (2019)
Red mullet (D) <i>Mullus barbatus</i>	Summer	22-37	Muntoni (2015) Carbonara et al. (2015)
Common pandora (D) <i>Pagellus erythrinus</i>	Summer	44	Vrgoč et al. (2004)
Common sole (B) <i>Solea solea</i>	Winter	31-38	Paoletti et al. (2021) Fanelli et al. (2022)

From left to right: Marine species are the organisms to which the results of this work may apply, with a code that indicates their corresponding habitats (P, Pelagic; D, Demersal; B, Benthonic); spawning season is the average reproductive period; PLD is the length of time the propagule is pelagic; bibliography indicates the source(s) where information was obtained. n.f. (not found/not reported) in the AS.

compromise between a stable value for connectivity in the AS and an affordable computational time. To test the sensitivity to PLD, connectivity was recalculated for time windows ranging from 15 to 90 days (Section 4.3).

### 3.3 Construction and analysis of connectivity

Two different methods were followed to address hydrodynamic connectivity (Figure 4). First approach consisted in the so-called "connectivity matrix" (Figure 4A), which represents the probability of larval exchange among geographically separated sites (Cowan and Sponaugle, 2009). In this matrix, each cell is the number of particles ( $p$ ) released from a certain source  $i$  (along the vertical axis) and collected in a certain destination  $j$  (along the horizontal axis), so

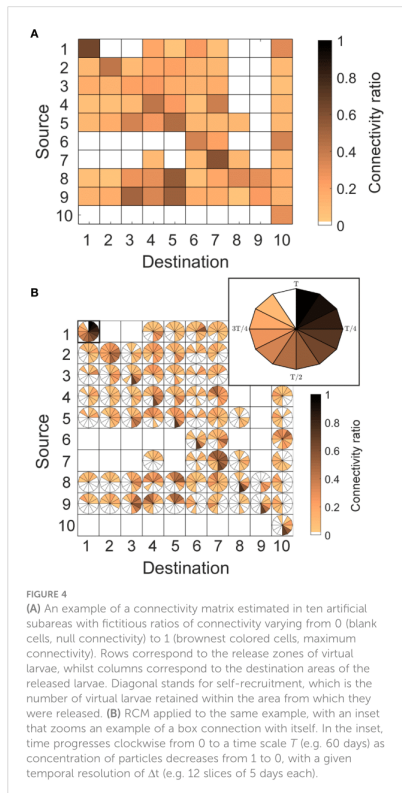


$C_{ij}$  is the probability that an individual or group of individuals of population  $i$  will move to population  $j$  after a certain tracking time ( $C_{(i,j)} = \frac{p_{(i,j)}}{p(i)}$ ). Diagonal cells of this matrix (where  $i = j$ ) stand for the self-recruitment, i.e., the number of individuals that remain in the same region from which they were originally released, including particles that eventually return to the sourcing area (Cowen et al., 2006). Connectivity ratios ( $C$ , with values ranging from 0 to 1), therefore, quantify the strength of connectivity between different sites, with higher values indicating more favorable connections. Source-sink dynamics of larval dispersal can be elucidated with this approach, revealing the direction and intensity of connections. It further enables to estimate the potential and effectiveness of a given area as a nursery ground for developing larvae. Despite this, connectivity matrices only offer a partial depiction of larval connectivity complexity, neglecting crucial information such as the identification of areas that are rapidly dispersing, both dispersing and recruiting, or only recruiting for individuals through time.

Prompted by this lack of temporal information in the network, the second method used a more-recent approach developed by Defne et al. (2016). The method, called a “retention clock matrix” (RCM, hereafter), uses a clock in each cell to track the temporal changes in source-sink connections, evaluating the time-dependent connectivity (see Figure 4B). Specifically, each retention clock describes the release event as a circular clock that tracks the number of particles ( $p$ ) over the entire time scale of interest ( $T$ ) (see inset of Figure 4B). The time scale is discretized into slices with a temporal resolution of  $\Delta t_{(i,j)}$  ( $C_{(i,j,t)} = \frac{p_{(i,j,t)}}{p(i,t_0)}$ ). As in the conventional connectivity matrix, in all RCMs, the horizontal axis represents the boxes from which particles are released, and the vertical one is where the particles end up. The strength of connectivity between

each possible combination of source-destination is depicted with a color scale, in which slices with the darkest color intensity indicate the larger fraction of particles moving from their origin to the destination. Naturally, domains with different retention characteristics have unique retention clocks, which reflect the rate at which particles are retained or lost within a domain through time. In slowly dissipating environments, the particle concentration, hence the clock, would gradually approach zero, indicating that individuals are being spawned at a slower rate than they are being dispersed. In rapidly dispersing domains, the clock would approach zero faster and a larger portion of it would remain at null values, suggesting that tracers are subjected to strong currents that result in direct connections to other domains. The opposite behavior is depicted by retentive domains, identified by clocks with connectivity values close to 1 at all-time scales, which indicate that spawned individuals are effectively retained due to physical or biological features that prevent their advection.

To account for the discrepancy in sizes and shapes of source and destination polygons (see Figure 3), the estimated connectivity in both cases was normalized by the areas ( $a$ ) of each cell involved in the connection  $C = C \times \frac{a(i)}{a(j)}$ , so that the maximum value of the matrix is 1. In both methods, connectivity was only considered significant if the ratio  $C$  satisfied a minimum threshold of 0.01, meaning that at least 1% of the particles released from the source reached the destination polygon. Thus, the presence of either colored cells (in method 1) or clocks (in method 2) indicate a connection between the source and destination polygon, while a blank cell indicates that the connection is zero or less than 1%, and thus, negligible. The connectivity ratios  $C$  are hereinafter interpreted in the text as  $S\# - D\#$ , indicating particle transport from source (row number) to destination (column number),



respectively. A numerical code made available to the scientific community by [Defne et al. \(2016\)](#) was adapted to calculate the RCMs in this study.

## 4 Results and discussion

### 4.1 Connectivity matrix

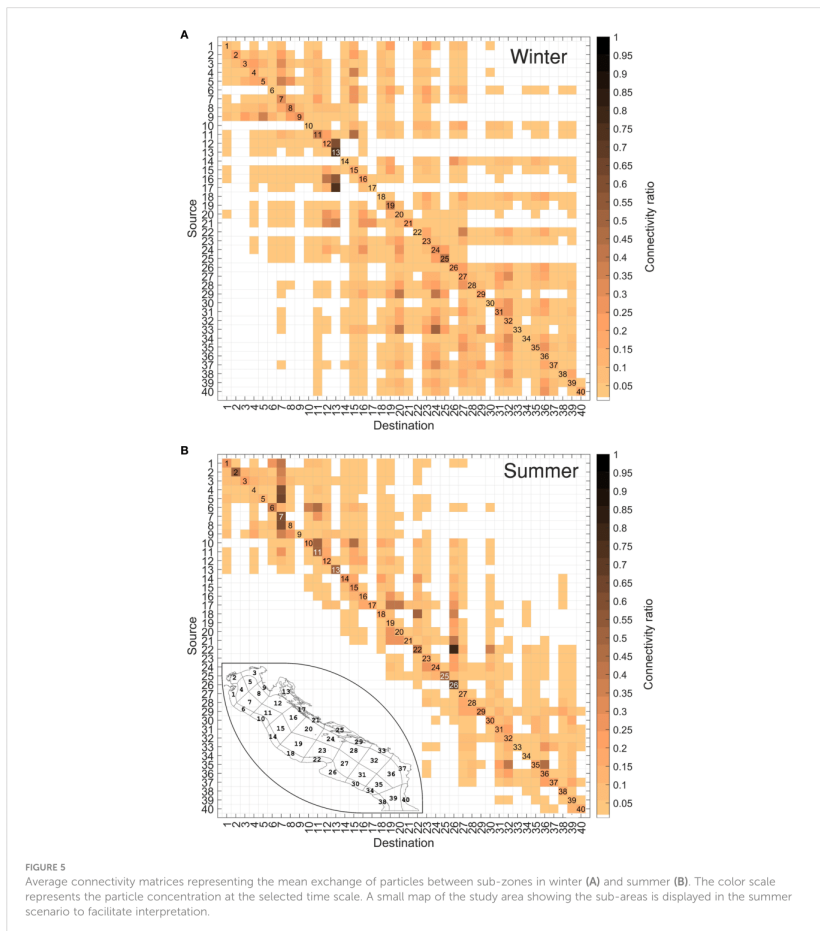
The mean connectivity matrix estimated at winter and summer for the year 2018 is illustrated in [Figures 5A and B](#) respectively, and the result of its difference (summer minus winter) is provided separately in [Supplementary Figure S2](#).

A characteristic feature of both winter and summer scenarios is the prevalence of high connectivity rates along the diagonal of the matrix. This indicates that these regions are characterized by a certain level of

auto-retention of propagules. Self-retention probability differs greatly between the distinct boxes, ranging from 60% in the Kvarner Gulf (S13-D13) to 5% in Bosnia (S33-D33) for winter ([Figure 5A](#)), and from 55% in Manfredonia (S26-D26) to 4% in Brindisi (S34-D34) for summer ([Figure 5B](#)). This spatial difference is foreseeable, as the complex system of islands in the Kvarner Gulf, and the existence of a small cyclonic eddy in the Gulf of Manfredonia (see [Figure 1](#)) act as trap of propagules ([Specchiulli et al., 2016; Sciascia et al., 2018](#)), whilst Brindisi and Bosnia coasts, nearby the Strait of Otranto, are subjected to stronger advection by the EAC-WAC circulation system. Overall, self-retention in the northern and middle Adriatic sub-basins (areas 1-25) is more likely than in southern Adriatic sub-basin (areas 26-40), denoted by the darker color intensity of the former diagonal cells compared with the latter elements (~28% in areas 1-25, compared to ~13% in areas 26-40, in both winter and summer scenarios).

Considering also the connectivity values out of the diagonal, Gargano (D22) and Manfredonia (D26) during summer ([Figure 5B](#)), display a large fraction of particles arriving from S14-20 and S18-22, with mean connectivity values of 10% and 20%, respectively, and maximum reaching 50% (S18-D22) and 70% (S22-D26). This spatial pattern is to be expected, since the WAC acts as the main advection process along the Italian shelf, although it is also subject to seasonal fluctuations ([Supplementary Figure S1](#)). Contrastingly, Istria (D9), Kvarner Gulf (D13), and the Kornati (D17), Korcula (D25), and Elaphiti (D29) Islands, exhibit external particle reception rates less than 5%. Extreme case is provided by D17 ([Figure 5B](#)), which shows zero reception of individuals from external boxes. These areas harbor relatively closed populations, receiving particles from a limited number of grounds, but suggest their potential as self-sustaining areas. During winter ([Figure 5A](#)), isolated self-sustaining areas are less obvious, although the shielding capacity of the Kornati Islands (D17), northern Croatia (D21) and the Korcula Islands (D25) is noteworthy, as they receive nearly null abundance of particles from the northern part of the basin. Areas D2 (Venice), D3 (Trieste), D5 (OpenSea2) and D9 (Istria) only receive particles from a small part of the southern sub-basin, while source areas S12 (OpenSea6), S13 (Kvarner Gulf), S17 (Kornati Islands), S21 (North Croatia), S24 (OpenSea12) and S25 (Korcula Islands) do not send any particles to the southern sub-basin. A striking example is the Kvarner Gulf (D13), which paradoxically shows minimal external particle receptions in summer, but high external particle exchange in winter, while remaining self-retaining (elevate connection with itself). This suggests that this area may play a hatchery and nursery role for marine species, as suggested by the previously cited authors ([Zorica et al., 2020](#)), and suggest the existence of physical processes determining the temporal evolution of the particles in the basin.

Based on the averaged result, we can derive macro-regions as combinations of boxes of our network. For instance, more evident in summer than in winter, areas 1-9 and 26-40 may be identified as two isolated regions with a slight or null inter-connection. A third area can be identified in 10-25 (central Adriatic), where the particle reception is mainly limited to the upper part of the connectivity matrix (northern and central Adriatic), with limited or no exchange with the southern sub-basin during summer. During winter, the prevailing currents over the AS inject more energy in the basin,



leading to a wider dispersion of particles and a less distinct delineation of macro-regions. The seasonality is also evident by the significantly higher number of valid elements, i.e., cells with connectivity probabilities higher than 1%, in winter (~900 out of 1600, Figure 5A) compared to summer (~600 out of 1600, Figure 5B). The likely reason is the atmospheric forcing, which is less variable and more stable in summer, resulting in diminished velocities and consequently shorter drifter paths in this period. The much more dispersed transport because of the more variable

atmospheric forcing during winter may create otherwise less structured connectivity patterns within the basin.

#### 4.2 Time-dependent connectivity

Temporally averaged connectivity matrices (Figure 5; Supplementary Figure S2) highlight the role of circulation structures on particle dispersion and provide predictable



connectivity patterns that show seasonal variability. However, it also shows that the selection of a temporal snapshot is subjective and can limit the analysis due to loss of information. It is more adequate to preserve the temporal information of connectivity, while benefiting from the simplicity of a connectivity matrix (Defne et al., 2016). To this end, the RCM for all source-destination pairs in the AS basin has been estimated for the same temporal configurations (winter and summer). A maximum time scale of 60 days is used for all model scenarios. Each slice on all retention clocks represents 5 days. The color scale in each clock represents the particle concentration at the selected time slice, with darker colors indicating larger fraction of particles moving from source to destination.

#### 4.2.1 Auto-connectivity

Auto-connectivity, the ability of a system to receive and retain particles from and within itself, is a pivotal determinant of population persistence. It represents the self-sustaining capacity of a population structure, a factor intricately influenced by the physical processes that mediate the propagules transport (Cowen et al., 2006). The quantification of self-recruitment probability, a direct metric of auto-connectivity, is made by evaluating the diagonal cells of the connectivity matrix (where  $i = j$ ), with higher values signifying a more robust tendency for particles to remain within the area from which they were initially released. The cells corresponding to these diagonal matrices are extracted from the estimated RCMs and depicted in Figure 6, illustrating the time-dependent self-recruitment probabilities for both winter and summer seasons.

In the winter experimental configuration (Figure 6A), a low self-sustained clock pattern is evident along the Italian coast, indicating rapid southward transport within the western Adriatic shelf, with particles leaving the source area within a maximum of 10 days. This is consistent with the winter WAC pattern shown in Figure 2B. Regions located above the northern Adriatic gyre show retentive characteristics, as indicated by elevated clock values in both intensity and duration, particularly observed in Po (1), Venice (2), OpenSea5 (11), and OpenSea6 (12). The summer scenario (Figure 6B) presents a stark contrast, with the exception of the Croatian coast, which shows similar auto-retention characteristics. Specifically, the Kornati Islands (17) and northern Croatia (21) retain their winter characteristics for an extended period of up to 50 days, and the Gulf of Kvarner (13), along with the islands of Korcula (25) and Elaphiti (29), exhibit clock patterns almost identical to the winter configuration throughout the 60-day tracking period. This suggests that the coastal topography of the eastern Adriatic coast, rather than the seasonal regime, plays the primary role in influencing its auto-retention behavior. Po (1) and Venice (2), which contain complex lagoon systems, also maintain their behavior in both seasons due to their topographic conformation. Conversely, the coastal areas of Gargano (22) and Manfredonia (26) along the Italian shelf, exhibit higher auto-retention values in summer than in winter, in both intensity and duration, which persist for almost the entire 60-day period. Similarly, the onshore regions along the western Italian coast

south of the Po estuary (6, 7, 10, 11) show high retention rates, in agreement with previous findings in this region (Revelante and Glimartin, 1992; Bray et al., 2017).

#### 4.2.2 Winter connectivity

When the RCM estimated in winter (Figure 7) is analyzed, more granular temporal information becomes available with respect to the time-averaged analysis. For instance, among the previously identified macro-regions, the one corresponding to the northern Adriatic Sea (boxes 1-9), not only shows low ratios but also exhibits poor retention capacity with decreased persistence of connectivity over time. This is especially noticeable in the OpenSea3 (S7), which exhibits high average connectivity ratios (~40%, Figure 5A) but, when evaluated temporally, reveals consistently short and variable durations, with peak rates occurring at 40 days of tracking for particles originating from Trieste (S3-D7) and OpenSea2 (S5-D7).

The central macro-region (10-25) shows a more extensive distribution of connections, encompassing both the northern and southern sub-basins, with particle transfers to the southern Adriatic being significantly stronger and more persistent throughout the tracking period. Retention areas in this part of the basin occur in the Kvarner Gulf (D13), OpenSea10 (D20), OpenSea12 (D24) and the Korcula Islands (D25). It is particularly noteworthy in the case of the Kvarner Gulf (D13), which, despite the extremely complex rocky coastline, shows the highest connectivity receptions within the RCM (S16-D13, S15-D13, S12-D13 with a ratio of >60% sustained over longer periods). This pattern is likely due to enhanced atmospheric variability during winter, which induces rapid and direct transport of particles into these coastal areas. A strong and persistent rate of particle reception is further in the OpenSea6 (D12), which maintain a strong connectivity throughout the 60-day tracking period with the OpenSea8 (S16-D12), the Kornati Islands (S17-D12), the OpenSea10 (S20-D12) and North Croatia (S21-D12). These four areas shape a continuously well-connected water parcel compatible with the effect of the central Adriatic gyre, and likely identify one of the most productive areas for fish and important spawning and nursery grounds for commercially valuable fish species. Other important connections with the southern subbasin occur in the OpenSea9 (D19) and in the OpenSea10 (D20), which receives particles from Gargano (S22), OpenSea11 (S23), OpenSea12 (S24), and Korcula Islands (S25). These areas build a corridor of connection south of the Pelagosa Sill, with connectivity percentages of 45% throughout the 60-day clock period. The area D20 receives particles secondarily from S26-40, with special intensity in a period from 25 to 45 days from areas S29, S33, S37 which represent the pattern of the EAC. The connection of the central Adriatic with the northern is relatively weak and variable, as evidenced by the low (<30%) and delayed (>40 days) ratios in the upper portion of the matrix, attributed to the northward transport of currents towards the end of the tracking period. A relevant connection in this part of the basin occur in the OpenSea7 (D15) for particles arriving from the northernmost Adriatic (S1-D15, S2-D15, S4-D15, S5-D15, S7-D15, S10-D15 and S11-D15), indicating a particularly retentive area south of the Po River, corroborating previous findings in the region (Bray et al., 2017).

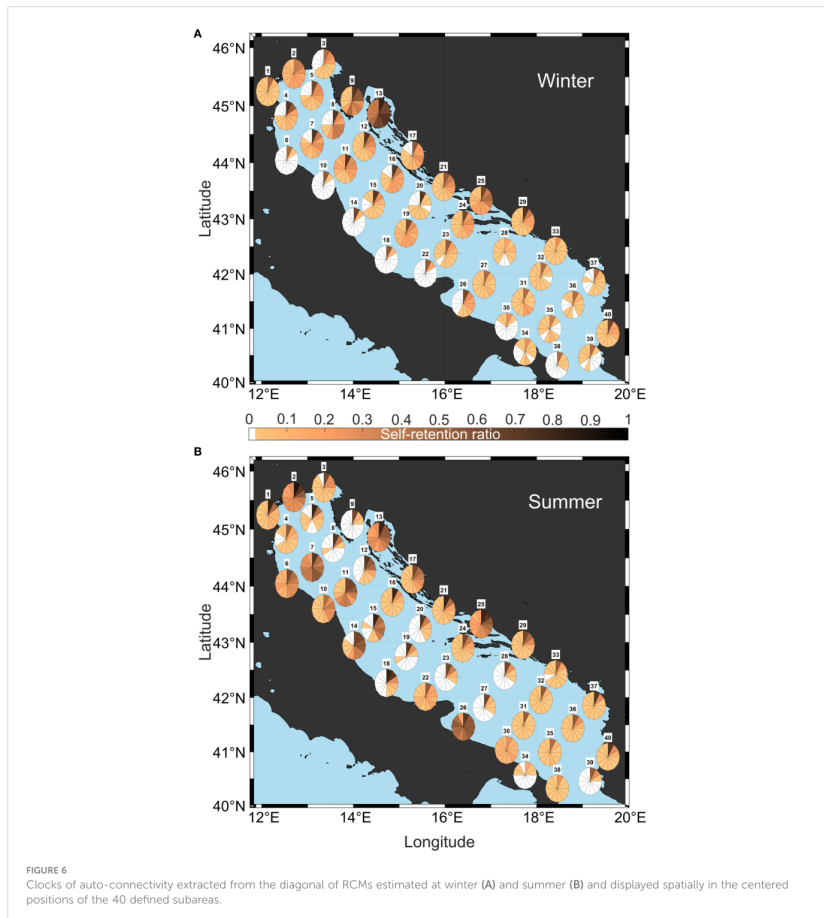
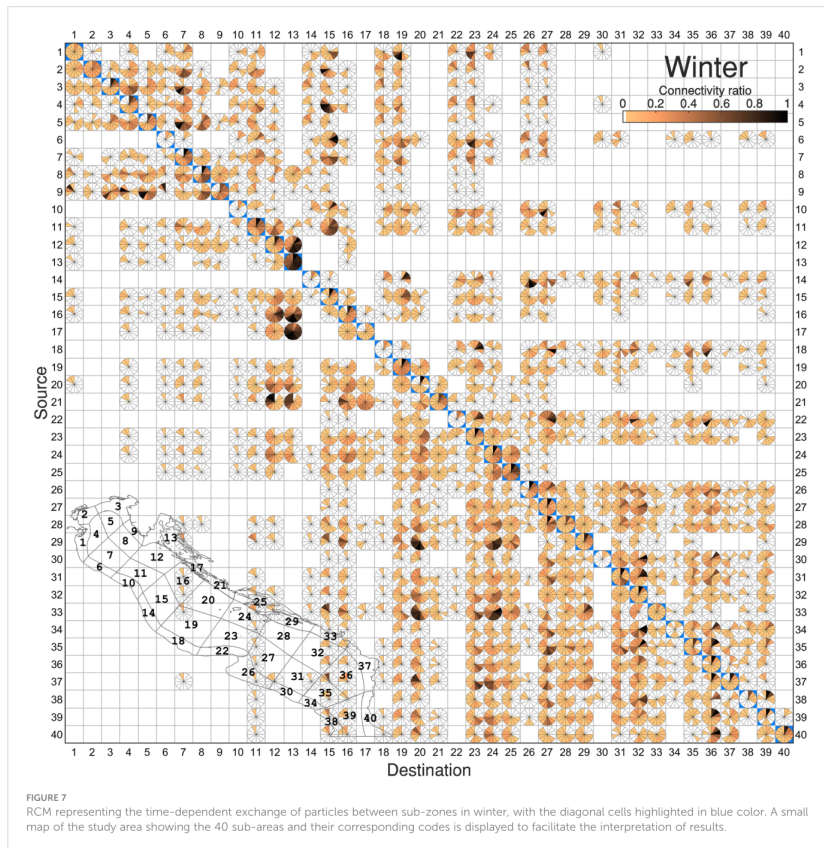


FIGURE 6  
Clocks of auto-connectivity extracted from the diagonal of RCMs estimated at winter (A) and summer (B) and displayed spatially in the centered positions of the 40 defined subareas.

Among the three identified macro-regions, the southern one (26-40) emerges as the most retentive. It maintains a generally persistent connectivity, being particularly significant in specific regions of the central macro-region (S28-D24, S33-D24), with a high rate of connections (>70%) persisting 35 days. Additionally, it exhibits a high degree of inter-connectivity, with the most extensive and enduring connection occurring between areas 31, 32 and 35, 36. This pattern is likely attributable to the presence of the south gyre, which is particularly prominent during winter (Figure 2B; Supplementary Figure S1).

#### 4.2.3 Summer connectivity

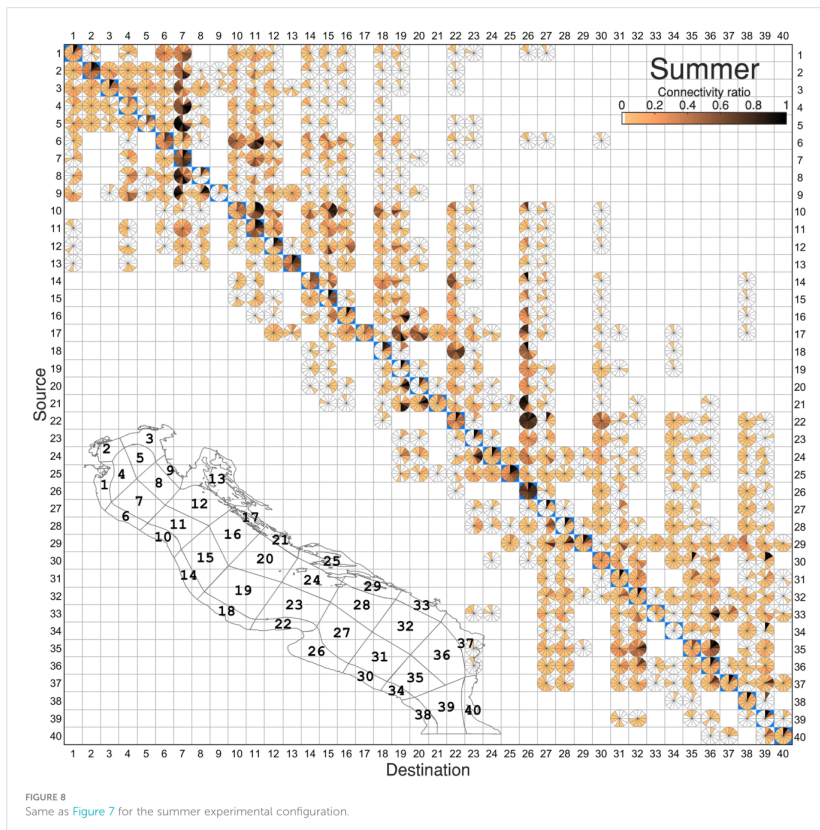
The rather scattered and variable connections seen in winter contrast with the much more unidirectional connectivity pathways in summer (Figure 8). This becomes apparent in the less heightened variability observed in both direction and duration of connections compared to the winter RCM. The northern macro-region (boxes 1-9), which showed a reduced ratio and persistence over time in winter, shows not only the highest but also the most persistent connectivity percentages in summer, denoted by the clocks with probabilities above 20% on all time scales (S2-D1, S3-D2, S4-D2,



S5-D2, S4-D3, S2-D3, S2-D4, S3-D4, S3-D5). The darker color intensity in the matrix indicates a significant influx of individuals into destination 7 (OpenSea3), with a concentration of elements ranging from 20% to 60% between S1-D7 (Po-OpenSea3) and from 30% to 90% between S8-D7 (OpenSea4-OpenSea3) during the tracking time. Within the same box, particles originating from source boxes 3 (Trieste), 4 (OpenSea1), and 5 (OpenSea2), once arriving, maintain connectivity percentages above 70% for the rest of the tracking period. The particles reaching these areas exhibit rapid travel times (5 to 15 days), which is within the range of the PLD of the relevant species (Table 1) and indicates their potential for retention. Overall, the entire northern macro-region requires a longer time (approximately 30-60 days) to establish a connection with the central part of the basin (D10-25), with slight or null

transport towards the southern macro-region (D26-40). This pattern is consistent with the slower flow conditions seen during summer (Figure 2C), but also provides important information regarding species strategy, as individuals arrive in that region at advanced developmental stages.

Regarding temporarily sustained connectivity, the southern macro-region 26-40 follows, with the highest and longest connectivity observed between the boxes 35 and 36 (OpenSea17 and OpenSea18). These two sites also exhibit strong connectivity for the entire 60-day tracking period to boxes 31 and 32 (OpenSea15 and OpenSea6), forming a well-connected water parcel consistent with the isolation effect of the southern Adriatic gyre. Paradoxically, a notable connectivity is observed between Bosnia (S33) and Montenegro (D37), with 67% of particles flowing in the opposite



direction of the EAC. This unexpected behavior is attributed to the reversal of currents very close to the shore due to instability created by the weakening of the coastal current during summer. In the southern macro-region, a mirrored relationship emerges in comparison to the northern counterpart along the south shore, characterized by a limited number of connections with the northern areas at longer times of arrival (>45 days). This pattern confirms that the northern and southern Adriatic, while internally connected, act as isolated water bodies within the region, which maximizes their potential as unique nursery environments.

The opposite situation is seen in the areas of the central macro-region 10-25, which reveal connections with a wider portion of the AS and demonstrates both retention and dispersal traits.

Destination areas D10-12,14-16,18-19 consistently exhibit longer arrival times (>45 days) and poor retaining capacity for particles originating from the northern sub-basin compared to other boxes. In contrast, Gargano (D22) and Manfredonia (D26) are identified as top retaining areas, with connectivity consistently exceeding that of other destinations throughout all time slices. The majority of particles observed in the Manfredonia Gulf (D26), previously identified as a recruiting area in the averaged analysis (Figure 5B), are primarily and nearly continuously transported from the adjacent Gargano (S22) during the simulation period, with secondary and slightly delayed contributions from S23 and S24 (>15 days). This pattern arises from east-to-west shore transport, particularly noticeable during summer due to the displacement of

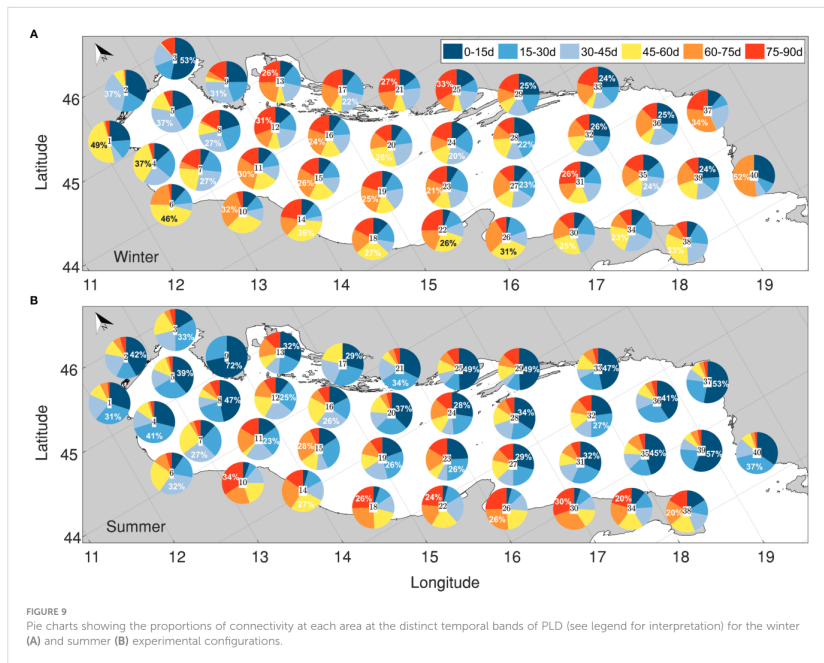
the Adriatic central gyre (see Figure 2C). In the same area, particles require more than 30 days to arrive both from North Croatia (S21) and the Kornati Islands (S17), and more than 40 days from Ancona (S10) and the OpenSea areas of the northern Adriatic (S11, S12, S15, S16). This temporal pattern is to be expected: as the distance increases, the time of arrival of particles also does. But the point to note here is that the high rate of particles reaching Manfredonia stays and recirculates nearly continuously within the same box for the rest of the simulation period. This observation confirms the Gulf's role as a particle receptor during the summer and subsequently as a nursery ground for larvae, a finding that could not be obtained in the time-averaged analysis (Figure 5B).

The spatial pattern observed between Gargano and Manfredonia (S22-D26) is consistent with patterns observed between San Marino and Ancona (S6-D10), and similarly with Pescara (S10-D14), and Vasto (S14-D18). This is likely attributable to the WAC, the primary advection mechanism transporting particles southward along the Italian shelf. Particularly during this season, the wind regime indicated a Mistral event blowing northeasterly (Supplementary Figure S1, July-August), which further supports the local displacement of particles onshore, despite the usual tendency of the coastal current to be detached from the shore during summer (Vilibić et al., 2012).

### 4.3 Effects of PLD on connectivity

The temporal component of connectivity between specific areas must be directly related to the species-specific PLD to ensure the practical application of the research. Determining the time that propagules spend drifting with currents is a key issue in shaping the dispersal potential and population connectivity of a given area. As mentioned in Section 3.2, the range of plausible durations is broad and uncertain (Table 1). While continuing to use the numerical model as a tool, it is worth exploring the dependence of connectivity on PLDs. To address this, we investigated the rate of particle reception in each area across a range of PLD windows from 15 days to 90 days, with intervals of 15 days (Figure 9).

In the winter configuration (Figure 9A), subareas show particle receptions evenly distributed across the PLD windows, with the most significant connections forming after at least 30 days of simulation. This is particularly noticeable along the Italian shelf (areas 6, 10, 14, 18, 22, 26, 30, 34), where the probability of receiving particles is less than 5% within the initial 15 days and remains below 20% within the first 30 days. This hinders the possibility of early life stages persisting in these areas, but suggests the eventual occurrence of individuals at more-advanced developmental stages, a phenomenon partially supported by works reporting the Gulf of





Manfredonia's role as a nursery ground (Sciascia et al., 2018). An exception to this trend is evident in the northernmost Adriatic, specifically in Venice (1) and Trieste (2), where the highest rate of particle reception occurs within the initial 15 days (35% and 53%, respectively), indicating a higher probability of occurrence of early life stages in these regions.

During the summer (Figure 9B), the arrival times are remarkably short, characterized by an average probability of reception of 30% and a maximum of 70% within the first PLD window (0–15 days). The most favorable scenario is observed in Istria (9), where the highest probability of receipt is concentrated in the first 15 days, with no further particle arrivals after 30 days of tracking. This observation indicates a prevalence of individuals in early life stages in this subarea, aligning with prior research highlighting Istria's role as a spawning ground (Zorica et al., 2020). Other potential spawning grounds are discerned in the southeastern Adriatic, specifically in OpenSea17 (35), Montenegro (37), and OpenSea19 (39). Favorable scenarios are also evident along the northern edges of the Adriatic gyres, favoring cross-shore connections, with peak reception occurring between 15 and 30 days of individual tracking.

From a biological perspective, these findings offer valuable insights into spawning strategies. According to our results, species with shorter PLD, such as the red mullet or anchovy (<40 days), would likely thrive along the Croatian coast in the summer, benefiting from the shorter arrival times and the more favorable oceanographic conditions. Conversely, species with longer PLD, such as sardine or hake (>40 days), would find the northern Adriatic and Italian shelf during winter advantageous.

#### 4.4 Implications for the species inhabiting the AS

Identifying the unique retentive characteristics of different areas in the AS is a crucial step in comprehending the distribution of marine species and designing effective conservation strategies in the basin. Our results indicate that particles exhibit a strong preferential direction along the coasts. The behavior in the Italian shelf was notably diverse, with some areas maintaining high self-sustaining ability during the summer and values shifting offshore in the winter. The Istrian coast (Figure 1) is identified as a crucial habitat for species spawning success, particularly in the summer, where arrival times fall within the ranges of PLD estimated for abundant species in the basin, such as anchovy, red mullet, and common pandora (Table 1). Areas distributed along the Italian shelf can be identified as essential nursery grounds, particularly when the region's productivity is influenced by wind-induced upwelling and river discharges, creating favorable environmental conditions for larvae. During the summer, when the velocity is reduced, retention is promoted, coinciding with the spawning period of anchovy, Mediterranean horse mackerel, and hake (Table 1). The variability observed during winter is attributed to environmental fluctuations, specifically the prevalence of strong winds that significantly affect the displacement of drifters. This phenomenon

provides advantageous opportunities for marine species with longer PLD and spawning periods concentrated in winter, such as sardines and common soles (refer to Table 1). Many particles arrive after undergoing recirculation, a process that requires longer times and results in extended arrival durations.

## 5 Conclusions

In this study, a hydrodynamic model integrated into the AS, coupled with a lagrangian module, was employed to systematically identify and evaluate sub-areas with distinct particle retention characteristics. While traditional connectivity matrices offer a valuable visualization tool for assessing the probability of individual exchange between zones, the challenge lies in extending this analysis across multiple time scales, often overlooked in existing approaches (Cowen et al., 2006; Crochet et al., 2016; Gamoyo et al., 2019). To overcome this limitation, our study introduces an innovative application of the "retention clock" methodology, originally developed by Defne et al. (2016), and previously applied only in a few back-barrier estuaries (Barnegat Bay, in New Jersey, USA; Defne et al., 2016; Goodwin et al., 2019 and Chincoteague Bay, in Maryland/Virginia, USA; Beudin et al., 2017). Therefore, our research represents a pioneering effort and the first large-scale application of the temporal approach in the AS and, to our knowledge, in Europe.

The proposed methodology was tested in 2018 as a case study with representative hydrographic patterns of the AS, and in areas with known ecological characteristics. This allowed the verification of the distribution patterns of specific areas in the AS with the existing scientific literature (Morello and Armeri, 2009; Coll et al., 2010; UNEP/MAP-RAC/SPA, 2015; Fanelli et al., 2022). It also established a correlation between the findings and the life cycle traits of different organisms. Future research should aim to improve the coupling of connectivity and biological knowledge at larger spatiotemporal scales. The spatial discretization, as shown in Figure 3, followed a logical subdivision of the domain into a limited number of releasing sub-regions. A more detailed subdivision of space may be necessary in future applications, especially in areas where prior knowledge is lacking. This will require significant computational effort, which can be reduced by using computer clusters. Similarly, the analysis of connectivity over multiple years requires the development of an algorithm-based method to synthesize information and highlight the most relevant aspects. Such a study is currently in progress. All in all, the tool will improve the accuracy of the AS connectivity estimates which could, for example, inform the design of networks of marine protected areas (MPAs), fisheries assessment tools, and management policies.

## Data availability statement

Publicly available datasets were analyzed in this study. This data can be found here: <https://iws.ismar.cnr.it/thredds/catalog/emerget/catalog.html>.

## Author contributions

IN: Conceptualization, Data curation, Formal analysis, Visualization, Writing – original draft. MP: Data curation, Formal analysis, Writing – review & editing. FF: Conceptualization, Data curation, Methodology, Supervision, Writing – review & editing. JG-L: Conceptualization, Formal analysis, Supervision, Writing – review & editing. SS: Investigation, Methodology, Visualization, Writing – review & editing. MG: Conceptualization, Data curation, Formal analysis, Investigation, Methodology, Supervision, Writing – original draft, Writing – review & editing.

## Funding

The author(s) declare financial support was received for the research, authorship, and/or publication of this article. The publication of this work was financially and scientifically supported by the research activities of CNR ISMAR.

## Acknowledgments

Authors are grateful to the Institute of Marine Sciences of the National Research Council of Italy for providing the model data necessary to conduct the numerical experiments (accessed at <https://iws.ismar.cnr.it/thredds/catalog/emerge/catalog.html>), with special thanks to Dr. Christian Ferrarin for his availability. IN

## References

- Abuauza, P., Gordo, L., Karlou-Riga, C., Murta, A., Eltink, A. T. G. W., Santamaría García, M. T., et al. (2003). Growth and reproduction of horse mackerel, *Trachurus trachurus* (Carangidae). *Rev. Fish Biol. Fisher.* 13, 27–61. doi: 10.1023/A:1026334532390
- Alvarez, P., Fives, J., Motos, L., and Santos, M. (2004). Distribution and abundance of European hake *Merluccius merluccius* (L.), eggs and larvae in the North East Atlantic waters in 1995 and 1998 in relation to hydrographic conditions. *J. Plankton Res.* 26, 811–826. doi: 10.1093/plankt/fbh074
- Arneri, E., and Morales-Nin, B. (2000). Aspects of the early life history of European hake from the central Adriatic. *J. Fish Biol.* 56, 1368–1380. doi: 10.1111/j.1095-8649.2000.tb02149.x
- Bajo, M., Ferrarin, C., Dinu, I., Umgiesser, G., and Stanica, A. (2014). The water circulation near the Danube Delta and the Romanian coast modelled with finite elements. *Continental Shelf Res.* 78, 62–74, 0278–4343. doi: 10.1016/j.csr.2014.02.006
- Basilone, G., Ferreri, R., Aronica, S., Mazzola, S., Bonanno, A., Gargano, A., et al. (2021). Reproduction and sexual maturity of european sardine (*Sardina pilchardus*) in the central mediterranean sea. *Front. Mar. Sci.* 8, doi: 10.3389/fmars.2021.715846
- Basilone, G., Guisande, C., Patti, B., Mazzola, S., Cuttitta, A., Bonanno, A., et al. (2006). Effect of habitat conditions on reproduction of the European anchovy (*Engraulis encrasicolus*) in the Strait of Sicily. *Fisheries Oceanography* 15, 271–280. doi: 10.1111/j.1365-2419.2005.00391.x
- Bastari, A., Micheli, F., Ferretti, F., Pusceddu, A., and Cerrano, C. (2016). Large marine protected areas (LMPAs) in the Mediterranean Sea: The opportunity of the Adriatic Sea. *Mar. Policy* 68, 165–177. doi: 10.1016/j.marpol.2016.03.010
- Bellafore, D., and Umgiesser, G. (2010). Hydrodynamic coastal processes in the North Adriatic investigated with a 3D finite element model. *Ocean Dynamics* 60 (2), 255–273. doi: 10.1007/s10236-009-0254-x
- Beudin, A., Ganju, N. K., Defne, Z., and Aretxabaleta, A. L. (2017). Physical response of a back-barrier estuary to a post-tropical cyclone. *J. Geophysical Research: Oceans* 10.1002/2016JC012344 122 7, (5888–5904). doi: 10.1002/2016JC012344
- Bignami, F., Sciarra, R., Carniel, S., and Santoleri, R. (2007). Variability of Adriatic Sea coastal turbid waters from SeaWiFS imagery. *J. Geophysical Res.* 112, C03S10. doi: 10.1029/2006JC003518
- Book, J. W., Signell, R. P., and Perkins, H. (2007). Measurements of storm and nonstorm circulation in the northern Adriatic: October 2002 Through April 2003. *J. Geophysical Res.* 112, C11S92. doi: 10.1029/2006JC003556
- Bray, L., Kassis, D., and Hall-Spencer, J. M. (2017). Assessing larval connectivity for marine spatial planning in the Adriatic. *Mar. Environ. Res.* 125, 73–81. doi: 10.1016/j.marenvres.2017.01.006
- Candelma, M., Marisaldi, L., Bertotto, D., Radelli, G., Gioacchini, G., Santojanni, A., et al. (2021). Aspects of reproductive biology of the european hake (*Merluccius merluccius*) in the northern and central adriatic sea (GSA 17-Central Mediterranean sea). *J. Mar. Sci. Eng.* 9, 389. doi: 10.3390/jmse9040389
- Carbonara, P., Intini, S., Modugno, E., Maradonna, F., Spedicato, M. T., Lembo, G., et al. (2015). Reproductive biology characteristics of red mullet (*Mullus barbatus* L. 1758) in Southern Adriatic Sea and management implications. *Aquat. Living Resour.* 28, 21–31. doi: 10.1051/alr/2015005
- Cavirao, F., Anelli Monti, M., Matić-Skoko, S., Caccin, A., and Pranovi, F. (2022). Vulnerability of the small-scale fishery to climate changes in the northern-central Adriatic sea (Mediterranean sea). *Fishes* 8, 9. doi: 10.3390/fishes8010009
- Ciannelli, L., Bailey, K., and Olsen, E. (2014). Evolutionary and ecological constraints of fish spawning habitats. *ICES J. Mar. Sci.* 72, 285–296. doi: 10.1093/icesjms/fsu145
- Cvitarese, G., Gacic, M., Vetrano, A., Boldrin, A., Bregant, D., Rabitti, S., et al. (1998). Biogeochemical fluxes through the Otranto Strait (Eastern Mediterranean). *Cont. Shelf Res.* 18, 773–789.
- Coll, M., Santojanni, A., Palomera, I., and Arneri, E. (2010). Ecosystem assessment of the North-Central Adriatic Sea: Towards a multivariate reference framework. *Mar. Ecol. Prog. Series* 417, 193–210. doi: 10.3354/meps08800
- Costa, A. M. (2013). Somatic condition, growth and reproduction of Hake, *Merluccius merluccius* L., on the Portuguese Coast. *Mar. Sci.* 3, 12–30. doi: 10.4236/ojms.2013.1002

acknowledges a predoctoral fellowship from the Spanish Ministry of Science and Innovation under the project BLUEMARO (PID2020-116136RB-I00). The constructive suggestions and advices of the reviewers are gratefully acknowledged.

## Conflict of interest

The authors declare that the research was conducted in the absence of any commercial or financial relationships that could be construed as a potential conflict of interest.

## Publisher's note

All claims expressed in this article are solely those of the authors and do not necessarily represent those of their affiliated organizations, or those of the publisher, the editors and the reviewers. Any product that may be evaluated in this article, or claim that may be made by its manufacturer, is not guaranteed or endorsed by the publisher.

## Supplementary material

The Supplementary Material for this article can be found online at: <https://www.frontiersin.org/articles/10.3389/fmars.2024.1360077/full#supplementary-material>

- Cowen, R. K., Paris, C. R., and Srinivasan, A. (2006). Scaling of connectivity in marine populations. *Science* 311, 522–527. doi: 10.1126/science.1122039
- Cowen, R. K., and Sprounle, S. (2009). Larval dispersal and marine population connectivity. *Annu. Rev. Mar. Sci.* 1, 443–466. doi: 10.1146/annurev.marine.010908.163757
- Cozzi, S., and Giani, M. (2011). River water and nutrient discharges in the Northern Adriatic Sea: Current importance and longterm changes. *Continental Shelf Res.* 31, 1881–1893. doi: 10.1016/j.csr.2011.08.010
- Crochetet, E., Roberts, J., Lagabirre, E., Obura, D., Petit, M., and Chabanet, P. (2016). A model-based assessment of reef larvae dispersal in the Western Indian Ocean reveals regional connectivity patterns—Potential implications for conservation policies. *Regional Stud. Mar. Sci.* 7, 159–167. doi: 10.1016/j.rsmas.2016.06.007
- D'Agostini, A., Gherardi, D. F., and Pezzi, L. P. (2015). Connectivity of marine protected areas and its relation with total kinetic energy. *PLoS One* 10, e0139601. doi: 10.1371/journal.pone.0139601
- Dagestad, K.-F., Röhrs, J., Breivik, Ø., and Ådlandsvik, B. (2018). OpenDrift v1.0: a generic framework for trajectory modelling. *Geosci. Model. Dev.* 11, 1405–1420. doi: 10.5194/gmd-11-1405-2018
- Da Ros, Z., Fanelli, E., Cassatella, S., Biagiotti, I., Canduci, G., Menicucci, S., et al. (2023). Resource Partitioning among “Ancillary” Pelagic Fishes (*Scomber* spp., *Trachurus* spp.) in the Adriatic Sea. *Biol. (Basel)* 12, 272. doi: 10.3390/biology12020272
- Defne, Z., Ganju, N. K., and Artxabaleta, A. (2016). Estimating time-dependent connectivity in marine systems. *Geophys. Res. Lett.* 43, 1193–1201. doi: 10.1002/2015GL066888
- Fanelli, E., Da Ros, Z., Menicucci, S., Malavolti, S., Biagiotti, I., Canduci, G., et al. (2023). The pelagic food web of the Western Adriatic Sea: a focus on the role of small pelagics. *Sci. Rep.* 13, 14554. doi: 10.1038/s41598-023-40665-w
- Fanelli, E., Principato, E., Monfardini, E., Da Ros, Z., Scarcella, G., Santoianni, A., et al. (2022). Seasonal trophic ecology and diet shift in the common sole *Solea solea* in the central Adriatic sea. *Animals* 12, 3369. doi: 10.3390/ani12233369
- Ferrarin, C., Davolio, S., Bellafiore, D., Ghezzi, M., Maicu, F., Mc Kiver, W., et al. (2019). Cross-scale operational oceanography in the Adriatic Sea. *J. Operational Oceanography* 12, 86–103. doi: 10.1080/1755876X.2019.1576275
- Fogarty, M., and Botsford, L. (2007). Population connectivity and spatial management of marine fisheries. *Oceanography* 20, 112–123. doi: 10.5670/oceanog.2007.34
- Gaines, S., White, C., Carr, M., and Palumbi, S. (2010). Designing marine reserve networks for both conservation and fisheries management. *Proc. Natl. Acad. Sci. United States America* 107, 18286–18293. doi: 10.1073/pnas.0906473107
- Gamoyo, M., Obura, D., and Reason, C. (2019). Estimating connectivity through larval dispersal in the Western Indian Ocean. *J. Geophysical Research: Biogeosciences* 124, 2446–2459. doi: 10.1029/2019JG005128
- García-Lafuente, J., Sánchez-Garrido, J. C., García, A., Hidalgo, M., Sammartino, S., and Laiz, R. (2021). “Biophysical processes determining the connectivity of the Alboran Sea fish populations.” in *Alboran Sea—Ecosystems and marine resources*. Eds. J. C. Baez, J. T. Vázquez, J. A. Caminas and M. Malouf (Springer Nature, Switzerland AG). doi: 10.1007/978-3-030-65516-7\_12
- GFCM (2009). *Resolution GFCM/33/2009/2 on the establishment of geographical subareas in the GFCM area of application, amending Resolution GFCM/31/2007/2*.
- GFCM (2021). *Recommendation GFCM/A4/2021/2 on the establishment of a fisheries restricted area in the Jabuka/Pomo Pit in the Adriatic Sea (geographical subarea 17), amending Recommendation GFCM/A1/2017/3*.
- Ghezzi, M., De Pascalis, F., Umgiesser, G., Zemly, P., Sigovini, M., Marcos, C., et al. (2015). Connectivity in three European coastal lagoons. *Estuaries Coasts* 38, 1764–1781. doi: 10.1007/s12237-014-9908-0
- Ghezzi, M., Pellizzato, M., De Pascalis, F., Silvestri, S., and Umgiesser, G. (2018). Natural resources and climate change: A study of the potential impact on Manila clam in the Venice lagoon. *Sci. Total Environ.* 645, 419–430. doi: 10.1016/j.scitotenv.2018.07.060
- Goodwin, J., Munroe, D. M., Defne, Z., Ganju, N. K., and Vassilides, J. (2019). Estimating Connectivity of Hard Clam (*Mercaenaria mercenaria*) and Eastern Oyster (*Crassostrea virginica*) Larvae in Barnegat Bay. *J. Mar. Sci. Eng.* 7, (167). doi: 10.3390/jmse7060167
- Grati, F., Aladrux, A., Azzurro, E., Bolognini, L., Carbonara, P., Cobani, M., et al. (2018). Seasonal dynamics of small-scale fisheries in the Adriatic Sea. *Mediterr. Mar. Sci.* 19, 21–35. doi: 10.12681/mms.2153
- Hersbach, H., Bell, B., Berrisford, P., Biavati, G., Horányi, A., Muñoz Sabater, J., et al. (2023). ERA5 hourly data on single levels from 1940 to present. Copernicus Climate Change Service (C3S) Climate Data Store (CDS). doi: 10.24381/cds.adbb2d47
- Hidalgo, M., Ligas, A., Bellido, J.M., Bitetto, L., Carbonara, P., Carlucci, R., et al. (2019). Size-dependent survival of European hake juveniles in the Mediterranean Sea. *Sci. Mar.* 83S1, 207–221. doi: 10.3989/scimar.04857.16A
- Jardas, I., Santic, M., and Pallarós, A. (2004). Diet composition and feeding intensity of horse mackerel, *Trachurus trachurus* (Osteichthyes: Carangidae) in the eastern Adriatic. *Biol. Mar.* 144, 1051–1056. doi: 10.1007/s00227-003-1281-7
- Khoufi, W., Ferreri, R., Jaziri, H., El Fehri, S., Gargano, A., Mangano, S., et al. (2014). Reproductive traits and seasonal variability of *Merluccius merluccius* from the Tunisian coast. *J. Mar. Biol. Assoc. United Kingdom* 94, 1545–1556. doi: 10.1017/S0025315414000356
- Kuzmić, M., Janeković, I., Book, J. W., Martin, P. J., and Doyle, J. D. (2006). Modeling the northern Adriatic double-gyre response to intense bora wind: A revisit. *J. Geophys. Res.* 111, C03S13. doi: 10.1029/2005JC003377
- Largier, J. (2003). Considerations in estimating larval dispersal distances from oceanographic data. *Ecol. Appl.* 13, 71–89. doi: 10.1890/1051-0761(2003)013[0071:CIEDLD]2.0.CO;2
- Lester, S. E., Halpern, B. S., Grorud-Colvert, K., Lubchenko, J., Ruttenberg, B. I., Gaines, S. D., et al. (2009). Biological effects within no-take marine reserves: a global synthesis. *Mar. Ecol. Prog. Ser.* 384, 33–46. doi: 10.3354/meps08029
- Lipizer, M., Partescano, E., Rabbitti, A., Giorgietti, A., and Crise, A. (2014). Qualified temperature, salinity and dissolved oxygen climatologies in a changing Adriatic Sea. *Ocean Sci.* 10, 771–797. doi: 10.5194/os-10-771-2014
- López-Márquez, V., Templado, J., Buckley, D., Marino, I., Boscarì, E., Micu, D., et al. (2019). Connectivity among populations of the top shell *Gibbula divaricata* in the Adriatic sea. *Front. Genet.* 10. doi: 10.3389/fgene.2019.010077
- Martin, P. J., Book, J. W., Burrage, D. M., Rowley, C. D., and Tudor, M. (2009). Comparison of model-simulated and observed currents in the central Adriatic during DART. *J. Geophysical Res.* 114, C01R05. doi: 10.1029/2008JC004842
- McKiver, W. J., Sannino, G., Braga, F., and Bellafiore, D. (2016). Investigation of model capability in capturing vertical hydrodynamic coastal processes: a case study in the north Adriatic Sea. *Ocean Sci.* 12, 51–69. doi: 10.5194/os-12-51-2016
- Medvedev, I. P., Vilibić, I., and Rabinovich, A. B. (2020). Tidal resonance in the Adriatic Sea: Observational evidence. *J. Geophysical Research: Oceans* 125, e2020JC016168. doi: 10.1029/2020JC016168
- Molinari, E., Peschiutta, M., and Rizzetto, F. (2023). Long-term evolution of an urban barrier island: the case of Venice Lido (Northern Adriatic Sea, Italy). *Water* 15, 1927. doi: 10.3390/w15101927
- Morales-Nin, B., and Moranta, J. (2004). Recruitment and post settlement growth of juvenile *Merluccius merluccius* on the western Mediterranean shelf. *Scientia Marina* 63, 399–409. doi: 10.3989/scimar.2004.68n3
- Morello, E., and Arneri, E. (2009). “Anchovy and sardine in the Adriatic sea— an ecological review.” in *Oceanography and marine biology: an annual review*. Eds. R. N. Gibson, R. J. A. Atkinson and J. D. M. Gordon (Boca Raton, FL: CRC Press), 209–256. doi: 10.1201/9781420094220.ch5
- Motos, L. (1996). Reproductive biology and fecundity of the Bay of Biscay anchovy population (*Engraulis encrasicolus*, L.). *Scientia Marina* 60, 195–207.
- Muntoni, M. (2015). *A multidisciplinary approach for puzzling over fish connectivity in the Mediterranean Sea: The role of early life history stages of red mullet (Mullus barbatus)* (Università degli Studi di Cagliari).
- Murua, H., and Motos, L. (2006). Reproductive strategy and spawning activity of the European hake *Merluccius merluccius* (L.) in the Bay of Biscay. *J. Fish Biol.* 69, 1288–1303. doi: 10.1111/j.1095-8649.2006.01169.x
- Nadal, I., Sammartino, S., García-Lafuente, J., Sánchez Garrido, J. C., Gil-Herrera, J., Hidalgo, M., et al. (2022). Hydrodynamic connectivity and dispersal patterns of a transboundary species (*Pagellus bogaraveo*) in the Strait of Gibraltar and adjacent basins. *Fisheries Oceanography* 31, 384–401. doi: 10.1111/fog.12583
- Orlić, M., Gačić, M., and La Violette, P. E. (1992). The currents and circulation of the Adriatic Sea. *Oceanologia Acta* 15, 109–124.
- Orlić, M., Kuzmić, M., and Pasarić, Z. (1994). Response of the Adriatic Sea to the bora and sirocco forcing. *Continental Shelf Res.* 14, 91–116. doi: 10.1016/0278-4343(94)90007-8
- Paoletti, S., Bekaert, K., Barbut, L., Lacroix, G., Volckaert, F. A. M., Hostens, K., et al. (2021). Validating a biophysical dispersal model with the early life-history traits of common sole (*Solea solea* L.). *PLoS One* 16, e0257709. doi: 10.1371/journal.pone.0257709
- Pasarić, Z., Belušić, D., and Chiggiato, J. (2009). Orographic effects on meteorological fields over the Adriatic from different models. *J. Mar. Syst.* 78, S90–S100. doi: 10.1016/j.jmarsys.2009.01.019
- Pasarić, Z., Belušić, D., and Zvezdana, B. C. (2007). Orographic influences on the Adriatic sirocco wind. *Earth System Dynamics* 12, 939–973. doi: 10.5194/esd-12-939-2021
- Patti, B., Torri, M., and Cattitta, A. (2020). General surface circulation controls the interannual fluctuations of anchovy stock biomass in the Central Mediterranean Sea. *Sci. Rep.* 10, 1554. doi: 10.1038/s41598-020-58028-0
- Pineda, J. (1991). Predictable upwelling and the shoreward transport of planktonic larvae by internal tidal bores. *Science* 253, 548–549. doi: 10.1126/science.253.5019.548
- Poulain, P. M. (2001). Adriatic Sea surface circulation as derived from drifter data between 1990 and 1999. *J. Mar. Syst.* 29, 3–32. doi: 10.1016/S0924-7963(01)00007-0
- Revelante, N., and Glimartin, M. (1992). The lateral advection of particulate organic matter from the Po delta region during summer stratification, and its implications for the northern Adriatic. *Estuar. Coast. Shelf Sci.* 35, 191–212. doi: 10.1016/S0272-7714(05)80113-1
- Russo, A., and Artegiani, A. (1996). Adriatic sea hydrography. *Scientia Marina* 60, Suppl. 2, 33–43.
- Ružić, I., Dugonjić Jovančević, S., Benac, C., and Kravica, N. (2019). Assessment of the coastal vulnerability index in an area of complex geological conditions on the krk island, Northeast Adriatic sea. *Geosciences* 9, 219. doi: 10.3390/geosciences9050219
- Sciaccia, R., Berta, M., Carlson, D. F., Griffa, A., Panfilii, M., La Mesa, M., et al. (2018). Linking sardine recruitment in coastal areas to ocean currents using surface drifters and



HF radar: A case study in the Gulf of Manfredonia, Adriatic Sea. *Ocean Sci.* 14, 1461. doi: 10.5194/os-14-1461-2018

Somarakis, S., Palomera, I., Garcia, A., Quintanilla, L., Koutsikopoulos, C., Uriarte, A., et al. (2004). Daily egg production of anchovy in European waters. *ICES J. Mar. Sci.* 61, 944–958. doi: 10.1016/j.jcesjms.2004.07.018

Specchiulli, A., Bignami, F., Marini, M., Fabbrocini, A., Scrocco, T., Campanelli, A., et al. (2016). The role of forcing agents on biogeochemical variability along the southwestern Adriatic coast: The Gulf of Manfredonia case study. *Estuarine Coast. Shelf Sci.* 183, 136–149. doi: 10.1016/j.ecss.2016.10.033

Tonani, M., Pinardi, N., Dobricic, S., Pujol, I., and Fratianni, C. (2008). A high-resolution free-surface model of the Mediterranean Sea. *Ocean Science* 4 (1), 1–14. doi: 10.5194/osd-4-213-2007

Tremblé, E., Roberts, J., Chao, Y., Halpin, P., Possingham, H., and Riginos, C. (2012). Reproductive output and duration of the pelagic larval stage determine seascape-wide connectivity of marine populations. *Integr. Comp. Biol.* 52, 525–537. doi: 10.1093/icb/ics101

Tsikliras, A., Antonopoulou, E., and Stergiou, K. (2010). Spawning period of Mediterranean marine fishes. *Rev. Fish Biol. Fisheries.* 20, 499–538. doi: 10.1007/s11160-010-9158-6

Umgiesser, G., Canu, D. M., and Cucco, A. (2004). A finite element model for the Venice Lagoon Development: set up, calibration & validation. *J. Mar. Syst.* 51, 123–145. doi: 10.1016/j.jmarsys.2004.05.009

Umgiesser, G., Ferrarin, C., Bajo, M., Bellafiore, D., Cucco, A., De Pascalis, F., et al. (2022). Hydrodynamic modelling in marginal and coastal seas — The case of the Adriatic Sea as a permanent laboratory for numerical approach. *Ocean Model.* 179, 102123. doi: 10.1016/j.oceanmod.2022.102123

Umgiesser, G., Ferrarin, C., Cucco, A., De Pascalis, F., Bellafiore, D., Ghezzi, M., et al. (2014). Comparative hydrodynamics of 10 Mediterranean lagoons by means of numerical modeling. *J. Geophys. Res.-Oceans* 119, 2212–2226. doi: 10.1002/2013JC009512

UNEP/MAP-RAC/SPA (2015). *Adriatic Sea: Description of the ecology and identification of the areas that may deserve to be protected*. Eds. C. Cerrano, D. Cebrían and S. Requena (Tunis: RAC/SPA), 92. doi: 10.13140/RG.2.2.14080.79368

Ungaro, N., Rizzi, E., and Marano, G. (1993). Note sulla biologia e pesca di *Merluccius merluccius* (L.) nell'Adriatico pugliese. *Biol. Marina* suppl. 1, 329–334.

Van Beveren, E. (2012). *Patterns of recruitment and early life history traits of *Trachurus trachurus* in a nearshore temperate reef* (Faro: Universidade do Algarve), 45.

Van Sebille, E., Griffies, S. M., Abernathy, R., Adams, T. P., Berloff, P., Biastoch, A., et al. (2018). Lagrangian ocean analysis: Fundamentals and practices. *Ocean Model.* 121, 49–75. doi: 10.1016/j.oceanmod.2017.11.008

Viette, M., Giulianini, P. G., and Ferrero, E. A. (1997). Reproductive biology of scad, *Trachurus mediterraneus* (Teleostei, Carangidae), from the Gulf of Trieste. *ICES J. Mar. Sci.* 54, 267–272. doi: 10.1006/jmsc.1996.0185

Vilibić, I., Matijević, S., Šepić, J., and Kušpilić, G. (2012). Changes in the Adriatic oceanographic properties induced by the Eastern Mediterranean Transient. *Biogeosciences* 9, 2085–2097. doi: 10.5194/bg-9-2085-2012

Vrgoč, N., Arneri, E., Jukū-Peladiū, S., Krstulović Šifner, S., Mannini, P., Marjeta, B., et al. (2004). Review of current knowledge on shared demersal stocks of the Adriatic Sea. *FAO-MIPAF Sci. Cooperation to Support Responsible Fisheries Adriatic Sea. GCP/RER/010/ITTA/TD-12. AdriaMed Tech. Documents* 12, 91.

Williams, P. D., and Hastings, A. (2013). Stochastic dispersal and population persistence in marine organisms. *Am. Nat.* 182, 271–282. doi: 10.1086/671059

Zardoya, R., Castilho, R., Grande, C., Favre-Krey, L., Caetano, S., Marcato, S., et al. (2004). Differential population structuring of two closely related fish species, the mackerel (*Scomber scomber*) and the chub mackerel (*Scomber japonicus*), in the Mediterranean Sea. *Mol. Ecol.* 13, 1785–1798. doi: 10.1111/j.1365-294X.2004.02198.x

Zore (1956). On gradient currents in the Adriatic Sea. *Acta Adriat.* 8, 1–38.

Zorica, B., Anđelić, I., and Čikeš Keč, V. (2019). Sardine (*Sardina pilchardus*) spawning in the light of fat content analysis. *Sci. Mar* 83 (3), 207–213. doi: 10.3989/scimar.04898.07A

Zorica, B., Čikeš Keč, V., Vrgoč, N., Isajlović, I., Piccinetti, C., Mandić, M., et al. (2020). A review of reproduction biology and spawning/nursery grounds of the most important Adriatic commercial fish species in the last two decades. *Acta Adriat.* 61, 89–100. doi: 10.32582/aa.61.1.7

## PLOS ONE

## RESEARCH ARTICLE

# Could secondary flows have made possible the cross-strait transport and explosive invasion of *Rugulopteryx okamurae* algae in the Strait of Gibraltar?

Jesús García-Lafuente<sup>1\*</sup>, Irene Nadal<sup>1</sup>, Simone Sammartino<sup>2</sup>, Nathalie Korbee<sup>3</sup>, Félix L. Figueroa<sup>3</sup>

**1** Physical Oceanography Group, Instituto de Biotecnología y Desarrollo Azul (IBYDA), Universidad de Málaga, Málaga, Spain, **2** Physical Oceanography Group, Instituto de Ingeniería Oceánica (IO), Universidad de Málaga, Málaga, Spain, **3** Department of Ecology and Geology, Instituto de Biotecnología y Desarrollo Azul (IBYDA), Universidad de Málaga, Málaga, Spain

\* [glafuente@ctima.uma.es](mailto:glafuente@ctima.uma.es)



## OPEN ACCESS

**Citation:** García-Lafuente J, Nadal I, Sammartino S, Korbee N, Figueroa FL (2023) Could secondary flows have made possible the cross-strait transport and explosive invasion of *Rugulopteryx okamurae* algae in the Strait of Gibraltar? PLoS ONE 18(5): e0285470. <https://doi.org/10.1371/journal.pone.0285470>

**Editor:** Atsushi Fujimura, University of Guam, GUAM

**Received:** August 11, 2022

**Accepted:** April 25, 2023

**Published:** May 23, 2023

**Copyright:** © 2023 García-Lafuente et al. This is an open access article distributed under the terms of the [Creative Commons Attribution License](https://creativecommons.org/licenses/by/4.0/), which permits unrestricted use, distribution, and reproduction in any medium, provided the original author and source are credited.

**Data Availability Statement:** Data can be found in the following three repositories: García-Lafuente Jesús, Sammartino Simone (2023). Current profiles at Camarinal Sill (Strait of Gibraltar) | Jun-Sep 2013. SEANOE. <https://doi.org/10.17882/92892> García-Lafuente Jesús, Sammartino Simone, Sánchez-Leal Ricardo (2023). Current profiles at Camarinal Sill (Strait of Gibraltar) | Aug 2020 - May 2021. SEANOE. <https://doi.org/10.17882/92898> García-Lafuente Jesús (2023). Current at Eastern margin of the Strait of Gibraltar |

## Abstract

Presently, the Strait of Gibraltar is undergoing an unprecedented invasion of the alien alga *Rugulopteryx okamurae* of North Pacific origin. According to the scarce literature, the algae first settled in the south shore, probably following commercial exchanges with French ports where it was accidentally introduced together with Japanese oysters imported for mariculture. There is no certainty, however, that the algae first colonized the south shore of the Strait and, from there, spread to the north. It could well have been the opposite. Whatever the case, it spread all over the Strait and surrounding areas with amazing rapidity. Human-mediated vectors (algae attached to ship hulls or fishing nets, for example) can be behind the spread from the shore initially settled to the algae-free shore on the opposite side. But it could also have happened by means of hydrodynamic processes without direct human intervention. This possibility is assessed in this paper by revisiting historical current meter profiles collected in the Strait of Gibraltar searching for secondary cross-strait flows. All the stations present an intermediate layer of northward cross-strait velocity near the interface of the mean baroclinic exchange along with a surface layer above of southward velocity, whose lower part also overlaps the interface zone. The first one would back the south-to-north transport of algal fragments, the second one, the north-to south. In both cases, algae must reach the depth of the interface. The vertical velocity field in the area, which far exceeds the small sedimentation velocity of the algae, allows their vertical displacements throughout the water column. Its endurance to survive under the weak or no light conditions that will prevail during the cross-strait transport and its capability of reactivating the metabolism after this unfavorable period, offers chances for colonizing the opposite shore. Therefore, the propagation of the algae by hydrodynamic processes, without human intervention, cannot be ruled out.

Oct 1995 - Mar 1998. SEANOE. <https://www.seanoe.org/data/00817/92900/>.

**Funding:** IN acknowledges a predoctoral fellowship of the Ministerio de Asuntos Económicos y Transformación Digital, Gobierno de España funded project PID2020-116136RB-I00 (Interdisciplinary research for blue management of the invasive alien alga *Rugulopteryx okamurae* in the Mediterranean (BLUEMARO)). This work is a scientific contribution to this project. The funders had no role in study design, data collection and analysis, decision to publish, or preparation of the manuscript.

**Competing interests:** The authors have declared that no competing interests exist.

## Introduction

Since the mid-2010s, the coasts around the Strait of Gibraltar (SoG, hereinafter) and neighboring basins (Fig 1) are suffering from a drastic invasion of the algae *Rugulopteryx okamurae* [1], a brown macroalga belonging to the Dictyotaceae family (Dictyotales order), original from the northwestern Pacific Ocean [2]. The alga was detected in the small Mediterranean lagoon of Thau, southwest of France, in year 2002 for the first time in Europe [3] where, according to these authors, it was probably introduced along with Japanese oysters imported for mariculture purposes. In year 2015 the alga was found off Ceuta in the south coasts of the SoG [4–7] where it could have arrived following commercial exchanges with Tangier-Med port (Fig 1). Leisure boats and their marinas have been also shown to be important components of the hub-and-spoke model of invasion in coastal systems [8]. On the other hand, algae could have already been present on the north coast at that time and not have been identified due to its resemblance to other algae already established in the area, although a benthic community monitoring program at some fixed sentinel stations established on the north coast did not detect algae up until 2016 [1]. In spite of this fact, which gives weak support to the southern pathway, the precise route of entry still remains uncertain. Regardless this uncertainty, the point is that, in few years, the alga has occupied the illuminated rocky seafoam of large extended coastal areas in both shores of the SoG and adjacent basins [1], featuring an aggressive invasion with no precedents in European coastal waters (Fig 2A and 2B). Northern Africa

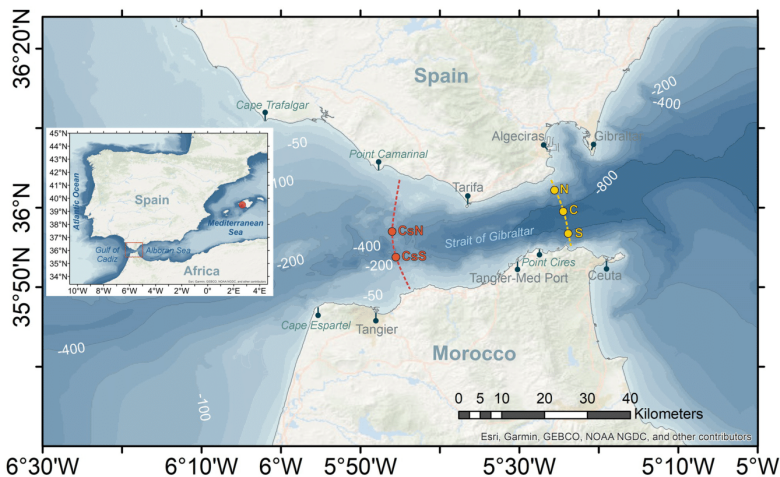


**Fig 1. Map of the Strait of Gibraltar showing bathymetric features and locations and geographic sites mentioned in the text.** Dots labelled N, C, and S in the eastern part and CnN and CsS in Camarinal section are the stations where current meter data used in this study come from. Red dot in the inset indicates Palma de Mallorca in the Balearic Islands. Sources: Esri, GEBCO, NOAA, National Geographic, DeLorme, HERE, Geonames.org, and other contributors. Maps were created using ArcGIS<sup>®</sup> software by Esri. ArcGIS<sup>®</sup> and ArcMap<sup>®</sup> are the intellectual property of Esri and are used herein under license. Copyright Esri. All rights reserved. For more information about Esri<sup>®</sup> software, please visit [www.esri.com](http://www.esri.com).

<https://doi.org/10.1371/journal.pone.0285470.g001>

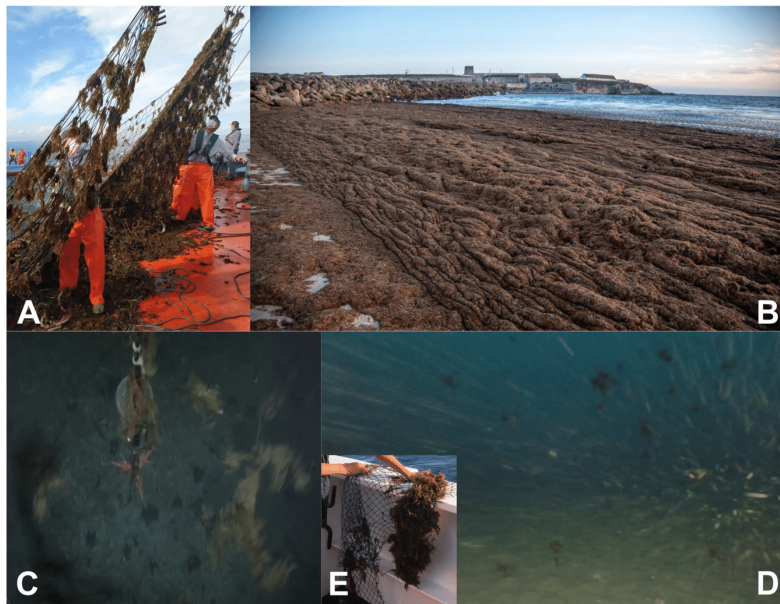


**Fig 2.** A) Tuna fishing net (Almadraba) pulled from the sea in Tarifa nearly covered with *Rugulopteryx okamurae*. B) Massive *Rugulopteryx okamurae* beaching nearby Tarifa. C) Frame taken from a video recorded by a Remotely Operated Vehicle during a rescue operation of a mooring line off Cape Espartel (see Fig 1) showing thalli of *Rugulopteryx okamurae* drifted by the Mediterranean outflow. Sea floor (identified by the grey spots in the background) is at 360m depth. D) Frame taken from a video recorded by a camera attached to a trawling net showing several fragments of *Rugulopteryx okamurae*. The fishing vessel was working to the northeast, but near of the eastern limit of the SoG and the videocamera was at 120m depth. E) Fragments of *Rugulopteryx okamurae* attached to scientific equipment deployed at 350m depth off Espartel which were collected when the instruments were brought to the surface for maintenance.

<https://doi.org/10.1371/journal.pone.0285470.g002>

and the southern Iberian Peninsula are the most intensely affected area, but it continues expanding towards the west and east with the threat of monopolizing the sea rocky bottom to the detriment of photophilous resident biota [1, 9]. Currently, the exotic alga has colonized the Marsella coast [10] and even the Azores islands [11]. More worrisome is the risk pointed out by [12] that it could cover the whole Mediterranean coasts.

The explosive spreading would be linked to favorable environmental conditions, since the photic zone in the area gathers suitable year-round temperature for growth and reproduction of this subtropical species [1, 13], but also to the fact that broken thalli serve as seeding population, since their specimens present vegetative propagules [4, 14]. A remarkable fact to this regard is that thalli and propagules are actually found drifting not only in the illuminated zone where they are also fixed to the bottom but also at practically any depth of the SoG (Fig 2C–2E).

The plausible hypothesis that algae first settled in a shore of the SoG, likely the south one according to the scarce available literature, poses the question of how did it spread to the other shore. Different mechanisms could be behind the spreading. The first and more plausible one is linked to the heavy ship traffic in the area, which includes continuous north-to-south ferry and other commercial ships crossing the Strait. The alga shows huge capability to colonize any type of hard substrates, not only rocky seafloor but glass, ceramic, iron, tires, etc. [15], so the eventual crossing attached to ship hulls, fishing nets, including scientific sampling nets [16], or other human-mediated vectors as the mentioned recreational boats [8] cannot be ruled out. Neither ballast waters from remote shipments can be discarded [17, 18]. Another possibility, however, is that the algae managed to cross the SoG taking advantage of hydrodynamic processes without human intervention. Such possibility is revised in this paper. Interestingly, it would be also applicable to pelagic larvae and propagule of other marine species that last for weeks in the pelagic realm. This opens new hypothesis about transport mechanisms between Lusitanian and Mauritanian biogeographical regions, which could eventually be testable by applying molecular techniques among populations.

### Possible mechanisms for cross-strait connection

The SoG holds a well-known two-way (baroclinic) exchange necessary to compensate for the freshwater and buoyancy losses in the Mediterranean basin. It results in intense, zonal-oriented currents: an eastward Atlantic inflow into the Mediterranean Sea at the surface, and a subsurface Mediterranean outflow towards the Atlantic Ocean beneath (see [19] or [20], for instance). Under such a system of currents, the spreading of alga and further substrate colonization in west-east direction would be achievable relatively easily, but it will not be that easy in the cross-strait direction. The intense along-strait currents behave as hydrodynamic barriers for cross-strait transport [21] that, moreover, would carry propagules out of the dimensions of the SoG well before they have chances to get to the opposite shore.

There is, however, a loophole for this dynamic constriction, which is the necessary vanishing of the along-strait current at the depth of the interface between the Atlantic and Mediterranean layers. Should exist a cross-strait secondary flow at this depth, even if weak, the chances to successfully cross the Strait would be no null. Secondary flows are linked to rotation and friction with the solid boundaries, which are the ingredients of Ekman boundary layers [22, 23]. The along-strait inflow and outflow are density driven flows, as there is no geostrophic balance (pressure gradients balanced by Coriolis force) in the along-strait equation. However, the earth rotation acting upon them, forces a pressure gradient that leads to geostrophic cross-strait balance [19, 20, 24], a pattern known as semi-geostrophy or semi-geostrophic flows. Fig 3 shows the good agreement between that pressure gradient, as given by the sea level difference between south and north shores, and the along-strait velocity in the Atlantic layer at the eastern SoG.

The semi-geostrophic balance tends to accumulate water of the surface layer in the south coast of the SoG to build up the pressure gradient, a process that favors the north-to-south transport within this layer. Near the lateral boundary the geostrophically-balanced current is reduced by friction, so that the pressure gradient is able to drive cross-isobar ageostrophic flows (see Fig 4 and caption there) and generate a secondary cross-strait circulation [25, 26]. Laboratory experiments of two-layer exchange through channels of half-circular cross section [27] suggest that this flow is partially driven by the dynamics of Ekman boundary layers, where the net Ekman transport is to the left of the jet that induces the layer, looking downstream (Fig 4A). These authors suggest the existence of robust interfacial Ekman layers contributing to the secondary flow, although the behavior of these layers in the laboratory

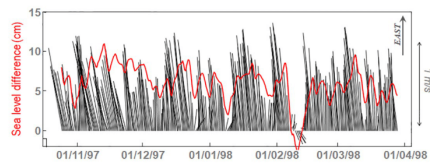


**Fig 3.** Black lines: Stick diagram of the velocity (scale on the right) recorded at 50m depth in site "C", station C2 (Fig 1, Table A in S1 File). Vectors are oriented with reference to the East, indicated in the upper-right corner. Red line is the sea level difference between south (Ceuta, see Fig 1) and north (Algeciras) shores. Positive values indicate northward sea surface downslope (higher sea level in the south) as predicted by the geostrophic adjustment of an eastward surface current. (Adapted from [34]).

<https://doi.org/10.1371/journal.pone.0285470.g003>

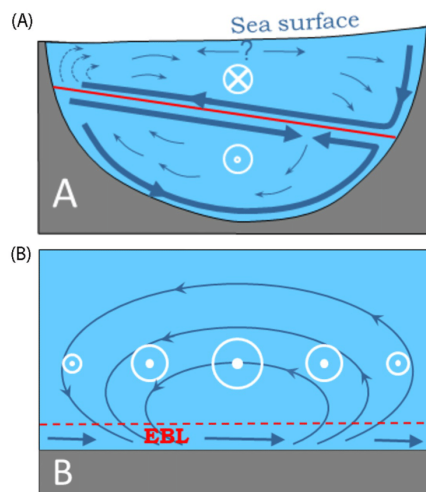


**Fig 4.** A) Schematic of a two-layer exchange through a channel of half-circular geometry, adapted from Johnson and Ohlsen (1994). Encircled white cross (dot) indicates flow into (out of) the page, thus resembling the exchange through the SoG as observed from the Atlantic looking to the Mediterranean, with the north (south) shore in the left (right). Northward downslope of the free surface and southward downslope of the interface (solid red line) are disclosed. Thick arrows indicate the solid boundary and interfacial boundary Ekman layers, whereas thin arrows illustrate the return flow in the interior (secondary circulation). B) Sketch of the interior ageostrophic circulation (thin arrows) driven by the convergence and divergence of the Ekman transport (horizontal thicker arrows) in the Ekman boundary layer (EBL, dashed red line) beneath a spatially-variable jet, represented by the (size) of the white encircled dots. Since outside of the EBL the flow is geostrophic (water moves along isobars) the secondary circulation represented by the thin arrows crosses the isobars and is therefore ageostrophic or out of geostrophic balance.

<https://doi.org/10.1371/journal.pone.0285470.g004>



experiments was more complicated than expected as they did not extend all the way to the lateral boundaries, but apparently converged somewhere by the central part.

On the other hand, a spatially-variable jet flowing over the seafloor causes convergence and/or divergence in the bottom Ekman boundary layer (Fig 4B), in the same manner as a spatially-changing wind stress over the sea surface drives downwelling/upwelling in the open ocean. The jet forces an interior across-jet flow, sketched by the thin blue lines in Fig 4B that, in addition to slightly diminishing the jet strength via the Coriolis force (spin-down process; [23]), it facilitates across-jet transport of particles. Near-bottom Mediterranean outflow in the SoG shares spatial characteristics with this idealized jet [28] for which it would provide chances for south-to-north connections in the present case.

The previous discussion has assumed a steady state exchange, which is far from being the case in the SoG. Tidal currents are strong enough to reverse the mean currents at semidiurnal time-scales [19, 28, 29] and, therefore, to cancel the intense flows during short time intervals. A first question is whether tidal dynamics could offer opportunity windows of diminished east-west flows for achieving north-south transport in a complete way. Tidal ellipses (over a tidal cycle, the tips of the tidal velocity vector trace out an ellipse called tidal ellipse) tend to have its major axis aligned with the shoreline and, therefore, its minor axis characterizes the cross-strait tidal velocity. Ellipses are highly polarized [30] with minor axis less than  $10 \text{ cm s}^{-1}$  in all cases. A periodic velocity of this size causes periodic displacements of 1.4 km at semidiurnal frequencies, twice this value at diurnal ones, which are clearly insufficient to achieve a successful crossing. However, the shoreline orientation of the SoG changes noticeably from place to place. In the north, the shore veers almost  $90^\circ$  around Tarifa, changing orientation from NW-SE in the west to SW-NE in the east (Fig 1). Something alike happens in the south around Punta Cires (Fig 1). These important changes of orientation cause local misalignments of the ellipses that leave them partially oriented in the cross-strait direction [31]. Tidal currents around such singular sites would then contribute to eventual cross-strait transport more efficiently.

Another potential mechanism is the interaction of the total current with the lateral boundaries. It mainly entails the surface layer, which experiences the effect of abrupt changes of the shoreline orientation more than the Mediterranean layer, where bathymetry hardly changes orientation (Fig 1). [31] or [32], using Lagrangian trajectories of passive tracers computed from the output of a numerical model, show cross-strait intrusions of the tracer in the neighborhood of these particular sites, opening new chances for a successful north-south connection. The mechanism is similar to the previous one, except for the fact that it deals with total current, not only tidal ones.

A detailed investigation of whether these processes can eventually lead to a successful hydrodynamic connection between the opposite shores of the SoG should be carried out by means of high spatial resolution advection schemes coupled to fully 3D, non-hydrostatic numerical models. Previously to such numerical effort, however, searching for observational evidences of cross-strait flows in existing records is an interesting exercise that can assist in future research. This is the objective of this work, which analyses different current meter data collected in the SoG to assess the potential of the recorded currents as vectors for the cross-strait spreading of the *Rugulopteryx okamuræ* algae in the area.

### Summary of current meter observations and other data sets

Velocity observations come from three different sources: i) point-wise current meter data collected at points N, C, and S in the eastern SoG (see Fig 1) in the second half of 1990's decade within the frame of CANIGO project, which have been already employed in several

publications (e.g. [20, 33–35]), ii) Acoustic Doppler Current Profiles (ADCP) collected in year 2013 in the main sill of Camarinal (points CsS and CsN in Fig 1) used to investigate high frequency phenomena caused by flow-topography interaction [36], and iii) recent ADCP collected at point CsS (Fig 1) in years 2020–2021, which have not been used yet. Annex A provides more information about locations, time coverage and depths of all these observations.

Atmospheric pressure is provided by Puertos del Estado, Spain, (<https://portus.puertos.es>) for the period August 2020–July 2021 at a 1-minute sampling rate in the buoy of Palma de Mallorca (see Fig 1), taken as a representative of the Western Mediterranean basin. Wind data in the sub-region of the SoG during the same time period have been retrieved from the ERA5 reanalysis model [37], which is provided by the Copernicus Climate Change Service (C3S) (<https://climate.copernicus.eu>) with 1-hour temporal and  $\sim 25$  km spatial resolutions.

The available current meter time-series have been projected into a rotated Cartesian system aligned with the axis of the SoG (rotated  $20^\circ$  anticlockwise respect the east-north reference system). The  $y$ -component of the velocity in the new system is the cross-strait velocity, positive northwards, and the  $x$ -component is the along-strait velocity, positive to the east. The time-average of both velocity components as a function of depth is plotted in Fig 5 for the velocity series collected at the eastern section and in Fig 6 for the series collected at Camarinal sill.

The surface of instantaneous null velocity, which is the intuitive interface separating inflow and outflow, exhibits large tidally-driven oscillations. Even more, it often disappears because the entire water column moves in one direction during parts of the tidal cycle [19, 20]. Only after removing tidal motions (by a low-pass filtering), this surface can be tracked, although it undergoes noticeable oscillations (Fig 7B) of meteorological origin [24, 33] that can exceptionally lead to its collapse during short intervals [34].

A mean local interface has been defined as the time-averaged depth of the surface of null velocity obtained from the vertical profiles of velocity at each station. The horizontal black

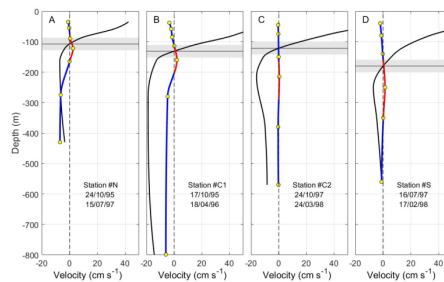


**Fig 5. Time-average cross-strait (blue and red line) and along-strait (black line) velocity as a function of depth in the stations of the eastern section.** Panel A corresponds to site N, panels B and C are for site C in two different periods, and panel D is for site S (see Fig 1 and Annex A for details). Horizontal black line is the depth of null time-average along-strait velocity, that is, the interface that separates inflow and outflow (notice the greater depth towards the south, in agreement with the sketch of Fig 4A). Shaded rectangle indicates  $\pm$ std (standard deviation) of the subinertial fluctuations of this interface estimated in station CsS2 (see text for details). In all panels, solid lines are interpolated profiles from observations, whose depths are indicated by yellow circles. The depth range of positive (northwards) cross-strait velocity is marked in red. The  $\pm 1$  std interval of this velocity is indicated by light-blue thin lines.

<https://doi.org/10.1371/journal.pone.0285470.g005>



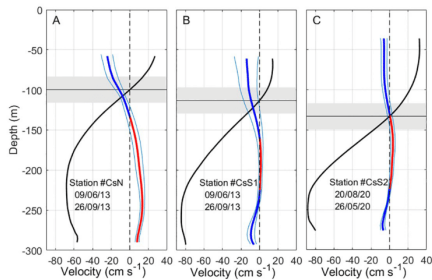


**Fig 6.** Same as Fig 5 for Camarinal sill section. Panel A is for site CsN and panels B and C are for site CsS in two different periods (see Fig 1 for locations). The profiles are directly computed from ADCP observations (no interpolation required) and circles indicating instrument depths do not apply.

<https://doi.org/10.1371/journal.pone.0285470.g006>

lines in Figs 4 and 5 show the interface depth along with a confidence interval, which shows up as a shaded rectangle. This interval has been taken as the standard deviation of the subinertial fluctuations of the interface observed at station CsS2 (cf. Fig 7). The reason for choosing station CsS2 is the high spatial resolution provided by ADCP observations, necessary for the accurate determination of the null-velocity depth, and the length of the series, the longest of the ADCP stations (see Table B in S1 File).

### Assessment of the possible cross-strait transport

#### Observation-based cross-strait mean secondary circulation

The successful algae spreading between both shores depends on the cross-strait current, as the floating spores or seaweed fragments eventually torn from the substrate behave as passive nearly neutrally-buoyant particles (see next Section). However, the success is mediated by the along-strait current, which can displace those particles beyond the open boundaries of the SoG

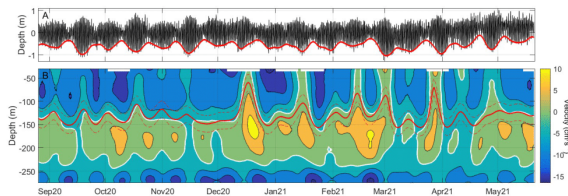


**Fig 7.** A) Pressure oscillations (converted to meters of water column) recorded by the pressure sensor of the ADCP after removing the mean pressure. The spring-neap tidal cycle is easily recognizable and has been made clearer by the smoothed low-water envelope represented by the thick red line. B) Contours (every  $5 \text{ cm s}^{-1}$ ) of the subinertial cross-strait velocity. Reddish colors indicate positive (northwards) velocity whereas bluish tones are for negative, the white line being the contour of cross-strait null velocity. Solid red line indicates the depth of along-strait null velocity (interface) flanked by two dashed red lines at  $\pm 1$  std of the mean interface depth. All time series correspond to station CsS2 in Camarinal sill.

<https://doi.org/10.1371/journal.pone.0285470.g007>

before they are transported from one shore to the other. A favorable coupling between both velocity components is thus necessary.

All the profiles in Figs 4 and 5 show a mid-depth layer of positive cross-strait velocity flanked by negative layers on the surface and at depth, except for CsN site (Fig 6A), where the deeper part is lacking. Accordingly, south-to-north connection would be feasible within the intermediate layer (red line in profiles), whereas north-to-south transport could take place within either the surface or the deep layer (in the eastern SoG, in this case). Figs 4 and 5 show values of cross-strait velocity of around  $5 \text{ cm}\cdot\text{s}^{-1}$  ( $4 \text{ km}\cdot\text{day}^{-1}$ ) or less in the intermediate and deep layers, thus requiring about 4 days at least to cross the SoG at its narrowest section ( $\sim 14 \text{ km}$ ) and longer through other sections. Along-strait mean velocity in the Mediterranean layer changes with depth and geographical location. In its core, the velocity increases from few tens of  $\text{cm}\cdot\text{s}^{-1}$  in the eastern part to nearly  $1 \text{ m}\cdot\text{s}^{-1}$  in the west (Figs 4 and 5). Even assuming a moderate spatial mean value of  $40 \text{ cm}\cdot\text{s}^{-1}$ , the along-strait displacement undertaken in 4 days is close to 150 km, well above the dimensions of the SoG. The same or even more unfavorable considerations apply to the surface layer. Therefore, only by avoiding the core of greater velocities and remaining close to the interface could the algae have chances to cross the SoG.

According to Figs 4 and 5, the last condition discards connectivity within the deeper layer and reduces the chances to the upper and intermediate layers. South-to-north (north-to-south) transport could be achieved in the depth range where the red (blue) profile in Figs 4 and 5 overlaps the shaded grey rectangle. The depth range of positive cross-strait velocity overlaps this rectangle more clearly in the eastern part (red lines in Fig 5), suggesting that this section of the SoG gathers better conditions for successful south-to-north connection within the intermediate layer. The contrary would happen in Camarinal sill (Fig 6) where north-to-south transport in the upper layer is favored.

### Time variability of the cross-strait secondary circulation

The previous description based on time-average values of the velocity must be revised when subinertial variability (from days to few tens of days) is considered. Fig 7B shows contours of the cross-strait velocity after filtering the series with a low-pass filter of 3-day cutoff period that removes tides. The depth of the interface of null along-strait velocity together with the  $\pm 1$  std interval (red lines) have been superposed to the contours. Fig 7A has been included to disclose the fortnightly spring-neap tidal cycle that modulates the semi-diurnal tides.

The intermediate layer of positive cross-strait velocity displayed in Fig 6C is easily recognizable in Fig 7B, despite its thickness fluctuations. Periods of enhanced velocity alternate with other periods of reduced or, even, reversed (negative) velocity. The point of interest is the existence of sustained periods of enlarged velocity nearby the interface depth that provides good chances for south-to-north transport. According to Fig 7, they seem to occur preferably in winter (December 2020 to February 2021). Similar velocity and thickness fluctuations are seen in the surface layer, affecting in this case the north-to-south connectivity. Therefore, subinertial variability offers windows of enhanced cross-strait velocity lasting long enough to allow for successful connection between both shores, a result that applies for both directions.

Velocity fluctuations in Fig 7B may have different origins. A correlation study for investigating relationships between the velocity field and external drivers has been done. Absolute velocity values have been used to avoid the unintuitive detail that higher values of negative velocities mean lower intensities and vice-versa. Panels 7A to 7D show the results for along-strait velocity. Since exchanged flows are computed from this component and the response of those flows to external agents is well established [24, 33], these panels are used here as quality tools. They are expected to show confirmation of this response, which in turn will provide

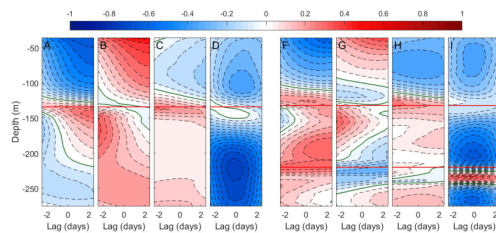


**Fig 8.** Left panels: contours of lagged correlation as a function of depth between the modulus of along-strait velocity with A) the atmospheric pressure in Palma de Mallorca (see red dot in Fig 1), taken as representative of the Western Mediterranean basin, B) the local zonal component of wind, C) the meridional component of wind and D) the strength of the spring-neap tidal cycle as determined by the envelope displayed in Fig 7A. Contour lines are every 0.05 units of correlation with the zero contour shown in green. Horizontal red line indicates the depth of zero-crossing of the along-strait velocity (see Fig 6C). Right panels: same as left panels but for the cross-strait velocity. Red lines indicate the depths of cross-strait zero velocity. In all cases, positive lags correspond to "forcing" (i.e., atmospheric pressure, wind, strength of the tide) leading the "response" (i.e., the velocity components).

<https://doi.org/10.1371/journal.pone.0285470.g008>

support to the conclusions drawn from panels 7E to 7H for the much less studied cross-strait velocity, the one of interest in this work.

**Meteorologically-induced fluctuations.** The along-strait velocity is negatively correlated with the atmospheric pressure over the western Mediterranean above the interface and positively below it (Fig 8A). High pressure will reduce the inflow and increase the outflow, giving rise to a barotropic fluctuation of the net flow towards the Atlantic. Westerlies (positive zonal winds) increase the velocity in the upper layer, easterlies (negative zonal winds) diminish it (Fig 8B). Lower layer velocities show positive correlation too, suggesting that wind-stress induces baroclinic fluctuations of the exchange. These results have already been reported [24, 33, 34, 38, 39] and provide indirect support to those inferred from the correlation analysis for cross-strait velocities, which are discussed next.

Focusing on the upper and intermediate layers that extend over the depth range occupied by the interface (Figs 4 and 5), Fig 8F shows negative and positive correlations, respectively, with the modulus of the cross-strait velocity. Therefore, high atmospheric pressure will diminish the southward current in the upper layer and increase the northward one in the intermediate layer. It shares characteristics of its counterpart Fig 8A in the sense that the response is a barotropic fluctuation that shifts the secondary cross-strait circulation towards a situation of decreased surface current. The opposite would happen under low pressures. Zonal winds (Fig 8G) produce positive correlation in the top of the upper layer and in the intermediate layer. Westerlies would increase the velocity in these segments of the water column and enhance the secondary cross-strait circulation. The opposite effect would happen with easterlies. The effect of meridional winds (Fig 8H) recalls the one of atmospheric pressure (Fig 8F). Northward (positive) wind reduces the mean southward cross-strait velocity in the upper layer and increases the northward one in the intermediate layer. The opposite would happen with southward winds. Both results are expectable.

**The fortnightly tidal cycle.** One of the clearer features in Fig 7B is the fortnightly fluctuations of the cross-strait velocity, which reveals their tidal origin. Fig 8I, in fact, shows extended negative correlation with the strength of the tide in the upper and intermediate layers, meaning that the secondary cross-strait circulation is diminished during spring tides and enhanced

during neap tides. A similar conclusion is drawn from the negative correlation between the strength of the tide and the modulus of the along-strait velocity in practically the entire water column displayed in Fig 8D. The correlation is particularly high in the lower Mediterranean layer, which implies weaker subinertial, tidal-free currents in spring tide and stronger in neap tide. This somewhat unintuitive result has been discussed in [20, 35], and is ascribed to enhanced mixing during spring tides which diminishes the horizontal density gradient that drives the flow. Fig 8D is encouraging in the sense that depicts a contrasted result that supports the findings for the cross-strait velocity component.

The joint consideration of the outcome of the correlation analysis allows to stress favorable opportunity windows and unfavorable scenarios for cross-strait connections. Regarding meteorological forcing, northward flow within the intermediate layer would increase under high pressure over the western Mediterranean basin and local winds from the southwest. If, moreover, these particular conditions are met during neap tides, the resulting scenario would gather the best conditions for south-to-north connectivity. The opposite would happen under low pressure and local northeasterly in spring tides, which would diminish the chances. As for the upper layer, the southwards flow that favors north-to south connection would increase under low atmospheric pressure and local northwesterly along with neap tides. Chances would decrease with low pressure and southeasterly in spring tides.

### Other requirements for a successful connection

Let us consider one of the shores of the SoG with algae settlements while the other is still free of them. What conditions must be met to achieve a successful colonization of the algae-free shore without human intervention? First of all is the existence of the cross-strait system of flows described in the previous sections. The current to take advantage of depends on which shore holds the initial settlement: should it be the north one, the right current is that at the surface layer, but if the initially colonized is the south shore, the proper current lays in the intermediate layer. In addition to this secondary circulation, the successful colonization requires other set of circumstances that include physiological traits and endurance of algae.

The weak cross-strait flow is able to transport products from a shore to the other only if they are available. For south-to-north transport, for instance, algal fragments must reach the interface, situated 100–150 m below the sea surface in the south, be carried to the north at these depths and, once there, be moved upwards into the illuminated layer to settle and thrive. The journey will take days to weeks and be done in dark conditions. The colonization success will thus depend on whether or not the algae arrive in good conditions for reproduction after that period of weak light or no-light conditions.

### Reaching the right depth for crossing and returning to illuminated layers

Macroalgal strains are attached to rocky illuminated bottom and other type of substrates in the subtidal nearshore zone of the SoG to a maximum observed depth of 40 m [1]. There are also evidences that they are drifting freely well below this depth (Fig 2). They must be torn out from the substrate to provide free spores, propagules or seaweed fragments for transportation. Density of algae and vertical velocity of the flow come into play at this stage. *Rugulopteryx okamurae* is very slightly denser than seawater. Simple experiments performed in calm sea conditions in which thalli were dropped near the surface and allowed to fall freely, yielded sedimentation velocities in the range of 1 to 4 cm·s<sup>-1</sup>, depending on the size and shape of the thalli and on whether they form larger aggregates. Similar experiments carried out under more controlled conditions in the laboratory gave a little broader sedimentation velocity range (from 1 to 6.5 cm·s<sup>-1</sup>) and confirmed its dependence on the shape and size of the specimens.

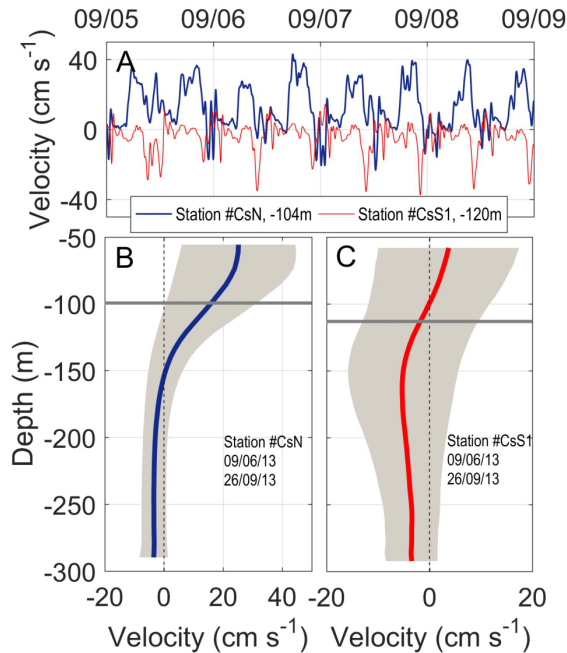


**Fig 9.** A) Vertical velocity recorded at stations CsN and CsS1 at depths of 104m and 120m, respectively, close to the time-averaged interface depth. Dates on the top axis correspond to September 2013. Velocities were recorded every two minutes and have been smoothed by a 5min cut-off period filter. B) Vertical profile of the time-averaged vertical velocity at station CsN (blue line). Shaded area stretches over  $\pm 1$ std and the horizontal grey line indicates the (mean) interface depth. C) Same as B) but for station CsS1.

<https://doi.org/10.1371/journal.pone.0285470.g009>

Variations of seawater density within realistic intervals will hardly change that velocity. The small density difference makes the algae be easily re-suspended by wind-induced or current-induced turbulence, carried to the surface and eventually beached on the shores, often in astonishing amounts [1, 5, 15, 40] see Fig 2B.

Flow-topography interaction in the SoG forms internal hydraulic jumps with high levels of turbulence nearby Camarinal sill [41]. They decay as short-period, large-amplitude internal waves [42] with associated vertical velocities of tens of  $\text{cm s}^{-1}$  [43], greater than the measured sedimentation velocity. Fig 9A shows a short time series of vertical velocity near the interface at stations CsN and CsS1 and illustrates the fact. It changes sign and exhibits semidiurnal fluctuations that disclose their tidal origin. Absolute values exceed the sedimentation velocity and can therefore displace algal fragments up or down vertically. Profiles in Fig 8B and 8C suggest that this result applies to the whole water column. However, nearby the interface, downward

advection is more likely to occur in the south and upward advection in the north, as it can also be deduced from Fig 9A.

The combination of the very small negative buoyancy of algal fragments and the structure and strength of vertical velocities in the SoG makes it feasible for the algae to reach the suitable depth to be advected across the SoG. They would do it in one direction or the other, depending on the depth range in which they stay (cf., Fig 4). Once on the other side, vertical currents could bring them into the illuminated surface layers and allow them to begin colonizing new environments.

### Keeping the right conditions for spreading

The colonization will depend on the health status the algae arrive with after a relatively long journey made in low light or, even, no light conditions. To gain insight into this issue, *Rugulopteryx okamuræ* specimens collected in Tarifa (see Fig 1 for location) were placed in darkness inside a culture chamber of nutrient-rich seawater at 17°C. After 13 days, they showed a considerable health decay, measured as its photosynthetic capacity. However, these specimens were able to recover partially when they were re-exposed to light after the dark period. Even though the initial condition was not fully achieved, they were able to reactivate their metabolism again, thus offering chances for colonizing the new region of arrival. This outcome agrees with other studies. Photosynthetic measurement using *in vivo* chlorophyll fluorescence in algae collected in nets during fish activities between 50–100m depth in the same area gave satisfactory value of electron transport rate as indicator of photosynthetic activity [44]. Also, [18] observed that adult thalli of the species had survival rates between 80–100% after being cultivated in dark conditions for three weeks, depending on the temperature during cultivation, and that these thalli even increased their biomass during this period.

This outcome is not new in the algae realm. Microscopic stages of macroalgae can withstand long periods of darkness and subsequently develop when conditions improve [45–47]. *Aureococcus anophagefferens* (Pelagophyceae), a heterokont alga responsible for the harmful brown tides, was able to survive for at least 30 days in the dark according to [48]. Otherwise, arctic macroalgae (Laminarians and some Rhodophytes) and different polar phytoplankton can survive during the polar night with up to six-month darkness, when they are unable to photosynthesize. They do it by evolving specific strategies during darkness, like maintaining low metabolic state to decrease the consumption of storage compounds and energy. When light returns after the dark period, they re-initiate the growth [49–51]. The mechanisms involved in survival during darkness are not yet well known for these species, nor for *Rugulopteryx okamuræ*. Further studies are required on this. However, the point of interest here is that there are real possibilities of survival during the time interval needed for transportation from one shore to the other.

### Summary and final remarks

Simultaneous appearance of *Rugulopteryx okamuræ* in both shores of the SoG few years ago seems highly improbable. A much more likely situation is that the algae settled in one shore, from which it invaded the opposite one. Favorable environmental conditions propitiated its subsequent explosive spreading. Algae capability to colonize any type of hard substrates [15] opens the possibility of accidental crossing attached to ship hulls, fishing nets or other human-mediated mechanisms, but the possibility still remains that it could have managed to cross the SoG taking advantage of hydrodynamic processes without human intervention.

The possibility has been assessed in this study using current meter observations collected in the area, which show layers of no null velocity in the cross-strait direction. Chances for cross-

strait transport reduce to the depth range around the interface of null along-strait velocity, located at around 100–150 m depth. Within this range, layers of weak cross-strait currents heading south and north have been identified above and below the interface, respectively. They could be used by nearly-neutral buoyant seaweed fragments for being transported from one shore to the other. Outside of this depth range, possibilities drop null, as particles will be advected beyond the lateral open boundaries of the SoG by the strong inflow and outflow.

The successful connection, however, relies on a chain of circumstantial links. Algae should be ripped out from the seafloor by natural (wind-induced or current-induced turbulence) or human (bottom-trawling nets) agents in the surface illuminated layer at the colonized shore. Their propagules or spores should be displaced offshore in the horizontal and to the depth range of the interface in the vertical. Then they should be transported across the deepest part of the SoG until reaching the opposite continental slope, be raised to the surface and displaced to the shore and, finally, settle and thrive in the new environment. The process will take weeks, much of the time the algae being in extreme low or even no-light conditions. This study argues that each and every of these contingencies, considered one by one, are surmountable. For a single experiment, however, the concatenation of the full sequence of events leading to a successful connection is extremely improbable. Obviously, it is only the massive amount of available specimens for transport that can provide a number of successful connections. Even if this number of connections is reduced, it would be enough to colonize the new ecosystem taking into account the huge adaptability of the algae. The feasibility of this possibility could be tested with the help of very high resolution fully 3D numerical models coupled to high resolution advection schemes. The results of these numerical experiments would either support the possibility of a successful hydrodynamic connection between both shores or, on the contrary, they would provide additional proofs to confirm its high improbability and, therefore, reject it. Such a study is currently in progress.

### Supporting information

**S1 File. Appendix: Summary of current meter observations.**  
(PDF)

### Acknowledgments

Authors are grateful to Antonio Vergara, Gojko Kremenec, Antonio Muñoz and J.L. Ferres-García for providing graphical information.

### Author Contributions

**Conceptualization:** Jesús García-Lafuente.

**Data curation:** Jesús García-Lafuente, Irene Nadal, Simone Sammartino.

**Formal analysis:** Jesús García-Lafuente, Irene Nadal, Simone Sammartino.

**Funding acquisition:** Nathalie Korbee, Félix L. Figueroa.

**Investigation:** Jesús García-Lafuente.

**Methodology:** Irene Nadal, Nathalie Korbee.

**Resources:** Félix L. Figueroa.

**Validation:** Jesús García-Lafuente, Simone Sammartino, Nathalie Korbee.

**Visualization:** Jesús García-Lafuente.



**Writing – original draft:** Jesús García-Lafuente, Irene Nadal.

**Writing – review & editing:** Jesús García-Lafuente, Irene Nadal, Simone Sammartino, Nathalie Korbee.

## References

- García-Gómez JC, Sempere-Valverde J, González AR, Martínez-Chacón M, Olaya-Ponzzone L, Sánchez-Moyano E, et al. From exotic to invasive in record time: The extreme impact of *Rugulopterix okamuræ* (Dictyotales, Ochrophyta) in the strait of Gibraltar. *Science of The Total Environment*. 2020 Feb; 704:135408. <https://doi.org/10.1016/j.scitotenv.2019.135408> PMID: 31836226
- Huang ZG. *Marine Species and Their Distributions in China's Seas*. China Ocean Press. Beijing; 1994.
- Verlaque M, Steen F, De Clerck O. *Rugulopterix* (Dictyotales, Phaeophyceae), a genus recently introduced to the Mediterranean. *Phycologia*. 2009 Nov; 48(6):536–42.
- Altamirano-Jeschke M, de la Rosa Álamos J, Martínez Medina FJ. Arribazones de la especie exótica *Rugulopterix okamuræ* (EY Dawson) I.K. Hwang, W.J. Lee & H.S. Kim (Dictyotales, Ochrophyta) en el Estrecho de Gibraltar: primera cita para el Atlántico y España. 2016. RIUMA. <http://hdl.handle.net/10630/12433/>
- El Amri F, Idhalla M, Tamsouri MN. Occurrence of the invasive brown seaweed *Rugulopterix okamuræ* (E.Y. Dawson) I.K. Hwang, W.J. Lee & H.S. Kim (Dictyotales, Phaeophyta) in Morocco (Mediterranean Sea). *Mediterranean Fisheries and Aquaculture Research (MedFAR)*. 2018. 1(2), 92–96.
- Navarro-Barranco C, Muñoz-Gómez B., Saiz D, Ros M, Guerra-García JM, Altamirano M, et al. Can invasive habitat-forming species play the same role as native ones? The case of the exotic marine macroalga *Rugulopterix okamuræ* in the Strait of Gibraltar. *Biological Invasions*. 2019 Nov 1; 21(11):3319–34.
- Katsanevakis S. Unpublished Mediterranean records of marine alien and cryptogenic species. *BioInvasions Records*. 2020; 9(2):165–82.
- Ashton GV, Zabin CJ, Davidson IC, Ruiz GM. Recreational boats routinely transfer organisms and promote marine bioinvasions. *Biological Invasions*. 2022 Jan 17; 24(4):1083–96.
- García-Gómez JC, Florido M, Olaya-Ponzzone L, Rey Díaz de Rada J, Donazar-Aramendia I, Chacón M, et al. Monitoring Extreme Impacts of *Rugulopterix okamuræ* (Dictyotales, Ochrophyta) in El Estrecho Natural Park (Biosphere Reserve). Showing Radical Changes in the Underwater Seascapes. *Frontiers in Ecology and Evolution*. 2021 Apr 15; 9.
- Ruitton S, Blanfuné A, Boudouresque CF, Guillemain D, Michotey V, Roblet S, et al. Rapid Spread of the Invasive Brown Alga *Rugulopterix okamuræ* in a National Park in Provence (France, Mediterranean Sea). *Water*. 2021 Aug 23; 13(16):2306.
- Faria J, Prestes ACL, Moreu I, Cacabelos E, Martins GM. Dramatic changes in the structure of shallow-water marine benthic communities following the invasion by *Rugulopterix Okamuræ* (Dictyotales, Ochrophyta) in Azores (Ne Atlantic). *Marine Pollution Bulletin*. 2022; 175:113358. <https://doi.org/10.1016/j.marpolbul.2022.113358> PMID: 35092932
- Román Muñoz A, Martín-Taboada M, De la Rosa J, Carmona R, Zanolla M, Altamirano M. La modelación de la distribución de especies como herramienta en la gestión de invasiones biológicas en el medio marino: el caso de *Rugulopterix okamuræ* (Dictyotaceae, Ochrophyta) en el Mediterráneo. *Algas*. 2019. 55e: 37–41 (in Spanish).
- Mercado JM, Gómez-Jakobsen F, Korbee N, Aviles A, Bonomi-Barufi J, Muñoz M, et al. Analyzing environmental factors that favor the growth of the invasive brown macroalga *Rugulopterix okamuræ* (Ochrophyta): The probable role of the nutrient excess. *Marine Pollution Bulletin*. 2022 Jan; 174:113315. <https://doi.org/10.1016/j.marpolbul.2021.113315> PMID: 35092937
- Hwang IK, Lee WJ, Kim HS, De Clerck O. Taxonomic reappraisal of *Dilophus okamuræ* (Dictyotales, Phaeophyta) from the western Pacific Ocean. *Phycologia*. 2009 Jan; 48(1):1–12.
- García-Gómez JC, Sempere-Valverde J, Ostalé-Valriberas E, Martínez M, Olaya-Ponzzone L, González AR, et al. *Rugulopterix okamuræ* (EY Dawson) I.K. Hwang, W.J. Lee and H.S. Kim (Dictyotales, Ochrophyta), alga exótica "explosiva" en el estrecho de Gibraltar. Observaciones preliminares de su distribución e impacto. *Almoraima. Revista de Estudios Campogibraltareños*. 2018. 49, 97–113. ISSN 1133-5319.
- Wejnerowski Łukasz, Tümer Orhun Aykut, Aleksandra Pelechata, Rybak M, Dulic T, Jussi Meriluoto, et al. Plankton hitch-hikers on naturalists' instruments as silent intruders of aquatic ecosystems: current risks and possible prevention. *NeoBiota*. 2022 May 25; 73:193–219.
- Hyun B, Shin K, Jang MC, Jang PG, Woo Jung Lee, Park CB, et al. Potential invasions of phytoplankton in ship ballast water at South Korean ports. *Marine and Freshwater Research*. 2016 Dec 16.



18. Rosas-Guerrero J, Meco YE, Altamirano M. Could *Rugulopteryx okamuræ* (Dictyotales, Ochrophyta) have been introduced by ballast waters? *Algas*. 2018; 54, 52.
19. Bryden HL, Candela J, Kinder TH. Exchange through the Strait of Gibraltar. *Progress in Oceanography*. 1994 Jan; 33(3):201–48.
20. García-Lafuente J, Vargas JF, Francisco Jorquera Plaza, Sarhan T, Candela J, Burkard Bascheck. Tide at the eastern section of the Strait of Gibraltar. *Journal of Geophysical Research*. 2000 Jun 15; 105 (C6):14197–213.
21. García-Lafuente J, Sanchez-Garrido JC, García A, Hidalgo M, Sammartino S, Laiz R. *Biophysical Processes Determining the Connectivity of the Alboran Sea Fish Populations*. Springer eBooks. 2021 Jan 1;459–87.
22. Gill A. *Atmosphere-Ocean Dynamics*. Academic Press, San Diego, California, USA. 1982. 662 pp.
23. Garrett C, MacCready P, Rhines PB. Boundary Mixing and Arrested Ekman Layers: Rotating Stratified Flow Near a Sloping Boundary. *Annual Review of Fluid Mechanics*. 1993 Jan 1; 25(1):291–323.
24. Candela J, Winant CD, Bryden HL. Meteorologically forced subinertial flows through the Strait of Gibraltar. *Journal of Geophysical Research*. 1989; 94(C9):12667.
25. Garrett C. Frictional processes in straits. *Deep-sea Research Part II-topical Studies in Oceanography*. 2004 Feb 1; 51(4–5):393–410.
26. Pratt LJ, Whitehead JC. *Rotating Hydraulics*. Atmospheric and oceanographic sciences library. Springer Nature (Netherlands); 2007.
27. Johnson GC, Ohlsen DJ. Frictionally Modified Rotating Hydraulic Channel Exchange and Ocean Outflows. *Journal of Physical Oceanography*. 1994 Jan 1.
28. Baschek B, Send U, García-Lafuente J, Candela J. Transport estimates in the Strait of Gibraltar with a tidal inverse model. *Journal of Geophysical Research: Oceans*. 2001 Dec 15; 106(C12):31033–44.
29. Sammartino S, Lafuente J, Naranjo C, Garrido S, Sanchez F, Sánchez Román A. Ten years of marine current measurements in E spartel S ill, S trait of Gibraltar. *Journal Of Geophysical Research: Oceans*. 2015 Sep 1; 120(9):6309–28.
30. García-Lafuente J, Sammartino S, Sánchez Garrido JC, Naranjo C. On the role of the bay of algeciras in the exchange across the strait of Gibraltar. *Regional Studies in Marine Science*. 2019 May 1.
31. García-Lafuente J, Bruque Pozas E, Sánchez Garrido JC, Sannino G, Sammartino S. The interface mixing layer and the tidal dynamics at the eastern part of the Strait of Gibraltar. *Journal of Marine Systems*. 2013 May 1; 117–118:31–42.
32. Nadal I, Sammartino S, Jesús García-Lafuente, Garrido JA, Gil-Herrera J, Hidalgo M, et al. Hydrodynamic connectivity and dispersal patterns of a transboundary species (*Pagellus bogaraveo*) in the Strait of Gibraltar and adjacent basins. *Fisheries Oceanography*. 2022 Apr 18.
33. García Lafuente J. Subinertial variability in the flow through the Strait of Gibraltar. *Journal of Geophysical Research*. 2002; 107(C10).
34. García Lafuente J, Delgado J, Criado F. Inflow interruption by meteorological forcing in the Strait of Gibraltar. *Geophysical Research Letters*. 2002 Oct; 29(19):20–120–4.
35. Vargas JM, García-Lafuente J, Candela J, Sánchez AJ. Fortnightly and monthly variability of the exchange through the Strait of Gibraltar. *Progress in Oceanography*. 2006 Aug; 70(2–4):466–85.
36. García-Lafuente J, Sammartino S, Sánchez-Garrido JC, Naranjo C. Asymmetric baroclinic response to tidal forcing along the main sill of the Strait of Gibraltar inferred from mooring observations. In Velarde, M.G., Tarakanov, R.Y. and Marchenko, V. (editors) *The Ocean in motion*. Springer Oceanography, Switzerland AG. 2018.
37. Hersbach H, Bell B, Berrisford P, Biavati G, Horányi A, Muñoz Sabater J, et al. ERA5 hourly data on single levels from 1979 to present (Copernicus Climate Change Service (C3S) Climate Data Store (CDS)). 2018.
38. Peliz A, Teles-Machado A, Marchesiello P, Dubert J, García-Lafuente J. Filament generation off the Strait of Gibraltar in response to Gap winds. *Dynamics of Atmospheres and Oceans*. 2009 Jan 1; 46(1–4):36–45.
39. Boutov D, Peliz A, Pedro, Soares P, Cardoso RM, Prieto L, et al. Inter-annual variability and long term predictability of exchanges through the Strait of Gibraltar. *Global and Planetary Change*. 2014 Mar 1; 114:23–37.
40. Altamirano-Jeschke M, de la Rosa J, Gil FJM, Gallego ARM. Prolifera en el Estrecho un alga nunca citada en nuestro litoral de origen asiático, "*Rugulopteryx okamuræ*" ocupa ya una gran extensión. *Quercus*. 2017. 374, 32–33.
41. Wesson JC, Gregg MC. Mixing at Camarinal Sill in the Strait of Gibraltar. *Journal of Geophysical Research*. 1994; 99(C5):9847.

42. Farmer DM, Armi L, Armi L, Farmer DM. The flow of Atlantic water through the Strait of Gibraltar. *Progress in Oceanography*. 1988 Jan; 21(1):1–103.
43. Sánchez-Garrido JC, Sannino G, Liberti L, García Lafuente J, Pratt L. Numerical modeling of three-dimensional stratified tidal flow over Camarinal Sill, Strait of Gibraltar. *Journal of Geophysical Research*. 2011 Dec 17; 116(C12).
44. Figueroa FL, Vega J, Gómez-Valderrama M, Korbee N, Bañares E, Flores-Moya A. Invasión de la especie exótica *Rugulopteryx okamuræ* en Andalucía: I. Estudios preliminares de la actividad fotosintética. *Algas*. 2020. 56:35–46 (in Spanish).
45. Leukart P, Klaus Lüning. Minimum spectral light requirements and maximum light levels for long-term germling growth of several red algae from different water depths and a green alga. *European Journal of Phycology*. 1994 May 1; 29(2):103–12.
46. Santelices B, Aedo D, Hoffmann A. Banks of microscopic forms and survival to darkness of propagules and microscopic stages of macroalgae. *Revista Chilena de Historia Natural*. 2002 Sep 1; 75(3).
47. Carney LT, Edwards MS. Cryptic Processes in the Sea: A Review of Delayed Development in the Microscopic Life Stages of Marine Macroalgae. *ALGAE*. 2006 Jun 30; 21(2):161–8.
48. Popels LC, Hutchins DA. FACTORS AFFECTING DARK SURVIVAL OF THE BROWN TIDE ALGA *AUREOCOCCUS ANOPHAGEFFERENS* (PELAGOPHYCEAE)1. *Journal of Phycology*. 2002 Aug; 38(4):738–44.
49. LaCour TG, Morin PI, Sciandra T, Donaher NA, Campbell DA, Ferland J, et al. Decoupling light harvesting, electron transport and carbon fixation during prolonged darkness supports rapid recovery upon re-illumination in the Arctic diatom *Chaetoceros neogracilis*. *Polar Biology*. 2019 Oct 1; 42(10):1787–99.
50. Li H, Scheschonk L, Heinrich S, Valentin KU, Harms L, Gernot Glöckner, et al. Transcriptomic Responses to Darkness and the Survival Strategy of the Kelp *Saccharina latissima* in the Early Polar Night. *Frontiers in Marine Science*. 2020 Dec 23; 7.
51. Gordillo F, Carmona R, Jiménez C. A Warmer Arctic Compromises Winter Survival of Habitat-Forming Seaweeds. *Frontiers in Marine Science*. 2022 Jan 13; 8.



El trabajo se ha realizado en el Departamento de Física Aplicada II de la Universidad de Málaga, y parcialmente gracias a las ayudas para la realización de estancias encaminadas a la obtención de la mención de Doctor Internacional concedidas por el Plan Propio de la Universidad de Málaga.